DUCTILITY IN HIGH CHROMIUM SUPER-FERRITIC ALLOYS

by

Ira M. Wolff

A thesis submitted to the Faculty of Engineering, University of Cape Town in fulfilment of the requirements for the degree of Doctor of Philosophy

Department of Materials Engineering
University of Cape Town
March 1989

ABSTRACT

The competition between microfracture and plastic flow has been studied in relation to the thermomechanical processing parameters and minor element chemistry of wrought super-ferritic alloys based on a composition of Fe-40wt% Cr. These alloys have been developed for corrosion-resistant applications, specifically by micro-alloying with platinum group metals to induce cathodic modification, but their use has been hampered by inadequate toughness at ambient temperatures.

Brittle cleavage of the alloys is a consequence of the high resistance to plastic flow required to accommodate local stresses, such as those found ahead of a loaded crack. Once initiated, a crack propagates in a brittle manner with minimal ductility. The impact toughness therefore relies on the ability of the alloys to withstand crack initiation. The frequency of the crack initiation events is related to the distribution of secondary phases within the matrix and at the grain boundaries. A direct means of improving the toughness and the ductility is accordingly via annealing cycles and minor alloying additions to control the precipitation of second phases.

The ductility is enhanced by raising the mobile dislocation density, and this may be achieved by pre-straining recrystallised material, or increasing the number of dislocation sources in the otherwise source-poor material. The generation of mobile dislocations by prismatic punching at second phase particles in response to local or tessellated stresses was found to increase the ductility and the impact toughness of the alloy.

The addition of nickel also increases the brittle fracture resistance by promoting stress accommodation at the crack tip, a result which can, in principle, be explained on the basis of enhanced dislocation dynamics.

The tendency of the alloys to form a stable recovered substructure was identified as a critical parameter for both the mechanical and corrosion properties. The low-angle dislocation sub-arrays contribute to overall strain-hardening, but destabilise the passivity of the alloys in acid media.

In practice, rationalisation of the microstructural parameters has enabled the practicable fabrication of tough, corrosion-resistant alloys, suitable for commercial development.

ACKNOWLEDGEMENTS

It is a pleasure to express my appreciation to the following people for their assistance during the course of this work :

Professor A. Ball, for his able supervision

Dr P.T. Wedepohl, for his advice and support

Mrs H. Böhm and Mrs S. Betz, for their experimental assistance

Mrs P. Park-Ross, for her help with the corrosion work

Mr B. Greeves and Mr J. Petersen, for their photographic expertise

Mr N. Dreze, Mr G. Newins and Mr J. Maskrey, for their technical assistance

Mrs J. Geldenhuys, Mrs B. Hartley, Mrs A.C. Ball and Ms S. Hamilton, for their help with the final manuscript

The staff and my colleagues in the Department of Materials Engineering, UCT, for their encouragement

Lastly, I am indebted to the Physical Metallurgy Division, MINTEK, for the use of equipment and materials, and financial sponsorship.

Dedicated to my mother
and in memory of my father

CONTENTS

Page

LIST OF ABBREVIATIONS

at%	atomic percent
bcc	body centered cubic
(C+N)	total carbon + nitrogen content
CR	cold reduction
CRE	controlled residual element
CSL	coincidence site lattice
C_V	Charpy V-notch Energy
DBTT	ductile-brittle transition temperature
EDA/P	electron diffraction analysis/patttern
EDS	energy dispersive spectroscopy
%El	percentage elongation
ELI	extra low interstitial
FATT	fracture appearance transition temperature
fcc	face centered cubic
hcp	hexagonally close-packed
H_V	Vickers pyramid hardness
IGF	intergranular fracture
ITT	impact transition temperature
OR	orientation relationship
PGM	platinum group metals
ppm	parts per million
0,2%PS	0.2% proof stress
RDE	rhenium ductilising effect
REM	rare earth metals
RT	room temperature
SCC	stress corrosion cracking
SFE	stacking fault energy
SHT	solution heat treatment
tcp	topologically close packed
UTS	tensile strength
WQ	water quench
wt%	weight percent*

* unless otherwise indicated, all compositions refer to wt%

CHAPTER 1

INTRODUCTION

1.1 DEVELOPMENT

Poor impact toughness in the Fe-Cr system is associated primarily with a ductile-brittle transition common to metals with a body-centred cubic or bcc crystal structure. This transition can be seriously influenced by the state of the interstitial elements. Provided that the interstitials are retained in solid solution, good toughness and ductility are displayed at ambient temperatures. These properties may, however, be impaired if the interstitials are allowed to precipitate, with a concomitant loss of corrosion resistance. Both of these difficulties have been overcome to some extent in modern commercial grades by minimising the total (C+N) content.

Since the sensitivity of the alloys to the interstitial elements increases as the chromium increases, high chromium alloys require a commensurate tightening in the interstitial tolerances, which has implications for both the economics as well as the fabrication procedures. Considerable energy has therefore been expended in the past in an attempt to describe the mechanical and corrosion properties as a function of the microstructural parameters. The practical limitations in combatting the inherent brittleness of the system have led to wide-ranging attempts to promote ductility in the alloys by external means. These include grain refinement by cold-working, the use of gettering agents to stabilise the impurities, and "ductilising" additives to improve the impact toughness. It is the contention of this dissertation that ductility can be promoted by enhanced stress accommodation processes ahead of a crack-tip. The most straightforward means of achieving this is by increasing the mobile dislocation density and/or the dislocation mobility. To this end the effects of annealing cycles, pre-straining, prismatic punching at second-phase particles, and minor alloying additions on the plastic response of alloys based on a composition of Fe-40wt% Cr have been studied.

1.2 MOTIVATION

The collaborative research programme of the Physical Metallurgy Division of MINTEK (South Africa) has as one of its leading objectives the extension of the knowledge base of alloy systems derived from South Africa's raw materials. In the long term the successful development of new commerical applications for local products leads to a greater market for the export of commodities and technology. The present study constitutes an aspect of the alloy development programme focussing on the utilisation of ferrochromium in the form of high chromium alloys. Following early work by Soviet researchers, which showed that the passive characteristics of stainless steels in acid media could be dramatically enhanced by micro-alloying with platinum group metals (PGM), the current work has as its objective the parallel exploitation of high chromium ferritic stainless steels in conjunction with PGM's as highly corrosion-resistant alloys for use in specific environments.

There exist today more than 170 specially developed types of stainless steels with alloying additions to provide particular properties or ease of fabrication. The progressive improvement in the general and localised corrosion resistance with increasing chromium content has led to the development of steels with chromium contents greater than 30wt%, with more stringent requirements for refinement.

The generic class of stainless steels known as super-ferritics represents an example of high chromium steels developed for special applications. Their resistance to chloride stress-corrosion-cracking (SCC), and the cost-effective elimination of nickel as an alloying addition, has made them competitive in applications where their austenitic or high nickel counterparts are unsuitable.

The passivity of stainless steels relies on the chromium content, which provides a protective oxide film at the corrosion surface over a large passive region. The addition of a PGM to the alloy causes a spontaneous shift of the cathodic potential into the passive region, a phenomenon generally known as cathodic activation. Enhanced corrosion resistance by cathodic modification is understood to be an electrochemical effect as compared with the mechanical protection of the impervious oxide layer. The PGM addition causes an increase in the rate of hydrogen evolution under

reducing acid conditions, thereby shifting the corrosion potential into the stable passive region. It therefore requires only a small alloying addition (of the order of a few tenths of a percent) to effect spontaneous passivation.

Early work by Tomashov's group in the U.S.S.R. showed that the primary passivation potential of Fe-Cr alloys continues to move in the favourable (negative) direction with an increase in the chromium content, but that the critical current density for passivation greatly increases beyond a composition of 40wt% Cr. In the case of Fe-Cr alloyed with a PGM, the Fe-40Cr composition also records the minimum corrosion rate and time to self-passivation in acid media (Figure 1.1). Thus the Fe-40Cr composition represents the optimum balance between passivation and the corrosion kinetics, and was selected to maximise the passivity obtained by cathodic modification. The enhanced corrosion resistance following cathodic element additions is demonstrated in Table 1.1.

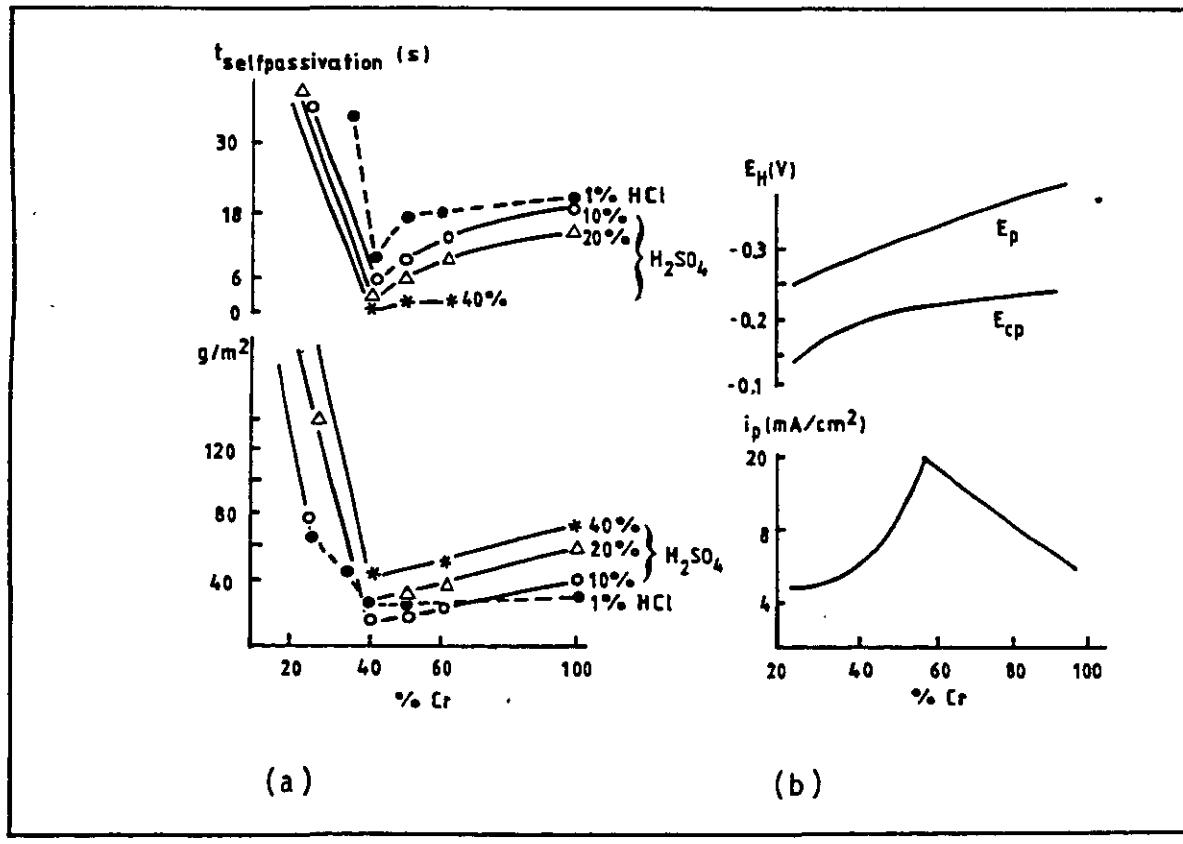

FIGURE 1.1 Effect of Cr content on (a) the self-passivation and weight loss of alloys with 0.2 Pd in H_2SO_4 at 100°C and in boiling HCl, and (b) passivating characteristics of alloys passivation (E_p) and complete passivation (E_{cp}) potentials in H_2SO_4 at 25°C [Chernova et al (1978)]

TABLE 1.1 Corrosion Rates for Alloys in 40wt% H_2SO_4 at 100°C [Higginson (1987)]

Alloy	Corrosion Rate (mmpy)
Fe-40Cr	10^4
Fe-40Cr - 0,2Pd	0,05
Hastelloy C	3,0
Hastelloy A,B	0,2

Streicher (1977) has used all of the PGM's to produce passivity in boiling sulphuric acid. The minimum concentration required to polarise the alloy decreases with increasing chromium content. While none of the PGM additions affect the resistance to SCC, only iridium, osmium and ruthenium do not impair the resistance to pitting and crevice corrosion. In addition, weight-loss tests performed at MINTEK on Fe-40Cr-0.2Ru and Fe-40Cr-0.2Pd alloys have indicated that ruthenium is more effective than palladium on a weight for weight basis [Harding (1984)]. Since ruthenium is also the cheapest of the PGM's it is the most likely cathodic modificant for use in stainless steels.

Higginson (1987) has studied the passivation of Fe-Cr-Ru alloys in acidic environments and has confirmed the expanded range of passivity. Spontaneous passivation of Fe-40Cr with 0.2%Ru was shown to occur in 0.5M H_2SO_4 and 0.5M HCl solutions. Mechanical tests be De Marsh (1986) and Hermanus (1986) subsequently demonstrated that good toughness could be achieved in Fe-40Cr alloys provided the interstitials were controlled.

The requirements for high purity necessitate costly production procedures, whereafter the addition of 0.2%Ru approximately doubles the cost of the Fe-40Cr alloy. This puts it in a regime where it must compete with the high nickel alloys. The potential market is therefore small, apart from

which it must face a challenge from well established alternative alloys such as the Hastelloys. Nevertheless, it has been estimated that the successful development of a 0.2%Ru alloy could, within five years, provide a market for an additional $1,5x10^3$ kg of ruthenium annually, a substantial proportion of the estimated total worldwide demand of $5,1x10^3$ kg per annum. [MINTEK (1986)].

Development of commercial alloys based on cathodic element additions is therefore deemed practicable in light of the above. In order to make the Fe-40Cr alloy an economic feasibility, it is necessary to develop alloys which have either the technical refinement of the super-alloys, or the cost competitiveness of the less sophisticated ferritic stainless steels. In either case an understanding of the alloy system is paramount for further development, particularly as regards the mechanical properties. From the corrosion point of view, the disproportionate cost of the PGM addition may lead to the reduction in the PGM content by partial substitution with other alloying additions. From the production point of view, it is desirable to establish whether lesser degrees of refinement may be tolerated. While this study is concerned primarily with the development of the mechanical properties of the system and the effect of the alloy chemistry, the above considerations need to be kept in mind.

1.3 SCOPE

Despite the large research effort worldwide, uncertainty exists in several important areas of ferritic stainless steel development. These include:

(a) The impact toughness as a function of the microstructural parameters.
(b) The role of mobile dislocations in determining the fracture toughness.
(c) Phase relationships and distribution of the secondary phases.
(d) The independent effect of the minor alloying additions and residual impurities on the mechanical properties.
(e) The relationship between corrosion resistance and ductility.

An experimental programme to examine the behaviour of the Fe-40Cr system on a micro-level was therefore undertaken. Work has encompassed a range of thermomechanical treatments and alloying additions, with two fundamental aims, viz

(1) To gain an understanding of the fracture mechanisms to enable modification of the alloys via alloying additions and heat treatment cycles.

(2) To study the minor element chemistry, especially in relation to improving the odds for plasticity in competition with factors promoting brittle fracture.

CHAPTER 2

LITERATURE REVIEW

2.1 INTRODUCTION

This chapter draws on several major fields of research which have a direct bearing on the present study. While the scope is enormous, it must be pointed out that despite the considerable research into fields such as substitutional alloying, and fracture mechanisms in bcc alloys, a basic mechanistic understanding remains lacking in several fundamental areas. Thus it is only recently, with the refinement of the dislocation theory, that intrinsic phenomena such as alloy softening, and the deformation at the head of a crack, have come to be explained. With an understanding of the basic mechanisms have come attempts to model the processes at a micro-level. These mathematical models provide a qualitative understanding of the processes involved, but as yet are far from correlation with experiment. Attention is therefore confined to more recent developments, and salient observations have been extracted.

The first section is an overview of the generic class of stainless steels known as super-ferritics, with which the Fe-40Cr alloys may be grouped. Some of the initial work on Fe-40Cr alloys is also examined. The role of alloying in simple bcc systems is dealt with in some detail in the following section, with particular emphases on the phenomenon of alloy softening, and the control of residual impurities. A section is given over to a synopsis of the evolution of the fracture theory in recent years, which is followed by an examination of the plastic deformation processes which control the fracture mode. Finally, attention is given to the creation of mobile dislocations by prismatic punching at second phase particles.

2.2 THE SUPER-FERRITIC STAINLESS STEELS

2.2.1 Classification

The ferritic stainless steels may best be defined with reference to the Fe-Cr phase diagram in Figure 2.1. They are binary alloys which are ferritic up to their melting points, with residual impurities low enough to preclude the formation of austenite or martensite on cooling. Under ideal conditions the ferritic stainless steels exhibit good general corrosion resistance, but their main advantage lies in their resistance to SCC in chloride environments, to which their austenitic counterparts are susceptible. In addition, the elimination of nickel as an alloying element has cost benefits.

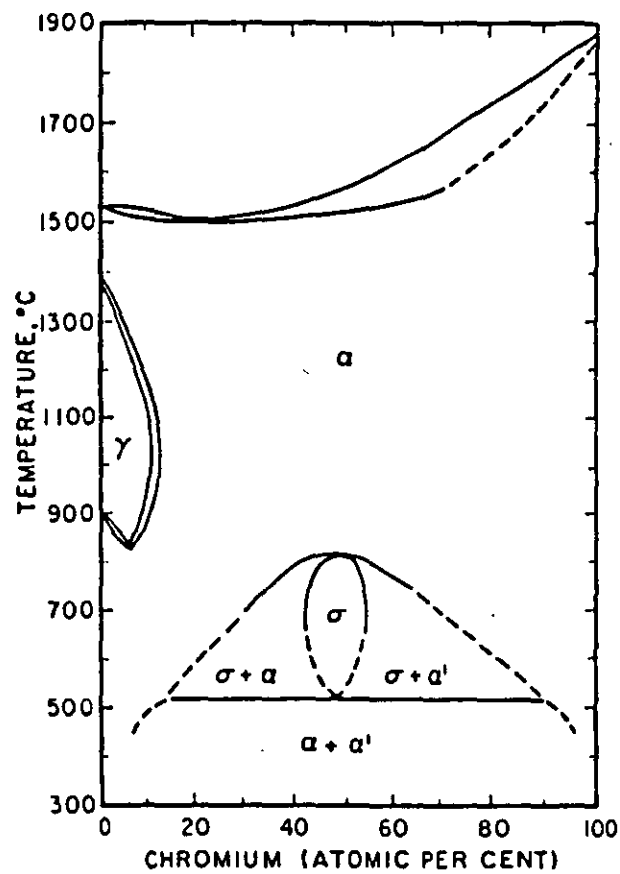

FIGURE 2.1 General Fe-Cr equilibrium diagram [Wright (1980)]

The demonstration by Binder and Spendlow (1951) that toughness in high chromium alloys is a function of the interstitial levels led to a heightened interest in the ferritic grades, but this knowledge was not utilised until the advent of vacuum melting and refining processes in the 1970's made the economical production of high purity alloys possible [Streicher (1977)]. The development of extra-low interstitial (ELI) grades with chromium contents greater than 25% gave rise to the class of alloys known as 'super-ferritics'. The intensive research of the past 15 years has generated an astonishing volume of experimental data, but since this is mainly empirical in nature, a detailed analysis serves no useful purpose. Comprehensive reviews have been given by Demo (1977) and Wright (1980). Attention is therefore confined to general observations of direct relevance to the current investigation.

2.2.2 Secondary Phases

INTERSTITIAL COMPOUNDS

Carbonitrides are present as the principal secondary phases in the super-ferritics. The concept that the ferritic structure may be rendered sufficiently tough by holding the (C+N) below 200 ppm is well established, but this is contingent on the C+N being retained in solid solution [Wright (1980)]. The precipitation of carbonitride phases is generally agreed to have a deleterious effect on the mechanical and corrosion properties of the alloy.

The Cr-Fe-N and Cr-Fe-C systems have been extensively studied. Figure 2.2(a) shows a section of the Fe-Cr-N phase diagram [Brewer and Chang (1973)]. The predominant interstitial phase at a composition of 0.1% N and 40% Cr is the hexagonal Cr_2N precipitate, which is totally dissolved above 1050°C. The precipitation of Cr_2N has been rationalised by Bywater and Dyson (1975). Cr_2N forms within the ferrite with an acicular morphology, the orientation relationship (OR) being given by :

$$(0001)_{Cr_2N} \;//\; (011)_{\alpha}$$

$$[210]_{Cr_2N} \;//\; [2\bar{1}1]_{\alpha}$$

Analysis has shown that the acicular precipitates have a <113> growth direction, which corresponds to the minimum mismatch of interatomic distances along parallel matrix and preciptate crystallographic directions.

(a)

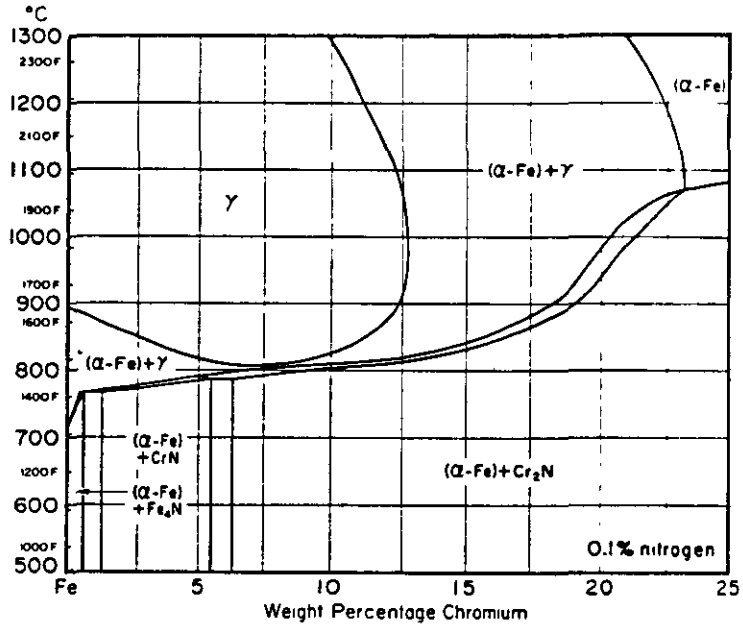

(b)

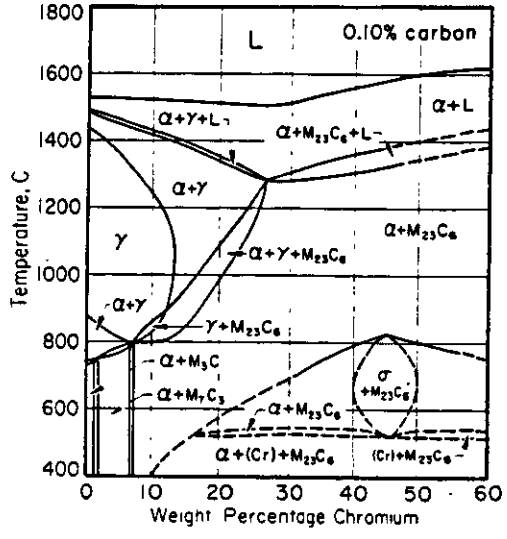

FIGURE 2.2 Constitutional diagrams for (a) Cr-Fe-N and (b) Cr-Fe-C systems [Brewer & Chang (1973), Forgeng and Forgeng (1972)]

The dominant carbide species predicted by the constitution diagram in Fig. 2.2.(b) is the complex fcc $M_{23}C_6$, containing up to 30% Fe [Forgeng and Forgeng (1972)]. The thermodynamics of the Fe-Cr-C system have recently been re-assessed by Dawson and Sale (1977) and

Anderson (1988), and Woodyatt and Krauss (1976) have determined the Fe-Cr-C 870°C isothermal section by equilibrating a series of alloys containing up to 30% Cr. The only carbides present in the system were shown to be M_3C, M_7C_3 and $M_{23}C_6$, but the M_3C and M_7C_3 are not in equilibrium with the ferrite phase.

The two types of carbide M_7C_3 and $M_{23}C_6$ are reported to be morphologically similar by Beech and Warrington (1966) and cannot be distinguished on the basis of shape. The $M_{23}C_6$ carbides precipitate preferentially on grain boundaries, twin boundaries, and lastly intragranularly and on inclusions. Cold work increases the rate of nucleation by providing additional nucleation sites in the form of dislocations. An increase in the carbon content increases the carbide stability at elevated temperatures [Weiss and Stickler (1972)].

The crystallography of the $M_{23}C_6$ precipitation has received much attention. The OR for $M_{23}C_6$ and ferrite has been found by Kuo and Jia (1985) to be:

$$(001)_\alpha \;//\; (011)_{M_{23}C_6}$$
$$(110)_\alpha \;//\; (\bar{1}1\bar{1})_{M_{23}C_6}$$
$$(\bar{1}10)_\alpha \;//\; (\bar{2}\bar{1}1)_{M_{23}C_6}$$

In systems containing both C and N, a certain degree of substitution occurs. Pollard (1974) found that irrespective of the cooling rate of Fe-26Cr alloys, with a high N and low C level the precipitate formed was $Cr_2(C,N)$, whereas with a low N and high C level the precipitate was invariably $M_{23}C_6$. The major precipitates in stabilised heats were carbonitrides of the form M(C,N). Pollard indicated that the important factor in determining ductility was the precipitate morphology, not its chemical composition. The harmful effect of the plate-like Cr_2N precipitates in particular has also been recognised by others [Patskevich et al (1975) and Grubb and Wright (1979)], the plates readily opening up to serve as fast crack paths.

INTERMETALLIC COMPOUNDS

The high chromium ferritic stainless steels are also prone to embrittlement and loss of corrosion resistance by two types of intermetallic phase transformations. One of these is the age-

hardening formation of the chromium-rich bcc alpha-prime phase over the temperature range 370-550°C, which has come to be known as '475°C Embrittlement'. [Nichol et al (1980)]. This is generally understood to be the result of spinodal decomposition derived from the miscibility gap in the Fe-Cr phase diagram [Brenner et al (1982) and others] although the presence of interstitial nitrogen can cause precipitation hardening by the preferential nucleation and growth of Cr-N zones in the same temperature regime [Leitch (1987)]. Since the present studies involve heat treatment cycles terminating in a quench from above 800°C, the 475°C Embrittlement reaction is not expected to play a role in determining the mechanical properties.

The second type of transformation consists of the precipitation of intermetallic phases such as sigma, chi and Laves, which form over the 600-1000°C temperature range. Of particular concern to the Fe-Cr binary system is the formation of the topologically close-packed (tcp) sigma phase, which is highly brittle and has a reported hardness of $940H_V$ [Dean and Plumbridge (1982)]. The unit cell is tetragonal with lattice parameters a = 8,799Å and c = 4,54Å. Sigma forms predominantly as grain-boundary allotriomorphs, but lower soaking temperatures favour intragranular precipitation. The intrinsic brittleness of the sigma plates lead to characteristic "intersigmatic" brittle fracture. Once nucleated, sigma grows congruently from the ferrite, and the regions in the immediate vicinity of the sigma phase boundaries contain a high density of dislocations induced by transformation strains [Brown et al (1983)].

The presence of even small amounts of other elements can greatly accelerate the sluggish sigma formation kinetics, and the ferrite stabilisers such as Nb, Ti and Mo are particularly effective in this regard. In as-cast alloys the time for sigma formation is greatly reduced due to large amounts of solute segregation. Other factors which promote sigma formation are cold work [Ludwigson and Link (1965)] and grain refinement, which reduces the diffusion paths [Barak (1983)]. Working with duplex ferrite-austenite stainless steels, Chandra and Kuchlmayr (1988) have found that sigma formation is also enhanced by hot working, and that the volume proportion of sigma decreases as the strain rate increases. The prior precipitation of TiC particles are reported by Lewis (1966) to enhance sigma formation.

Generally sigma formation is promoted by secondary phases which act as chromium reservoirs. An interesting relationship between sigma and $M_{23}C_6$ has been reported in the literature. $M_{23}C_6$ carbides have a complex cubic structure which, if the carbon atoms are removed, closely approximates the structure of the tcp sigma phase. Sims and Hagel (1972) have suggested that carbon is depleted through the sequence:

$$MC - M_7C_3 - M_{23}C_6 - \text{Sigma}$$

Coherency between $M_{23}C_6$ and sigma is high, and plates have been seen nucleating on $M_{23}C_6$ particles [Briant and Banerji (1983)]. White and Le May (1970) have postulated that sigma phase formation is in competition with $M_{23}C_6$ since both phases are enriched in chromium. Barcik (1987) reports that the presence of $M_{23}C_6$ accelerates both the nucleation and dissolution of sigma phase.

Results of corrosion studies indicate that sigma is more prone to corrosion than the ferrite in most environments, and no chromium depletion mechanism need be invoked to explain the reduced corrosion resistance in sigmatic alloys [Steigerwald (1977)].

2.2.3 High Temperature Embrittlement

The solubility of C+N in Fe-26Cr has been determined by Pollard (1974) and is shown in Figure 2.3. Clearly carbon levels above about 100 ppm result in super-saturation below 900°C, and quenching from elevated temperatures causes a precipitation-hardening reaction in higher interstitial alloys as a result of the relief of super-saturation. This can lead to the degradation of the toughness, ductility and corrosion resistance of the alloy, and has broadly been defined as 'high temperature embrittlement'.

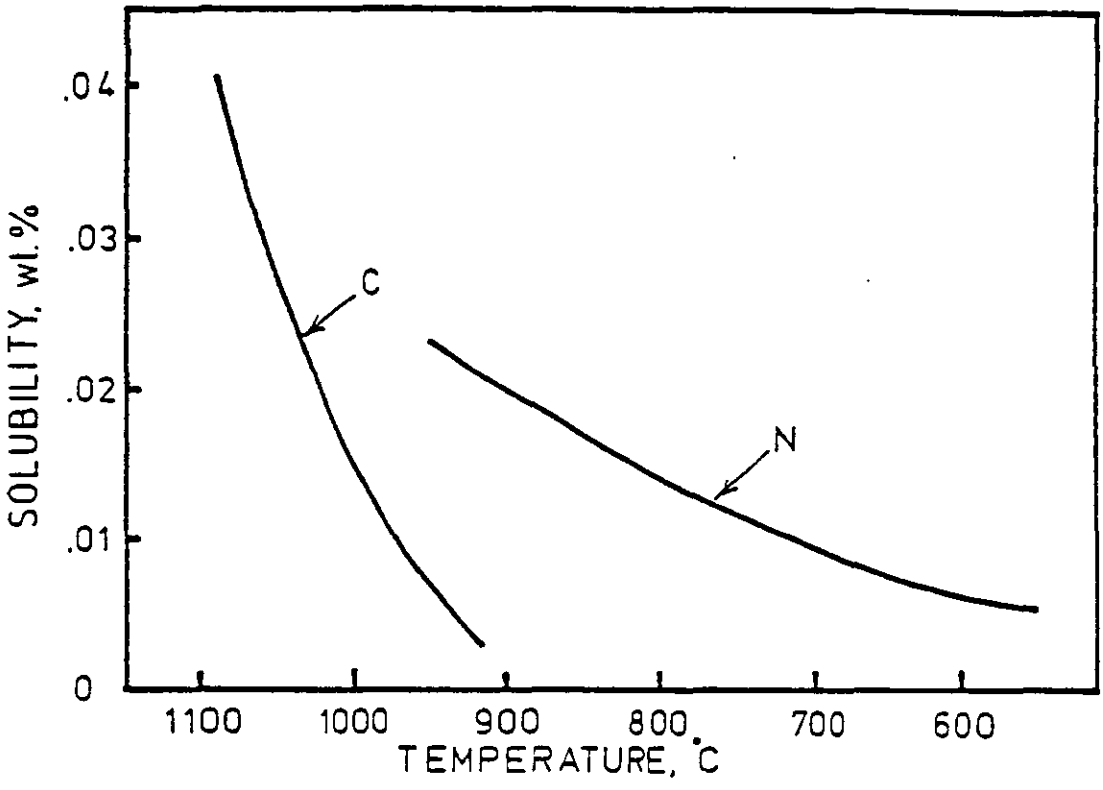

FIGURE 2.3 Solubility of (C+N) in Fe-26Cr [Pollard (1974)]

The mechanism of high temperature embrittlement has been argued from several perspectives. Sensitisation of steels quenched from high temperatures was the subject of research by Demo (1971), who found that high interstitial alloys quenched from 1100°C had decorated dislocations when viewed under the TEM. Demo reasoned that the intragranular precipitation was promoted by the high driving force of supersaturation for rapid precipitation on all high energy surfaces. The rejection of C+N coupled to the simultaneous nucleation of dislocations was suggested as the cause of embrittlement, these factors being absent in alloys which were slow-cooled and which retained their ductility. Reheating to 850°C resulted in precipitate-free dislocations, and it was thought that migration of the C+N to the higher energy grain boundaries had occurred. This has been substantiated by a recent study of Haoquan et al (1987), who link embrittlement in a Type 446 ferritic stainless steel quenched from 1100°C to the formation of intra granular precipitates, and C+N segregation to dislocation cores, both of which act as barriers to slip. Intermediate annealing at 850°C following quenching improved the ductility by

Ostwald ripening of initially large intragranular precipitates, and dissolution of precipitates formed at dislocations.

Pollard (1974), and Plumtree and Gullberg (1974) attributed embrittlement to chromium nitrides and carbides at the grain boundaries. Studying a range of high chromium ferritic steels, Gol'dshteyn et al (1983) in turn concluded that the controlling mechanism was a combination of fine intragranular precipitation and grain boundary films of $M_{23}C_6$-type carbides. The most comprehensive study of the precipitation of excess phases associated with high temperature embrittlement was carried out by Grubb and Wright (1979), on alloys of differing interstitial contents subjected to various annealing practices. Their observations are worth reporting:

(a) Quenching from 1290°C prevented precipitation in low interstitial alloys (C+N = 67ppm) but not in high interstitial alloys (C+N = 540ppm);

(b) Slow cooling rates produced grain-boundary precipitates in the low interstitial alloys;

(c) Subsequent exposure to intermediate temperatures produced a variety of precipitation effects. At 870°C, intragranular and grain-boundary precipitation occurred; at 620°C - 790°C only semi-continuous grain-boundary precipitates were noticed; at 540°C only intragranular plate-like chromium-nitrides were identified in the low interstitial alloys. The high interstitial alloys were found to have both intragranular precipitates and grain-boundary films for all the treatments.

It follows that the ductility is intimately associated with the microstructural development of the precipitates as a function of the cooling rate [Thielsch (1951)]. However, observations by Shaw et al (1988) of Fe-40Cr alloys subjected to different cooling rates from 1050°C have suggested that the ductility may also be related to the formation and retention of dislocations. While rapid quenching is favourable to dislocation generation by condensation of point defects and thermal stresses, more extended cooling periods allow

sufficient time for diffusion and rearrangement processes to remove the dislocations which are required for ductility. (Appendix B1).

2.2.4 Processing Parameters

In addition to the effects of secondary phases on the mechanical properties, it is worth noting that several additional parameters may play a role.

Semchyshen et al (1971), Nichol (1977) and Saito et al (1980) all note improvements in the DBTT by refining the grain size. This is by no means as straightforward an observation as it suggests itself, for the effect of grain boundaries on the fracture process is not clear-cut. Plumtree and Gullberg (1974) observed DBTT variations with grain size that were consistent with a relationship of the form

$$DBTT = D\ln d^{\frac{1}{2}}$$

where d = grain diameter.

On the other hand Abo et al (1977), Deverell (1980) and Kinoshita (1984) all report a negligible effect of grain size. Grubb (1982) demonstrated that grain size had no effect on the room temperature yield strength or DBTT of precipitate-free Fe-26Cr alloys. However, in higher interstitial alloys, grain refinement was reported to be effective in reducing the DBTT by increasing the solubility of nitrogen and suppressing intragranular precipitation. The difficulty in isolating the influence of grain size from other variables which affect the impact behaviour has been put forward as the reason for this conflicting evidence [Deverell (1980)].

The fracture behaviour of high chromium steels is strongly dependent on the stress state. Saito et al (1980) showed that a Fe-30Cr-2Mo alloy displayed excellent ductility under conditions of low triaxial stress, but was brittle under high triaxial loads. Similarly Ohashi et al (1980) found that a reduced plate section was beneficial in lowering the transition temperature.

All the available literature cites an increase in the DBTT of ferritic stainless steels with cold work. For example, Grobner and Steigerwald (1977) reported a DBTT increase of 1-2°C per percent

cold reduction (%CR). This is thought to be the result of work hardening and an increase in the flow stress. The effect of cold work on the sigma formation kinetics has already been mentioned.

There is a well-known tendency for high chromium ferrite to recover rather than to recrystallise following deformation. This results in the production of a recovered and very stable sub-grain structure which causes an increase in strength but does not impede cleavage propagation [Pickering (1972)]. Consequently the yield and tensile strengths depend on the sub-grain size, but the impact properties are more directly related to the macro-grain size.

The recrystallisation behaviour of high chromium ferritic steels was the subject of publications by Sheppard and Richards (1987) and Uematsu and Yamazaki (1987). The predisposition to dynamic recovery rather than recrystallisation gives rise to coarse aligned grains which cause plastic anisotropy. The resultant recrystallised grain size depends on the sub-grain size. In order to refine the ferrite grains, a higher degree of non-uniformity in the substructure is necessary i.e. high rotation angles between deformation bands. Although this may be partially achieved by increasing the total strain, maximum grain refinement cannot be achieved in this way. The sub-structural features are governed primarily by changes in the temperature and stress rate, and grain refinement is most effective at higher strain rates and lower temperatures. Any variations of these parameters in the through-thickness direction cause substructural variations. Recrystallisation following deformation generally results in larger grains at the centre than at the surface due to fewer deformation bands. These deformation bands may be induced by rolling below 1150°C. Rolling below 900°C also increases the number of precipitates which act as stress concentrators for greater deformation, and subsequently as prime nucleation sites for recrystallisation. The second-phase particles also impede grain boundary migration.

Analyses of the texture development in ferritic stainless steel during high temperature processes have been reported by Lewis and Pickering (1982). The crystallographic texture was found to be a

function of the nucleation sites for recrystallisation. Hence pre-existing deformed grain boundary sites produced a texture in which the {100} planes were parallel to the rolling plane. Nucleation at deformation bands produced a texture in which {110} planes were parallel to the rolling plane. Nucleation at second phase particles produced textures in which the {111} planes parallelled the rolling plane, irrespective of the nature of the second phase particles.

2.2.5 Earlier Work on Fe-40Cr Alloys

The nominal Fe-40Cr composition represents the optimum passivation behaviour in reducing acid environments and was selected to maximise the cathodic modification achieved by PGM additions. The passivation of Fe-40Cr-Ru alloys in acidic solutions was studied by Higginson (1987). The alloys were found to be suitable for cathodic modification and the addition of ruthenium was shown to extend the range of passivity in reducing acid environments. The corrosion characteristics of the Fe-40Cr alloys are elaborated in Appendix A.

Developmental work on Fe-40Cr alloys established that, although brittle in the as-cast condition, good mechanical properties could be achieved by thermomechanical processing. Initial studies by De Marsh (1986) noted impact transition temperatures well below ambient temperature in 12mm plate, with C+N $\leq$ 100 ppm. Following rolling in the 950-650°C temperature range, the alloys received a one hour anneal and quench from 1050°C. A summary of the impact transition temperatures and upper shelf energies for alloyed Fe-40Cr is given in Table 2.1.

Alloying with stabilising additions of 0.2% niobium and 0,2% titanium respectively resulted in over-stabilisation of the melt. The addition of 0,05% titanium and 0,1% niobium in near stoichiometric proportion to the (C+N) shifted the DBTT to well below ambient temperature, and raised the upper shelf energy in both cases.

The addition of aluminium to getter the residual oxygen resulted in the greatest toughness. Ductile failure was achieved down to -10°C, with the upper shelf energy exceeding 360 J/cm^2.

TABLE 2.1 DBTT and Upper Shelf Energies for Alloyed Fe-40wt%Cr Determined from Charpy Impact Tests [De Marsh (1986)]

Ingot	Alloy Analysis (Wt.%)	Alloy Addition (Wt.%)	DBTT (°C)	Upper Shelf Energy (J)
A	-	base alloy	50	140
B	0.20 Nb	0.2 Nb	~ 90	-
C	0.07 Ti	0.2 Ti	> 90	-
D	0.12 Al	0.2 Al	- 10	> 360
E	0.19 Ru	0.2 Ru	40	125
F	0.03 Ti + 0.20 Ru	0.1 Ti + 0.2 Ru	0	170
G	2.0 Ni	2.0 Ni	- 25	150
H	< 0.02 Ti	0.05 Ti	- 15	330
I	0.19 Ru + < 0.02 Ti	0.2 Ru + 0.05 Ti	- 15	330
J	0.1 Nb	0.1 Nb	10	200
K	< 0.02 Al + 0.09 Nb	0.2 Al + 0.1 Nb	0	> 360
L	0.98 Ni	1.0 Ni	- 5	185
M	< 0.02 Al + 2.00 Ni	0.2 Al + 2.0 Ni	- 18	360
N	0.17 Ru + 2.02 Ni	0.2 Ru + 2.0 Ni	- 10	180

Nickel was the most effective in reducing the ITT. Alloying with 2% nickel reduced the ITT by over 70°C, while 1% nickel resulted in a favourable shift of some 50°C. The shelf energy in both cases was only marginally influenced by the nickel additions.

The addition of 0,2% ruthenium had a slight beneficial effect on the ITT of the Fe-40Cr alloy, but simultaneous alloying with nickel or titanium significantly improved the ductile-brittle transition.

In a study of rare-earth treated Fe-40Cr melts, Hermanus (1986) showed that good toughness and isotropic properties could be achieved in 12mm plate alloys rolled between 950°-650°C and annealed in the range 950°-1150°C prior to quenching. The addition of up to 0,15% Rare Earth Metals (REM) served to lower the DBTT to below 0°C, but the DBTT deteriorated with larger additions. In all cases the shelf energy displayed a noteworthy increase (Table 2.2)

TABLE 2.2. Impact Toughness as a Function of REM Additions [Hermanus (1986)]

Alloy	wt% REM	DBTT	Transition Temperature Range (°C)	Upper Shelf Energy (J)
V2/1/2	0	-10	20	155
V3/2	0.15	-12	10	210
V2/2/2	0.3	15	30	225

Dynamic fracture toughness tests of Fe-40Cr alloys were carried out by Van Zwieten (1987) in an attempt to quantify the effect of interstitials on the toughness properties. In an experimental programme in which the carbon, nitrogen and oxygen contents were varied independently, oxygen was shown to have a lesser effect on the toughness relative to carbon and nitrogen. Above a certain level of carbon and nitrogen, the toughness became independent of the amount of interstitials present, with carbon and nitrogen having similar effects on the impact toughness of Fe-40Cr with a high (C+N) content.

2.3 ALLOYING OF BCC METALS

The most important aspects of alloying additions in the present study are their effects on the corrosion resistance and on the impact toughness of the base alloy. The optimum alloy composition is achieved by a careful play-off between alloying elements to confer the necessary corrosion resistance while maintaining good ductility. The corrosion alloy-chemistry is dealt with in greater detail in Appendix A. The following discussion is concerned primarily with the effect of alloying elements on the mechanical properties, given the intention to use minor alloying additions to improve the toughness of the Fe-40Cr base alloy. The theory concerned with alloy-softening in so-called binary alloys is outlined in Section 2.3.1. Section 2.3.2 is concerned with substitutional interstitial (s-i) interactions which stabilise or getter residual impurities. Finally, consideration is given to elements conventionally classified as controlled residual elements (CRE), notably sulphur.

2.3.1 Alloy Softening

A vast body of literature documents the attempts to explain the plastic deformation characteristics of alloyed bcc metals. Of particular interest to engineering applications is the solid solution softening effect in bcc metals alloyed with dilute amounts of certain substitutional elements. The solute elements impart strength at ambient temperatures and nominal strain rates, but protect the alloy against cleavage at low temperatures and/or high strain rates. It is well established that solid solution softening is a general phenomenon in bcc metals, and Leslie (1972) describes alloy softening by no less than twenty-one different solutes in alpha-iron. While many authors believe that softening occurs as the result of changes by the alloying element on the distribution of impurity atoms in the lattice, others have invoked an intrinsic model of a modified lattice friction, which determines dislocation mobility. The results of rigorous experimental studies have recently advanced the understanding of the extrinsic or intrinsic nature of softening in ferrite.

The work of Leslie and associates (1972) encompassed the effects of a large range of alloying elements on the properties of iron which had had its impurities gettered. No evidence in support of substitutional-interstitial solute interactions was found. Instead, it was noted that solid solution softening is not confined to strong carbide or nitride formers, but is general for all solutes except those which are also ineffective solid solution strengtheners. A critical concentration of solute produced the maximum softening, and this was generally in the vicinity of 3 at%. The elements Ni, Ru, Rh, Re, Ir and Pt were all found to lower the DBTT of iron, with Pt having the greatest effect. Attempts to explain the toughening in terms of an increased ratio of the bulk modulus K to the shear modulus G bore no fruit. Similarly, toughness showed poor correlation with predictions based on the cohesive energy and electron configuration of the solute elements. Leslie concluded that the toughening was related intrinsically to the enhanced cross-slip of screw dislocations at high strain rates.

Recent findings have lent credence to the intrinsic model of solution softening in bcc models. Kubin and Louchet (1978) have formulated the energetics of dislocations at low temperatures in pure bcc metals. The interactions between mobile screw dislocations and interstitial atoms were described in terms of an intrinsic lattice frictional force which determines the rate of double-kink nucleation on screw dislocation segments. This rate-controlling slip mechanism has been extended to substitutional solutions by the work of authors such as Nagakawa and Meshii (1979), and Chomel and Cottu (1982). In a study of Fe alloyed with Ni, Ti, Ga, Al, Co, and Pt, Chomel and Cottu concluded that the alloy softening is in each case intrinsically controlled by the double kink nucleation mechanism. A similar finding has been reported by Botta, Christian and Taylor (1988) for Nb alloys. In all cases it was noted that solutes which exhibit the greatest hardening intensity at room temperature gave the most softening at low temperatures.

THE ADDITION OF NICKEL

The strengthening and toughening effect of nickel has long been known, but early research showed little agreement on the mechanism whereby this is achieved. The work of Jolley (1968) confirmed an effect of nickel independent of the grain size and grain boundary carbide in improving the impact properties of Fe and Fe-C alloys. Mc Evily (1966) suggested that local distortions of the ferrite lattice by nickel atoms may attract and trap interstitial atoms, thus reducing their action on dislocation drag. Some evidence has been cited by Stoloff (1969) to show a decrease in the magnitude of the dislocation locking in iron with nickel additions. The use of internal friction studies for the direct study of s-i interactions has subsequently been assessed by Hasson and Arsenault (1972). No effect of nickel on nitrogen was found, but it was suggested that carbon interaction may be slightly affected by the removal of random interstitials to Cottrell atmospheres. Saito et al (1988) have noted a reduction of intergranular fracture (IGF) in Fe-P alloys to which nickel was added. IGF is apparently circumvented by lowering the DBTT to below the IGF transition temperature. A reduction in the DBTT and also the shelf energy of Fe-25Cr steels with 3,6% Ni was also reported by Plumtree and Gullberg (1980), while a reduction in the FATT of Fe-29Cr-4Mo steels with a 2% Ni addition was observed by Deverell (1980). In each case the observation was purely qualitative, and no attempt was made to explain the effect of the nickel additions.

More comprehensive studies were performed by Petch (1987), who studied the influence of nickel on the cleavage transition temperature of several ferritic steels. The variation of the lattice friction σ_0 with temperature and nickel content at high strain rates is shown in Figure 2.4. These studies led Petch to conclude that lowering of the DBTT by nickel was due to alloy softening.

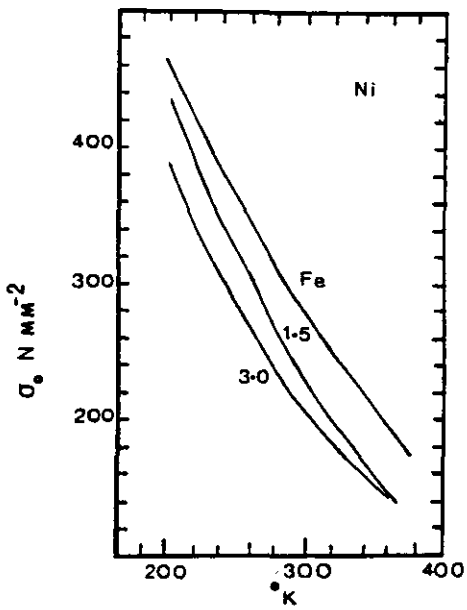

FIGURE 2.4 Temperature dependence of lattice friction at a strain rate of 10^3/s shown as a function of Ni content [Petch (1987)]

The effect of nickel additions of up to 10% on the low temperature deformation behaviour of Fe-26Cr alloys has been elegantly demonstrated by Nakano et al (1978). The response of the ITT and tensile ductility to the nickel content is shown in Figures 2.5(a) and (b). It can be seen that the addition of nickel causes solid solution hardening at ambient temperatures, and solid solution softening at low temperatures. The DBTT is progressively lowered with an increase in the nickel content, but is increased by quenching from a higher annealing temperature. The low temperature deformation is denoted by serrated flow indicative of twinning. A surprising increase in strength and ductility at lower temperature is demonstrated in Figure 2.5(c). Nakano et al account for this anomalous behaviour in terms of suppressed slip and enhanced twinning at lower temperatures. The behaviour of the low nickel alloys is therefore explained as follows: The deformation is governed by slip at room temperature, and the elongation falls off

with temperature. At a critical temperature the deformation becomes twin-controlled. In the absence of the nickel softening effect, the twin-induced stresses are not relieved, and fracture follows.

Nakano et al also noted that nickel promotes the 475°C decomposition reaction, and speculated that this reaction resulted in restricted cross-slip, and deformation predominantly by twinning. Evidence to support this hypothesis has been forthcoming from Magnin and Moret (1982). In a series of elevated temperature deformation studies, the twin density was shown to be roughly proportional to the nickel content over the 475°C interval. Anglada et al (1987) have agreed that the high temperature twinning of Fe-Cr-Mo-Ni alloys is a dynamic effect related to dynamic strain ageing, and have cited the results of Leslie (1982) to show that serrated yielding occurs with all solute species in Fe between about 230°C and 500°C. It seems clear from the above that nickel increases the incidence of twinning in Fe-Cr alloys, but the mechanism whereby this is promoted is not clear. The nature of the interrelationship between the deformation twinning and alloy softening remains a moot point.

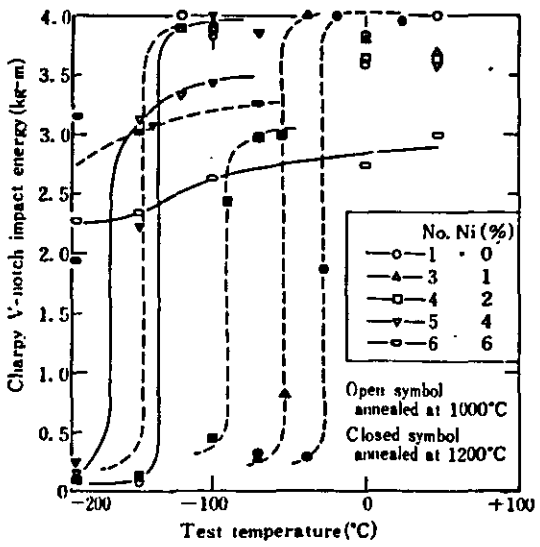

FIGURE 2.5(a) Effect of Ni content on impact transition curves of Fe-26Cr alloys annealed at 1000 and 1200°C [Nakano et al (1978)]

(b)

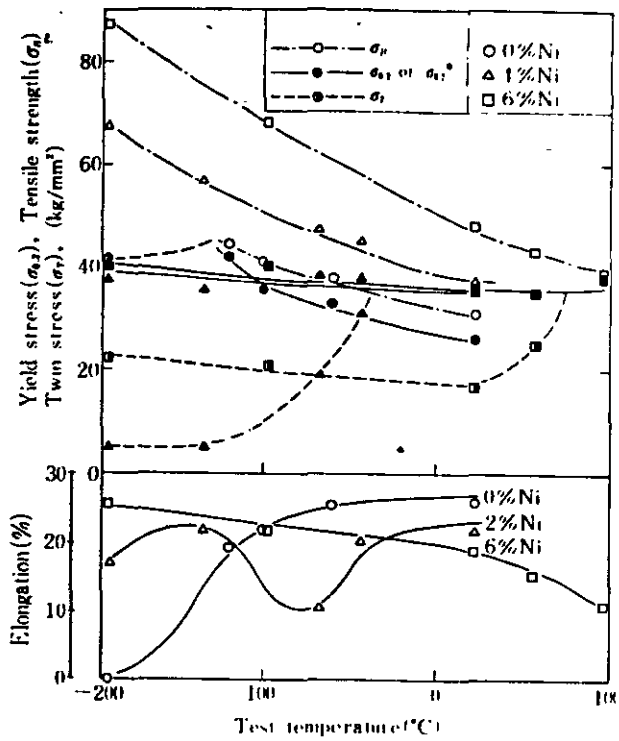

(c)

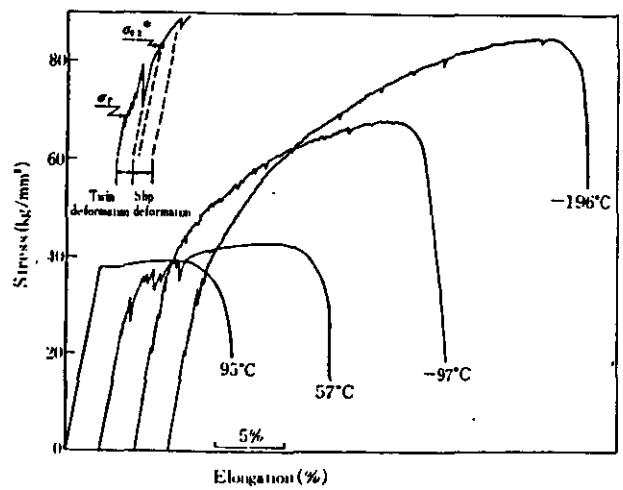

FIGURE 2.5 (b) Variation in tensile properties at low temperature (cont.) of Fe-26Cr alloys as a function of the Ni content

(c) Stress-strain curves of Fe-26Cr-6Ni annealed at 1200°C as a function of temperature [Nakano et al (1978)]

THE RHENIUM DUCTILISING EFFECT

The improved low temperature ductility of tungsten and molybdenum following alloying additions of rhenium was discovered in 1955 by Geach and Hughes, and came to be known as the 'Rhenium Ductilising Effect' or RDE. [Jaffee and Hahn (1963)]. The effect was subsequently shown to extend to the other Group VIA metal chromium. While the RDE results in improved toughness and ductility, it is qualitatively different to the solid solution softening effect discussed above in that it generally involves solute additions of the order of 25-45 at %, which result in large scale changes in the plastic deformation mode. The work of Stephens and Klopp (1968) showed the Cr-Fe and Cr-Ru systems to be rhenium analogues, and the RDE is therefore of particular interest to the Fe-40Cr system under investigation.

The DBTT and phase diagrams for Cr-Fe and Cr-Ru binary alloys are shown in Figure 2.6. Stephens and Klopp noted that the ductile alloys are characterised by high grain growth rates, enhanced tensile ductilities at elevated temperatures and a high degree of deformation twinning, all of which are evidence of a metastable structure in the system. The improved ductility was therefore explained in terms of:

(1) a high solubility and composition near the maximum solubility in chromium which favours a metastable structure with respect to sigma phase precipitation, and

(2) the production of localised stresses which act as dislocation and twin sources by the metastable structure during quenching and deformation at low temperatures.

Klopp (1975) has outlined several common characteristics of solutes promoting the RDE:

(a) The ductilising solutes are from Groups VIIA and VIIIA of the Periodic Table;

(b) The ductilising solutes form intermediate sigma phases with chromium;

(c) The ductilising solutes have relatively high solubilities in chromium;

(d) The maximum ductility occurs in saturated or super-saturated single-phase, solid solution alloys.

screw components of dislocations was attributed to a lower stacking fault energy (SFE). The low SFE hinders the polygonisation processes, resulting in:

- reduced climb and transverse slip of screw components;
- a reduced concentration of point defects;
- a reduced rate of climbing processes.

Even with deformations of up to 40%, the sub-grain misorientation was sufficiently low to indicate only one operative slip plane, and the DBTT increased at the early stages of plastic deformation due to the uniform dislocation distribution. It is interesting to note that for deformations in excess of 50%, the azimuthal sub-grain misorientation rapidly increased, effectively reducing the length of the slip and cleavage planes, with a corresponding drop in the DBTT.

Alloy systems that exhibit the RDE therefore exhibit characteristic deformation modes, which are expected to determine the ductility and fracture behaviour.

2.3.2 Stabilisation of Interstitials

Interstitial solutes are many times more potent as solid solution strengtheners than substitutional solutes, and even trace impurities can exert a dramatic effect on the mechanical properties of the base alloy. Considerable improvements in the ductility can therefore be achieved by relatively minor alloying amounts to render the interstitials innocuous by gettering, although this results in additional precipitate species which may be harmful.

Stabilisation of stainless steels is achieved by the addition of alloying elements which form thermodynamically more stable carbides or nitrides than chromium, and minimises the precipitation of chromium carbonitrides. This has important benefits for the corrosion resistance in that intergranular sensitisation by the precipitation of chromium carbonitrides is prevented. On the other hand, the stabilising elements strengthen the alloy, both in solid solution or in the form of a precipitated dispersoid.

The wide application of titanium and niobium as stabilising additions in austenitic stainless steels before the modern refining

processes for lowering the interstitial contents had been established, has made them the subject of research into similar applications in the ferritic stainless steels. The standard practice is to heat the alloy above 1100°C to ensure complete dissolution of all chromium carbonitrides, followed by cooling to 650-950°C and holding for several hours to allow reaction of the Ti and Nb with the interstitials.

The amount of Ti and Nb necessary for complete stabilisation has been the subject of several investigations. Ratio's of Ti/(C+N) and Nb/(C+N) of at least 6 and 8 respectively have been suggested by Demo (1977), but a point of diminishing returns for Nb occurs at a ratio of about 15 [Semschyshen et al (1971)].

Optimum Ti and Nb additions for fracture toughness have also been identified. An increase in the (C+N) content has been correlated with an increase in the DBTT and a decrease in the shelf energy, mainly as a result of an increase in the second phase, particularly at the grain boundaries [Plumtree and Gullberg (1980)]. A Ti/(C+N) ratio of 25:1 is reported to restore the shelf energy to that of low interstitial-content alloys, although this does not improve the DBTT. The results of De Marsh, discussed in Section 2.2.5, clearly show the unfavourable shift in the DBTT in alloys which are over-stabilised. Over-stabilisation in ferritic stainless steel has also been reported by Pollard (1974), Grubb et al (1980) and Redmond (1980). Pollard attributed this embrittlement to dispersion strengthening by MC-type precipitates. Wood (1980) on the other hand, found that excess Ti is a very potent solid solution strengthening element. The small volume fraction of fine Nb (C,N) precipitates in niobium-treated steels has been shown to increase the flow stress values, but not to have any material effect on the work-hardening rate [Pickering (1971)].

The precipitation characteristics of niobium carbonitrides has received extensive study [see for example Powell et al (1980)]. Dissolution of the carbides is achieved above 1100°C, and since chromium diffuses more rapidly in the ferrite on cooling, $M_{23}C_6$ forms at the grain boundaries first. With prolonged ageing times the $M_{23}C_6$ may be converted to niobium carbonitrides. These phases

precipitate in the range 650-850°C, following C-curve kinetics with an optimum at about 750°C. This presents a problem from the point of view of sigma phase formation, which may be expected over the same temperature range.

The Nb(C,N) precipitates nucleate extensively on dislocations, and random intragranular precipitation only occurs under conditions of high vacancy supersaturation. As a consequence the presence of a dislocation network increases the kinetics of precipitate formation. Intragranular precipitation is on a scale too fine to be resolved by the TEM, and only coarsening, typically over periods of up to 500 hours, reveals the presence of these precipitates.

The literature documents the wide-spread practice of stabilisation in ferritic stainless steels. The need for effective interstitial control will become more apparent during the assessment of the corrosion properties, and to that end stabilisation presents an efficient solution.

2.3.3 Sulphur Control

The occurrence of sulphur in steel melts has been the subject of research over as many years as modern steel making practices have existed. There is general agreement that the shape and distribution of second phase particles have a major effect on the mechanical properties of alloys, and the elongated sulphide stringers, typical of most wrought products, are particularly detrimental to the isotropic impact toughness. The present work seeks to illustrate a novel way of harnessing the unique properties of suphides, namely as dislocation sources. To that end, a brief discourse on the nature of sulphide inclusions is given here.

The effects of non-metallic inclusions on the ductility and toughness of low carbon steels have been quantitatively described by Pickering (1971). In tension the effect of second-phase particles is most clearly observed in the reduction in the total strain to fracture which is brought about by cavitation nucleation by stress concentrations around the particles. However, unlike oxides which have an interfacial strength of the order of

100-200 MPa and readily initiate cavitation by decohesion or fracture, sulphides may exhibit considerable resistance to cavity nucleation. Beremin (1981) has studied the conditions for cavity formation from elongated MnS inclusions in low alloy steel. In the longitudinal direction the sulphide inclusions break before the interface separates, at a critical local stress = 1120 ± 60MPa, whereas in the short transverse direction the interface breaks at a stress of 810 ± 50MPa, in the temperature range 77-373 K. Under conditions of stress, the sulphide particles are therefore expected to withstand considerable deformation of the surrounding matrix before cavitation occurs.

It is accepted that the impact toughness is adversely affected by a large brittle inclusion content. However, there is a clearly defined effect for higher sulphide levels to lower the DBTT, although the ductile shelf energy is reduced (Figure 2.7). The initial increase in the DBTT is attributed to an increased number of sulphides acting as crack initiation sites. With higher sulphur levels the stringers provide obstacles to crack propagation, particularly in the longitudinal directions. Altering the shape of the stringers to a spheroidal morphology virtually doubles the transverse shelf energy while leaving the longitudinal shelf energy essentially unaffected.

The response of the FATT of high chromium ferritic steels to sulphur is marginal. Abo and associates (1977) reported a small increase in the fracture transition temperature of Fe-21Cr-1Mo steels quenched from 1000°C with sulphur additions of up to 370 ppm. Similarly, Redmond (1980) reported a FATT rise from -57° at 40ppm S to -21°C at 310ppm sulphur. Increasing the sulphur levels contributes to more scatter but not to an absolute shift in the transition temperature. Within certain limits, the sulphur therefore appears to be relatively benign with respect to the mechanical properties.

The anisotropic properties of wrought sulphur-bearing steels has led to the well-established practice of inclusion shape-control. Reducing the average aspect rate improves the plane-strain fracture toughness K_{IC} [Tomita (1988)] but the microscopic cleavage fracture stress is independent of sulphur content and/or sulphur

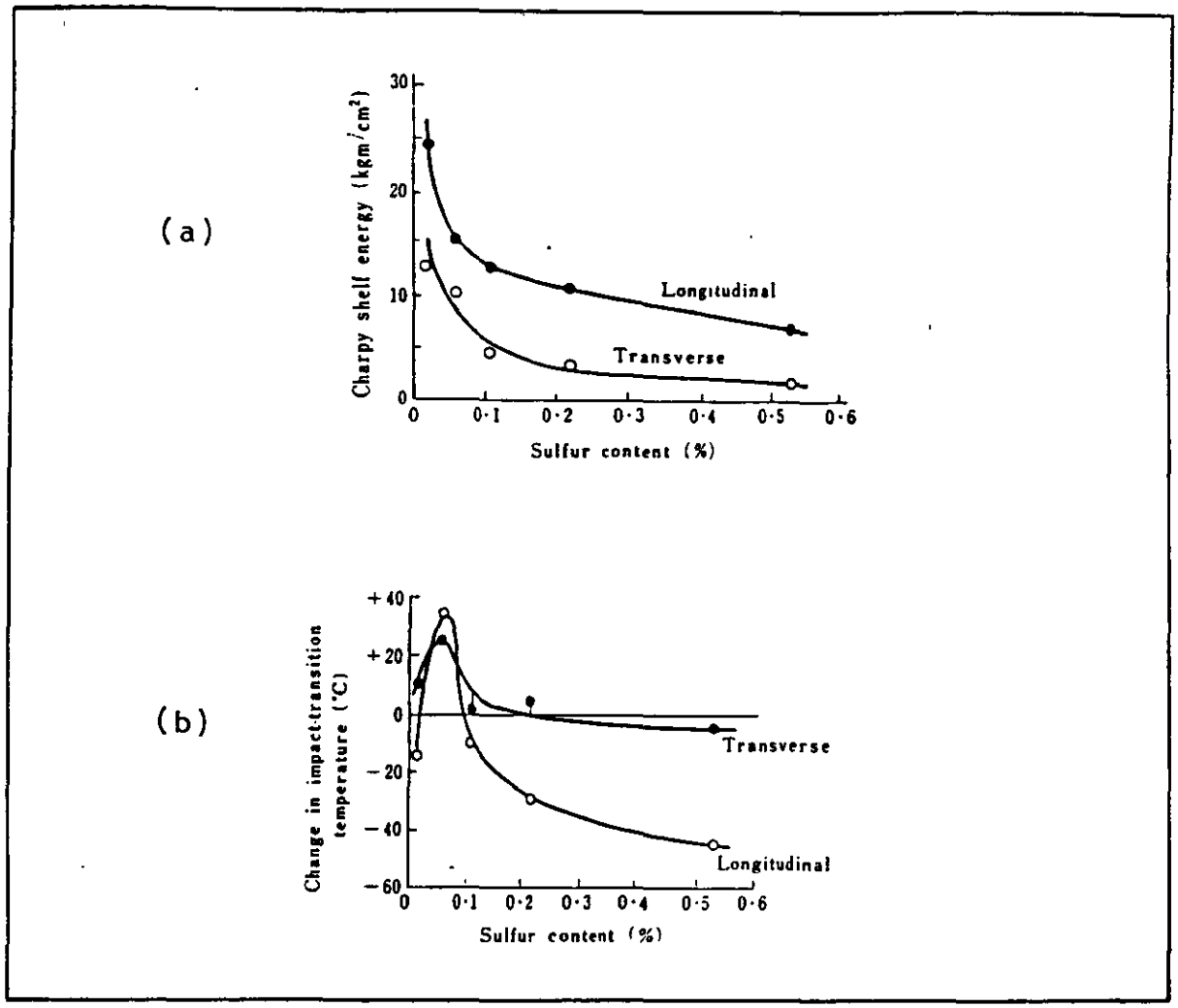

FIGURE 2.7 Effect of sulphur content on (a) Charpy shelf energy, and (b) ITT [Pickering (1971)].

shape control [Halim et al (1987)]. The addition of innoculants such as REM's to the melt changes the sulphide morphology from elongated stringers to rounded globules by the formation of higher melting point sulphides. The reduced plasticity then prevents the sulphides from being extruded to the same extent during deformation.The globular sulphides have lower stress-concentration factors and reduce the rate of void growth, thus improving the transverse ductility. The sulphide inclusion morphology may also be controlled by the cooling rate [Mohla and Beech (1969)], the oxygen content of the melt [Kiessling (1984)], the degree of hot reduction [Tomita (1988)] and the post-deformation heat treatment [Murty et al (1975)].

The distribution of sulphur in the wrought steel has been the focus of several studies. Homogenization of sulphide stringers has been described by Wilson (1977) and McFarland and Cronn (1981). Reheating of the wrought steel at temperatures in the range 815-1205°C results in the recovery of the plastic strain energy of the stringers by initial 'cylinderising', followed by segmentation and spheroidisation of the stringers. Schulz and McMahon (1973) found that heating CrS-type sulphides above 1250°C caused dissolution of the sulphides, followed by re-precipitation on cooling predominantly at grain boundaries. This gave rise to the phenomenon of "over-heating", characterised by failure of a primarily intergranular nature.

Recent work has shown that the segregation of elemental sulphur to grain boundaries in annealed and aged chromium steels is minimal. Given sufficient time during cooling, the sulphur concentration becomes great enough for the sulphur to re-precipitate as chromium-rich sulphides [Briant and Banerji (1981) and Briant (1987)]. In overheated alloys, the intergranular facets are subject to microvoid coalescence originating at the precipitated grain boundary sulphides, giving the grain boundaries a ductile appearance [Baker and Johnson (1973), and Ritchie and Knott (1974)]. Brittle intergranular failure is attributed to the low cohesive strength across the grain boundary caused by the unprecipitated sulphur. There is evidence to show that the grain boundary embrittlement caused by elemental sulphur is countered by a site-competition effect between sulphur and carbon [Suzuki et al (1987)].

2.4 MICROSTRUCTURAL INFLUENCES ON FRACTURE IN BCC METALS

An historical review of the theory that has evolved around the role of microstructure in brittle fracture has recently been given by Hahn (1984). A brief summary of the development provides a useful framework for the interpretation of observations of cleavage fracture.

Crack nucleation as a result of the stress concentration ahead of a blocked dislocation pile-up was proposed by Zener as far back as 1948, and the association of cleavage cracking with plastic deformation has since been ellaborated by Petch (1953), Stroh (1957) and Cottrell (1958). The fracture process was described by Tetelman and McEvily (1967) in terms of a critical stress, which is the stress at which the most difficult of three separate stages is overcome, viz:

(1) Nucleation of a crack by inhomogeneous plastic deformation;
(2) Growth of the crack through the grain;
(3) Transfer of the crack across the first barrier it encounters.

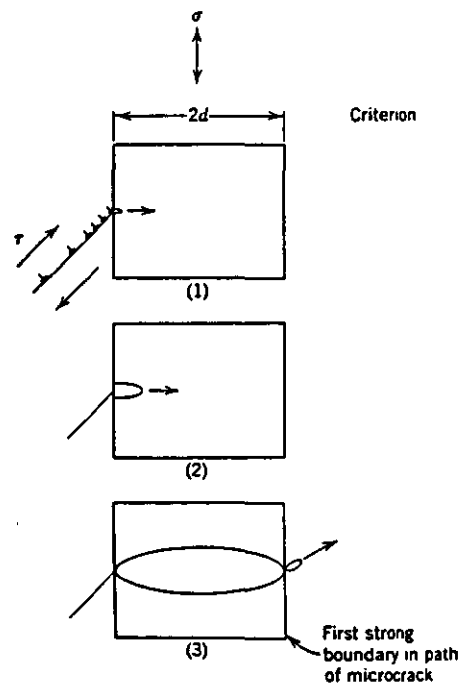

Three Stages Associated with the Development of an Unstable Cleavage Fracture

THE EQUILIBRIUM CARBIDE CRACK

The work of McMahon and Cohen (1965) first related cleavage to cracked carbide particles in the grain or at the boundaries, which led to the adoption of carbide rupture as an essential, intermediate event between the formation of the blocked slip band and propagation of the crack through the ferrite. Later models have therefore equated the nominal fracture stress σ_f for traversing the carbide/ferrite boundary to the sum of the contributions of the carbide film and the pile-up. In a model which examines the static-equilibrium stress at which the crack propagates into the ferrite, Smith (1966) proposed that the fracture stress

$$\sigma_f = \underbrace{\left[\frac{2}{\pi}\frac{(K_{Ia})^2}{c_0}\right]}_{\substack{carbide \\ film}} - \underbrace{\left[\tau_{eff}\left(\frac{d}{c_0}\right)^{0.5} - \frac{4\tau_i}{\pi}\right]^2}_{pile\text{-}up}{}^{0.5} \qquad (2.1)$$

where τ_{eff} = effective shear stress
τ_i = lattice friction stress
d = ferrite grain diameter
c_o = carbide film thickness

The static equilibrium fracture resistance is therefore related to two microstructural parameters, viz the grain size d, which determines the pile-up length, and the carbide thickness C_o. An argument for the refinement of both grain size and carbide thickness to improve the fracture strength was therefore presented. However, as Hahn points out, the necessity of the carbide in the nucleation process was not explained.

DYNAMIC CRACK PROPAGATION

A description of the fracture process by Rice and Thomson (1975) attempted to relate brittle fracture to bond rupture before plastic deformation could accommodate the stresses. For brittle fracture, therefore, the elastic strain energy release rate must exceed the plastic energy dissipated at the crack tip during growth. A stationary crack which is slowly loaded differs from a fast crack in that it allows more time for thermally assisted dislocation generation. Observations that the transition from brittle to tough behaviour in iron crystals probably occurs at temperatures as low -200°C shows the improbability of microcrack nucleation by pile-ups at ferrite boundaries - the crack simply blunts at higher temperatures. On the other hand, since the carbide has a low effective surface energy and is brittle, the nucleation of a crack in the carbide is easy. The fracture of the carbide consequently results in the production of a fast crack which can overcome plasticity at the carbide/ferrite interface.

The notion that cleavage across the carbide/ferrite interface is a dynamic process was taken into account by Curry and Knott (1978) who proposed that the cleavage crack would extend dynamically across the interface if the local tensile stress exceeded the effective particle strength S, given by

$$S = \left[\pi E G_{cf} \; / \; 2(1-\nu^2)\, d_p \right]^{0.5} \qquad (2.2)$$

where G_{cf} is the critical strain energy release rate for dynamic propagation into the ferrite matrix which has been plastically strained, and d_p is the particle size. If d_p is sufficiently small to cause S to be greater than the tensile stress, the crack arrests at the interface [Tsann et al (1987)].

GRAIN SIZE DEPENDENCE

Evidence to suggest that the carbide film thickness C_o, and not the ferrite grain diameter d is the controlling variable was first provided by Curry and Knott. In examining the Smith model, they noted an upper limit to the effective shear stress τ_{eff} due to yield in neighbouring grains. ($\tau_{eff} = d^{\frac{1}{2}}k_y$, where k_y = Hall-Petch parameter). By putting τ_{eff} proportional to $d^{-\frac{1}{2}}$ in Equation (2.1), the grain size dependence is lost.

Curry and Knott also pointed out that the pile-up term in Equation (2.1) is negligible for practical values of C_o and d, and that the apparent grain size dependence is linked to concurrent variation in the carbide film thickness. Furthermore, the brittle fracture stress shows a linear dependence on $C_o^{-0.5}$, but not on $d^{-0.5}$

This does not, however, negate the role of slip in crack nucleation. Cracked carbides have only been identified in the plastic zone of cracked regions, which suggests that significant plastic strain is necessary to create the crack nuclei. This is borne out by a comparison of the theoretical and experimental values of the local tensile stress needed to fracture carbide particles in a ferrite matrix [Argon and Im (1975)]. The fact that the carbide fractures well below its theoretical strength points to assistance by a local stress raiser, such as a defect in the particle, or a pile-up.

The contention between the grain size and the carbide thickness for pre-eminence in the brittle fracture process has been extended to more recent studies. In a study of the impact properties of stainless steel plate, Mintz and Arrowsmith (1980) found that the transition temperature could be lowered by as much as 60°C by refining the grain boundary carbides, independent of the grain size. However, in follow-up studies, it was found that an order of magnitude reduction in the grain size was effective in lowering the ITT by some 160°C, demonstrating a more dominant influence of the grain size [Mintz et al (1982)]. Interestingly enough, it was found that above a critical carbide thickness, no further deterioration in the impact behaviour occurred. This was reasoned to be the result of grain boundaries acting as effective barriers to crack propagation in many instances, with the result that the critical event was the ability to

propagate a grainsize microcrack across the boundary. The upper limit to the carbide thickness is therefore the point at which the energy to crack a carbide and propagate the crack into the ferrite matrix becomes insufficient to propagate the grain-size microcrack across the grain boundary.

Calculations by Petch (1986) assuming a non-equilibrium crack also show a grain size effect independent of the carbide thickness. The cleavage strength σ_c at yield was related to the carbide thickness and the grain size by:

$$\sigma_c = \left[\frac{8\mu\gamma_p}{\pi(1-\nu)c_0} - \frac{k_y^2 d}{8\pi^2 c_0^2}\right]^{0.5} - \frac{k_y d^{0.5}}{2\sqrt{2\pi c_0}} \qquad (2.3)$$

The cleavage strength for fracture at and after yield as predicted by Equation 2.3 is plotted in Figure 2.8 for various carbide thicknesses. The direct proportionality of the fracture stress to $d^{-0.5}$ (OA) shows the theoretical cleavage strength of ferrite unaffected by the carbide. As the carbide coarsens and the grain size is refined, the model predicts a more pronounced influence of the carbide, but shows a considerable effect of grain size nonetheless. Although the model has yet to be tested empirically, it appears to tie together a large number of experimental observations.

Of particular interest in Petch's model is an explanation of the effect of carbide thickness on the shape of the impact transition curve, illustrated in Figure 2.9. The sharp transition observed with fine carbides contrasts with the broad transition band displayed in the case of the coarser carbides. The effect is explained by comparing Figures 2.8(a) and 2.8(b) for a typical value of $k'k_y'$, where k_y is the grain size constant for the yield stress. It is assumed that after yield the availability of freshly introduced dislocation changes the grain size constant k and hence the cleavage strength. In the case of the fine carbide, a specimen which just fails to cleave at yield can sustain a large degree of deformation prior to attaining the new σ_c by work hardening because of the large change in k.

Hence ductile fracture ensues. The coarse carbide material, however, sees only a small change in the cleavage strength. Thus if cleavage is just missed at yield, the new cleavage stress is readily attained by strain hardening, although the amount of strain required gradually increases with temperature, causing the gradual transition.

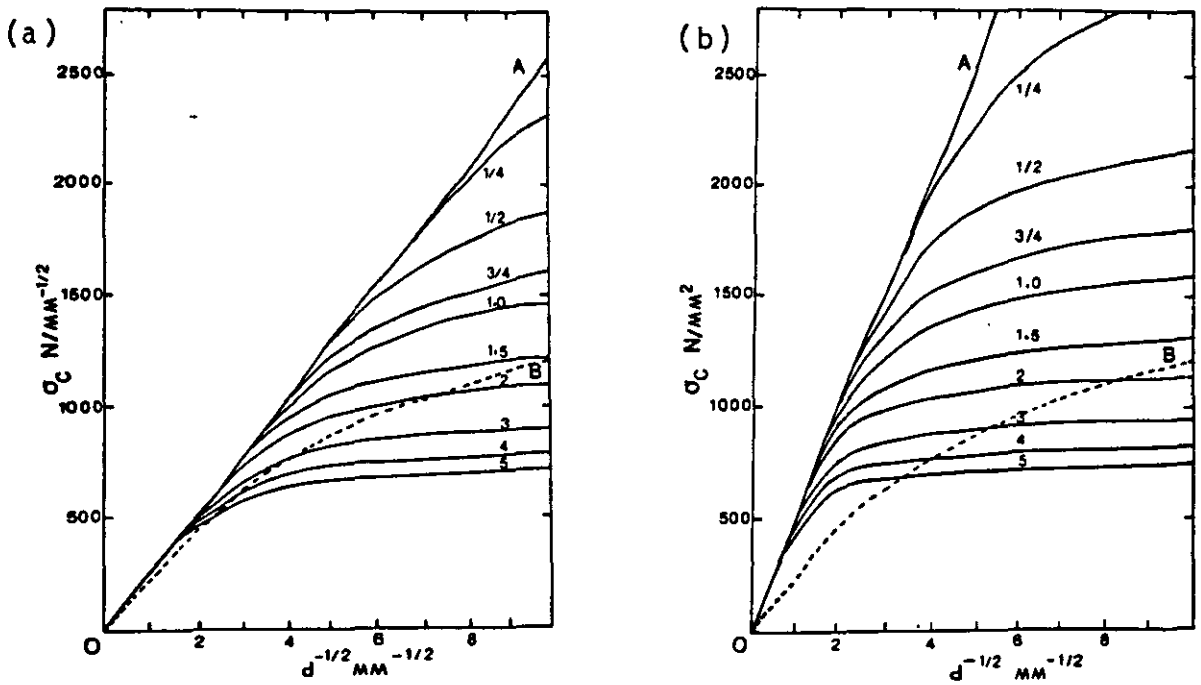

FIGURE 2.8 The cleavage strength for fracture (a) at yield and (b) after yield ($k = \frac{1}{2}k_y$) as a function of carbide thickness and grain size [Petch (1986)]

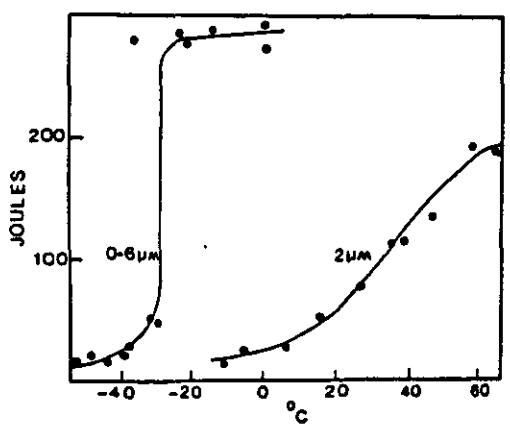

FIGURE 2.9 The change in the shape of the impact transition curve with carbide thickness [Petch (1986)]

CHARACTERISTIC DISTANCE

The cleavage fracture toughness of a material is further characterised by a critical microstructural distance X_0 ahead of the crack tip, postulated by Ritchie et al (1973). Cleavage occurs when the maximum tensile stress ahead of a crack exceeds the cleavage fracture stress over the distance X_0. The distance X_0 bears no straightforward relationship to the ferrite grain size. Curry and Knott (1979) have related X_0 to the statistical occurrence of "eligible" particles, eligibility being a measure of the probability that a given particle is capable of nucleating a crack. To be eligible a particle must:

(a) be associated with a suitable stress raiser, such as a twin or a pile-up;
(b) be suitably oriented to nucleate the crack;
(c) produce a low value of K_a.

Calculations are supposed to be based on the largest eligible particle within the stressed volume. The brittle fracture stress is therefore dependent on microstructural features that change the distribution of eligible particles. It is significant to note that statistical analyses attribute an overwhelming influence on the fracture process to a small fraction of the particle population (some 5 pct, those having the largest radii).

The relative importance of grain size and particle size has also been modelled statistically by Tsann et al (1987). Experiments conducted on low carbon steels in which the grain and particle sizes were varied independently tendered evidence to show that the low temperature toughness is related to the number of active particles generated ahead of a sharp crack. They noted an increase in toughness with increased grain size, which they linked to the reduction in the yield stress. This effectively lowered the stress gradient and decreased the plastic zone and the population of active particles at the crack tip. It was shown experimentally that, whereas for fracture ahead of a sharp crack (with a high, negative stress gradient) the toughness was decreased with a refinement in the particle size distribution, the toughness increased in the case of a rounded notch, which had a shallower, positive stress gradient. The high, negative stress gradient ahead of a sharp crack activated smaller, more numerous particles, and toughness was therefore decreased with a refinement in the particle size distribution.

2.5 MICROFRACTURE vs PLASTIC DEFORMATION

Ductility in a metal is associated with the ability of the metal to deform plastically under the influence of a local or applied stress. The parameters governing the dislocation kinetics and dynamics are therefore bound to determine the fracture response. The advent of the dislocation theory has led to the development of sophisticated models in an attempt to describe the fracture process. Consideration is given in this section to the interaction of mobile dislocations with the crack. The results of recent theoretical and experimental studies on dislocation emission from cracks has been reviewed by a set of papers introduced by Ohr (1986) and will receive only brief treatment here. Although it has been conclusively shown that dislocations can be emitted from a crack tip, the role of these dislocations as compared with dislocations generated at external sources in controlling the DBTT requires ellucidation.

MOBILE DISLOCATION DENSITY

The premise that the dislocation velocity v is related to the strain rate is given by the Orowan equation:

$$\dot{\varepsilon} = \rho_m b v \qquad (2.4)$$

where ρ_m = mobile dislocation density
b = Burger's vector

The dislocation velocity is further understood to be related to the effective shear stress to move the dislocation through the lattice σ_e by an equation of the form:

$$v = \left(\frac{\sigma_e}{\tau_o} \right)^n \qquad (2.5)$$

where τ_o = measure of the lattice friction
n = stress-velocity exponent

Although a large amount of information is available on the velocity of dislocations, the mobile dislocation density is still poorly understood and lacks quantitative characterisation. While a measure of the average slip-line length of mobile dislocations is generally obtained

experimentally from electron microscope observations, Montemayor-Aldrete and co-workers (1986) have proposed a relationship which gives as a function of mechanical parameters from energy conservation principles. Hence the creation rate of mobile dislocation is given by:

$$\dot{\rho}_m = \sigma\dot{\varepsilon} \,/\, (Gb^2) \qquad (2.6)$$

where σ = applied stress
G = shear modulus

Results in creep studies have shown good compatibility of Equation 2.6 with the Orowan equation.

A theory of mobile dislocation density has been evolved by Alden (1987) based on studies in a soft tensile machine. Although quantitative corroboration of the theory is still limited, the model embodies the modern understanding of inelastic deformation behaviour: When a metal is stressed beyond its elastic limit, dislocations are caused to move and multiply at a critical stress σ^*. The origin of these dislocations are unclear, but it is thought they are sourced at surfaces, grain boundaries, and the like. The dislocations travel over a mean free path at a velocity determined by the effective stress relative to the viscous drag, and are progressively trapped at an increasing rate as the velocity and dislocation density increase. The trapped dislocations confer additional strain hardening and reduce the effective stress and dislocation velocity. The total dislocation density ρ_t in single phase alloys is therefore composed of the mobile dislocations ρ_m and the network dislocations ρ_n. The stress is related to the total dislocaton density by the empirical relation

$$\sigma = \sigma^* + \alpha Gb\rho_t^{\frac{1}{2}} \qquad (2.7)$$

where α = numerical coefficient

$$\rho_t = \rho_m + \rho_n$$

Assuming Equation 2.7 to be time-independent, the rate of increase of the mobile dislocation density is given by:

$$\dot{\rho}_m = \frac{2\rho_t^{\frac{1}{2}}}{\alpha G b}\ \dot{\sigma} \qquad (2.8)$$

The concurrent trapping of dislocations gives the net result

$$\dot{\rho}_m = \frac{2\rho_t^{\frac{1}{2}}}{\alpha G b}\ \dot{\sigma} - \frac{\rho_m}{t^*} \qquad (2.9)$$

where t^* = mean dislocation lifetime over the distance r_o at velocity v

The important assumption to note is that the creation rate of mobile dislocations is determined by the rate of increase of external stress only, and any variation in the mobile dislocation density among different materials is caused by the trapping rate. For example, viscous drag on dislocations in stainless steels and Fe-3,5%Si are predicted to be high because of the large concentration of impurity atoms, and the dislocation velocity is consequently slow. The strain rate therefore responds slowly to increases in the applied stress rate.

While the Alden model is useful for conceptualising plastic deformation at nominal stress rates, the validity of the model falls short in certain important respects. In the first instance, the model makes no prediction as to the dislocation dynamics in microstructures containing precipitates or dispersions, either of which may act as sources for dislocations and alter the mean free path. Perhaps more important, dislocation generation is assumed to be an athermal process, dependent only on the rate of stress increase, whereas it is, in fact, linked to the velocity. Finally, the model does not extend to the dislocation dynamics at high stress rates.

A comprehensive analysis of the fracture process by Thomson (1986) provides overwhelming evidence to show that the fracture mode is determined by the interactions of dislocations with the crack. For our purposes it is

important to note that when the local stress or k-field at the crack tip is high enough to sustain cleavage, its magnitude is also of the order required to initiate shear flow in the vicinity of the tip. Thus the fracture event is the outcome of the competition between tensile Mode I fracture and shear flow. The emission of the dislocations relaxes the stress field around the crack tip, either by blunting the crack tip, or by creating a plastic zone that shields the crack tip from the external stress, and this inhibits cleavage propagation. It now seems apparent that mobile dislocations produced by external means may produce the same result.

INFLUENCE OF DISLOCATION DENSITY

Ashby and Embury (1985) have noted several instances of improved toughness in bcc metals by prior plastic working. As an alternative approach to considering the relative ease of bond-breaking and dislocation generation at the crack tip, they propose a simple model involving the dynamics of pre-existing dislocations in the crack-tip field. A crack such as that originating from the fracture of a carbide particle is shown schematically in Figure 2.11. Because of limited dislocation mobility in the bcc metal, the nearest dislocations lie beyond the effective crack tip field, and fail to be "captured". At higher dislocation densities the lattice resistance may be overcome and the crack tip field is sufficient to make the dislocations move and multiply, effectively blunting the crack.

Assuming that the transition temperature T_C is known at a particular value of the mobile dislocation density ρ_m, and velocity V (say T_C^*), the variation of the DBTT with ρ_m may be calculated from

$$\frac{T_c}{T_c^*} = \left[1 + \frac{kT_c}{\Delta F} \ln \left[\frac{V^*}{V} \left[\frac{(b\rho^{\frac{1}{2}})^{\frac{1}{2}} (1 - B(b\rho^{\frac{1}{2}})^{\frac{1}{2}}}{(b\rho^{*\frac{1}{2}})^{\frac{1}{2}} (1 - B(b\rho^{*\frac{1}{2}})^{\frac{1}{2}}}\right]^n\right]\right]^{-1} \qquad (2.10)$$

where ΔF = activation energy for lattice resistance controlled glide

k = Boltzmann constant

n = 40 at room temperature

$$B = \frac{(6\pi)^{\frac{1}{2}} \alpha\mu b^{\frac{1}{2}}}{K_{Ic}} \approx 1$$

Using order of magnitude calculations, the variation of the DBTT with dislocation density is shown in Figure 2.12. The model predicts a reduction in the DBTT up to an optimum dislocation density, whereafter work hardening leads to embrittlement. Ashby and Embury acknowledge two deficiencies in the model i.e.

(1) It assumes that the fields of static and moving cracks are identical. Tsann and colleagues (1987) point out that the plastic zone shrinks as the crack velocity increases. It has also been noted that the ability to cleave may be a dynamic property of cracks in the specific material (Section 2.3);

(2) The dislocations are considered to achieve a velocity equal to the crack velocity. This ignores viscous-drag effects on fast-moving dislocations. Furthermore, it is presumed that the crack is stable against dislocation emission.

Despite the model's shortfalls, it presents for the first time, a practical assessment of the DBTT response to the dislocation density.

Elastic analysis by Lin and Thomson (overview 1986) of cracks and dislocations under general loading displays considerable complexity, but theorems are developed to describe dislocation shielding by symmetrically arranged dislocations. In a refinement of the model suggested by Ashby and Embury, Lin and Thomson (1986) showed that the local k-field at the crack is indeed lowered by the activity of external dislocation sources, and that sufficient dislocations within the crack field lead to a reduced tendency to cleavage. This conclusion was arrived at by considering the triggering of a dislocation source by an approaching crack, shown schematically in 2-D in Figure 2.13. The dislocations are created in pairs, being in shielding and anti-shielding configuration. This destabilises the crack

crack resistance to dislocation emission, and locking of the external dislocations by emitted dislocations results in the primary effect of shielding by the remaining externally generated dislocations. Not only is the crack tip blunted, but the locked dislocations contribute to work-hardening in the wake of the crack. The model of Lin and Thomson provides a more general description of crack blunting and external plasticity. Nevertheless, a quantitative description of the dislocation source density and dislocation velocity in blunting the crack remains lacking.

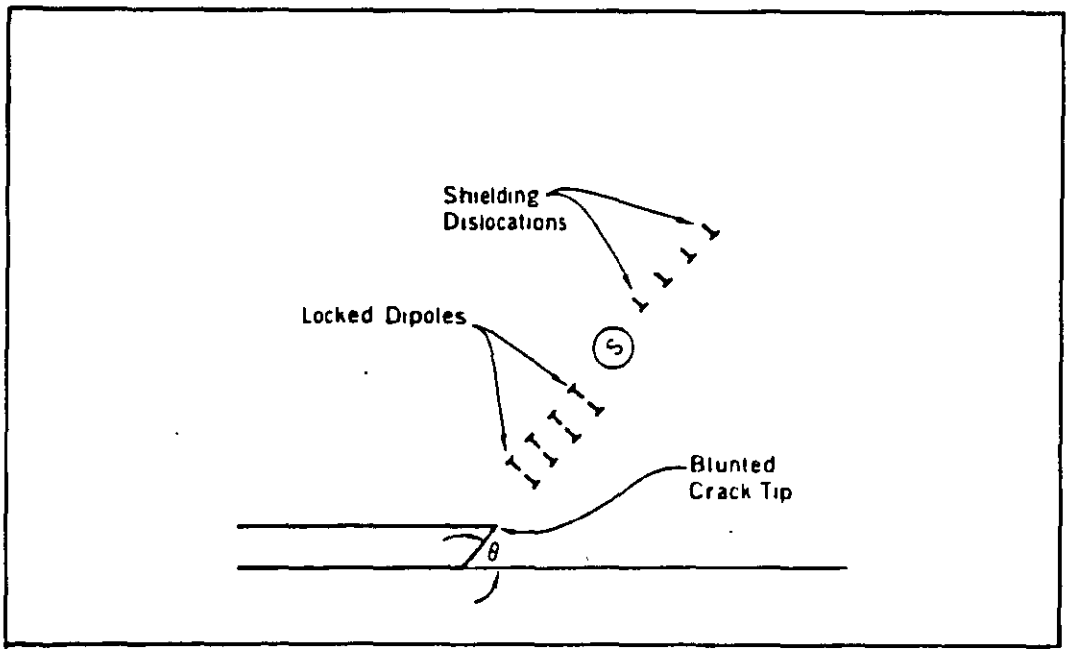

FIGURE 2.13 Induced dislocation emission. When the crack is influenced by the approaching antishielding dislocations, emission results in locked dipoles [Lin & Thomson (1986)]

Jokl et al (1989) have proposed a model which suggests that the real plastic work of brittle fracture is derived, not from a macroscopic plastic zone which shields the crack tip, but from the emission of localised shears within a few atomic spacings of the tip, which accompanies bond breaking, the sum of which may be less than the Burgers vector of a lattice dislocation. The conditions of existing cracks as well as injected cracks due to the cracking of a particle were studied dynamically assuming highly mobile dislocations. Provided that the dislocation velocities exceed 30% of the shear wave speed, the emission of dislocations from a pre-existing crack precludes crack propagation. However, in the case of materials like ferritic steels, the model allows for brittle fracture by rupture of second phase particles. The importance of this theoretical treatment lies in the outgoing premise that the emission and motion of the dislocations are not distinctly different processes, both being governed by the dislocation mobility. Dislocation mobility is high in the crack tip region because of the high stresses available. The model further acts to annex the microstructural observations of brittle fracture with the dislocation theory.

The general concept that the toughness may be improved by externally introduced plasticity has been recognised in several materials, but has received little practical attention. The ductility of chromium has been increased by pressurization or prior-working to introduce dislocations [Ball et al (1968)]. Gross and Knott (1975) subjected mild steel to varying degrees of pre-strain and found that the local tensile stress required to produce cleavage increased with pre-strain, although this increased the transition temperature. An increase in the ITT with pre-strain was also noted by Heslop and Petch (1958) in steels with carbide thicknesses of 2-3 microns.

DEFORMATION TWINNING

Twinning has been found in all bcc transition metals and is as common a form of plastic deformation as slip. [Drachinsky et al (1965)]. The nucleation of deformation twins in metal is generally considered to occur at localised stress concentrations under conditions of restricted slip.

Since brittle fracture and twinning occur under similar conditions i.e. high strain rates, low temperatures and coarse grain sizes, considerable energy has been expended in an attempt to link the occurrence of brittle fracture to mechanical twinning.

The crystallography of twinning has received particularly detailed study [see for example Priestner and Leslie (1964)] and has been fully rationalised. The twin-matrix interface may be represented by a series of partial dislocations which lie on successive {112} planes and have a Burgers vector of the type (a/6) <111> . In addition the effects of a large number of microstructural parameters on the incidence of twinning are known.

In a review of all the experimental evidence, Reid (1981) has categorised the results as follows:

(a) An independent response of twinning and brittle fracture to stress:
Twins are often absent from a brittle fracture, and twinning may occur under tensile loading without brittle fracture, or with brittle fracture only after large plastic strains;

(b) Crack-induced twinning:
The local k-field of the crack may cause twins to form on either side of the crack, but they are not continuous and parallel from one side of the crack to the other, and are not present at the origin of the crack.

(c) Twin-assisted brittle fracture:
When twins are involved in the nucleation of cracks, the cracks are usually found at the intersections of the twin with another microstructural feature such as another twin, a grain boundary, an inclusion or a free surface. In crack propagation, the twin-matrix interface is the preferred propagation path.

A concurrent review by Mahajan (1981) records that accommodation by slip and twinning can occur at a blocked or terminating twin, but microcracking is sometimes observed. Speculation that the twin growth rate determines the resulting stress concentration led Mahajan to suggest that the fracture stress is attained if the twin growth rate exceeds the accommodation process - a factor which has received little or no attention in the literature.

Reid points out that most of the evidence for twin-induced fracture is circumstantial, and conclusive correllation of twinning and brittle fracture in time and space has yet to be presented. Nevertheless, mechanical twinning is an important deformation mechanism in the system under investigation, and room temperature deformation twinning in ferrite stainless steels has been reported in several publications.

The results of Nakano et al have already been discussed (Section 2.2). In a study of Fe-19Cr alloys, Taillard (1982) concluded that the twinning is an intrinsic mode of deformation of high purity alloys. The presence of intermetallic particles were found to facilitate the twinning reaction by increasing the inhomogeneity in the slip character. Grubb and Wright (1979) have related twinning in Fe-26 Cr alloys to a reduced interstitial content and increased solid solution alloying. High temperature embrittlement, associated with restricted dislocation motion, was found to give rise to greater twinning.

Lagneborg (1967) suggested that fracture in 475°C embrittled Fe-30Cr alloys might be twin initiated. Enhanced twinning in 475°C embrittled alloys has also been reported by Nichol (1977), Yasunaka and Kanao (1979) and Park et al (1986). It is interesting to note that twinning can be suppressed by pre-straining, and that the twinning may be restored by ageing [Rosenfield et al (1963)]. The availability of dislocations therefore appears to be beneficial in accommodating the twin-induced stresses by plastic flow.

2.6 INTERFACIAL GENERATION OF DISLOCATIONS

It was recognised at an early stage in the development of the dislocation theory that homogeneous nucleation of dislocation loops by external stresses is negligible, and various heterogeneous mechanisms have subsequently been proposed. Li (1980) has given an overview of the main sources of dislocations, which include Frank-Read sources, condensation of point defects, grain boundary and surface sources , prismatic punching at second-phase particles and dislocations generated by cracks. The latter was discussed in Section 2.5. This section is concerned with the generation of dislocations at second-phase particles as a means of improving the ductility.

PRISMATIC PUNCHING OF DISLOCATIONS

Misfit between a particle and the hole it occupies can stem from causes such as phase changes, pressurization, thermal stresses and elastic and plastic deformation, which give rise to a localised strain energy and stress distribution. The misfit may be relieved in several different ways:

(1) The diffusion of point defects to or from the interface can relieve misfit at incoherent particles;

(2) Similarly, the precipitation of point defects to form dislocation loops in or around the particle can relieve misfit, regardless of the nature of the interface;

(3) Pre-existing dislocations can move by climb and glide to generate the necessary displacement to accommodate the misfit;

(4) Finally, if the kinetics for diffusion and dislocation motion are too slow, the misfit can be relieved by inducing plastic flow at the matrix/particle interface. This relaxation mechanism termed prismatic punching, whereby dislocation loops whose Burgers' vectors lie parallel to the punching directions are generated, was first noted by Mitchell's group (1958). Their results have subsequently been supplemented by direct observation of prismatic punching at small particles in a wide variety of materials.

The current level of development of the initial processes which lead to plastic deformation at particles has been assessed by Martin (1980) and Embury (1985). For small particles and small strains stress relaxation may occur by the formation of rows of primary prismatic dislocation loops pressed against the particle. These loops are predominantly interstitial in character and are of the same order in size as the particle diameter. At larger strains and larger particle sizes, the back stress from the prismatic loops raises the stress at the interface, giving rise to voids in some systems, or loops punched out on secondary systems. At the highest strains large lattice misorientations develop adjacent to the particle.

The critical misfit to begin to generate dislocations at the particle/matrix interface has to satisfy the conditions of stress, strain and energy. Plastic deformation of the matrix may be expected to occur if the operative reduced shear stress at the interface attains the matrix yield point. Similarly, an approximate condition for a particle to initiate a dislocation is that the mismatch between the particle and the matrix is of the order of one Burgers' vector. The energy condition expresses the stability of the dislocation at the interface.

Criteria for dislocation generation at the particle/matrix interface have been formulated in several studies, and the milestones in early work are given here with reference to the overview by Aaronson (1974).

The critical misfit above which prismatic loops are automatically punched as a function of the particle morphology was calculated by Weatherley and Nicholson (1968). It was found that the maximum shear stress is a function of the dilatation of the particle, and does not depend on the particle dimension beyond a critical percentage dilatation. From dislocation stability considerations Brown et al (1968) in turn gave the critical radius for an initially coherent spheroid to begin to generate dislocations as

$$r = \frac{b}{8\pi\varepsilon(1-\nu)}\left[\ln\frac{8r}{b} - 1 + \frac{3-2\nu}{4(1-\nu)}\right] \qquad (2.11)$$

where ν = Poisson's ratio
ε = particle strain parameter

Direct measurements of the minimum particle radius by Ashby et al (1969) gave values which fell between those predicted by Brown and Weatherley, which led Brown and Woolhouse (1970) to modify their treatment to consider additional criteria, including:

(a) The critical radius for prismatic loop punching in the absence of climb;
(b) The critical radius for coherency loss by plastic deformation;
(c) The critical misfit above which a dislocation is always formed at any particle radius.

The energy changes at the particle/matrix interface were analysed by Johnson and Ashby (1970) for incoherent particles using several simplifying assumptions. An energy barrier E must be overcome in order to nucleate a loop. This barrier decreases as the misfit increases, and an upper bound to the critical misfit is reached when E can be overcome by thermal fluctuations alone. A lower bound is obtained by assuming that E has been overcome, for example by stress concentrations, matrix dislocations or external stresses, and that a loop lowers the overall energy of the system. It was found by experiment that while coherent misfitting particles only generate dislocations when the upper bound is reached, dislocation generation at incoherent particles occurs at misfits close to the predicted lower bound.

The stress distribution at the matrix/particle interface has been modelled by various authors. The measurements of Weatherley and Ashby et al showed that the local stress is of order G/10 for a coherent particle, but of order G/100 for incoherent particles, depending on size. Furthermore, comparison with experimental observations showed that the calculated value of the maximum induced shear stress was below that required for nucleation because of particle irregularities which supply additional stress concentrations. Lee and Johnson (1978) re-analysed the elastic strain energy of an incoherent precipitate as a function of the ellipsoidal aspect ratio B. The strain energy was found to tend to zero when $B \to 0$ (disk) while reaching its maximum value when $B=1$ (sphere). Thus a number of descriptions of the formation of misfit dislocations have been accounted for.

TESSELATED (THERMAL) STRESSES

Structure-sensitive stresses derived from differential matrix/particle thermal expansion coefficients have come to be known as tessellated stresses. Brooksbank and Andrews (1972) have made estimates of the residual stress distributions surrounding inclusions in steels following thermal changes. They define a "strain potential of tessellation" which governs the stress level, given by:

$$\Phi \{(\alpha_2 - \alpha_1)\} \Delta T$$

where α_1 = inclusion thermal expansion coefficient
α_2 = matrix thermal expansion coefficient
Φ = function of the elastic moduli, and inclusion shape, size and distribution

The stresses at any point around a spherical inclusion may be calculated from the equations in Table 2.3(a). Detailed derivations are given by Brooksbank and Andrews and will not be reproduced here. The equations were arrived at from the following simplifying assumptions:

(a) The matrix and inclusions are elastically homogeneous and isotropic;
(b) The system cools from a stress-free state at some high temperature during heat treatment e.g. quenching;
(c) The inclusions are associated with an elastic matrix shell of influence.

This analysis has been extended by Dryden et al (1987) to include spheroids exhibiting transverse isotropy.

2.3(a) Inclusion (elastic conditions)

Type of stress (direction, etc.)	Inclusion (material 1) $(0 \leq R \leq R_1)$	Matrix (material 2) $(R_1 \leq R \leq R_2)$
Radial	$(\sigma_R)_1 = p$ (constant) . (1a)	$(\sigma_R)_2 = \frac{p}{(1-d^3)} \cdot \left[\frac{R_1^3}{R^3} - d^3\right]$. (4a)
Circumferential (or tangential)	$(\sigma_C) = p$ ..... (2a)	$(\sigma_C)_2 = \frac{-p}{(1-d^3)} \cdot \left[\frac{1}{2}\frac{R_1^3}{R^3} + d^3\right]$ (5a)
Reduced shear $(= \lvert\sigma_c - \sigma_R\rvert_.)$	$F_1 = 0$ ..... (3a)	$F_2 = \frac{3}{2} \cdot \frac{\lvert p \rvert}{(1-d^3)} \cdot \frac{R_1^3}{R^3}$ .....(6a)

where $p = \left\{\frac{(\alpha_2 - \alpha_1).T}{\frac{1}{2}(1+\nu_2) + (1-2\nu_2)d^3} + \frac{(1-2\nu_1)}{E_1}\right\}$ ..... (7a)

The maximum stresses in the matrix occur at the interface, so that σ_R', σ_C' and $(F_2)_{max.}$ are obtained from $(\sigma_R)_2$, $(\sigma_C)_2$ and F_2 respectively at $R = R_1$

- α = mean linear coefficient of thermal expansion over the given temperature range
- E = Young's modulus
- ν = Poisson's ratio
- T = temperature change: increase is positive
- R = distance from centre of inclusion: spherical case; distance from axis of inclusion: cylindrical case
- R_1 = radius of inclusion
- R_2 = outer radius of matrix shell associated with the inclusion
- $\frac{R_1}{R_2} = d$, and the volume fractions of inclusions for the spherical and cylindrical cases are d^3 and d^2 respectively
- σ = principal stress: positive tensile, negative compressive
- p = constant pressure throughout the spherical inclusion = radial and circumferential stresses in the cylindrical inclusion
- g = axial stress over cross-section of material for cylindrical case = σ_3
- σ_R' = radial stress at matrix/inclusion interface, $R = R_1$, in the matrix
- σ_c' = circumferential stress at matrix/inclusion interface, $R = R_1$, in the matrix
- F = reduced shear stress = 2 × max. shear stress

SUBSCRIPTS
- 1 refers to the inclusion
- 2 refers to the matrix
- c refers to circumferential direction
- R refers to radial direction

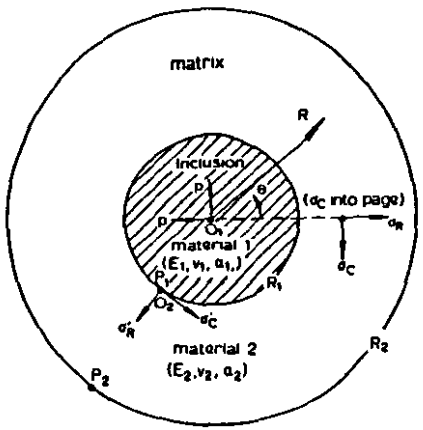

2.3(b) Stresses around a spherical inclusion in elastic-plastic matrix

Type of stress	Inclusion (1) $(0 \leq R \leq R_1)$	Plastic zone (matrix) (2y) $(R_1 \leq R \leq R')$	Plastic zone (matrix) (2e) $(R' \leq R \leq R_2)$
Radial	$(\sigma_R)_1 = p$ (constant) ..... (1d)	$(\sigma_R)_{2y} = -2Y_2\left\{\ln\frac{R'}{R} + \frac{1}{3}(1-h^3)\right\}$ .... (4d)	$(\sigma_R)_{2e} = -\frac{2}{3}Y_2\left\{\left(\frac{R'}{R}\right)^3 - h^3\right\}$ ..... (7d)
Circumferential	$(\sigma_C)_1 = p$ (constant) ..... (2d)	$(\sigma_C)_{2y} = Y_2 - 2Y_2\left\{\ln\frac{R'}{R} + \frac{1}{3}(1-h^3)\right\}$ .. (5d)	$(\sigma_C)_{2e} = +\frac{2}{3}Y_2\left\{\frac{1}{2}\left(\frac{R'}{R}\right)^3 + h^3\right\}$ ..... (8d)
Reduced shear	$F_1 = 0$ ..... (3d)	$(F_2)_{2y} = Y_2$ (by definition) ..... (6d)	$(F_2)_e = Y_2\left(\frac{R'}{R}\right)^3$ ..... (9d)

where $p = -2Y_2\left\{\ln\frac{R'}{R_1} + \frac{1}{3}(1-h^3)\right\}$ ..... (10d) and R' and Y_2 are related by:

$$\left(\frac{1-2\nu_2}{E_2} - \frac{1-2\nu_1}{E_1}\right) \cdot \left[3\ln\frac{R'}{R_1} + (1-h^3)\right] = \frac{3}{2}\left[(\alpha_2 - \alpha_1)\frac{T}{Y_2} + \left(\frac{1-\nu_2}{E_2}\right) \cdot \left(\frac{R'}{R_1}\right)^3\right] \quad \text{..... (11d)}$$

stresses at the boundaries (q_R, q_c, p', t_c, s_c, n_R, n_c) are obtained by substituting the appropriate value of R into the above equations

- p = hydrostatic pressure in the inclusion
- q = stress at inclusion/matrix interface, $R = R_1$, in the yielded zone of the matrix
- s = stress at elastic–plastic boundary in the yielded region of the matrix: $R = R'$
- t = stress at elastic–plastic boundary in the elastic region of the matrix: $R = R'$
- p' = radial stress across elastic–plastic boundary = $s_R = t_R$
- n = stress at outer radius of matrix sphere of influence: $R = R_2$; n_R = zero and $n_C \to$ zero for R_2 large
- Y_2 = yield stress of matrix
- R' = outer radius of the plastic zone of the matrix
- $\frac{R'}{R_2} = h$
- ϵ = strain

SUBSCRIPTS
- e refers to the elastic zone of the matrix
- y refers to the yielded, or plastic, zone of the matrix

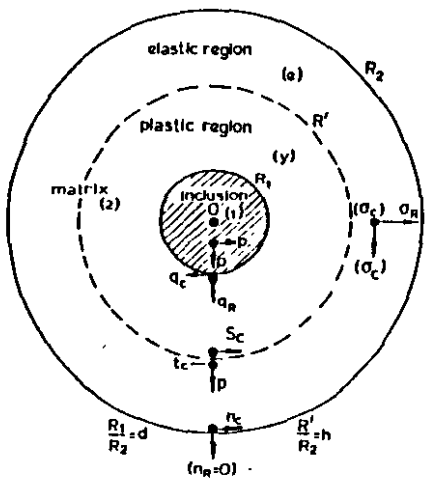

Analysis of Brooksbank & Andrews (1972)

The Brooksbank-Andrews model was later modified to take account of the residual stresses following matrix yielding adjacent to the particle. This necessitated the incorporation of an elastic-plastic boundary [Table 2.3(b)].

Brooksbank and Andrews distinguish between inclusions which have a "stress-raising" potential, and those which have a "void-forming" potential, and have categorised the relative expansion co-efficients of a variety of inclusions in Cr-C steels accordingly. (See Figure 2.14). The results of Stuart and Ridley (1970) for carbides have been included for the sake of completion. On the basis of the Brooksbank - Andrews analysis, residual micro-stresses are set up at inclusions where $\alpha_1 < \alpha_2$. However, they suggest that inclusions, and in particular sulphides, which have $\alpha_1 > \alpha_2$ do not give rise to stresses but form microvoids at the interface. They cite as evidence examples of improved fatigue properties, reduced hydrogen-cracking and a lower incidence of HAZ cracking in steels where the sulphur levels have been raised, effectively increasing the number of microvoids which act as hydrogen traps. Furthermore, they point out that etch-pitting studies of elongated MnS inclusions show no dislocation activity following quenching. This evidence appears to be circumstantial. The aspect ratio of the elongated sulphides would tend to minimise the strain-energy associated with tessellated stresses as discussed. Moreover, the beneficial influence of the sulphur on the mechanical properties may be interpreted microstructurally without invoking the influence of voids. The useful effect of sulphide inclusions on fatigue properties by crack blunting have been noted, inter alia, by Kiessling (1978) and Barbangelo (1985). Kiessling reports a high index of deformability in sulphides, which prevents crack formation at the interface and may neutralize the detrimental effects of non-deformable inclusions by forming a protective sulphide sheath around them. From experimental observation Kiessling concludes that "the binding forces at the interface between the (sulphide) inclusions and the steel are never broken and there is no tendency for cavity formation. The conditions given by Berenim (see Section 2.2.3) suggest that substantial stresses can indeed be withstood by the sulphide interface, and these would give rise to tensile micro-stresses on cooling.

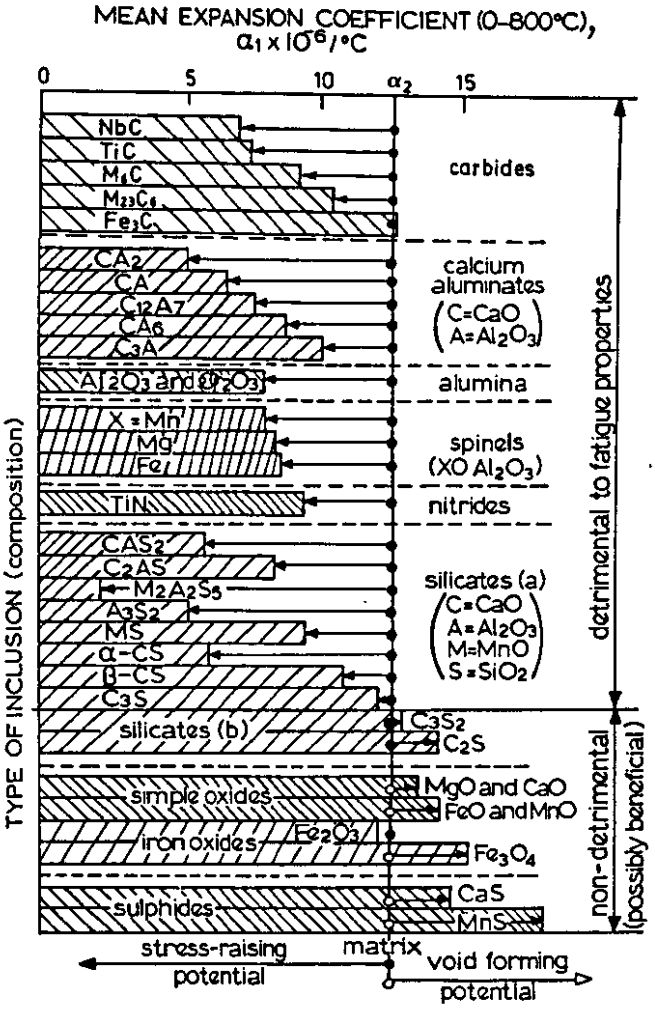

FIGURE 2.14 Stress-raising properties of inclusions in 1% C-Cr steel [Brooksbank & Andrews (1972) and Stuart & Ridley (1970)]

The nature of the primary prismatic loops may be illustrated by reference to an elastic analogue (Figure 2.15). For example, Ball and Bullen (1970) have described how elastically 'soft' inclusions can give rise to prismatic loops of the **vacancy** type by differential elastic contraction during compression. This is equivalent to thermal stresses at the interface where $\alpha_1 > \alpha_2$. On the other hand, inclusions with $\alpha_1 < \alpha_2$ may be expected to generate dislocations of an **interstitial** nature.

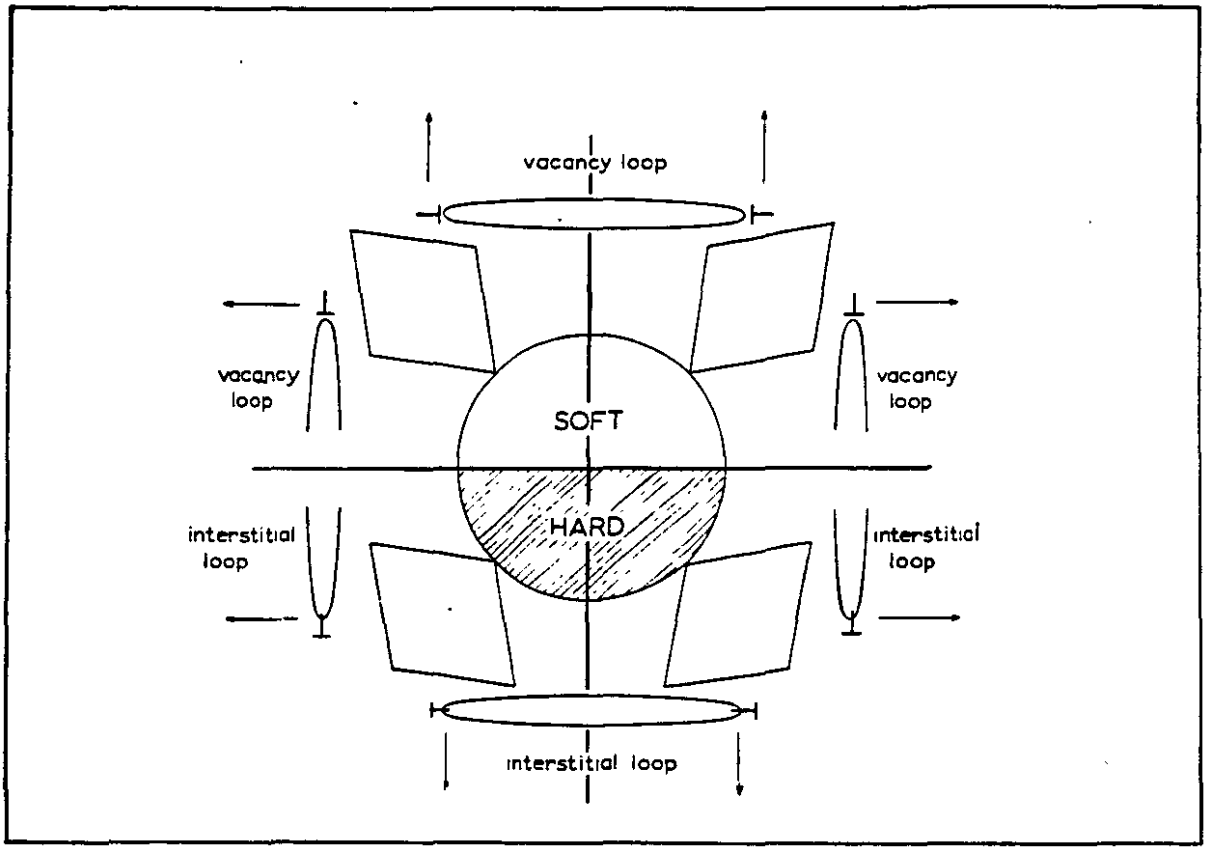

FIGURE 2.15 Schematic representation of the shear strains and dislocations generated near elastically "hard" and "soft" particles [Ball & Bullen (1970)]

2.7 CONCLUSIONS

It is well established that the toughness of ferritic stainless steel hinges on the interstitial content and form, and that the interstitials often have an overriding effect on other microstructural parameters. The mechanism whereby the interstitials and their precipitates degrade the ductility is less clearcut. The case for embrittlement by both inter- and intragranular precipitation of carbonitrides has been argued, but the evidence to link embrittlement to either or both of these variables remains largely circumstantial. Apparent conflict in the published literature regarding embrittlement may be attributed to at least three conditions which are not fully stipulated. In the first case, the separate contributions of the C and N and their respective precipitates to the overall ductility is an open question. Attempts to isolate their independent roles have been hampered by the low interstitial levels which make microstructural observation difficult. Furthermore, the relative proportions of C and N vary from one study to another. Secondly, there is a tendency to disregard the effect of strain rates when discussing ductility. It goes without saying that an alloy which satisfies the conditions for ductility in a tensile test does not necessarily qualify at higher strain rates, such as those present under impact conditions. Finally, there is a wide divergence in the annealing practices, which may, as has been seen, result in widely divergent microstructures with important implications for the mechanical properties.

It is also evident from the literature that strict control of the fabrication parameters is necessary to ensure reproducibility. Controlled rolling provides a viable method of governing the mechanical properties, these being dependent on the grain and subgrain structure, secondary phases, texture and geometry.

The results of the initial tests conducted on Fe-40Cr alloys make it clear that good impact toughness can be achieved by controlling the alloy chemistry. The addition of ductilisers such as nickel, and a melting practice which utilises additives for deoxidation, stabilisation and inclusion control in the melt are all effective in improving the conditions for ductile failure. Stabilisation of the residual interstitials holds advantages for both the corrosion and the mechanical properties, although the optimum stoichiometry has to be established by experiment.

The Fe-40Cr system on its own is expected to exhibit behaviour analagous to the Rhenium Ductilising Effect. Although the precise mechanism of ductilisation is not known, it is related to the propensity of the dislocations for cross-slip, which is central to the plastic and fracture behaviour of the alloys.

The phenomenon of solid solution softening by small additions of substitutional elements to the ferrite matrix is an intrinsic effect, probably the result of an enhanced dislocation mechanism which effectively reduces the lattice friction of the base alloy. The beneficial action of nickel in this regard is well established and holds considerable potential for improving the impact toughness of the Fe-40Cr alloys.

Provided that the state of the sulphur is controlled, higher sulphur levels appear to be tolerable, and hold several advantages from the point of view of the ductility and impact toughness.

The current understanding of brittle fracture in b.c.c. metals holds that the fracture process is either nucleation or growth controlled. Since carbide particles have a low effective surface energy, the nucleation of a crack in the carbide is easy. Cleavage is transferred across the carbide/ferrite interface by a dynamic process which prevents crack blunting. If fast-crack nucleation is the most difficult step, the crack once nucleated, automatically propagates, and is said to be nucleation controlled.

The relative size and occurrence of the particles with respect to the grain size determine the dominant microstructural parameter. It has been shown that the refinement of either the particle size or the grain size does not necessarily augur improved cleavage fracture resistance, although a reduction on the particle volume fraction favours improved toughness.

The prevalence of mechanical twinning in the ferritic stainless steels has not been unambiguously linked to brittle fracture initiation, and the contribution of twinning to the plastic deformation process is unclear.

The interaction of dislocations with the crack tip increases the energy of fracture, and, provided that the intrinsic dislocation mobility is sufficiently high, blunting of the crack is effected. In order to satisfy

the condition for the product of the mobile dislocation density and the average dislocation velocity to equal the strain rate, the odds for a ductile fracture response may be improved by increasing the mobile dislocation density.

The introduction of dislocations by second phase particles presents a way of increasing the mobile dislocation density. The occurrence of prismatic dislocations at second phase particles has been described by a large number of researchers and methods exist for calculating the residual stress distributions caused by differential contraction at the matrix/particle interface. Dislocation generation due to thermal stresses is particularly advantageous, especially in cast alloys where mechanical working of the alloy is precluded. The high thermal expansion coefficient of sulphides and the nature of the microstresses at the sulphide interface point to sulphide particles as being particularly effective in this regard. Apart from the role of inclusions in dislocation generation, there is evidence to suggest that they may be effective in dispersion toughening. A basis for the examination of the effect of a dispersoid on the fracture toughness has therefore been presented.

There remains the problem of quantitative prediction of brittle crack behaviour in practical terms, and a need for a coherent model of brittle cleavage relating the microstructural and mechanical parameters.

CHAPTER 3

EXPERIMENTAL TECHNIQUES

3.1 INTRODUCTION

This chapter describes the experimental procedures followed in the study of the mechanical and microstructural properties of the Fe-40Cr alloys. Use was made of the facilities of the Physical Metallurgy Division of MINTEK (South Africa), and the Department of Materials Engineering, University of Cape Town. The primary processing procedures draw on the practices established by Wolff (1985), De Marsh (1986) and Hermanus (1986), and are outlined here.

3.2 ALLOY PREPARATION

All the experimental alloys were made by vacuum induction melting (VIM) using a Leybold-Heraeus medium frequency facility. Commercial electrolytic iron and chromium were used to make up the base charge, with compositions as given in Table 3.1. The melting practice is summarised in Table 3.2.

TABLE 3.1: Analysis of Electrolytic Charge Fe and Cr

ELEMENT	IRON	CHROMIUM
C	0,003	0,05
N	0,003	0,02
O	0,050	0,05
Al	0,003	0,015
Si	0,005	0,04
Ni	0,007	
Cu	0,001	
P	0,003	
S	0,003	0,01
Sn	0,006	
Fe	Balance	0,35
Cr	0,002	99,5

TABLE 3.2: Melting Practice

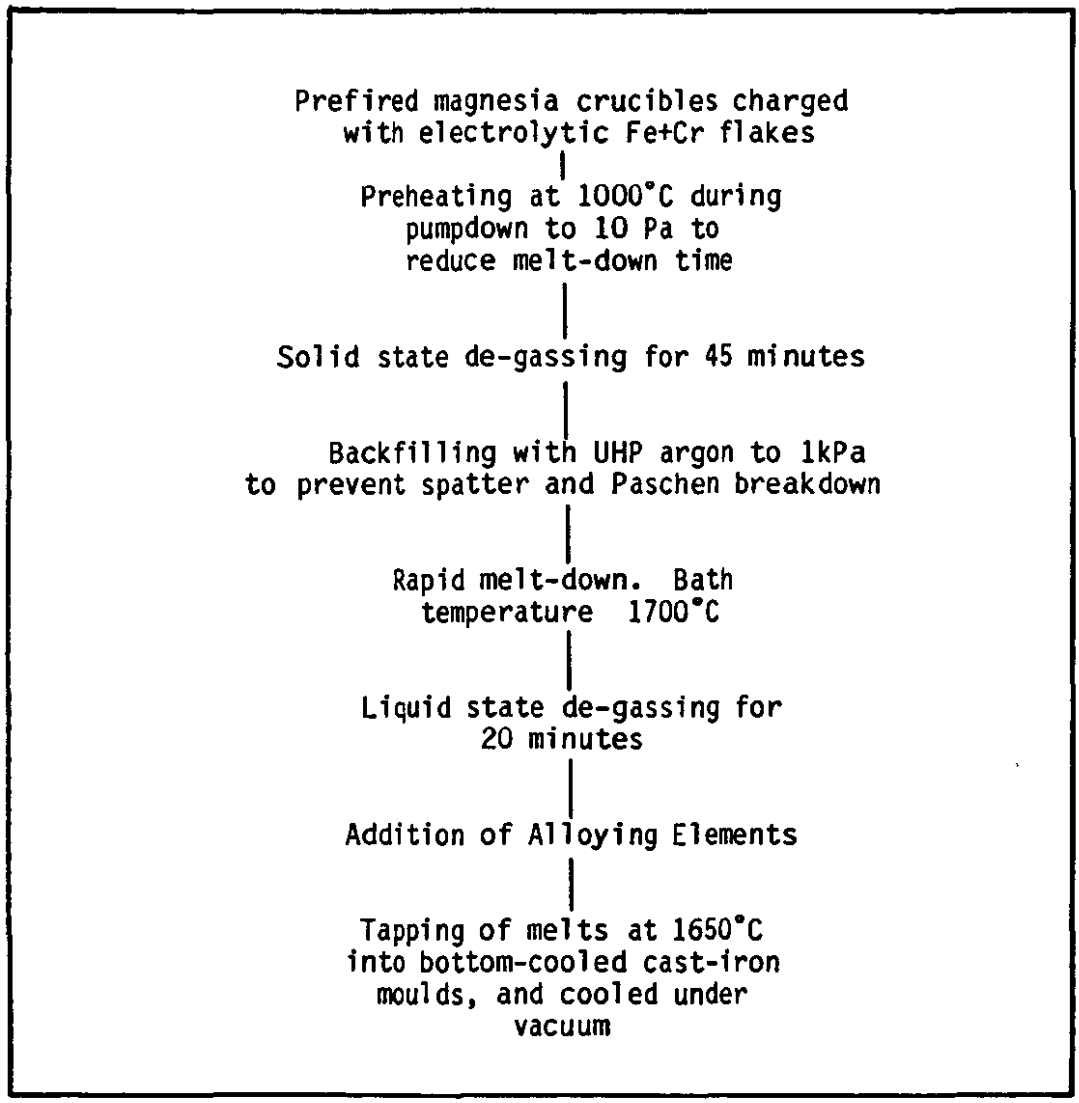

The alloying additions were introduced into the melt in ascending order of reactivity with the gaseous impurities. The nickel and ruthenium were charged with the iron and chromium flakes. The aluminium, niobium and sulphur were added to the melt immediately prior to tapping. Carbon was added to the melt in the form of electrolytic graphite, while nitrogen was charged in the form of high purity nitrided ferrochrome.

The capacity of the furnace allowed a maximum charge of 3-4kg, and cropping losses amounted to +/- 30% of the ingot. The limited scale of the melting practice had serious implications for the testing programme. It was

difficult to reduce the oxygen levels without compromising the carbon levels in the absence of more active refining processes such as argon bubbling, or melting under reducing atmospheres. Oxygen levels therefore tended to be high, although these could be expected to drop in the case of larger melts. Furthermore, the macroscopic grain structure and segregation profile of the ingots were of the order of the specimen dimensions in scale, and this inherently contributed to some degree of scatter in the results. It should be appreciated that the ingot size also limited the number of test specimens which could be derived from a single melt. In the base alloy, compositional variations between different melts were taken to be minimal, although slight changes in the interstitial levels couldsignificantly affect the DBTT.

3.3 CHEMICAL ANALYSIS

Analysis of the alloys was performed by wet chemistry. A summary of the compositions is given in Table 3.3.

3.4 FABRICATION

The ingots were rolled from an initial 50mm thickness to plates ranging from 4-12mm in section using a 50 ton, two-high reversing mill. Following earlier work to establish an optimum fabrication route, a standard rolling schedule was set up, and this is outlined in Figure 3.1. Using a thermocouple introduced into a hole in the ingot, an initial soak of one hour with re-heating times of 20mins, was shown to be the minimum time needed to obtain a homogeneous temperature in the material. The soaking temperature was low enough to prevent rampant grain growth, but effective in reducing cellular segregation in the ingot. A minimum finishing rolling temperature of 650°C was maintained to avoid the 475°C embrittlement regime. This was also below the recrystallisation temperature for the alloy, and the final passes down to 650°C ensured a warm-worked sub-structure. At most two re-heats and some ten passes were required to achieve the necessary reductions. Quenching from the finish temperature was executed to avoid embrittlement.

TABLE 3.3 Composition of Fe-40Cr Experimental Alloys

Designation	Description	Alloying Additions wt%	Amount Recovered wt%	wt% C	N	O	S	P
LI	Low interstitial	-	-	0,01	0,002	0,10	0,010	0,01
MI	Med. interstitial	-	-	0,017	0,003	0,08	0,009	0,005
HC	High Carbon	carbon	-	0,073	0,005	0,023	0,010	0,01
HN	High nitrogen	nitrogen	-	0,010	0,06	0,06	0,010	0,01
SD1	Sulphur doped	0,025 S	0,031 S	0,010	0,002	0,09	0,031	0,01
SD2	Sulphur doped	0,050 S	0,040 S	0,012	0,002	0,05	0,040	0,01
AL	Fe-40Cr-0,2Al	0,2 Al	0,12 Al	0,010	0,002	0,029	0,006	0,01
NB	Fe-40Cr-0,2Nb	0,2 Nb	0,20 Nb	0,010	0,002	0,06	0,010	0,01
RU	Fe-40Cr-0,2Ru	0,2 Ru	0,20 Ru	0,010	0,002	0,10	0,010	0,01
NI	Fe-40Cr-2Ni	2,0 Ni	1,95 Ni	0,011	0,002	0,10	0,010	0,01

3.5 HEAT TREATMENT

Initial tests to assess the mechanical response were performed on materials in both the wrought and as-cast conditions over a wide range of annealing schedules. From these studies it became clear that alloys displaying good tensile ductility did not necessarily exhibit good impact toughness. Similarly, tough material was usually related to a loss of tensile ductility. Based on these tests, six standard heat treatment cycles were established to rationalise the mechanical behaviour and are shown schematically in Figure 3.1. Solution heat treatments (SHT) were carried out by soaking for 1 hour at 1050°C and 1250°C, followed by quenching in iced water. Ageing was carried out by holding for 1 hour at 850°C prior to or subsequent to SHT, followed by quenching. All specimens were coated with a zircon-based protective ceramic during heat treatment. The ceramic coating was aimed at protectingthe high chromium material against internal oxidation and nitrogen pick-up at elevated temperatures. Typically, the nitrogen pick-up during heat treatment was found to be in the range 20-30 ppm.

3.6 MECHANICAL TESTING

Charpy-format impact specimens and metric Hounsefield tensile species were sectioned from the plate as shown in Figure 3.2. The impact specimens were taken in the worst-case transverse-longitudinal directions. Specimens were notched subsequent to heat treatment and tested at a strike velocity of 5 m/s. The tensile specimens were taken in the longitudinal direction for greater microstructural consistency in the deformation studies. The specimens were tested to failure at an initial strain rate of 10^4/s (cross-head speed 0,15mm/min) on a Zwick 1484 universal testing machine. Modifications to enable isothermal tensile tests and three point bending studies were built for use in conjunction with the Zwick.

Following heat treatment, pre-straining was performed by cold-rolling of the plate on a Dinkel Type K65E laboratory rolling mill. Reductions of up to 10% were performed at a rate of 1,3% per pass.

Hardness tests were performed using a Vickers pyramid indenter under a 50kg load. The hardness values represent an average of at least five determinations.

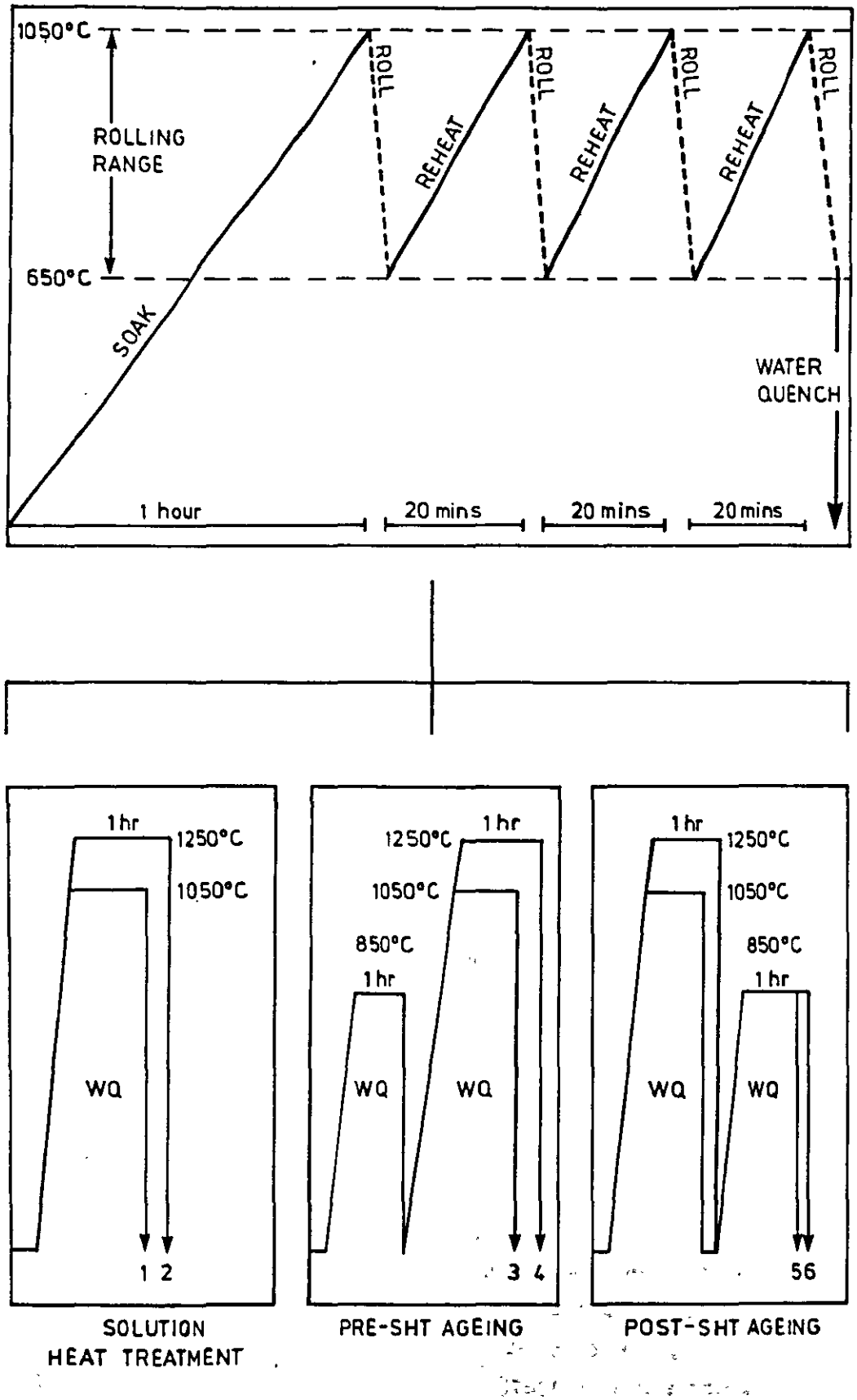

FIGURE 3.1 Schematic diagram for fabrication and isothermal heat treatment cycles

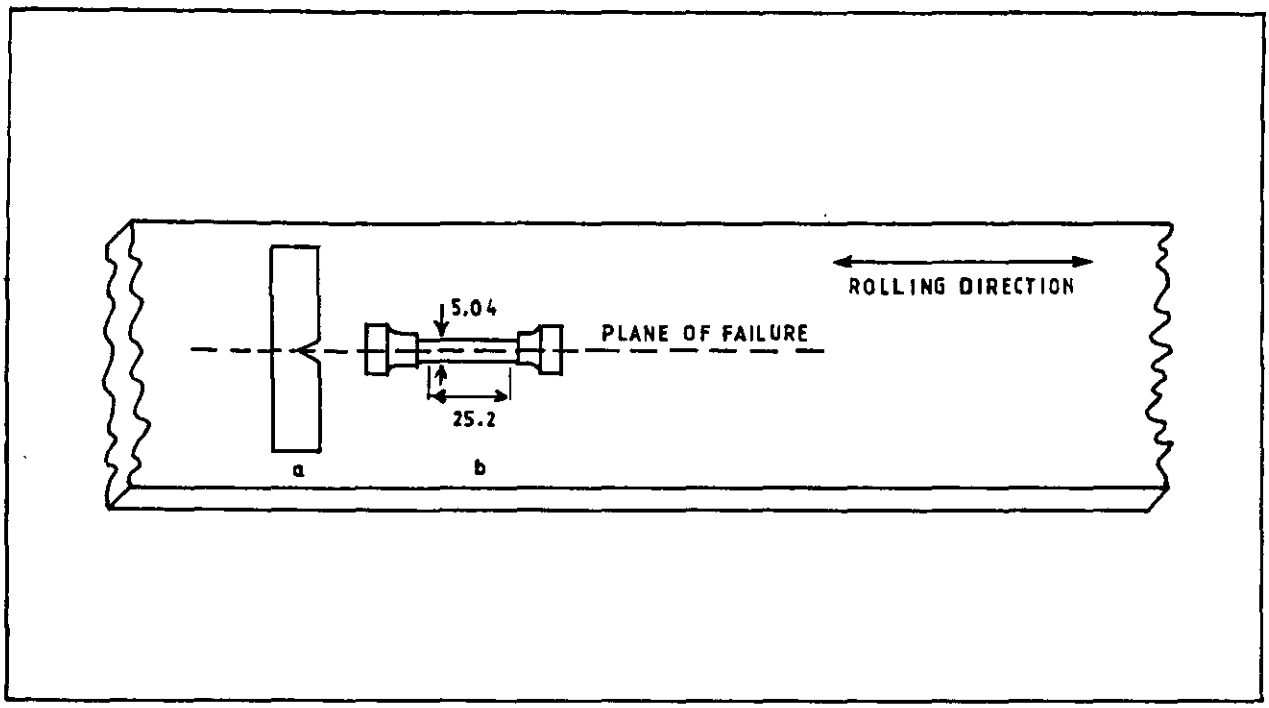

FIGURE 3.2 Specimen geometry

3.7 DILATOMETRY

Phase transformation and thermal expansion studies were conducted using a Leitz UBD dilatometer. Dilation-time studies of the material soaked at 750°C in the sigma phase formation region proved to be insensitive to the alpha-sigma change, and were abandoned. The mean thermal expansion coefficient was determined over the range 0-850°C.

3.8 OPTICAL METALLOGRAPHY

Samples taken for metallographic examination were mechanically lapped to a 0,25 micron finish. Similarly, the gauge length of the tensile and Charpy specimens were polished to enable study of the surface deformation features. In most cases electropolishing was performed to remove the deformed surface layers and to highlight the microstructure by selective attack. A list of the chemical reagents used is given in Table 3.4. Metallography was carried out using optical and stereomicroscopy. The surface topography was revealed by Nomarski interference techniques.

TABLE 3.5 List of Etchants.

Design-ation	Composition	Conditions	Application
A	5g Oxalic Acid 100ml Distilled Water	Electrolytic RT; 5V	Etching microstructure, surface deformation
B	Murakami's Reagent 10g $K_3Fe(CN)_6$ 10g KOH 100ml Distilled water	Immersion Boiling solution 3-5 mins	Etching sigma phase
C	133ml Glacial Acetic Acid (99,5 wt%min) 25g CrO_3 7ml Distilled water	Electrolytic 20°C max. 20V; 2-4 mins	Electropolishing
D	As above	Electrolytic 0,025A; 20mins	Etching microstructure

3.9 ELECTRON MICROSCOPY

Scanning electron microscopy was carried out on a Cambridge S.200 SEM with a Tracor TN5400 Energy Dispersive analytical facility. High resolution microscopy was made possible by operating in high vacuum with a LaB_6 emitter, using a balance of back-scattered and secondary electrons.

Thin foil specimens for transmission electron microscopy were prepared by automatic twin-jet techniques using a refrigerated 5 % perchloric acid in ethanol solution. These were examined in a JEOL 200CX TEM with double-tilt facilities at an operating voltage of 200kV. Analytical work on the specimens was conducted on a Phillips 420 TEM in conjunction with an EDAX 9900 Energy Dispersive System, operated at 120kV.

3.10 CORROSION STUDIES

A selection of specimens were taken for general and pitting corrosion studies. Conventional potentiodynamic polarisation techniques using a Princeton corrosion module were supplemented by scanning electron microscopy to assess the localised corrosion processes for different alloy conditions. These results are detailed in Appendix A.

CHAPTER 4

RESULTS

4.1 THE EXPERIMENTAL MATRIX

Fe-40Cr alloys with minimised interstitial levels were characterised in terms of their wrought properties. A description of some of the microstructural parameters is outlined in Section 4.2 in order to facilitate discussion in the following sections.

Following a study of the response of Fe-40Cr base alloys to isothermal heat treatment cycles, six standard heat treatment procedures were established. These comprised solution heat treatments (SHT) in conjunction with ageing cycles at an intermediate temperature prior to and subsequent to SHT. The mechanical properties were evaluated in response to heat treatment, and pre-straining by controlled deformation.

The effect of the isothermal annealing cycles in relation to the precipitation processes in Fe-40Cr base alloys was studied in greater detail, and is described in Section 4.3. An understanding of the way in which the precipitation influences the ductile behaviour was gained by examining alloys with a higher interstitial content. The higher interstitial levels had the advantage of enhancing the microstructural development, which facilitated microscopic analysis. Analytical electron microscopy to identify the secondary phases was undertaken (Section 4.4).

Following observations in the low interstitial alloys that inclusions could be harnessed as prismatic dislocation sources, parallel tests were also conducted on experimental Fe-40Cr alloys doped with sulphur, with a view to increasing the free dislocation density. A description of these results is contained in Section 4.5.

The addition of minor alloying elements to the Fe-40Cr alloy resulted in a wide range of responses to deformation and fracture. The effect of three substitutional alloying additions is described in Section 4.6:

1. The addition of 2.0% nickel was made with a view to increasing the impact resistance;
2. Ruthenium additions of 0,2% added to induce cathodic modification, were examined to evaluate the effect on ductility;
3. A Niobium addition of 0,2%, which is well in excess of the interstitial stoichiometry, was alloyed to establish whether higher levels of stabiliser could be tolerated, given the need for complete gettering of the interstitials.

Supplementary studies were undertaken to establish the compromise between the mechanical properties and the corrosion resistance of the alloy. Changes in microstructural parameters such as the volume fraction of second phase particles and the dislocation substructure were expected to affect the localised corrosion processes in particular; thus potentiodynamic general corrosion and pitting studies were carried out, and are reported on in Appendix A.

Each section is treated as a separate study, the essence of which is contained in a brief comment on each set of results. These are drawn together in Section 4.7 prior to a more general discussion.

4.2 CHARACTERISATION OF THE WROUGHT CONDITION OF Fe-40Cr

4.2.1 Recovery of the Wrought Sub-Structure

The Fe-40Cr alloys exhibit behaviour typical of most bcc ferritic structures during hot rolling. Dynamic recovery during rolling leaves the alloy with an elongated grain structure, and a series of bands aligned in the rolling direction on the micro-level. The bands comprise a series of cells of a relatively low dislocation density, contained by walls of dense dislocation tangles [Figure 4.1(a)].

Rolling down to temperatures in the warm-working region ($T=0.4T_m$) causes a heavily dislocated substructure. Following rolling, static recovery becomes noticeable after soaking above 700°C, and rearrangement of the dislocation network occurs by classic polygonization processes. The dislocations are swept into low-angle boundaries, leaving regions of strain-free metal. The formation of large and small-angle boundaries after soaking for 5 hours at 750°C can be seen in Figure 4.1(b).

Recrystallisation in the base alloy is detectable after soaking for 1hr at 850°C, and with increasing annealing temperatures, recovery and recrystallisation occur as a merging process. On a macroscopic level, new grains are initiated at the prior ferrite grain boundaries and also inclusions, as shown in Figure 4.2. Transmission microscopy shows the nucleation of recrystallised grains in the region of the deformation band walls. Growth of the recrystallised grains is by migration of high angle boundaries, indicated by the fringe contrast lines, but this is limited at 850°C.

The sub-boundaries persist even after 3hrs at 850°C, at which time restoration is nearly complete (Figure 4.3). The effect of annealing at 850°C or below, therefore, is to leave the metal only partially recovered, with a diminished driving force for recrystallisation. The high stability of the sub-structure is further increased if it is pinned by second phase particles, and may

exist even after annealing at 1050°C. The sub-structure may be detected optically, and is responsible for the 'veining' effect noted in Figure 4.3(b).

Recovery at 850°C leaves a remnant of the directional wrought grain structure, delineated by the original 'pancake' grain boundaries. Annealing above 950°C gives rise to an equiaxed grain structure which tends to be coarse at an average grain diameter of 100 microns.

The metal recovered at 850°C shows good tensile ductility, which persists virtually unaltered with increased soaking times, as shown in Table 4.1.

TABLE 4.1 Effect of Recovery on Tensile Ductility

Heat Treatment	UTS (MPa)	0,2%PS (MPa)	%El
As-wrought	554	457	-
1h 850°C	480	377	27
2h 850°C	473	362	30
3h 850°C	462	352	30
18h 850°C	472	351	28

(a)

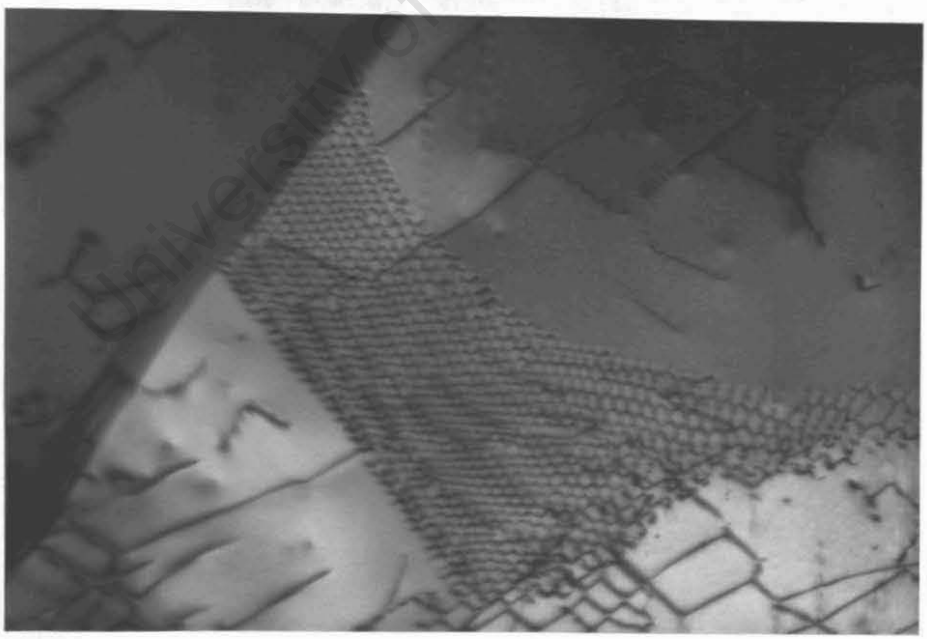

(b)

FIGURE 4.1 (a) As-wrought sub-structure, showing deformation bands
(b) Recovered sub-structure, showing large and small-angle boundaries after soaking for 5 hrs @ 750°C

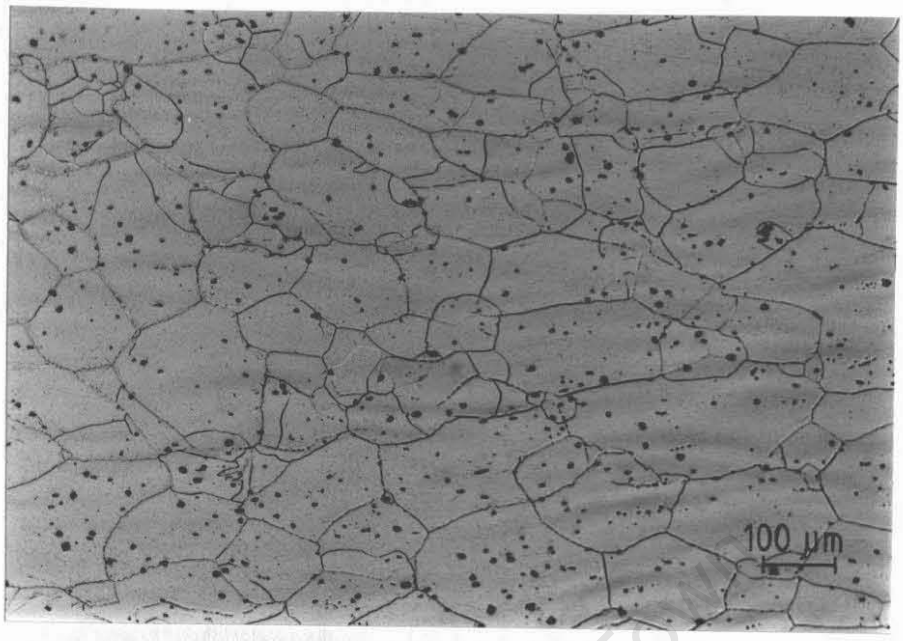

(a)

(b)

FIGURE 4.2 (a) Initiation of recrystallisation at the prior ferrite boundaries (1hr; 850°C) - Solution A

(b) Growth of recrystallised grains by the migration of high-angle boundaries

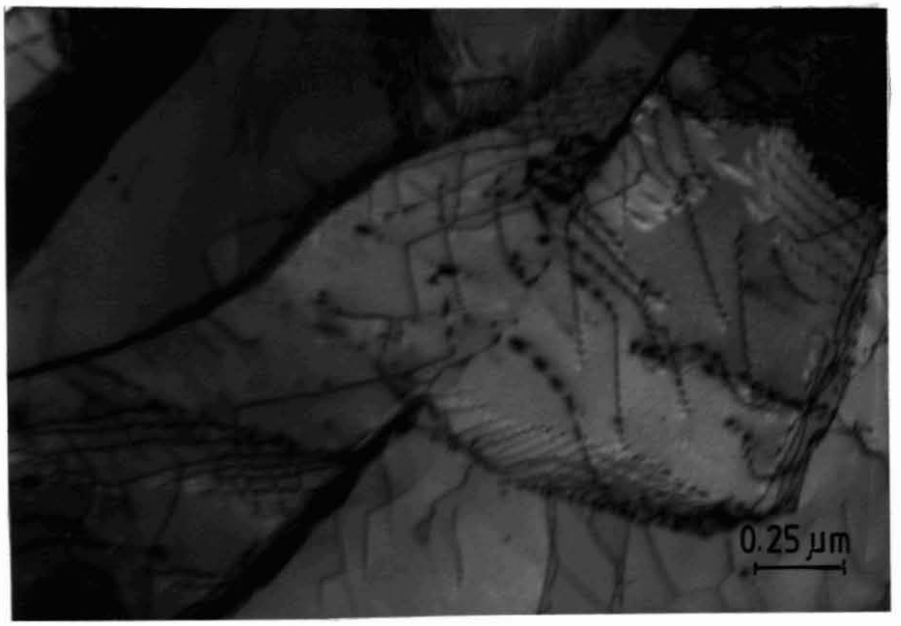

(a)

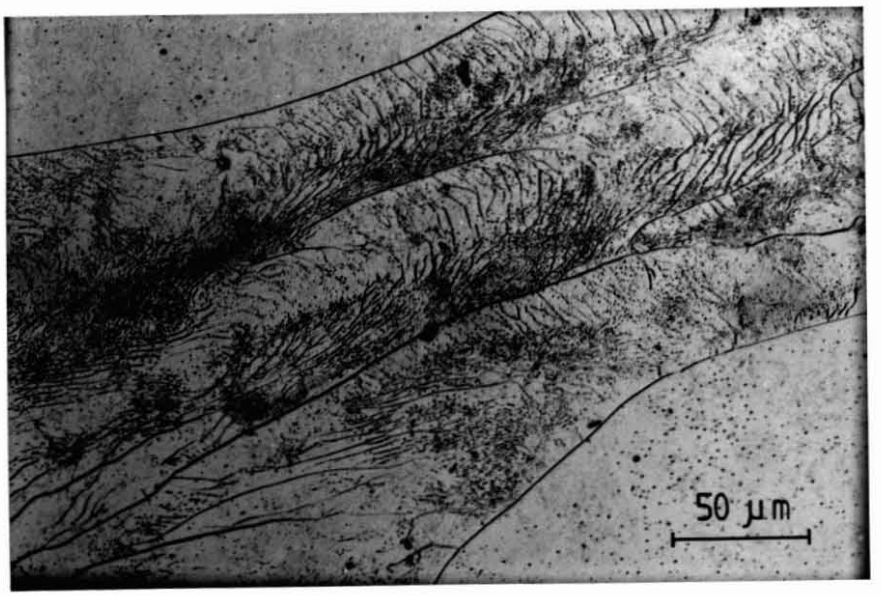

(b)

FIGURE 4.3(a) Formation of low-angle sub-boundaries during recovery (3hrs 850°C)

(b) Veining in the recovered ferrite, delineating the sub-grain structure - Solution A

4.2.2 Mode of Fracture

The polished deformation surface of a V-notched Charpy-format specimen loaded in three-point bending is shown in Figure 4.4. Fracture initially propagates from the notch in a catastrophic manner, but is arrested by blunting as it enters the region of compression. The transformation from brittle to ductile fracture is denoted by a change in the deformation mode, from mechanical twinning, in the form of Neuman bands, to plastic slip.

Under high strain rates, low toughness fracture is by brittle transgranular cleavage, which progressively changes to a bimodal failure comprising cleavage and 'dimple strips' as ductility increases. The edge of a crack is shown in the SEM micrograph in Figure 4.5. This illustrates fracture of a (100) plane, with a common herringbone pattern, in the <110> directions and along {112}<110> twin interfaces. Cleavage of the individual facets generally initiates at the boundaries. However, fracture of the alloy in the partially recovered condition leads to a type of quasicleavage with ill-defined facets, apparently initiated intragranularly, blending into dimpled regions.

Deformation changes from planar to wavy slip with decreasing strain rates. Failure in tension up to an initial strain rate of 3×10^{-1}/s (cross-head speed = 500mm/min, which represents the limit of the machine) is by microvoid coalescence.

The annealed material shows no characteristic load drop at the yield point, but a distinct yield point may be induced by strain-ageing, and, to a lesser degree, quench-ageing, at 150°C. Following ageing at 150°C, failure in tension remains ductile.

4.2.3 Analysis of Non-Metallic Inclusions

A large number of inclusions occur within the melt, and are visible optically, ranging in size from 1-5 microns in diameter. The results of analytical transmission microscopy performed on the inclusions are reported in Figure 4.6. Energy dispersive analysis indicates a high proportion of chromium, with smaller amounts of

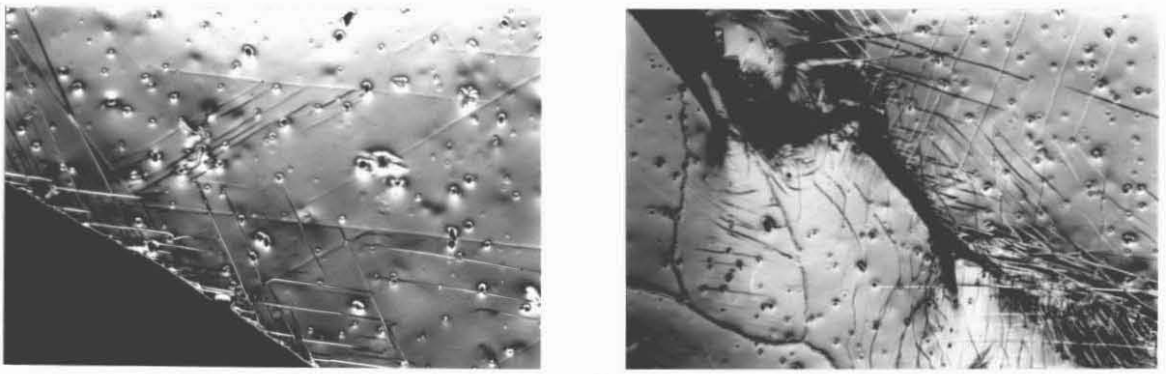

FIGURE 4.4 Polished deformation surface, showing the transition from deformation by mechanical twinning to slip

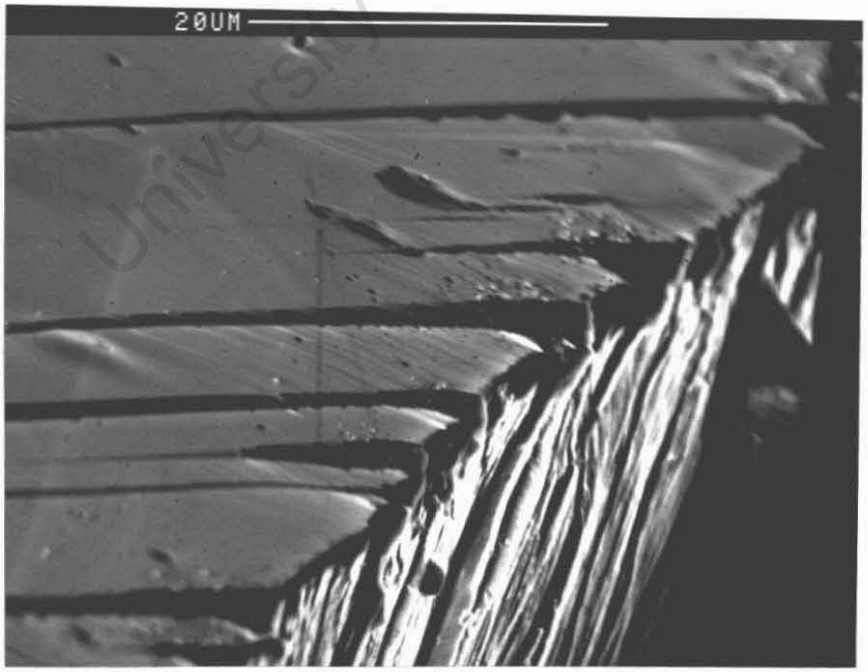

FIGURE 4.5 SEM micrograph of the fracture edge, showing cleavage of a (100) cleavage plane along $\{112\}\langle 110\rangle$ twin interfaces

iron and aluminium. This is confirmed by EDS analysis in the SEM. The electron diffraction pattern has been indexed as the hexagonal Cr_2O_3, or escolaite phase, with lattice parameters a=4,96A° and c=13,60A°. This has been reported as being isostructural with Fe_2O_3 and Al_2O_3, with each species showing complete mutual solubility [Kiessling (1978)].

The oxides are frequently to be seen acting as pinning sites for low and high angle boundaries, as well as nucleation centres for recrystallised grains. The oxides also play a key role in both the ductile and brittle fracture processes. Owing to their low interfacial strength with the matrix, the oxides initiate microvoids at low stress levels, and are the predominant species analysed within the dimples of the ductile fracture surfaces. Direct examination of the fracture surfaces in the SEM also reveals a mechanism for brittle crack initiation by the oxides. Fissure formation along planes perpendicular to the cleavage plane is shown in Figure 4.7(a).

Alloying with 0,2% aluminium results in gettering of the oxygen, with subsequent removal to the melting slag. Only a fraction of the aluminium is recovered in the melt, as seen in Table 3.3. Comparison of the microstructure of a deoxidised melt with that of the standard alloy showed a noticeable decrease in the inclusion content. Figure 4.7(b). Similarly examination of the fracture surfaces of deoxidised material tested below the DBTT showed only isolated cleavage initiation events at oxides. The resultant improvement in the impact toughness was demonstrated previously (Table 2.1).

4.2.4 Sigma Phase

The hard, brittle sigma phase occurs only after prolonged exposure of the base alloy in the sigma formation region. Bulk sigma phase is shown in Figure 4.8 after holding for 32 hours at 750°C. It occurs along grain boundaries, and nucleated around inclusions to give the characteristic bulls-eye appearance. The microfissures are a consequence of the mechanical polishing stresses.

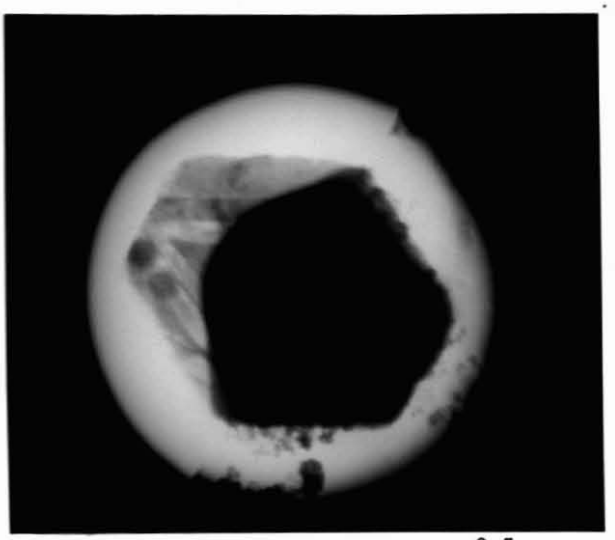

Composition (wt%)	Assuming Oxide Stoichiometry (wt%)
Al = 25	Al = 20,5
Cr = 71	Cr = 75
Fe = 4	Fe = 4,5

(a) TEM BF Image of Inclusion

(b) Standardless Semi-Quantitative Analysis in TEM

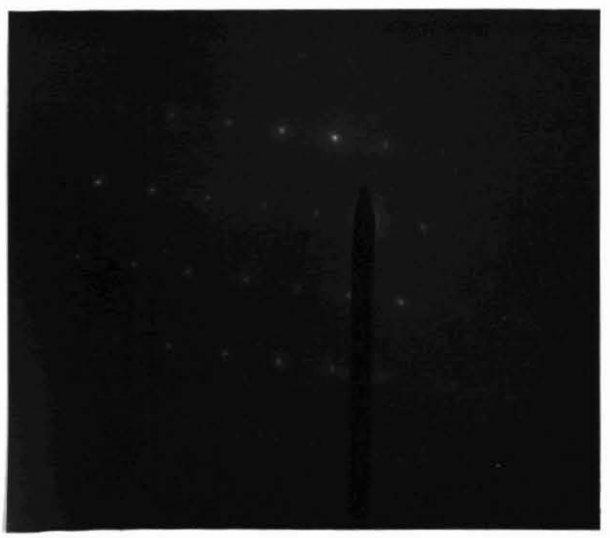

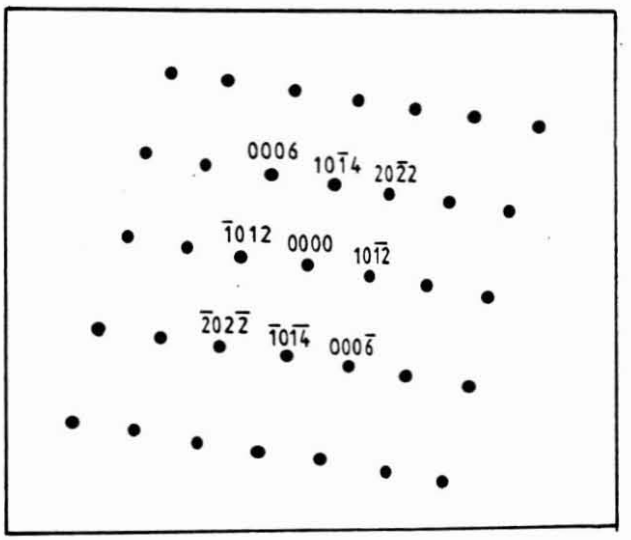

(c) SADP of Inclusion

(d) Indexed as hcp Cr_2O_3 'escolaite' Phase

FIGURE 4.6 Analysis of oxide inclusions

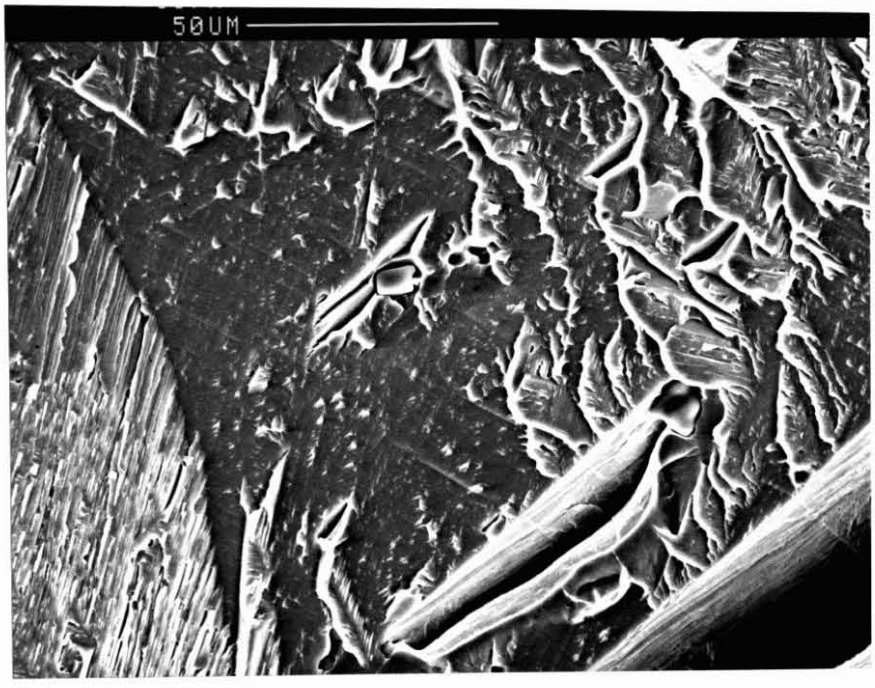

(a)

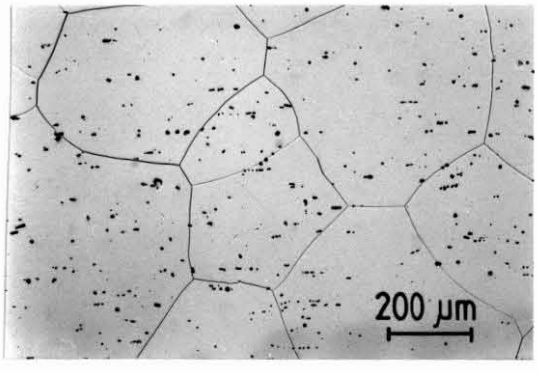

Base Alloy

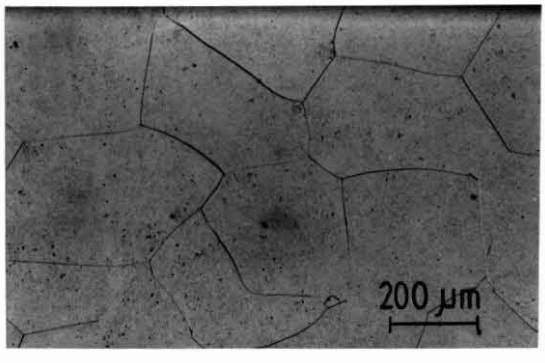

Deoxidised - 0.2% Al

(b)

FIGURE 4.7(a) Initiation of microcracks by oxide inclusions
(b) Effect of deoxidation with aluminium on the inclusion content - Solution A (1050°C)

Microhardness measurements indicate a hardness of some 1000 Vickers for the sigma phase. The sigmatised material shows severe embrittlement under all testing conditions.

The kinetics of the formation of the sigma phase are difficult to determine indirectly. Dilation-time curves measured by dilatometry show no volume change. This may be explained by calculation of the specific volume of the sigma phase, which shows only a slight increase over that of the ferrite matrix, from 84,6 to 85,5 atoms per nm^3.

EDS analysis in the SEM of bulk sigma phase shows minimal compositional variation between the sigma phase and the ferrite. This follows from the equilibrium phase diagram which puts the Fe-40Cr composition virtually on the sigma phase boundary. X-ray analysis showed no traces of sigma phase after soaking the base alloy for up to 3hrs at 850°C; nor was any evidence of sigma phase found optically or in transmission microscopy in any of the alloys following the standard heat treatment procedures. It therefore appears unlikely that the sigma phase plays a significant role on a macroscopic level under normal processing conditions, although the kinetics may be altered by a higher degree of alloying.

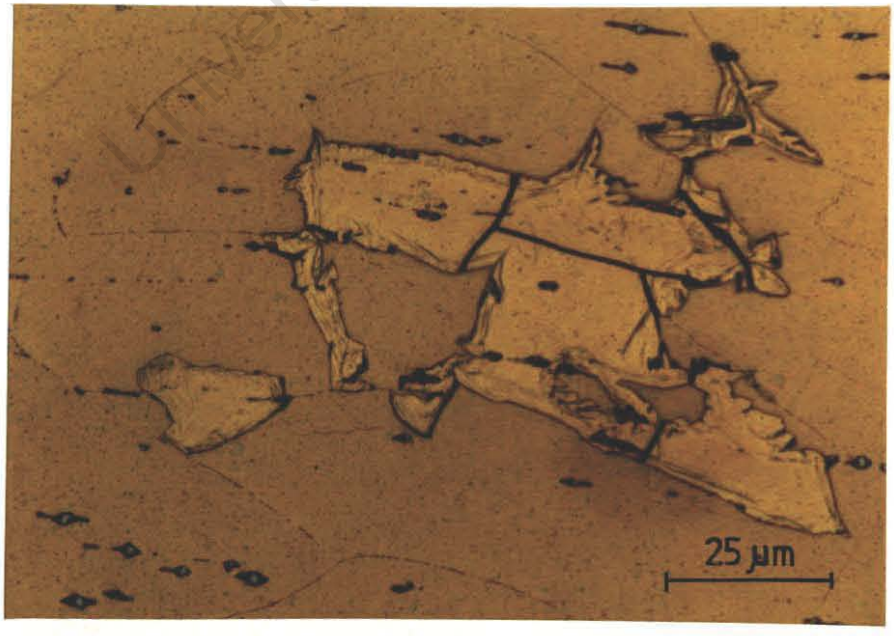

FIGURE 4.8 Sigma phase allotriomorphs (32hrs; 750°C) - Solution B

4.3 PROPERTIES OF LOW INTERSTITIAL Fe-40Cr

4.3.1 Results

The response of an Fe-40Cr base alloy in the wrought condition to isothermal annealing was studied with respect to its mechanical properties and microstructure. Specimens were sectioned from melt LI, which had a total (C+N) content of 100ppm. Six different annealing treatments were applied, based on a solution heat treatment (SHT) with or without ageing cycles prior to or subsequent to SHT. For the sake of clarity, material aged at an intermediate temperature before solutionising is referred to as 'prior-aged', whereas ageing after SHT is referred to as 'post-aged' or 'quench-aged'. Impact and tensile tests were carried out on the heat treated alloys, as well as material which had been pre-strained following heat treatment.

Further tests were performed with samples taken from melt MI, which had twice the interstitial levels of melt LI, in order to clarify the role of the interstitial content.

4.3.1.1 Mechanical Properties

The results of impact and tensile tests of samples taken from the low interstitial Fe-40Cr alloy are given below.

Figure 4.9 shows the impact transition curves for sub-size.7,5x10mm Charpy specimens. The ITT was taken as the midpoint between the upper and lower shelf energies.

The room temperature tensile behaviour is illustrated in Figure 4.10. A summary of the results is given in Table 4.2.

TABLE 4.2 Mechanical Properties as a Function of the Annealing Cycles

Cycle	Heat Treatment	UTS (MPa)	0,2%PS (MPa)	%El	HV_{50} (VPN)	ITT (°C)	Upper Shelf Energy (J/cm^2)
1	1h 1050°C	564	448	23	206	33	125
2	1h 1250°C	569	494	19	224	68	140
3	1h 850/1h 1050°C	554	448	22	212	25	107
4	1h 850/1h 1250°C	560	474	15	228	20	135
5	1h 1050/1h 850°C	491	321	26	187	63	79
6	1h 1250/1h 850°C	460	367	21	190	58	104

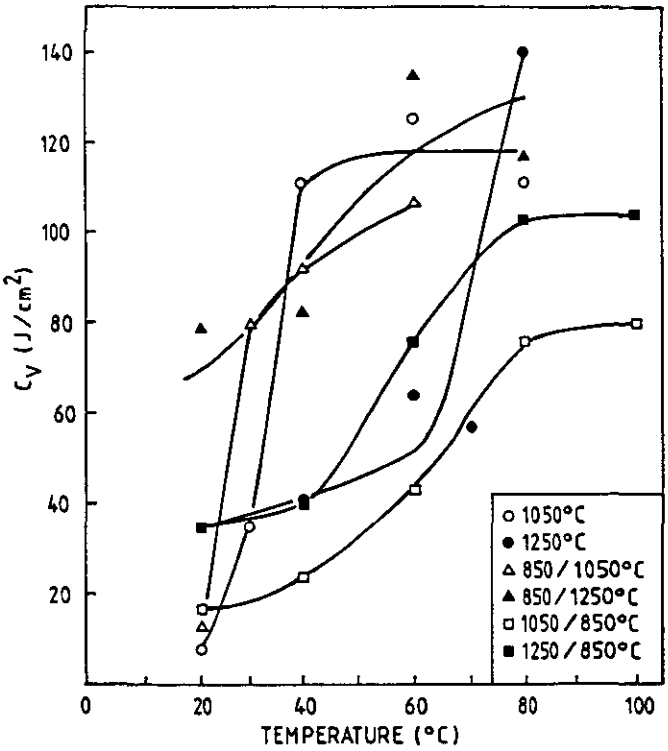

FIGURE 4.9 ITT curves as a function of the annealing cycles

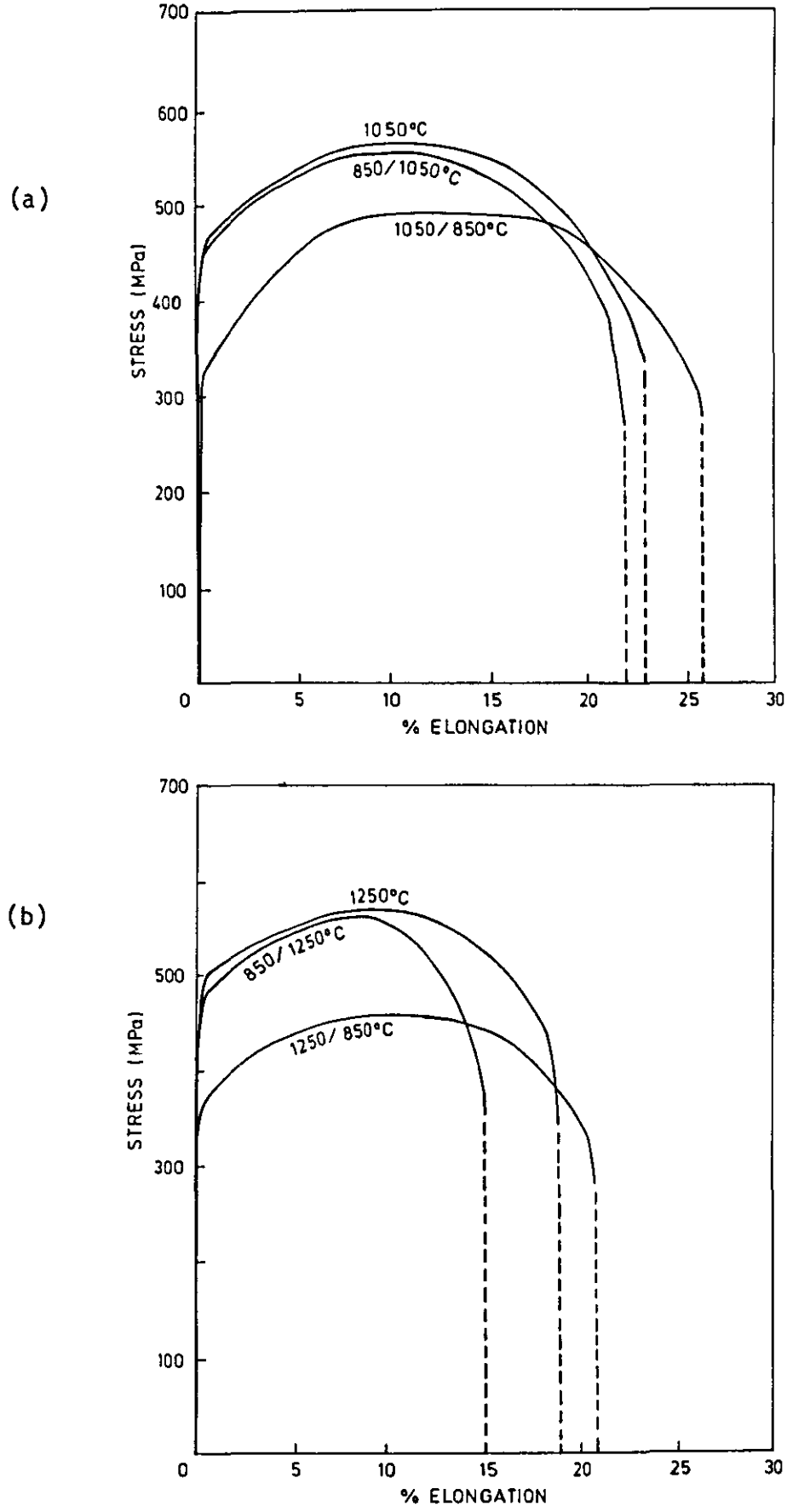

FIGURE 4.10 Tensile characteristics of low-interstitial Fe-40Cr Alloys for (a) SHT at 1050°C and (b) SHT at 1250°C

4.3.1.2 Microstructure

OPTICAL MICROSCOPY

The microstuctures of the heat-treated LI alloy studied under polarised light are shown in Figure 4.11.

Solutionising resulted in an equiaxed ferrite stucture, and grain growth at the higher 1250°C SHT gave rise to large polygonal ferrite grains. Ageing of the material left the ferrite morphology essentially unaltered. Ageing prior to SHT increased the tendency to 'veining', but this was largely eliminated in the 1250°C SHT. A coarse grain boundary precipitate could be resolved in the case of ageing subsequent to SHT, although this could be eliminated by reheating to the SHT temperature as shown, with complete restoration of the original properties. The occurrence of pitting in the alloy solutionised at 1050°C points to an intragranular precipitation effect, but this cannot be resolved in the case of the 1250°C treatment.

TRANSMISSION ELECTRON MICROSCOPY

(a) **Solution Heat Treatment:**

Material quenched from the SHT temperature was characterised by a low density of dislocations, typically shown in Figure 4.12. A large number of the dislocations were subject to a decorative effect and appeared to be pinned. (This should not be confused with the dynamical contrast effect apparent in Figure 4.12(a)). The presence of a fine background distribution of precipitates was refined by quenching from the higher 1250°C SHT. A fine, continuous precipitate film was present at the boundaries of higher misorientation. A triple point, with associated dislocation emission is shown in Figure 4.12(b). Spectrographic traces of the matrix and the grain boundary precipitate are shown in Figure 4.13. The precipitate was enriched in chromium, which, on the basis of observations in Section 4.2.4 appear to preclude it from being the inter-metallic sigma phase. There was also no evidence of sulphur at the grain boundaries. Insufficient quantities in this case prevented positive identification by EDA.

(b) **Ageing prior to SHT:**

This treatment was effective in alleviating the intragranular precipitation in the alloy solutionised at 1050°C, but not 1250°C. A recurrence of the grain boundary phase was noted. (Figure 4.14). Figure 4.16 shows a section taken in the slip plane where only one slip system is operative. There is a relatively high density of a/2 111 dislocation loops, and these frequently appear as linear arrays associated with a sparse distribution of globular spheroids, identified as sulphides (see Section 4.5). The spheroids were identified directly after soaking in the range 850°C - 1050°C, but were absent in material treated at 1250°C.

A high population of small elastic strain centres was swept out in the path of the arrayed dislocations. This structure is shown by the weak-beam series in Figure 4.17. They are readily distinguishable as smaller loops, many of them elongated.

(c) **Ageing after SHT:**

Material subjected to post-ageing was characterised by an absence of the fine intragranular precipitation in material solutionised at both 1050°C and 1250°C. Large, idiomorphic precipitates occurred in the grain boundary regions, showing coarsening of the grain boundary film, although regions of continuous precipitate persisted in those areas where coarsening did not occur. Figure 4.15 shows a section taken from a deformed specimen. The hexagonal particles were identified as $M_{23}C_6$ carbides. These are discussed in Section 4.4.

4.3.1.3. Effect of Pre-Straining

The influence of the mobile dislocation density on the mechanical properties was studied by annealing the Fe-40Cr alloy prior to cold rolling at ambient temperature to reductions of up to 10%. The mechanical properties and microstructure were evaluated in response to the degree of prior deformation.

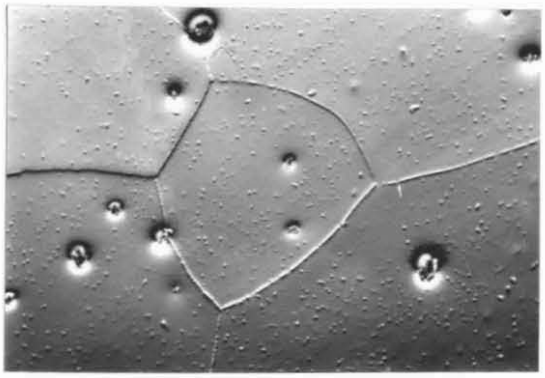

(a) 1050°C

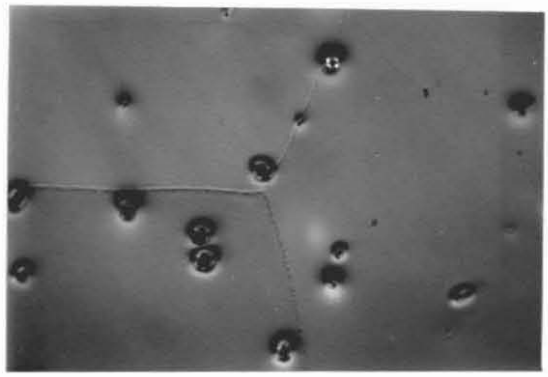

(d) 1250°C

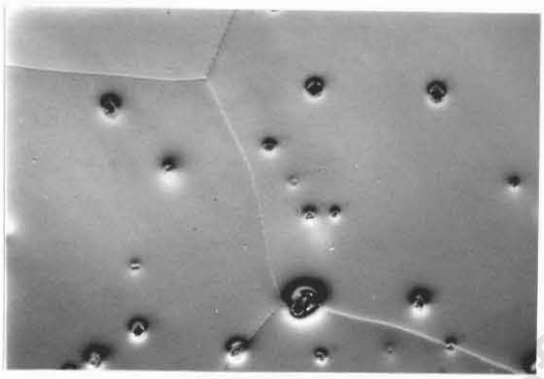

(b) 850/1050°C

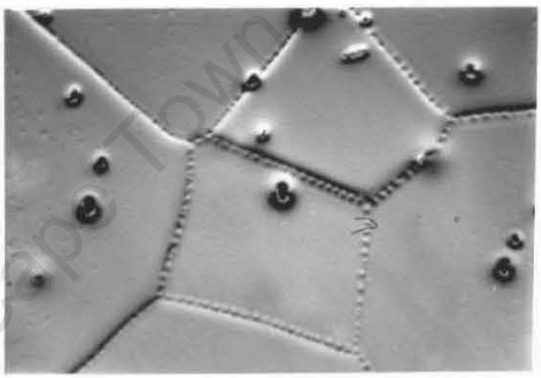

(e) 1250/850°C

(c) 1050/850°C

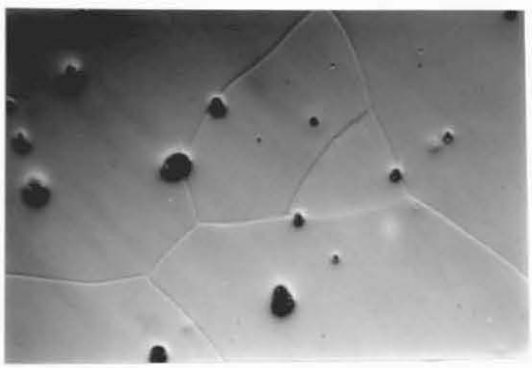

(f) 1250/850/1250°C

50 µm

FIGURE 4.11 Microstructure of low interstitial alloys under polarised light - Solution C

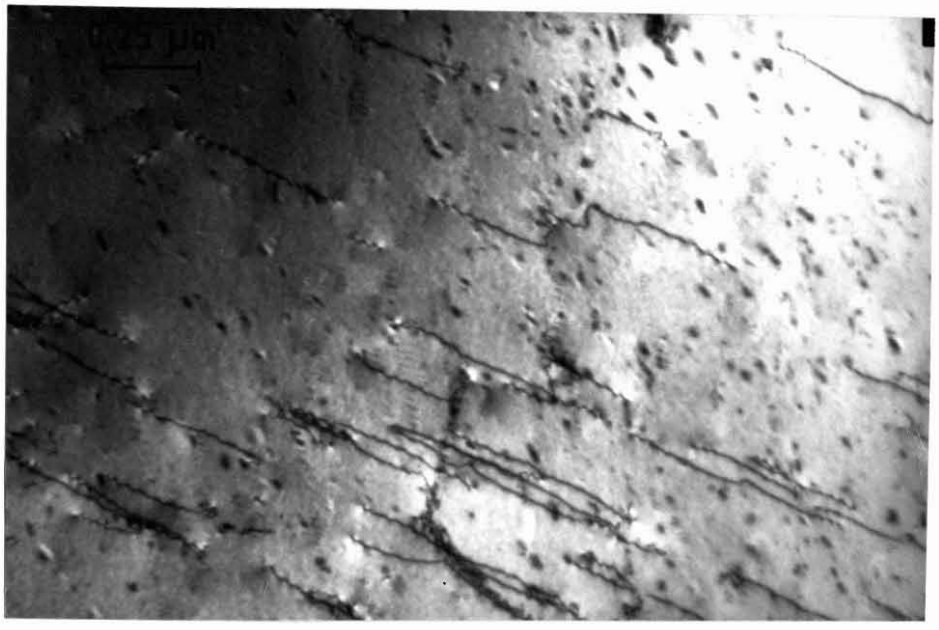

(a)

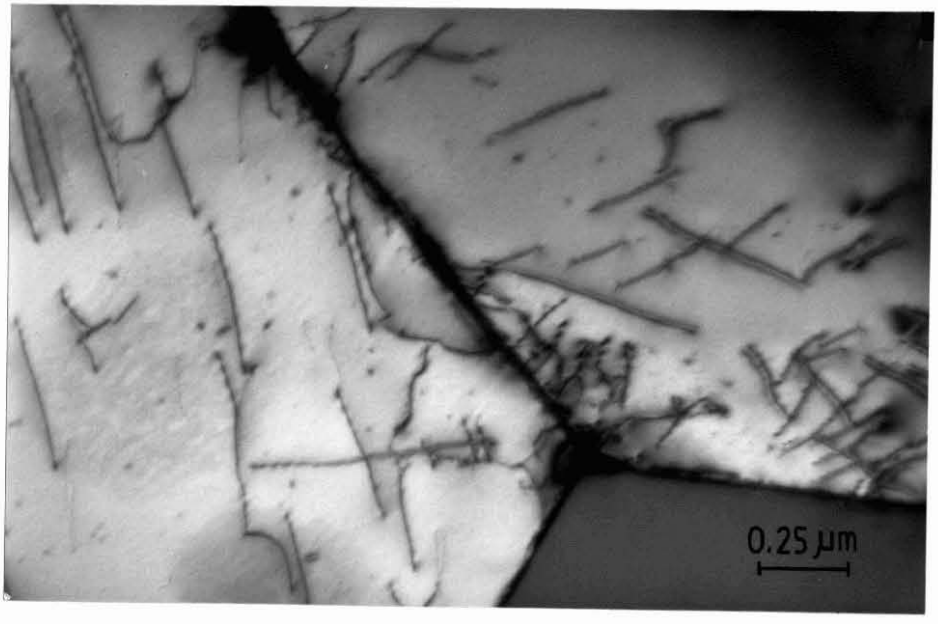

(b)

FIGURE 4.12 Microstructure of solutionised alloys (1050°C)

(a) Intragranular precipitation and dislocation pinning
(b) Triple point showing grain boundary phase

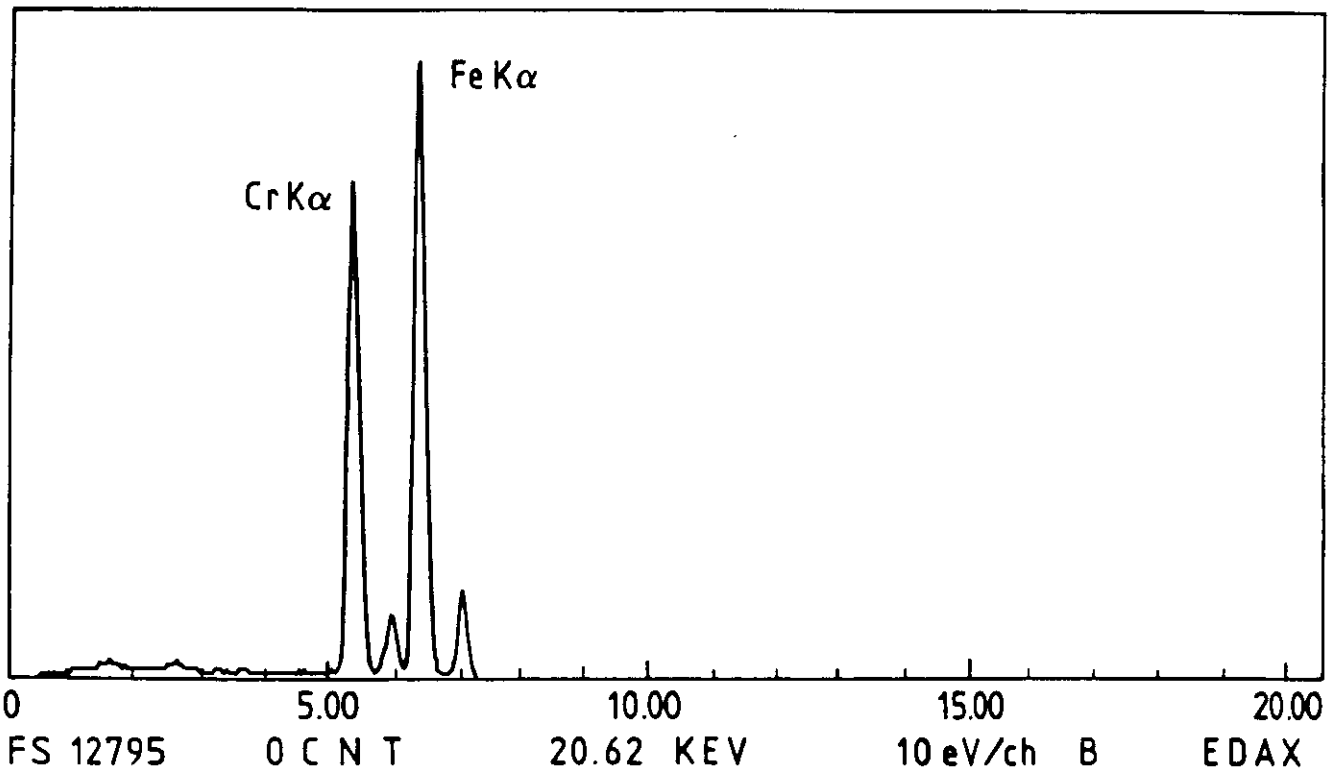

(a)

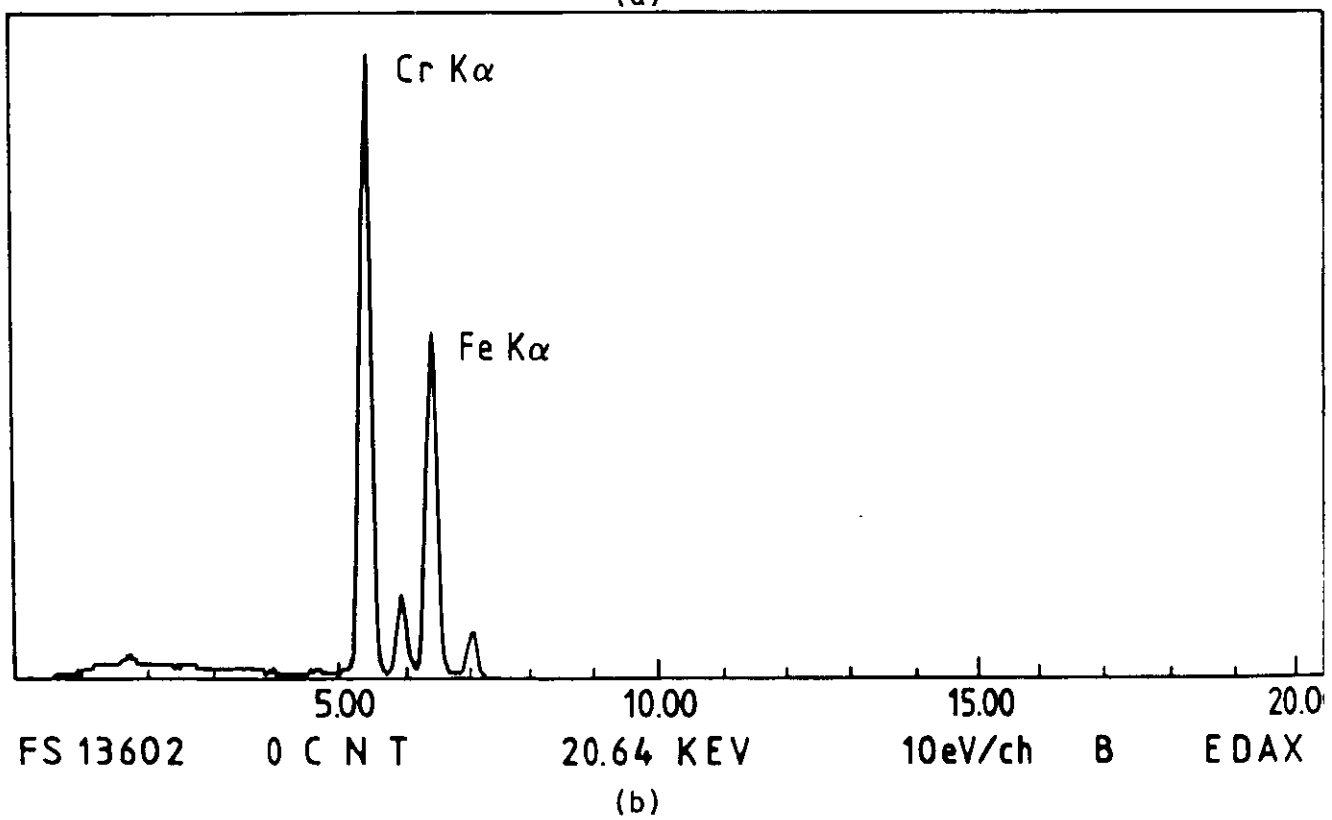

(b)

FIGURE 4.13 EDS Analysis (1050°C)

(a) Spectrographic trace of matrix
(b) Spectrographic trace of grain boundary phase

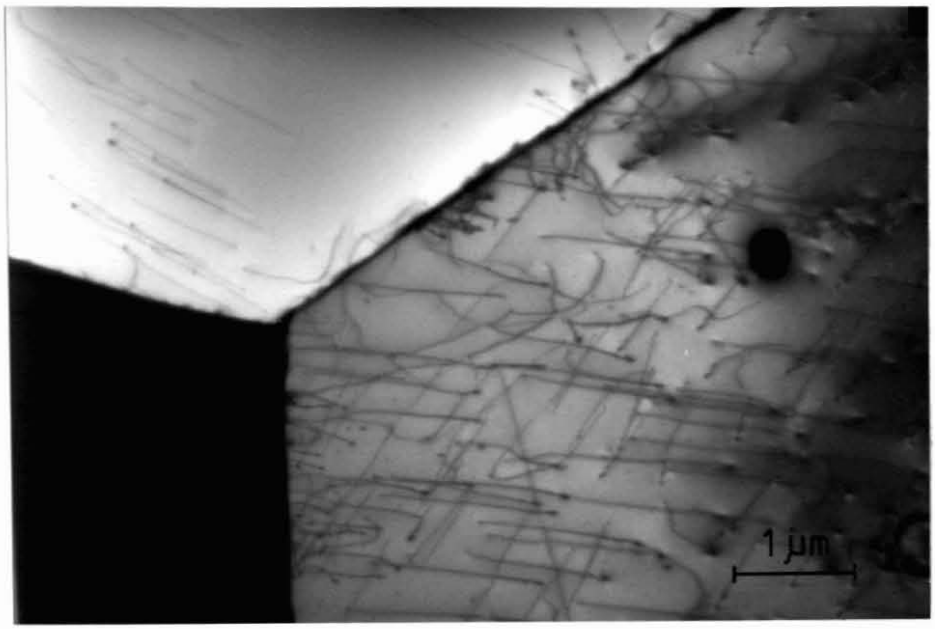

FIGURE 4.14 Triple point, showing grain-boundary phase and dislocation emission (850/1050°C)

FIGURE 4.15 Coarsening of grain boundary carbides. Section taken from a specimen pre-strained 5% (1050/850°C)

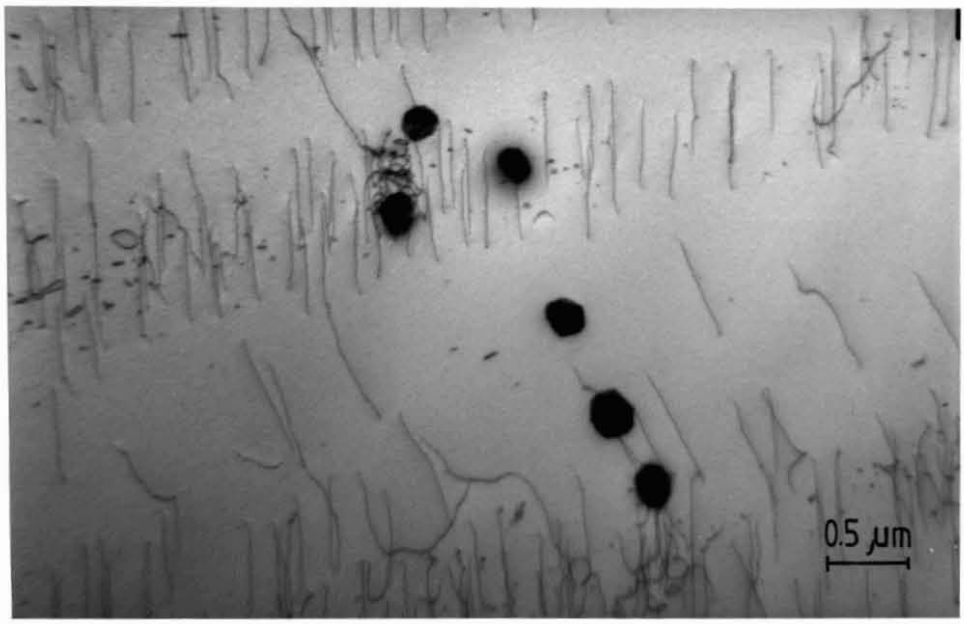

FIGURE 4.16(a) Primary prismatic arrays associated with sulphide inclusions (850/1050°C)

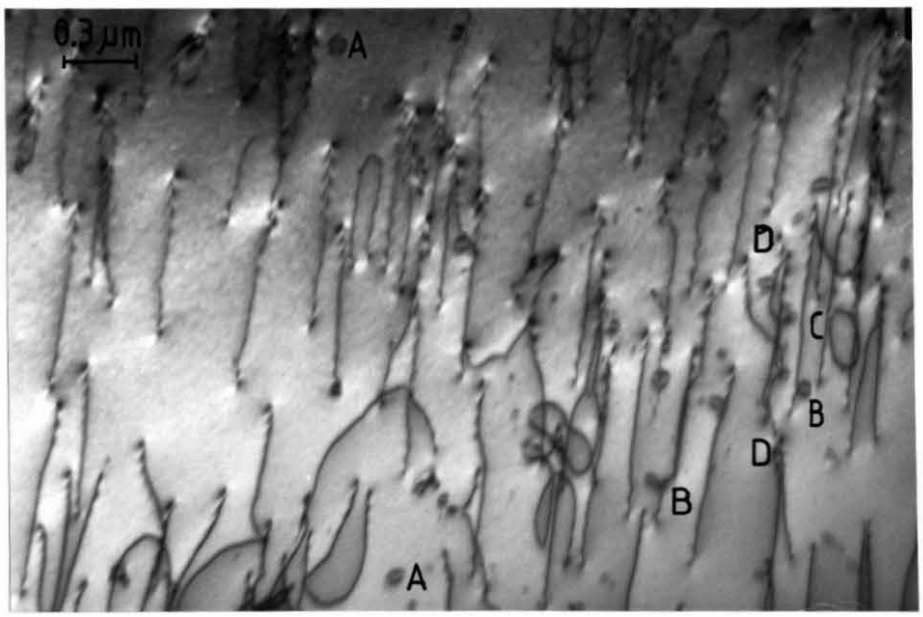

FIGURE 4.16 (b) Trails of the prismatic loops, showing dislocation debris

A - small loops derived from edge jogs on screw dislocations
B - dipole trail
C - single ended source; splitting of long loop into circular loop
D - jogged dislocation loop [after Hull (1975)]

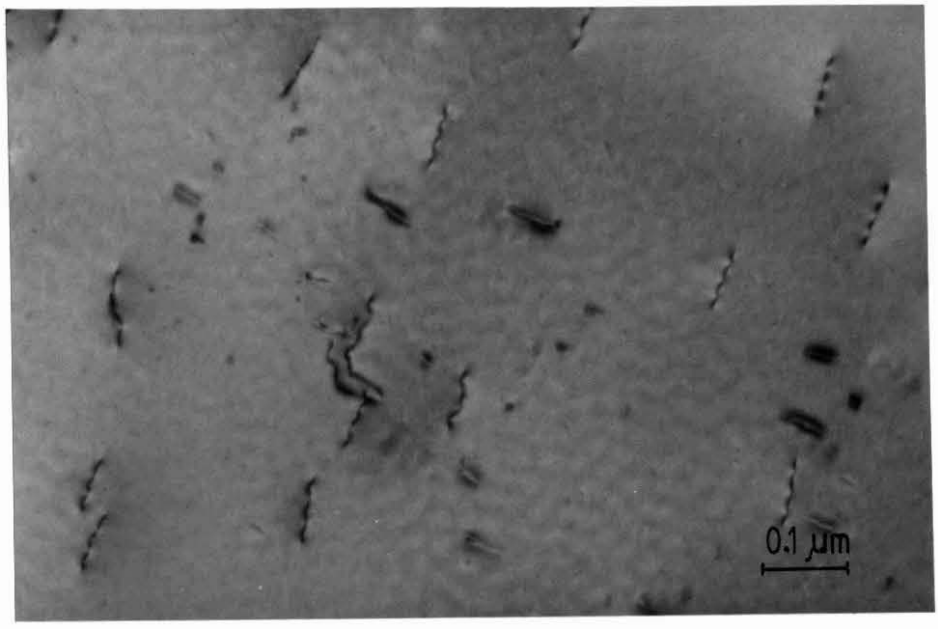

g_{110}

(a)

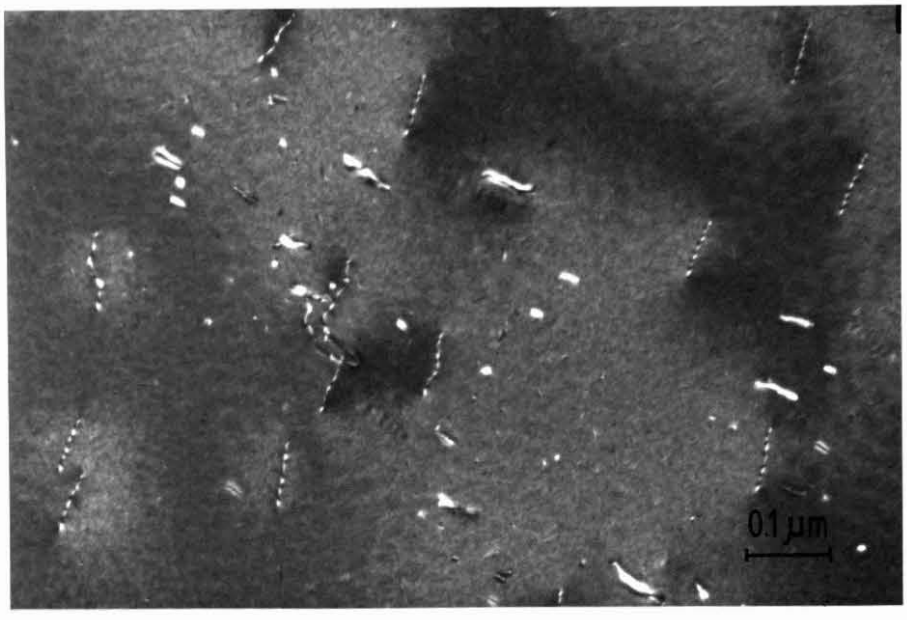

g_{110}

(b)

FIGURE 4.17 Structure of the small dislocation loops (850/1050°C). The segments show lines of no-contrast normal to the g-vector.

(a) Bright field image
(b) Centred weak-beam image

The effect of pre-straining on the room temperature (RT) tensile properties of 8mm plate annealed at 1050°C is shown in Figure 4.18. Tensile ductility fell off with an increasing degree of pre-strain and associated work hardening.

The response of the RT impact toughness of the base alloy to the prior deformation is shown in Figure 4.19. The behaviour may be summarised as follows:

(1) After an initial reduction in the toughness, there is a sharp increase up to an optimum percentage deformation in the solution annealed alloys. Failure in this case is 100% ductile. Thereafter the material becomes progressively embrittled;

(2) The optimum toughness is achieved with a smaller degree of pre-strain in material annealed at 1050°C than in the material annealed at 1250°C, although the upper shelf energy is approximately the same in each case;

(3) Given the optimum percentage cold reduction, the ITT is shifted to 0°C, with 100% ductile failure down to -10°C.

Three further observations were made:

(1) In the case of material aged subsequent to SHT, the material showed no improvement in the RT toughness with deformation;

(2) Pre-straining was not effective in specimens embrittled by slow cooling;

(3) Cold-rolling of the MI alloy, with C+N=200ppm, did not improve the RT impact toughness under any conditions.

MICROSTRUCTURE

The structure of the base alloy following pre-straining is shown in Figure 4.20. The material is characterised by a uniform density of dislocations, with evidence of the initial stages of dislocation band formation. A high degree of dislocation activity is evident at the grain boundary regions, and also at the inclusions.

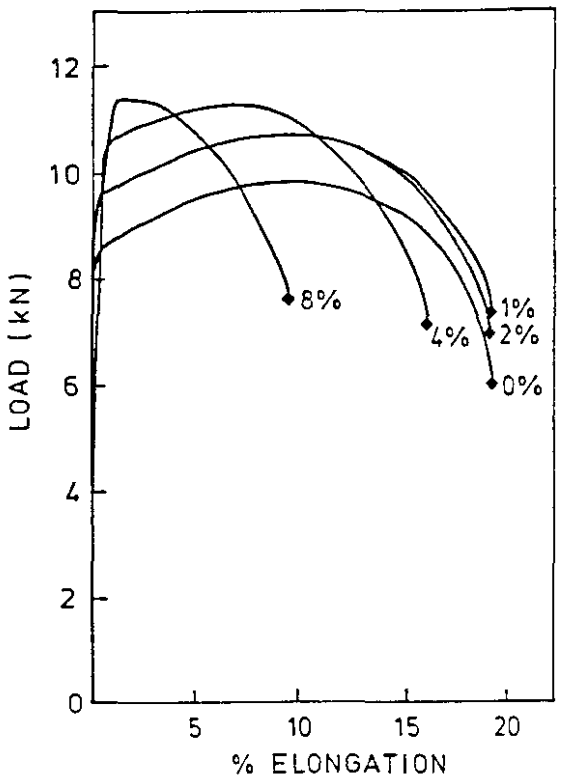

FIGURE 4.18 Effect of pre-straining on the RT tensile ductility (1050°C)

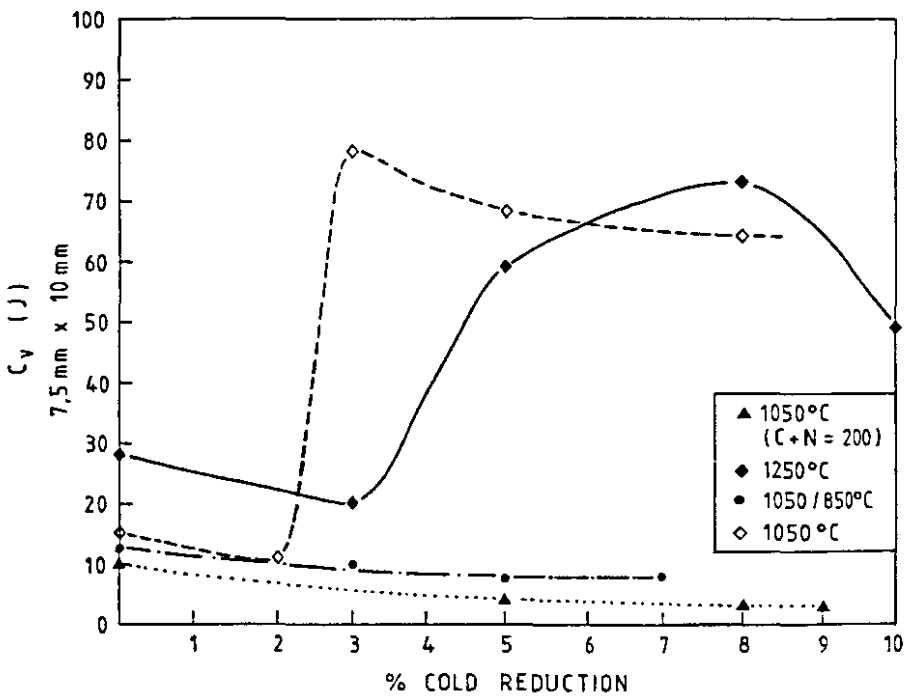

FIGURE 4.19 Effect of pre-straining on the RT impact toughness

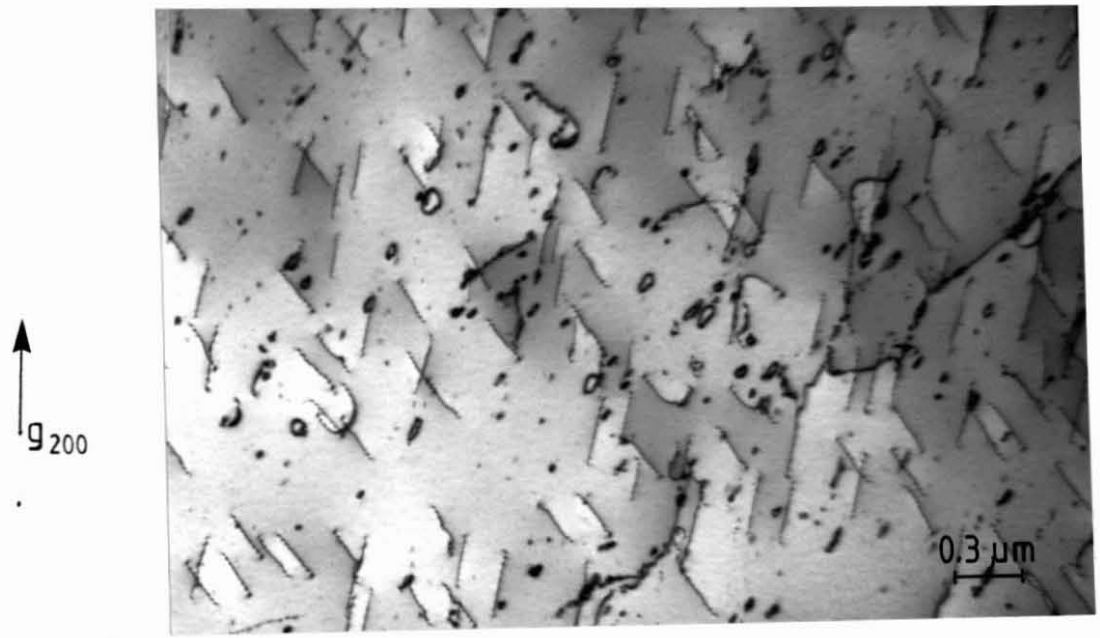

(a)

(b)

FIGURE 4.20 Effect of pre-straining on microstructure

(a) Uniform dislocation density
(b) Strain gradients at inclusions and grain boundaries (1050°C; 5% Cold Reduction)

4.3.2 Comment

From consideration of Figures 4.9 and 4.10, the overall effect of the isothermal heat treatment cycles may be summarised as follows:

(1) Quenching from the higher 1250°C SHT temperature reduces the tensile ductility and increases the strength and hardness as compared with material quenched from 1050°C;
(2) The absolute toughness, as measured by the impact energy, is improved by the higher SHT. Increased upper and lower shelf energies are achieved despite a concomitant increase in the macro-ferrite grain size, although the ITT is increased;
(3) Ageing at the intermediate 850°C temperature prior to solution annealing causes a small reduction in strength and ductility, which is accentuated in the case of the higher SHT, and a pronounced improvement in the impact toughness as compared with the single-stage SHT. The 1250°C treatment yields the greater absolute toughness, as well as the maximum reduction in the ITT;
(4) Ageing at 850°C subsequent to solution annealing causes the greatest depression in the yield strength, UTS, and hardness, and enhances the tensile ductility. However, the impact resistance is impaired, as reflected by a reduction in the shelf energy and an unfavourable shift in the DBTT.

Study of the microstructures following heat treatment suggests that the above results may be interpreted in terms of two parameters, these being the precipitation effects and the dislocation distribution. Several preliminary observations may be made:

With reference to Figure 4.12, material quenched from the SHT temperature, without the benefit of ageing, forces intragranular precipitation. This adversely affects the tensile ductility, ostensibly by a dispersion hardening effect. This becomes more pronounced at the higher SHT temperature where the greater solubility of the interstitials at 1250°C provides an increased driving force for relief of super-saturation on cooling. This is characteristic of the high temperature embrittlement phenomena noted in Section 2.2.3. In the case of the LI alloy under investigation,

however, the enhanced intragranular precipitation does not impair the impact toughness.

The occurrence of intragranular precipitation is countered by ageing, but the operative mechanism appears to differ qualitatively in the cases of prior and post-ageing. Given the absence of increased precipitation at the grain boundaries of higher misorientation, prior-ageing must somehow increase the solubility of the solutes, thereby limiting precipitation on cooling. The agency whereby this is accomplished is suggested by the increase in the dislocation area in the form of sub-arrays. This is given attention at a later stage. Post-ageing, on the other hand, serves to remove the intragranular phases by re-precipitation at energetically more favourable sites, notably the grain boundaries.

In all cases, heat treatment results in the formation of a grain-boundary deposit. Ageing at 850°C following SHT causes coarsening of the grain boundary precipitate, as shown in Figure 4.11, with a concurrent loss of toughness. The fact that the restoration of toughness, by subsequent re-annealing and quenching from 1250°C, is accompanied by a refinement of the grain boundary phase suggests the central role of the grain boundary phase in the fracture process.

It is possible to distinguish between embrittlement by the intragranular and the grain boundary precipitation respectively. The maintenance of good toughness by material quenched from SHT, despite a continuous grain boundary film as revealed by the TEM micrographs in Figures 4.12 and 4.14, indicates that brittle fracture at high strain rates is more directly related to a critical particle dimension, in agreement with the theory outlined in Section 2.4. This is supported by the observation that an increase in the interstitial levels causes a loss of toughness, commensurate with a greater degree of precipitation, both intragranularly and at the grain boundaries, and the attainment by a larger proportion of particles of the critical particle dimension. Since coarsening appears to occur mostly intergranularly, the effect of the grain boundary precipitates outweighs that of the finer intragranular particles.

At lower strain rates the coarsening of the grain boundary phase actually favours the overall ductility. Indeed, it is clear from Figures 4.12 and 4.14 that the grain boundary regions are active as dislocation sources, and evidently function as primary dislocation sources during macro-straining of the alloy.

The dependence of the impact resistance on the particle size is also reflected by the shapes of the impact transition curves in Figure 4.9. The occurrence of the coarse grain-boundary precipitates results in a decrease of the slope of the curve and a diffuse ductile-brittle regime. This was anticipated by Petch (Section 2.4) based on the limited degree of strain which the metal could sustain prior to achieving the cleavage strength by work-hardening. The studies elaborating the effect of pre-strain on the impact resistance make it clear that the coarse particle material shows little tolerance towards plastic deformation. It is important to note that in all cases pre-straining initially leads to a loss of cleavage resistance. Figure 4.19 shows the drop in the toughness following small amounts of deformation, which can be ascribed to the assisted initiation of flaws by the cracking of the particles ahead of blocked slip bands. Following the Petch model, the cleavage strength increases in proportion to the (carbide thickness)$^{-\frac{1}{2}}$. Thus initially, both the fine and coarse particles see an increase in the cleavage strength which is less than the increase in the constrained flow stress, so allowing attainment of the cleavage stress. At larger pre-strains, the fine particle material shows a relatively greater increase in the cleavage fracture stress, resulting in ductile failure.

The contribution of the heat treatment cycles to plastic flow may also be examined in terms of the dislocation dynamics. For the present it is sufficient to note that an increase in the dislocation density can account for improved toughness, as demonstrated by pre-straining. Study of the microstructures in Figures 4.12 through 4.17 establishes several sources of dislocations, viz:

(1) Dislocations introduced by warm-working and recovery, which occur as sub-arrays in low-angle boundaries;
(2) Prismatic dislocations typically associated with secondary phases;
(3) Small dislocation loops, which trail the larger matrix dislocations.

In addition, clustering of point defects as a result of the quenching process may be expected to give rise to dislocation loops within the matrix.

Recovery at 850°C prior to SHT diminishes the driving force for recrystallisation at SHT temperature and results in a remnant dislocation substructure, manifested optically as veining. This establishes two important considerations, which are mentioned here but will be discussed in following sections. The first is the obvious possibility of the sub-boundaries acting as both dislocation sources and obstructions to plastic flow. The second concerns the enhanced solution and rapid transport of solutes via the dislocation sub-structures, as shown by inter alia Stumpf (1968) and Angers et al (1987). Conditions therefore exist for depletion of matrix solutes by segregation to the dislocation cores, which would allow for a lesser degree of supersaturation and diminished precipitation.

In general, the solutionised alloys have a low density of dislocations, probably as a result of the increased flow stress brought about by the intragranular precipitation. The absence of a distinct yield point and the minimal influence of quench-ageing at 150°C to induce Cottrell locking testify, firstly to the sparsity of dislocations, and secondly to their high stability and impotency in aiding the plastic flow process.

By contrast, material aged prior to SHT is often characterised by linear arrays of mobile dislocations in close association with the globular inclusions. The absence of these dislocations in the post-aged material indicates that they are the product of the cooling process from the higher temperature. The generation of these dislocations by differential thermal expansion effects is developed in Section 4.5.

The formation of the smaller loops in the wake of the larger dislocation segments has been adequately described by Hull (1975) in terms of debris derived from the pinching off of dipoles, and edge jogs on screw dislocations. The absence of these loops in undeformed areas clearly points to their origin at the moving dislocations. One mechanism by which these loops may form is by the diffusion and coalescence of vacancies formed at a moving jog. Alternatively a dislocation dipole, formed by the interaction of dislocations on parallel slip planes, may break up and lower its overall energy by forming smaller loops.

The derivation of loops from super-saturation of point defects during the quenching process remains a point of some conjecture. While no such loops were identified, these may have been beyond the working resolution of the microscope. The role of the small loops is not clear except in so far as they raise the total dislocation density.

4.4 Fe-40Cr ALLOYS WITH HIGH INTERSTITIAL LEVELS

4.4.1 Results

Analysis of the precipitation effects in Fe-40Cr base alloys was carried out by subjecting high interstitial alloys to heat treatments parallel to those performed on the low interstitial alloys. This had two advantages:

- Microstructural development could be enhanced, allowing the characterisation of the excess phases;
- The effect of C and N could be studied by varying the respective levels independently.

Samples were taken from high carbon and high nitrogen melts HC (C+N=730+50 ppm) and HN (C+N= 100+600 ppm), which represent order of magnitude increases in the carbon and nitrogen levels over those of the low interstitial alloys.

4.4.1.1 Mechanical Properties

The variation of the RT tensile properties of the high carbon alloy is shown in Figure 4.21. The high nitrogen alloys failed in a brittle manner under tension.

The alloys exhibited a negligible RT impact toughness, and were brittle to well above 100°C in all cases.

The Vickers hardness values are given in Table 4.3. The values of the low interstitial alloy are included for purposes of comparison.

TABLE 4.3 Test Results: Vickers Hardness of High Interstitial Alloys:

Cycle	Heat Treatment	HV_{50} Low Interstitial	HV_{50} High Carbon	HV_{50} High Nitrogen
1	1h 1050°C	206	197	293
2	1h 1250°C	224	213	304
3	1h850/1h1050°C	212	193	305
4	1h850/1h1250°C	228	210	320
5	1h1050/1h850°C	187	190	211
6	1h1250/1h850°C	190	201	208

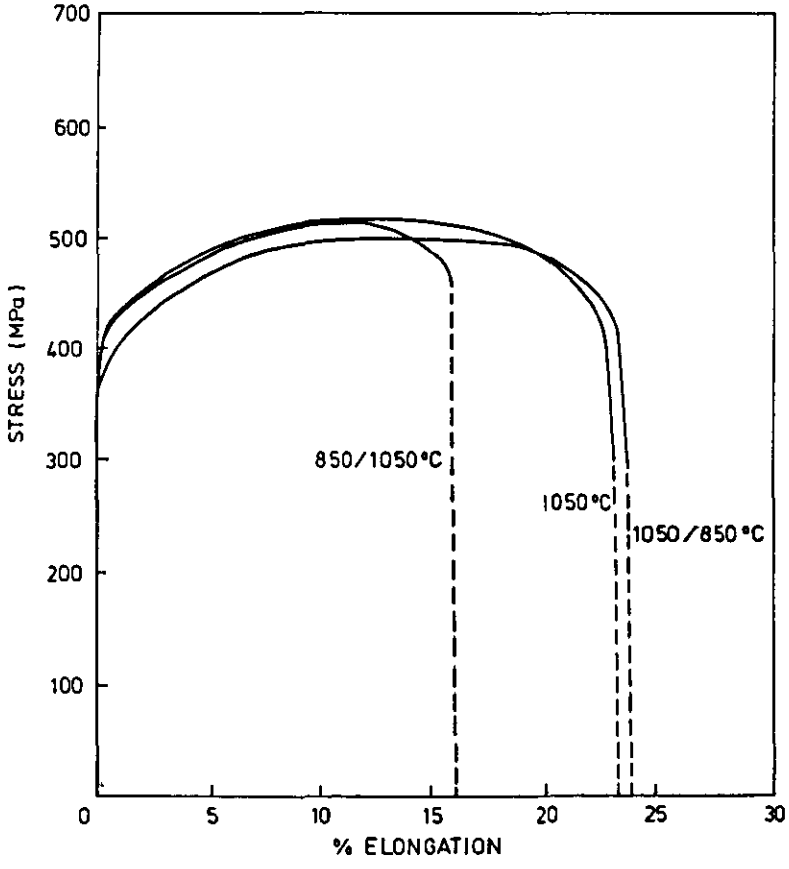

FIGURE 4.21 Tensile characteristics of the high carbon alloy

4.4.1.2 Microstructure

HIGH CARBON ALLOY

A selection of optical micrographs is shown in Figure 4.23. The following observations are made:

1. Figure 4.23(a) shows the alloy in the as-wrought condition. Long stringers of idiomorphic precipitates form a network aligned in the rolling direction. It is clear from Figure 4.23(b) that these stringers persist after solution annealing at 1050°C. The grain morphology appears unaltered after the 1050°C anneal, but a fine dispersion of precipitates occurs intragranularly.

2. Following solution annealing at 1250°C, the blocky precipitates are completely dissolved. The matrix is characterised by a fine distribution of plate or needle-like precipitates, oriented on specific crystallographic planes. The grain boundaries have a continuous film, while precipitate-free zones (PFZ) occur in the adjacent regions [Figure 4.23(c)].

3. The net effect of ageing prior to solutionising is to refine the intragranular precipitation. The large needle-like precipitates are replaced by a fine, homogeneous distribution of particles. The grain boundary deposit and depleted regions persist [(Figure 4.23(d)].

4. Ageing of the 1250°C solutionised material results in a reduction in the intragranular precipitation density, evidently by coarsening of the larger precipitates.

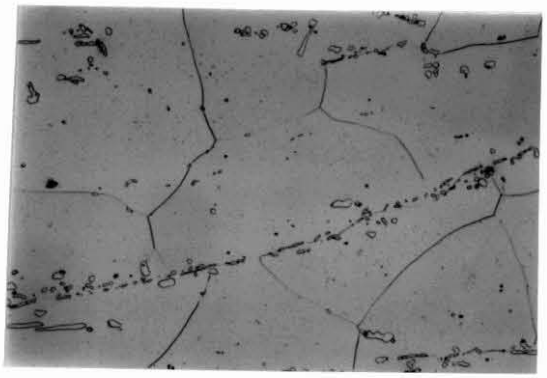

(a) As-wrought

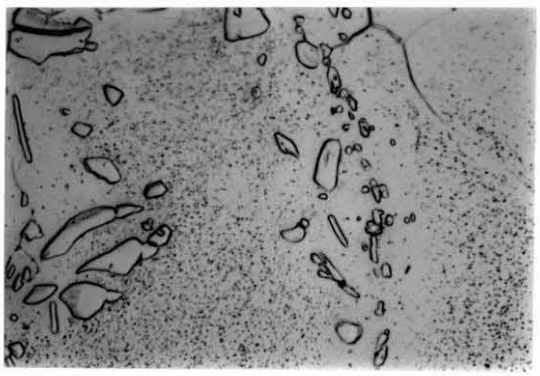

(b) 1050°C

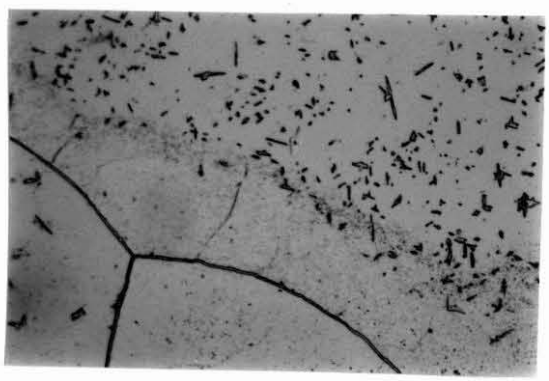

(c) 1250°C

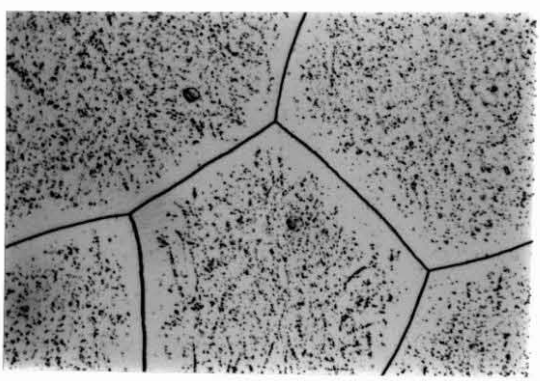

(d) 850/1250°C

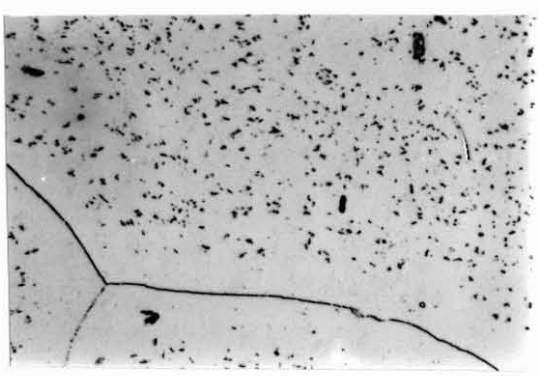

(e) 1250/850°C

50 μm

FIGURE 4.23 Microstructure of the high carbon alloys - Solution A

Acompanying SEM micrographs to the optical micrographs in Figure 4.23 are shown in Figure 4.24. The precipitates are shown in relief following selective etching. The following is noted:

1. The stability of the idiomorphic structure relative to grain boundary precipitation is demonstrated in Figure 4.24(a), which shows no grain boundary precipitate in the region of the blocky precipitates.

2. The precipitate morphology and crystallographic habit is shown in Figure 4.24(b). Examination of the precipitates in the aged material shows that ageing refines the occurrence of the precipitation, without modifying the precipitate morphology.

3. In the case of the prior-aged alloy the precipitates may be seen precipitating intragranularly in association with the sub-boundaries. [Figure 4.24(c)].

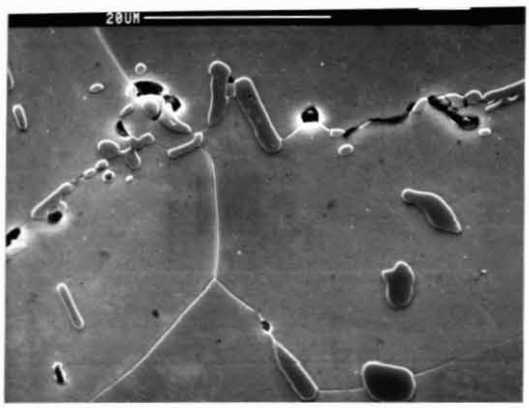

(a) 1050°C

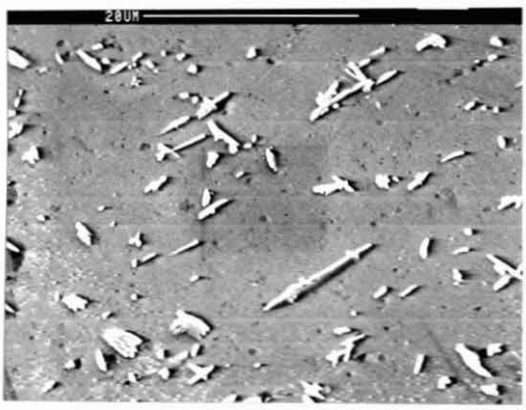

(b) 1250°C

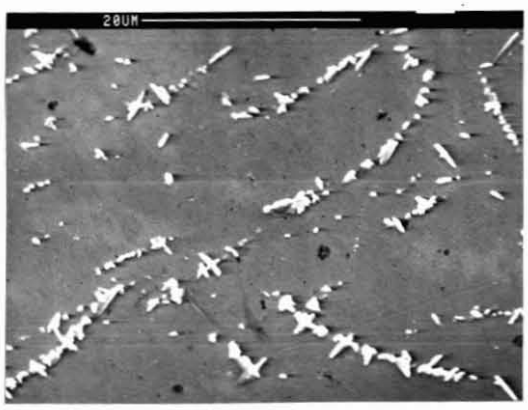

(c) 850/1250°C

FIGURE 4.24 SEM micrographs of etched high carbon alloys - Solution A

The microstructures studied by transmission microscopy are shown in Figures 4.25 to 4.26.

1. 1050°C Anneal:

The idiomorphic precipitates noted optically may be seen in Figure 4.25. Only partial recovery is effected and the action of the particles in stabilising the sub-boundaries is shown.

2. 1250°C Anneal:

The nature of the precipitated phases is modified as follows by the higher SHT temperature:

- The blocky phase is replaced by plate-like precipitates established on specific crystallographic axes as shown in Figure 4.26. This is typical of the Widmanstätten morphology characteristic of rapid precipitation from super-saturated solid solution. It is pertinent to note that the plates are generally associated with dislocation activity. These dislocations may be derived from a loss of coherency with the matrix during growth, and/or thermal stresses. In either event, the particles may act as sources of misfit dislocations.

- The matrix sustains fine intragranular precipitation. The depletion of these precipitates around dislocations decorated by precipitates in parallel orientation, and regions of plate precipitation is shown in Figure 4.26. Strain fields indicated by lines of no contrast normal to the g-vector, are evident around the smallest of these particles, which points to them being partially coherent initially.

- Heavy precipitation occurs at the grain boundaries. The plate-precipitates are absent in the grain boundary regions, but the incidence of the fine intragranular precipitation is unaffected to within less than 0,5 microns of the grain boundaries. The phase forms as separate grains, some of which show plate growth into the ferrite matrix.

3. Ageing 850°C/1250°C Anneal:

It is difficult to establish at the micro-level whether the distribution of the plate-like and intragranular precipitation is altered by the prior-ageing treatment. Both the plate and fine precipitates occur, and a high density of decorated dislocations are present.

4. 1250°C Anneal/Ageing 850°C:

Ageing of the SHT alloy eliminates the fine intragranular precipitation. The plate precipitates persist, as does the heavy grain boundary deposit.

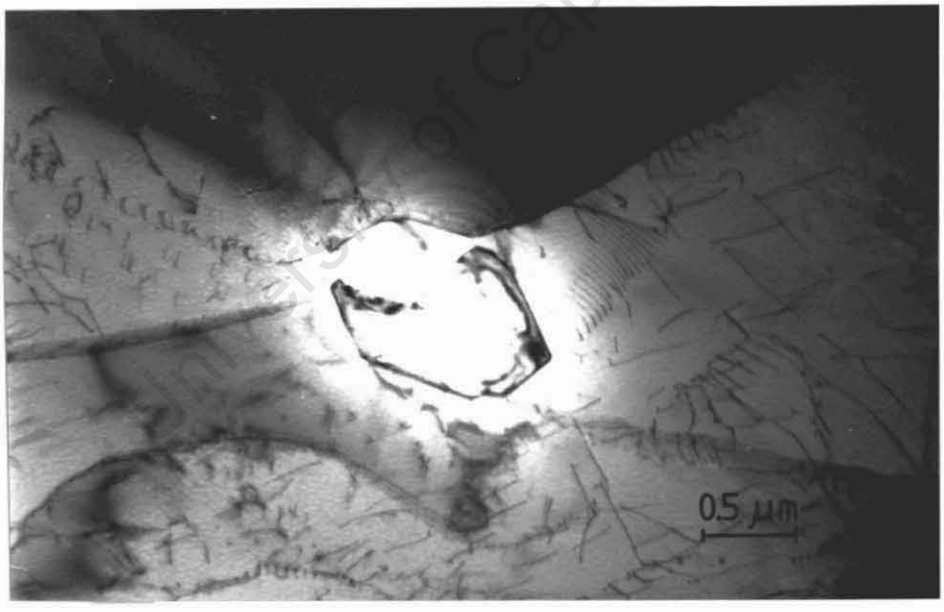

FIGURE 4.25 Idiomorphic carbides associated with pinning of the sub-structure (1050 °C)

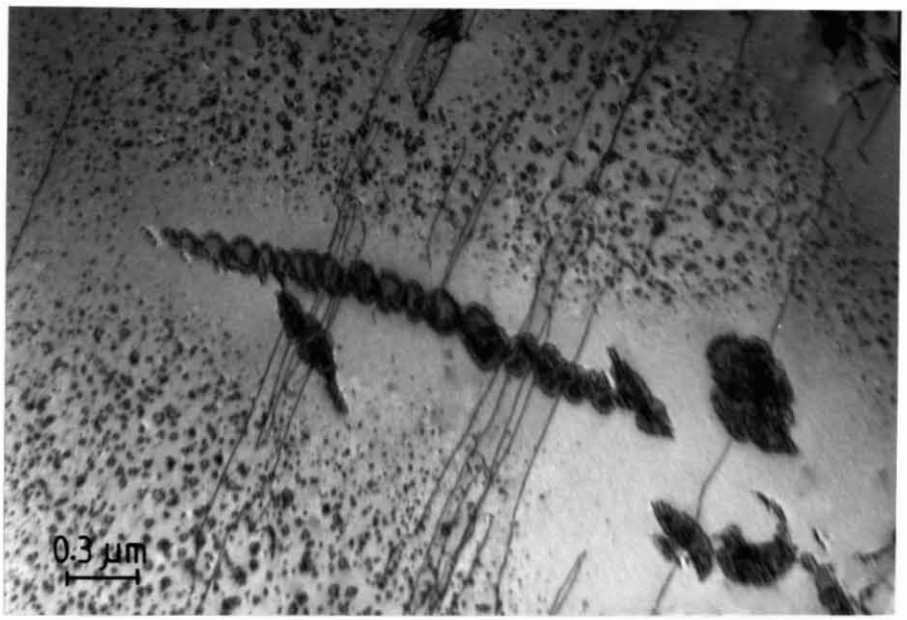

(a)

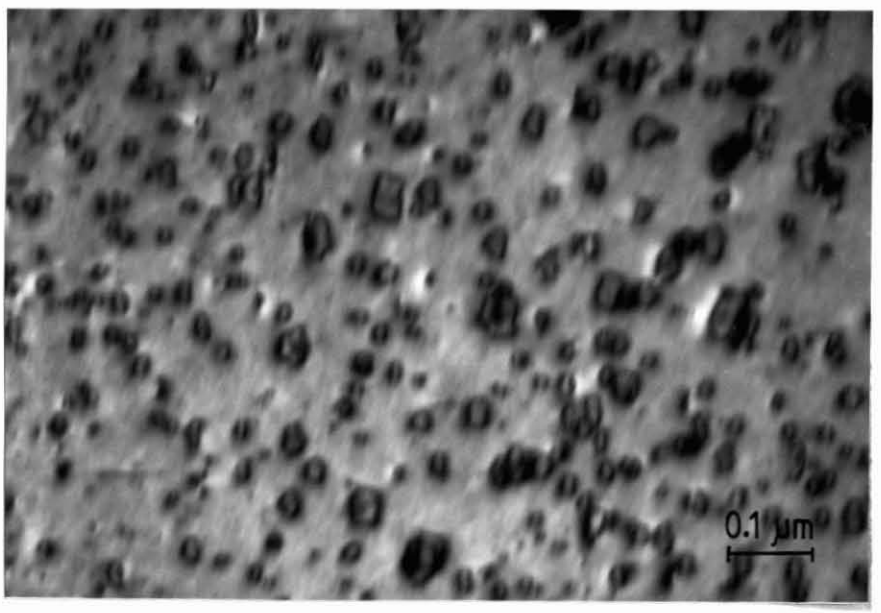

(b)

FIGURE 4.26 Intragranular precipitation in high carbon alloys (1250°C)

(a) Decorated precipitation sites showing PFZ
(b) BF Image of homogeneous precipitation

FIGURE 4.26 (c) Widmanstatten plate carbides, associated with precipitate-free zones and high dislocation density

FIGURE 4.26 (d) Intergranular precipitation, showing "saw-tooth" or plate growth

HIGH NITROGEN ALLOY

The precipitation effects in the high nitrogen alloy were studied by optical and transmission electron microscopy for:
(1) The solutionised condition;
(2) The post-aged conditions.
The occurrence of any precipitation was largely beyond the working resolution of the optical microscope.

The results of the transmission electron microscopy may be summarised by inspection of Figures 4.27-4.28:

1. 1250°C Anneal:

   Precipitation takes the form of a dense distribution of precipitates which occur preferentially at dislocations. Under two-beam diffracting conditions they appear as a homogeneous dispersion of fine strain centres.

2. 1250°C Anneal/Aged 850°C

   Following ageing, the precipitation is manifested as coarse plates aligned on the cube planes and a heavy grain boundary deposit. The plate precipitates are associated with a high degree of dislocation activity, which appears to indicate a loss of coherency with the matrix. The aged alloy also contains precipitates which appear to be multilayered, and have parallel habits. Figure 4.28(b) shows two such precipitates. The smaller precipitate, shown out of contrast, clearly shows the line of precipitation on a dislocation.

FIGURE 4.27 Intragranular precipitation in solutionised high nitrogen alloy, showing fine, homogeneous strain centres and decorated dislocations (1250°C)

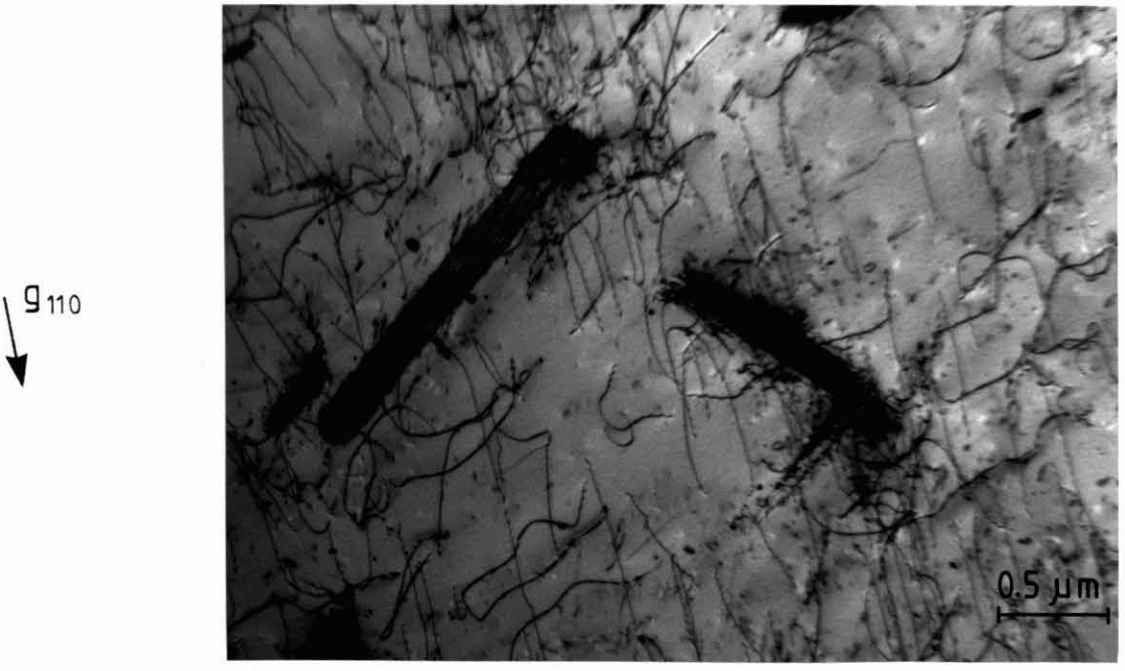

FIGURE 4.28 Precipitation in post-aged high nitrogen alloy (1250/850°C)
(a) Nitride plates, showing localised plastic strain

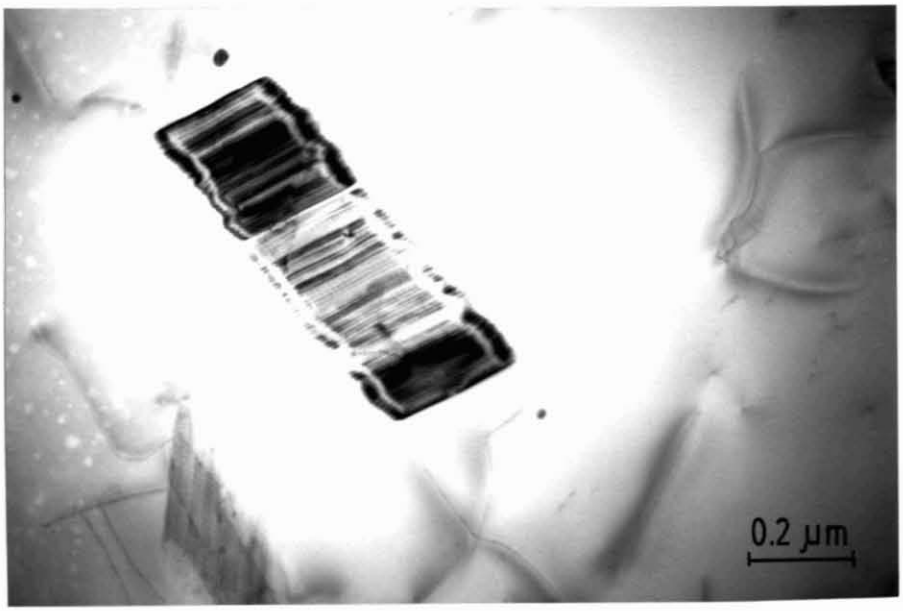

FIGURE 4.28(b) Multi-planar nitride plate precipitates (1250/850°C) (Cont)

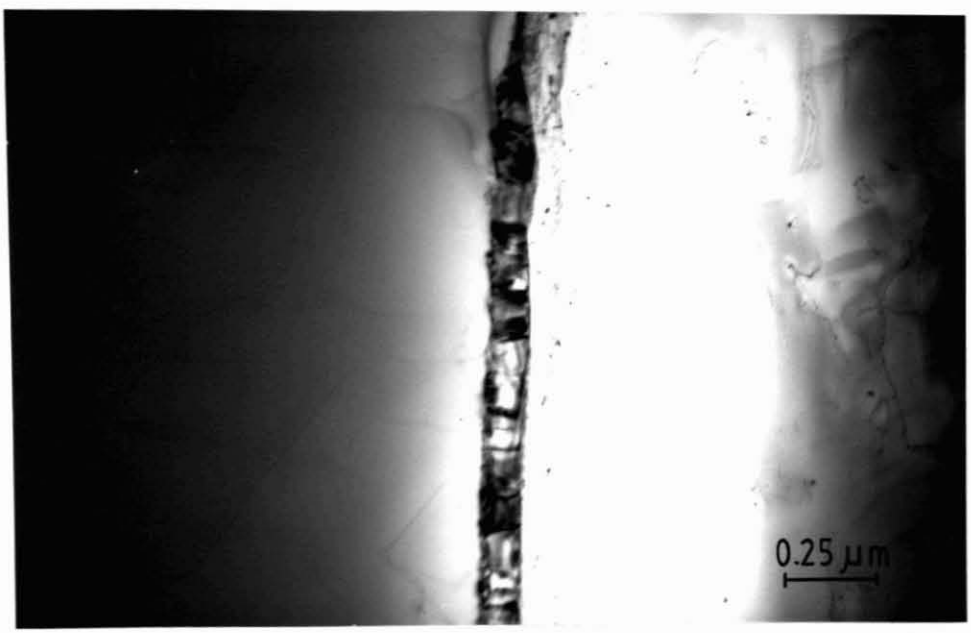

FIGURE 4.28(c) Grain boundary phase in post-aged high nitrogen alloy (1250/850°C)

4.4.1.3 Identification of Secondary Phases

The results of selected area diffraction analysis are shown in Figures 4.29 and 4.30.

HIGH CARBON ALLOYS

1. Idiomorphic carbides:

The polygonal precipitates are characteristic of the alloys annealed at 1050°C, and were also identified in the low interstitial alloys aged at 850°C. The multigranular nature of the precipitates is shown in Figure 4.29(a). The diffraction pattern yields a f.c.c. structure, with lattice parameter 10,69A, consistent with chromium carbides of the $M_{23}C_6$ type and close to that reported by the ASTM Powder Diffraction file as a=10,638A° for $Cr_{23}C_6$.

2. Widmanstätten Carbides:

Analysis of the plate precipitates shown in Figure 4.26 gives a similar crystal structure to that of the idiomorphic carbides. A f.c.c. structure with lattice parameter 10,70A was determined. The diffraction pattern reflects a cubic orientation relationship (OR) with the matrix, calculated to be:

$$(1\bar{1}1)_{M_{23}C_6} \;//\; (10\bar{1})_{\alpha}$$

$$[2\bar{2}\bar{4}]_{M_{23}C_6} \;//\; [\bar{1}3\bar{1}]_{\alpha}$$

This is in agreement with the OR for $M_{23}C_6$ with the ferrite reported by Kuo and Jia (Section 2.2.2).

3. Grain Boundary Carbides:

Two distinct grain boundary phases were identified, although these were morphologically similar:

All the annealing cycles resulted in the formation of $M_{23}C_6$, identified by the centred dark field image in Figure 4.29(c).

A second phase, the pseudo-hexagonal M_7C_3, was found in those alloys where the heat treatment had terminated in a quench from 1250°C. The phase was readily identified by characteristic streaking in the diffraction pattern, which has been explained in terms of stacking faults on and perpendicular to the basal plane by Beech and Warrington (1966). No evidence of the faulted M_7C_3 phase was found in alloys aged subsequent to solutionising.

4. Fine Intragranular Precipitation:

It was not possible to directly identify the fine, homogeneous intragranular phase. However, since no diffraction spots other than the parallel OR spots were detected in the matrix, it is assumed that these particles also exhibit the cubic $M_{23}C_6$ structure.

HIGH NITROGEN ALLOY

The diffraction pattern in Figure 4.30 was taken from the high nitrogen alloy aged subsequent to SHT and shows near coincidence of the precipitate spots with those of the matrix. The cubic parallelism is subject to some uncertainty following reports of precipitation of both the cubic CrN and the hexagonal Cr_2N in iron-chromium alloys by Bywater and Dyson (1975), and an intermediate phase with an atomic ratio between N/Cr : 1/4 and N/Cr : 1/2, studied by Woods and Ball (1973). However, the OR

$$(10\bar{1}0)_{Cr_2N} \;//\; (110)_\alpha$$

$$[\bar{1}100]_{Cr_2N} \;//\; [\bar{1}11]_\alpha$$

has been corroborated by the study of Bywater and Dyson for the precipitation of Cr_2N, which is in agreement with the phase diagram in Figure 2.2.

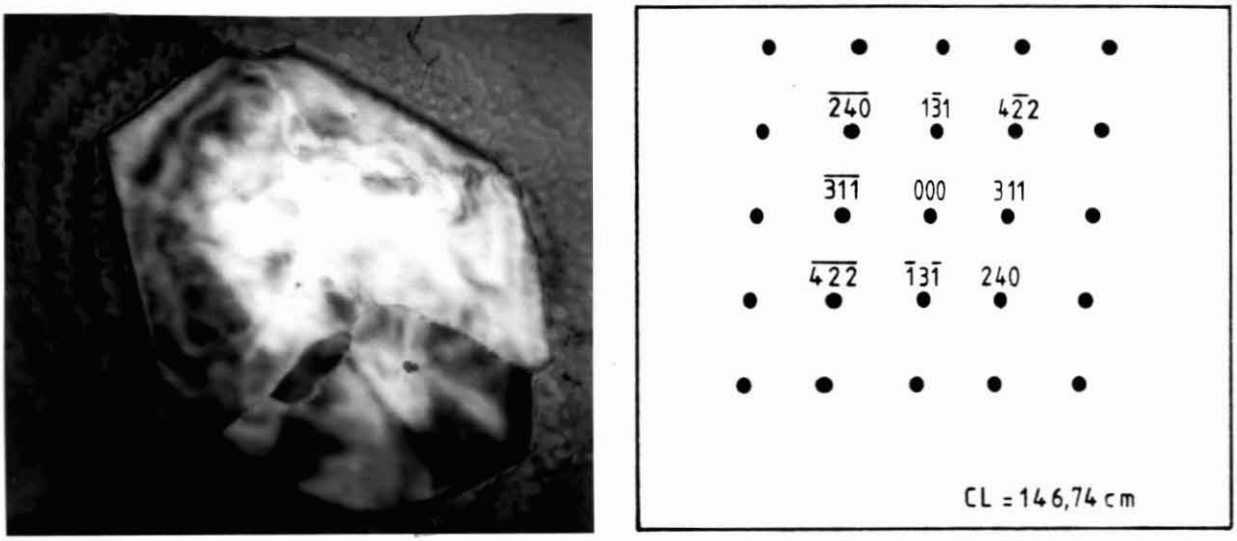

(a)

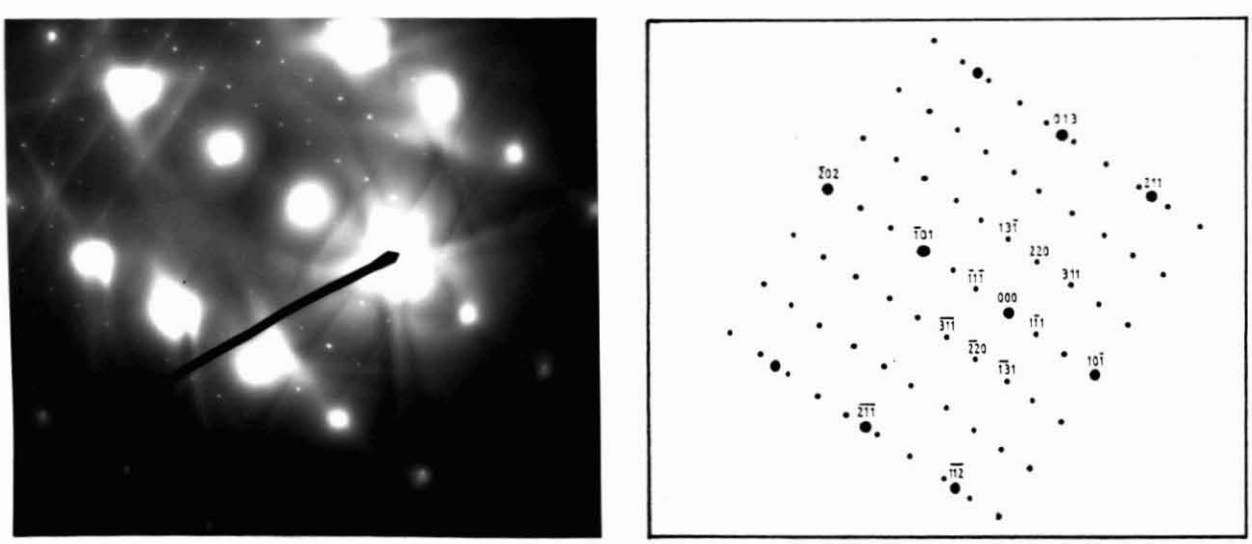

(b)

FIGURE 4.29 Analysis of carbides

(a) Idiomorphic carbides (1050°C)
(b) Widmanstatten carbides, showing parallel OR (1250°C)

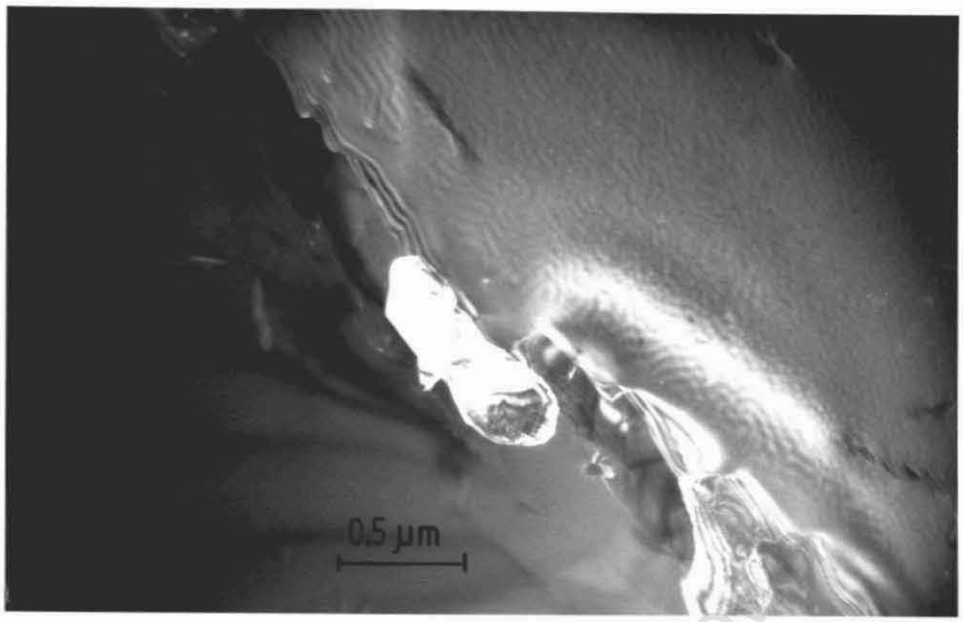

(c)

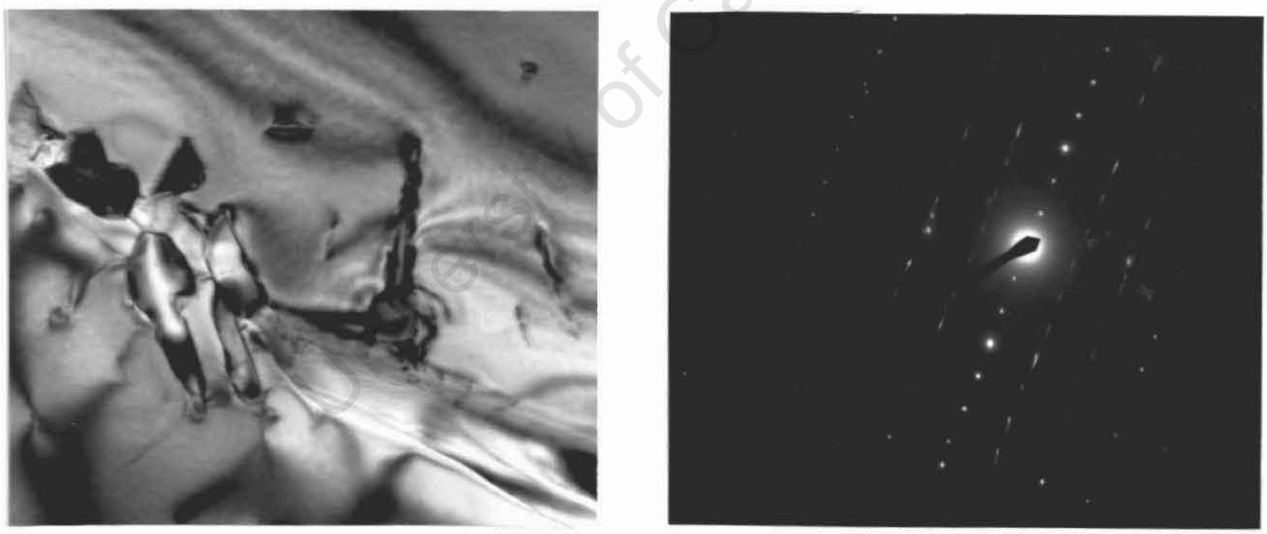

(d)

FIGURE 4.29 Analysis of carbides

(c) Centred DF image of intergranular carbide, identified as $M_{23}C_6$ (1250°C)

(d) Metastable M_7C_3 phase at grain boundaries. EDP shows streaking due to faults in the basal plane (1250°C).

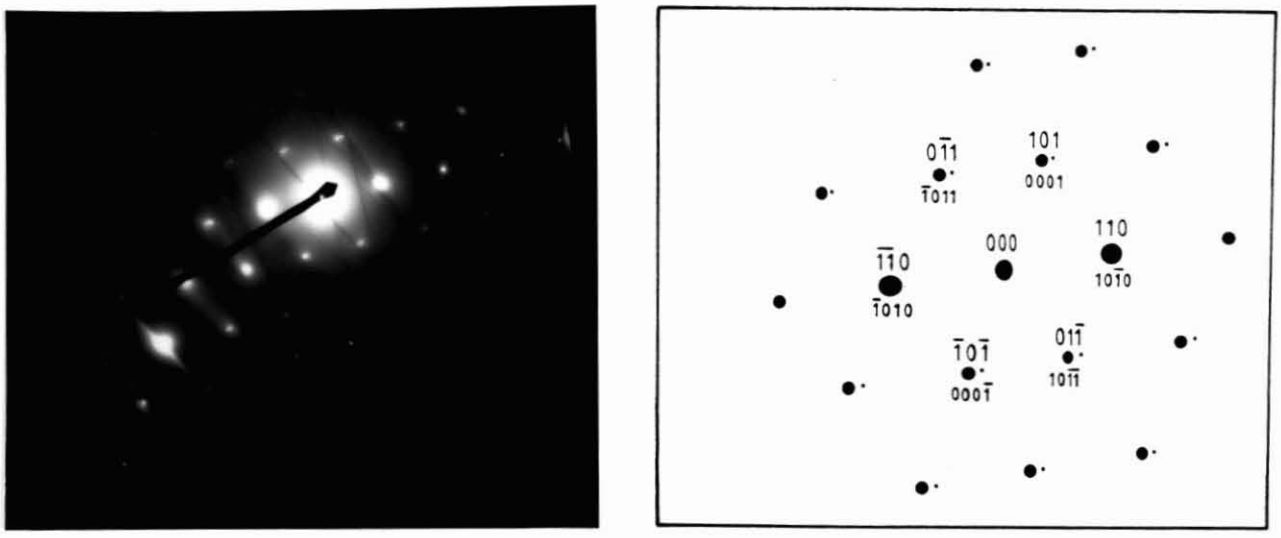

FIGURE 4.30 EDP of post-aged nitrogen alloy, showing coincidence of the plate precipitate reflections with those of the matrix. (1250/850°C).

4.4.2 Comment

Several important conclusions may be drawn from the preceding results. These may be summarised as follows:

(1) The plastic response of the Fe-40Cr alloy to the carbides differs in its response to that of the nitrides. An increase in the carbon content improves the overall tensile ductility, while nitrogen additions cause severe embrittlement;

(2) The tensile ductility is improved by coarsening of the second phase particles which promotes greater dislocation mobility. At the same time the particles become active as dislocation sources, partially as a result of a loss of coherency with the matrix;

(3) Quenching from greater degrees of supersaturation i.e. higher temperatures, change the nature of the precipitation;

(4) Prior-ageing to induce a substructure increases the nucleation rate of precipitation.

With regard to the mechanical properties, the above study has shown that strengthening of the ferritic matrix as a result of interstitial solutes is due primarily to the addition of nitrogen. While the strengthening due to nitrogen may be the result, in part, of solid solution hardening [Bell and Kumar (1978)], the present results support the finding of Leitch and Ball (1979) that the principal hardening mechanism in ferritic stainless steels is the precipitation hardening by small coherent nitride precipitates, whose strain fields cause a corresponding increase in the matrix flow stress. Ductility is restored by coarsening of the nitrides to form incoherent precipitates, both intragranularly and at the grain boundaries. The improvement in ductility emanating from the larger carbide precipitates, on the other hand, may be ascribed to the increase in the number of local centres for the initiation of plastic slip under shear stress. The fact that softening in the high carbon alloy is achieved despite the intense intragranular precipitation refutes the argument for high temperature embrittlement by fine intragranular precipitation of carbides.

Significantly, ageing subsequent to SHT to relieve intragranular precipitation results in hardening relative to the low interstitial alloy, which supports the case for embrittlement by grain boundary precipitation.

In the case of both the carbides and the nitrides, coarsening improves the overall ductility. This is manifestly the result of the greater dislocation mobility, but from examination of Figures 4.26 and 4.28 the coarse particles also act as strain centres for plastic slip.

The resistance of the particles to plastic deformation once again differs between the carbides and nitrides. The reduction in strength with the higher volume fraction of large particles is accounted for by an increase in the void nucleation events at the particle/matrix interfaces. It was found by Grubb and Wright (1979) that the plate-like Cr_2N precipitates readily open up during plastic deformation, thus initiating micro-voids. On the other hand the high interfacial decohesion strength of carbide particles, reported by Kwon (1988) to be as high as 1200 MPa, accommodates substantial plastic strain before cavitation leading to ductile fracture. TEM studies by Ashbrook and Marder (1985) have shown that large carbide particles have a larger deformation zone surrounding them than small particles following small strains, and that particles on grain boundaries have particularly large deformation zones, which is in accord with the above results. The contribution of dispersions of particles to the work-hardening rate by the generation of secondary dislocations has been correlated with several theoretical models, notably by Jones (1973).

At high strain rates, the presence of brittle secondary phases is detrimental to the impact toughness on the basis of kinetic factors as discussed previously. The precipitates foster fast crack initiation sites, and the low surface energy of the plate-precipitates arrayed on the habit planes are particularly conducive to brittle-crack propagation. The fracture toughness therefore falls off with particle size and volume fraction as expected.

The study of the high interstitial alloys has also illustrated the microstructural response to the different annealing regimes,

particularly in the case of the high carbon alloy. It is apparent that the idiomorphic chromium carbides are stable at 1050°C, notwithstanding limited dissolution as evidenced by some intragranular precipitation in Figure 4.23(b). Higher temperatures, in this case 1250°C, are necessary to ensure effective dissolution of the carbides, which advances an explanation for the improvement in the impact toughness observed in the low interstitial alloy in terms of the efficacy of grain boundary carbide dissolution.

Quenching from the 1250°C SHT replaces the idiomorphic carbides with the quasi-equilibrium Widmanstätten morphology, and introduces a metastable carbide phase, both of which are stimulated by the high driving force for precipitation. Precipitation is also nucleated homogeneously in both the carbon and the nitrogen alloys, and is in all probability vacancy-controlled under the excess vacancy conditions generated by the high cooling rates. This gives rise to the fine, uniform dispersoid in the matrix.

As a consequence of the dispersion of carbides, recovery is retarded by the pinning of sub-boundaries. The formation of the recovered sub-structure has already been noted, but two further observations are worth recording. From observation of the precipitation on the sub-boundaries (Figure 4.24) it is evident that prior-ageing increases the nucleation rate of precipitation by increasing the number of heterogeneous nucleation sites, namely the sub-boundaries. This creates more particles per unit volume and refines the scale of precipitation; the precipitate morphology is left unaltered. With reference to Figure 4.21, the prior-aged alloy exhibits a reduction in total elongation as compared with the alloys in the SHT and post-aged conditions. The net effect of the sub-structure on the ductility therefore appears to be a reduction in the dislocation mobility.

Post-ageing provides the energy for diffusive processes and causes the coarsening, or Ostwald ripening, of the larger matrix particles and grain boundary precipitate at the expense of the fine homogeneous intragranular precipitates. At the same time energy is provided for the transformation of the metastable M_7C_3 type to $M_{23}C_6$ in the carbon alloy.

4.5 Fe-40Cr ALLOYS DOPED WITH SULPHUR

4.5.1 Results

The following results record the plastic response of Fe-40Cr alloys to local stresses set up at second phase particles. The possibility of increasing the mobile dislocation density by tessellated strains was motivated by observations of dislocation activity at sulphide particles in the low interstitial alloy. (Appendix B2). Controlled amounts of sulphur were introduced into the alloy to promote the formation of a distribution of sulphide particles. Sulphide control was studied in relation to the standard heat treatment cycles. Mechanical test specimens were sectioned from Melts SD1 and SD2, with sulphur levels three to four times the normal residual levels encountered in the high purity alloys.

4.5.1.1 Analysis of Sulphide Inclusions

Analytical transmission microscopy was conducted on the spheroidal inclusions, and a spectrographic trace is shown in Figure 4.31. Standardless semi-quantitative analysis showed the chromium and sulphur to be present in the proportions 63wt% and 37wt% respectively. This is consistent with chromium sulphides of the type CrS, reported by Kiessling (1978) to have a monoclinic structure.

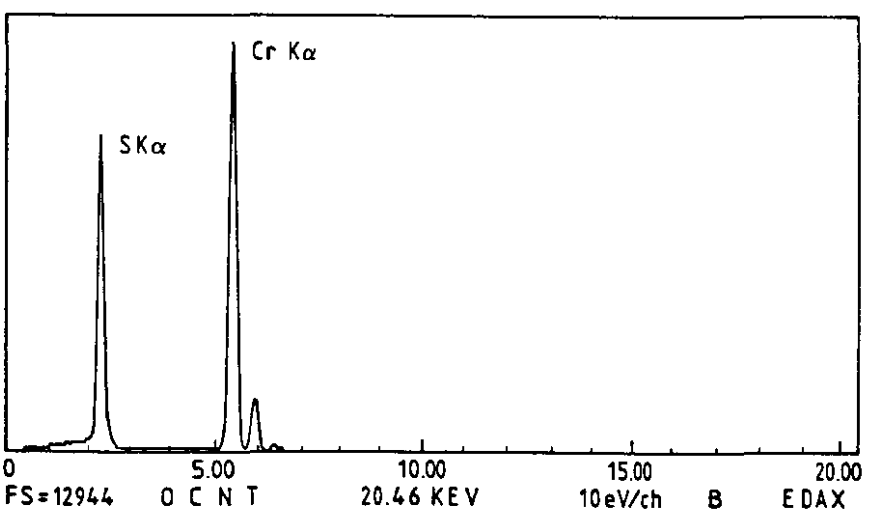

FIGURE 4.31 EDS trace of sulphide inclusions

4.5.1.2. Dislocation Generation by Prismatic Punching

ELASTIC ANALYSIS AT THE SULPHIDE/MATRIX INTERFACE

An elastic analysis of the stress distribution at the sulphide particles due to differential thermal contraction effects was performed based on the Brooksbank-Andrews model outlined in Section 2.6.

Brooksbank and Andrews have provided estimates of the thermal expansion coefficients and Young's Moduli of sulphides. The properties of the transition metal (Mn,M)S system were taken as an approximation to the behaviour of CrS.

The expansion coefficient of the Fe-40Cr alloy was measured by dilatometry and an average value over the 0-800°C temperature range was calculated, in keeping with the values quoted by Brooksbank and Andrews.

Based on values extracted from the literature, and summarised in Table 4.4, the interfacial stress profile was calculated by applying the equations in Table 2.3 (p56) over the temperature range 0-800°C.

TABLE 4.4 Properties of Sulphides and Matrix

Symbol	Magnitude	Source
α_1	18×10^{-6}	Brooksbank and Andrews (1972)
α_2	13×10^{-6}	By Experiment
ν_1	0,30	Brooksbank and Andrews (1972)
ν_2	0,28	Smithells (1976)
E_1	137,9 GPa	Brooksbank and Andrews (1972)
E_2	215,3 GPa	Smithells (1976)

From calculations performed by Brooksbank and Andrews, it appears that the stresses become small at a distance of one particle diameter from the interface (assuming that no yielding takes place

in the matrix). This they demonstrated by a photoelastic analogue. A similar effect may be shown by examination of a thin foil in the transmission electron microscope under highly diffracting conditions. The field of influence of the sulphide particle may be determined from the dynamic contrast effects, shown in Figure 4.32. It can be seen that the radius of influence is approximately one particle diameter in extent. Taking a mean particle size of 0,25 microns, the radius of matrix influence thus becomes 0.375 microns. In general the inter-particle spacing negates the possible interaction of inclusions in proximity.

Using Equation 7(a) in Table 2.3(a), the pressure in the inclusion, p, may therefore be calculated, and substituting into Equation 6(a) the maximum operative reduced shear stress is given by

$$F_2 = 1{,}285 \times 10^{-3}.(\Delta T)\ \text{GPa} \qquad (4.1)$$

The stress may be plotted as a function of the distance from the particle from

$$F_2 = 1{,}285 \times 10^{-3}.(\Delta T)(R^3_1)/(R^3)\ \text{GPa} \qquad (4.2)$$

This is shown in Figure 4.33. From a comparison of this data with the yield stress of Fe-40Cr, it is evident that tessellated stresses of sufficient magnitude to induce slip are generated at the CrS inclusion on cooling from 850°C and above.

EVIDENCE FOR PLASTIC YIELDING DUE TO COOLING STRESSES

Examples of stress relief at the sulphide interfaces by the formation of primary prismatic dislocation loops are shown in Figure 4.34(a). Figure 4.34(b) shows dislocation activity of considerable complexity around a particle where several slip systems are operating. In each case, residual debris may be seen in the wake of the dislocation loops.

Since there is clear evidence for plastic yielding at the inclusion interface, the elastic-plastic conditions become appropriate for residual stress analysis. In the present case this requires knowledge of the matrix yield stress at elevated temperatures and was therefore not undertaken. The elastic analysis therefore gives values regarded as maxima i.e. the theoretical interfacial stress at the unyielded interface.

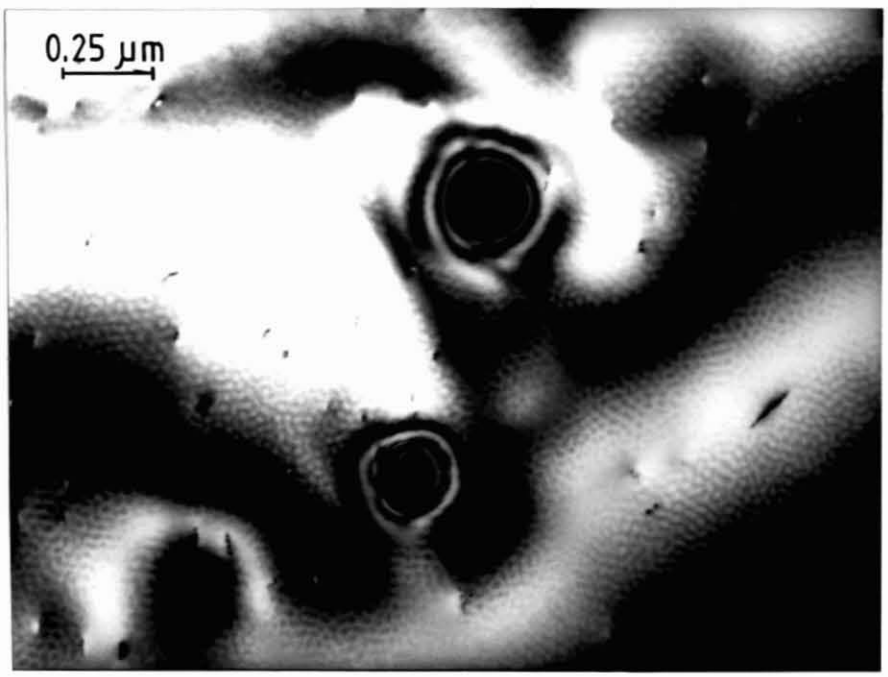

FIGURE 4.32 Stress field around sulphide inclusions, shown in 2-D under diffraction contrast in the TEM

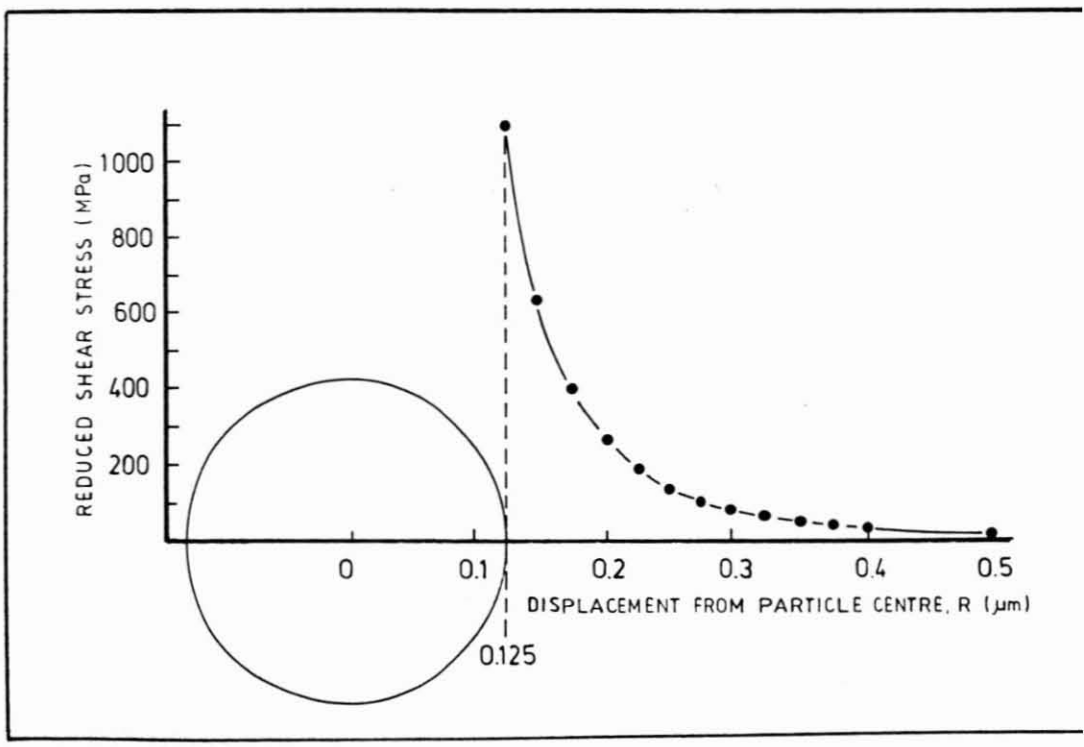

FIGURE 4.33 Calculated operative reduced shear stress around the sul spheroids in Fe-40Cr on cooling from 850°C

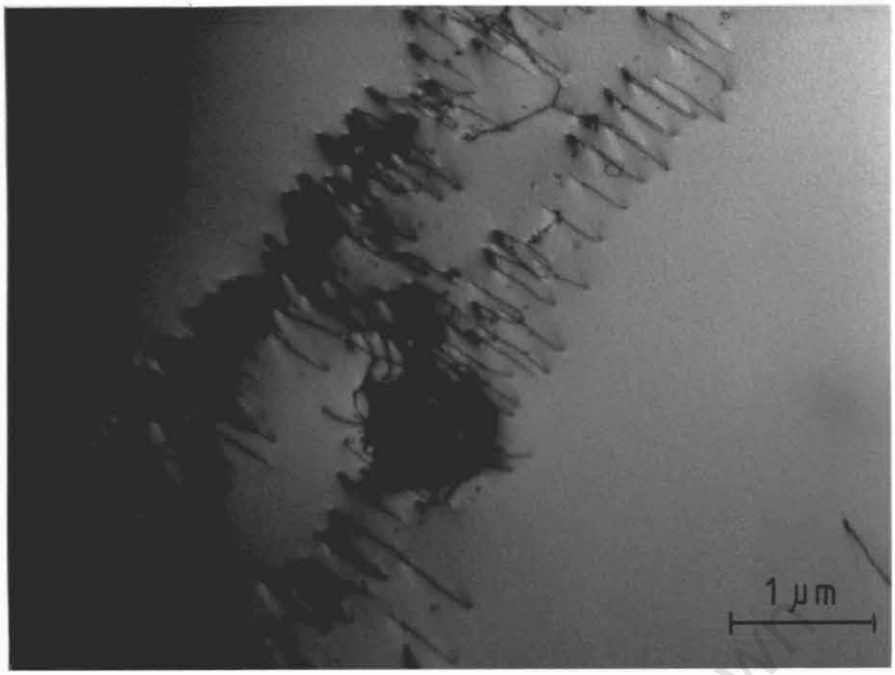

(a)

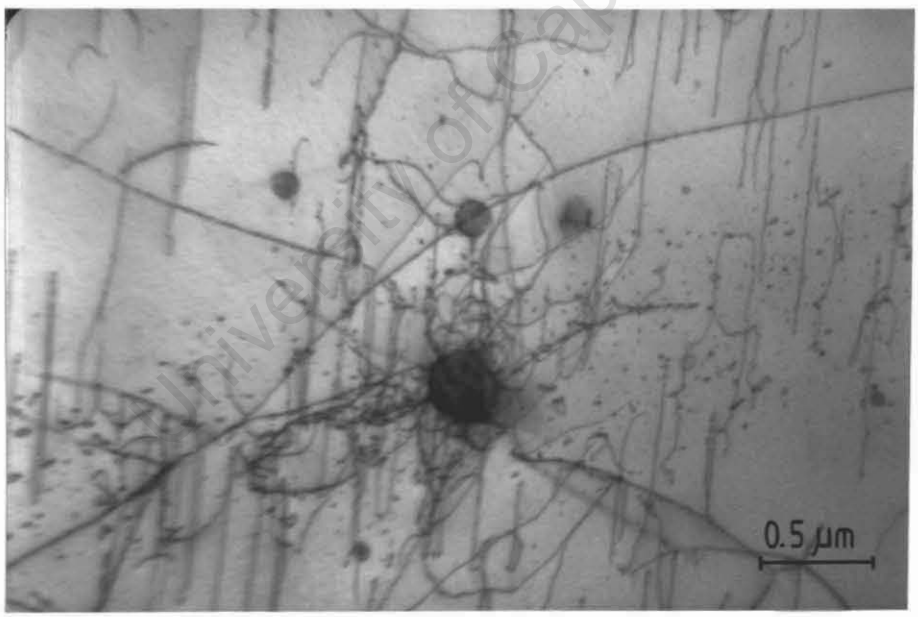

(b)

FIGURE 4.34 Plastic yielding at the sulphide particle/matrix interface 850/1050°C

(a) Prismatic punching of primary dislocation arrays
(b) Secondary slip on additional slip planes

4.5.1.3 Mechanical Properties

Tensile deformation curves for the high sulphur alloys following the various isothermal annealing cycles are shown in Figure 4.35. The results are summarised in Table 4.5, with the properties of the base alloy (LI) included for purposes of comparison.

The RT impact toughness is recorded in Table 4.6, while the dependence of the impact toughness on the sulphur content is shown in Figure 4.36 for full-size Charpy specimens.

TABLE 4.5 Test Results: Tensile Properties of Sulphur-Doped (SD2) Alloys, Compared with the Low Interstitial (LI) Base Alloy

Cycle	Heat Treatment	UTS (MPa)		0.2%PS (MPa)		%El		HV_{50}	
		LI	SD2	LI	SD2	LI	SD2	LI	SD2
1	1050°C	564	591	448	418	23	26	206	203
2	1250°C	568	536	494	484	19	3	224	334
3	850/1050°C	554	516	448	412	22	27	212	204
4	850/1250°C	560	505	474	420	15	18	228	193
5	1050/850°C	491	481	321	374	26	29	187	190
6	1250/850°C	460	463	367	397	21	27	190	204

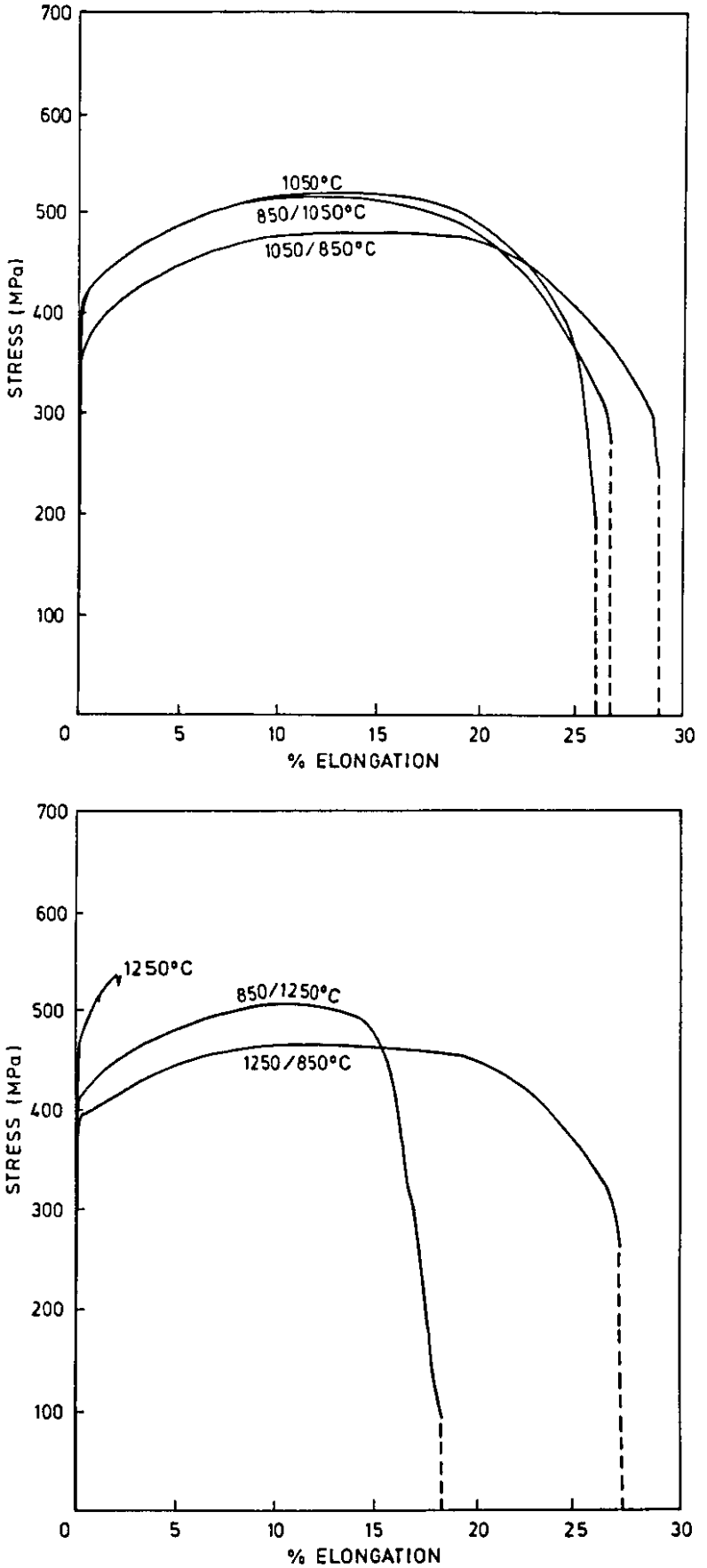

FIGURE 4.35 Tensile characteristics of sulphur-doped alloys

TABLE 4.6 Test Results: RT Impact Toughness of Sulphur-Doped Alloys

Cycle	Heat Treatment	Cv (J/cm^2) LI	SD2
1	1050°C	8	76
2	1250°C	35	38
3	850/1050°C	13	84
4	850/1250°C	79	9
5	1050/850°C	17	12
6	1250/850°C	35	14

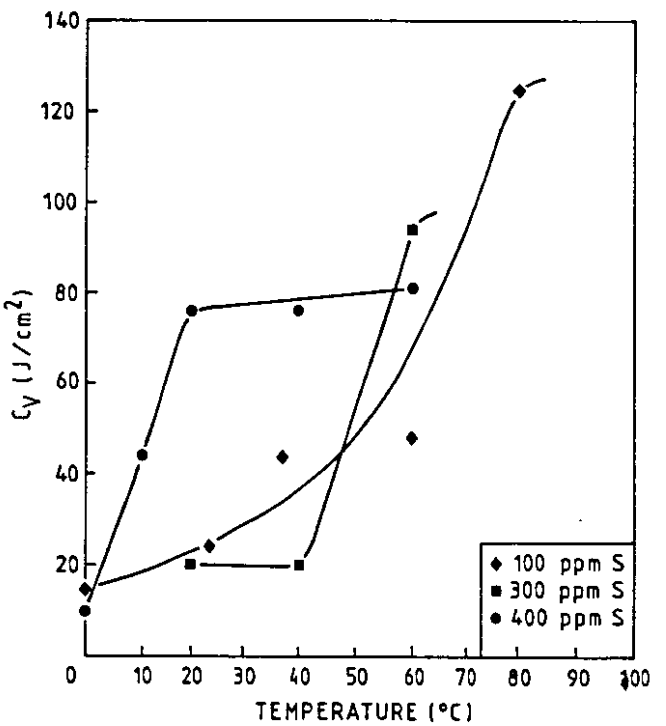

FIGURE 4.36 Impact toughness as a function of sulphur content

4.5.1.4. Fractography

The fracture modes of a selection of impact specimens was studied in the SEM, and are shown in Figure 4.37.

The tough material, obtained by ageing prior to 1050°C, exhibited bimodal fracture, with a diminishing transgranular cleavage component in favour of ductile tearing, as shown for the 850/1050°C alloy fractured at RT.

The fracture surface of the 1250°C specimen showed a brittle mode of failure, with large cleavage facets indicative of the grain size. A significant number of inter-granular facets was featuristic of this material, but note should be taken of the substantial component of dimpled surfaces normal to the fracture plane, indicating "intergranular ductile failure" (IDF).

Fracture of the 850/1250°C treated material showed lamellate fissure, characteristic of wrought alloys with a directional structure.

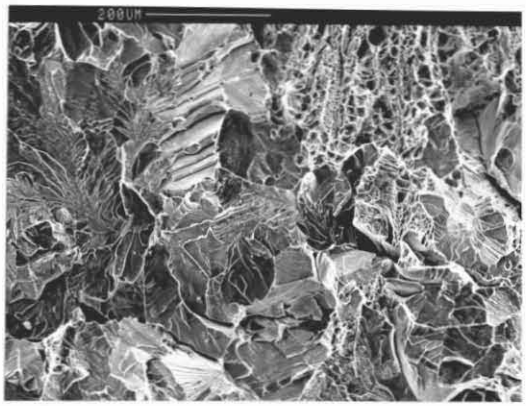

(a)

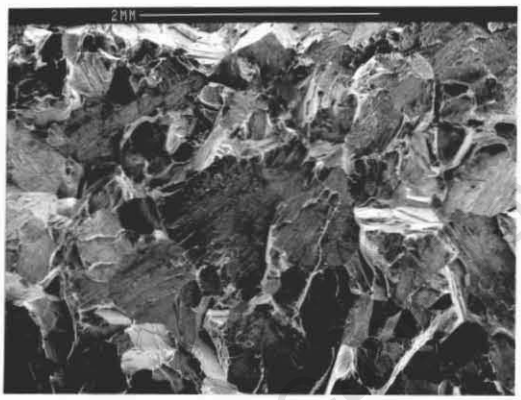

(b)

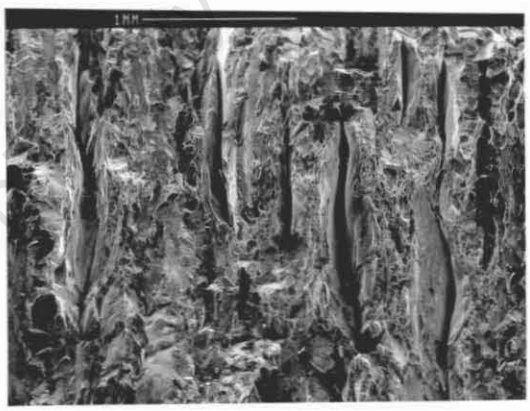

(c)

FIGURE 4.37 Fracture mode of sulphur-doped alloys

(a) 850/1050°C - Cleavage & ductile tearing
(b) 1250°C - Intergranular fracture sites
(c) 850/1250°C - Lamellate fissure

4.5.1.5 Microstructure

OPTICAL MICROSCOPY

A selection of polarised light micrographs relating the grain morphology to heat treatment is given in Figure 4.38.

1. Material receiving a simple SHT showed a fine equiaxed ferrite structure, with rapid grain growth occurring at 1250°C.

2. Ageing at 850°C prior to 1050°C once again resulted in a pronounced subgrain structure. Ageing prior to 1250°C resulted in a coarse pancake structure, with grain growth inhibited in the through-thickness direction. (Figure 4.38(e)).

3. Ageing subsequent to SHT left the grain structure unaffected, but led to enhanced grain boundary precipitation.

TRANSMISSION-ELECTRON MICROSCOPY

Transmission electron microscopy of the high sulphur alloy elicited the following features, shown in Figures 4.39-4.40.

1. Aged 850°C/Annealed 1050°C

   The tough material contained a large number of spheroids associated with arrays of dislocation loops aligned in the 111 slip directions. The spheroids occurred over an extremely narrow size range, being of the order of 0,25-0,5 microns in diameter. By tilting through exaggerated angles for diffraction contrast, most of the spheroids were shown to be sources of dislocation activity, ranging from primary loops to tangled and complex slip processes. Regions of the alloy showed only partial recrystallisation, and the spheroids could be observed pinning the sub-boundaries. Only a thin film of precipitate was seen to occur at the grain boundaries.

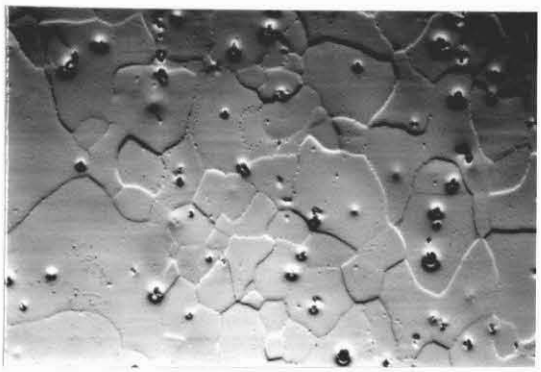

(a) 1050°C

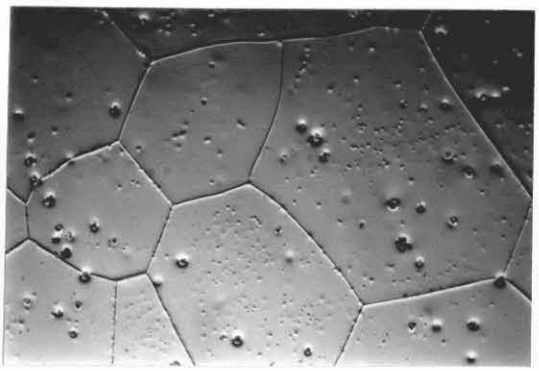

(d) 1250°C

(b) 850/1050°C

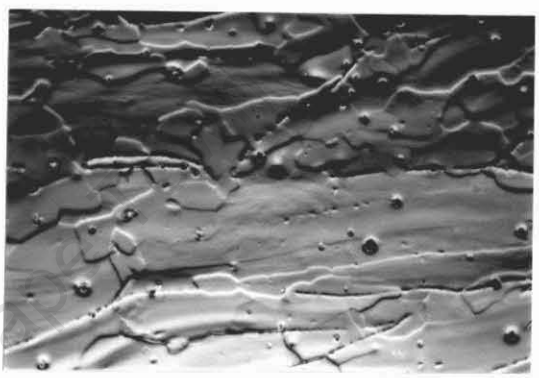

(e) 850/1250°C

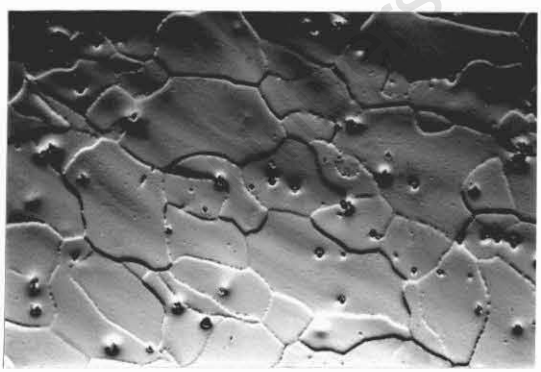

(c) 1050/850°C

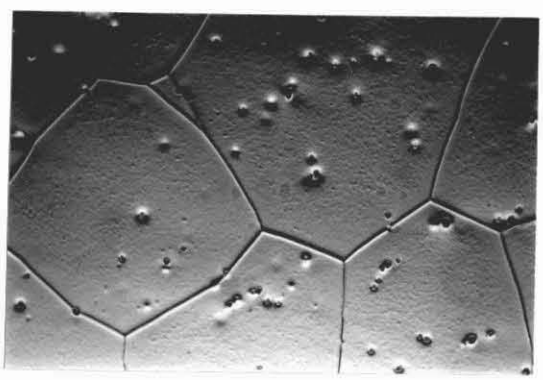

(f) 1250/850°C

50 μm

FIGURE 4.38 Microstructure of sulphur-doped alloys viewed under polarised light

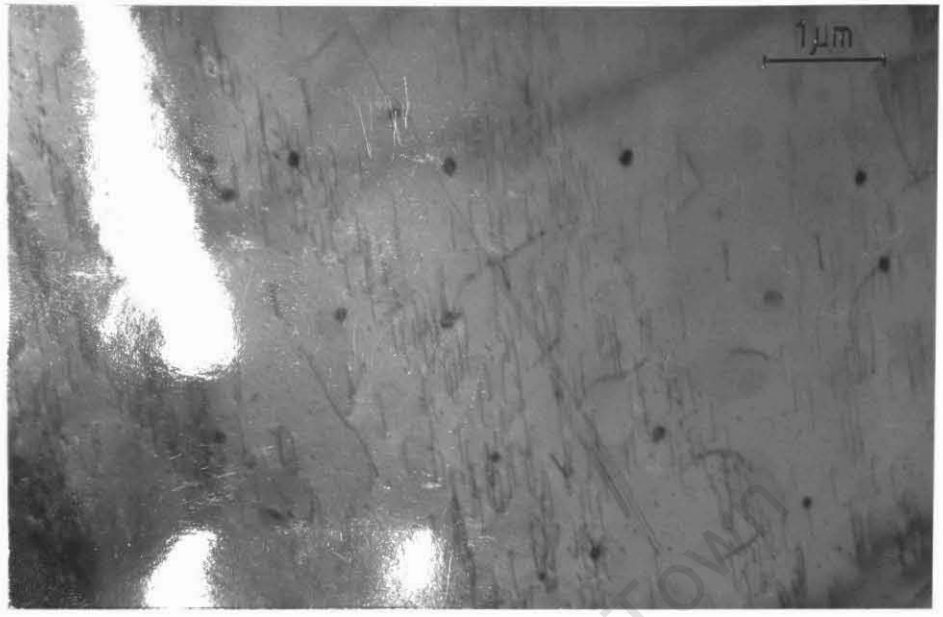

FIGURE 4.39 Sulphide inclusions with linear arrays of primary dislocations (850/1050°C)

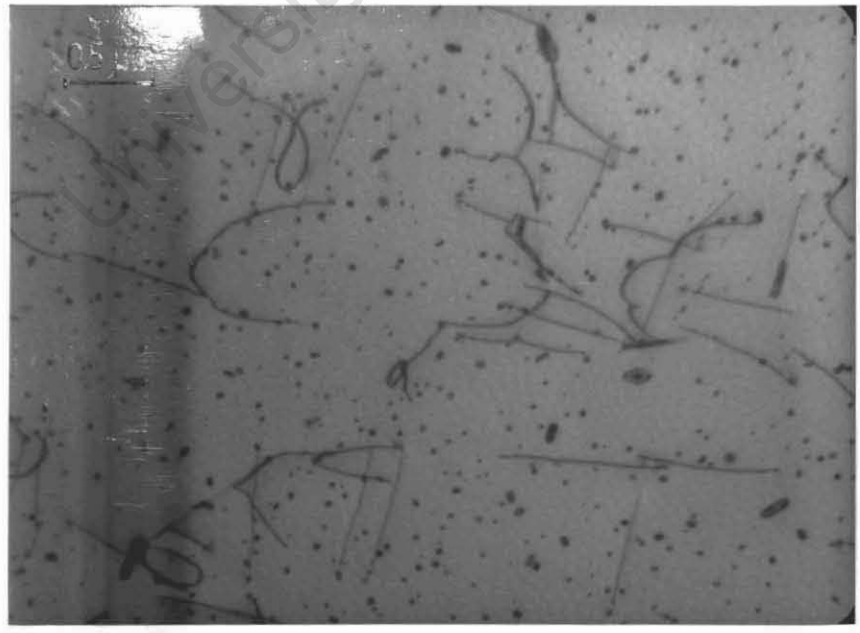

FIGURE 4.40 Intragranular precipitation and pinning of dislocations in over-heated sulphur alloy (1250°C)

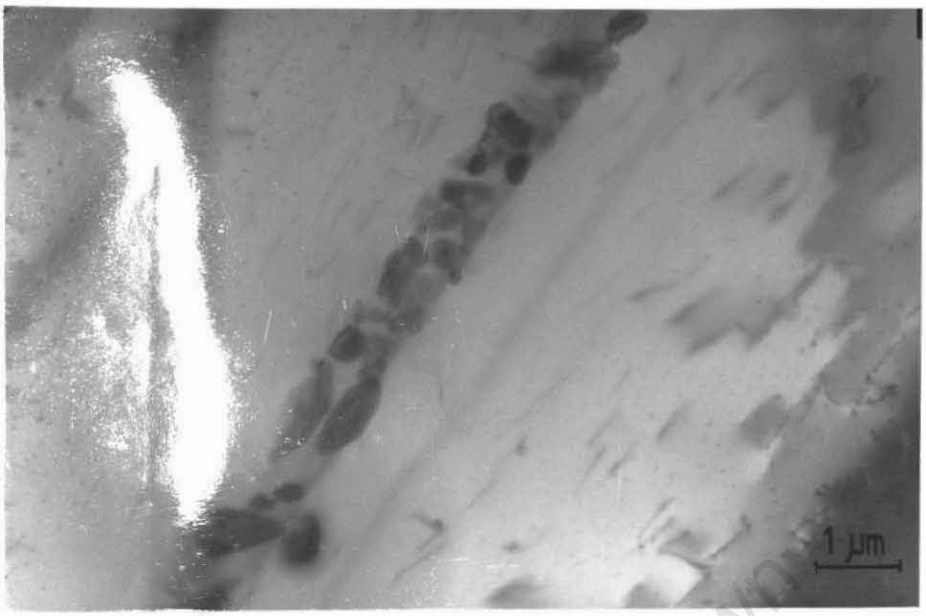

FIGURE 4.40 (b) (Cont) Contiguous grain boundary phase in over-heated sulphur alloy (1250°C)

4.5.1.6. Slip at Sulphide Inclusions

Use was made of high resolution scanning electron microscopy to study the polished and etched surfaces of the high sulphur alloys. The sulphides were revealed by imaging with secondary and back-scattered electrons, and are shown in Figure 4.41. The spheroids could be positively identified by a sulphur peak in the EDS trace. The spheroids generally occurred in rows arranged parallel to the rolling directions, which illustrated their derivation from stringers formed during hot deformation. The formation of the spheroids over the range 850-1050°C by cylinderisation and segmentation closely resembled that reported for the MnS system. It is not clear what proportion of the sulphides were removed by the etching process, but gaps in the regularly spaced intervals between the spheroids often indicated the removal of a spheroid.

Figure 4.41(b) shows the sulphides distributed across a plastically deformed surface which has been etched. The spheroids occur in association with the slip lines, and evidently act as initiation sites for slip.

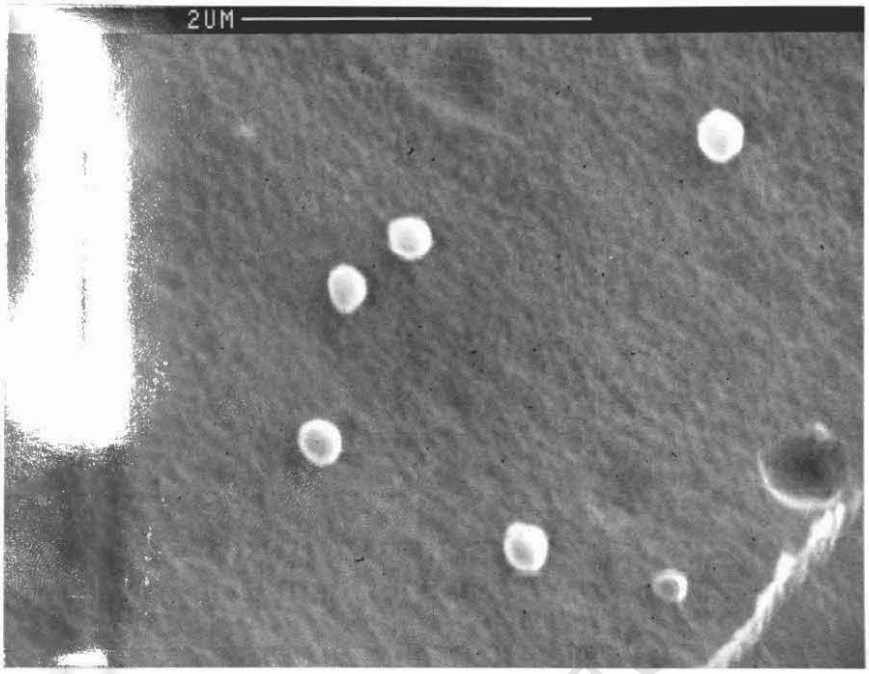

(a)

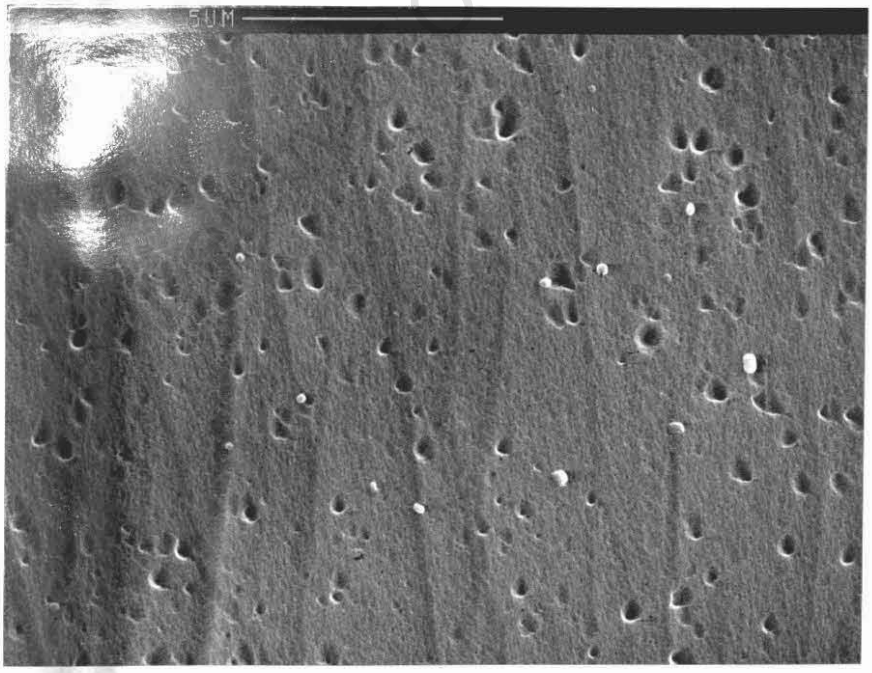

FIGURE 4.41 Mixed backscattered and secondary electron SEM image of polished and etched deformation surface - Solution A (850/1050°C)

(a) Sulphide inclusions
(b) Inclusions associated with slip-lines

4.5.2 Comment

The beneficial influence of a relatively sparse population of second phase particles is reflected in the mechanical properties given in Tables 4.5 - 4.6. The occurrence of the CrS inclusions improves the tensile ductility and the impact toughness relative to the base alloy over a wide range of heat treatment conditions. The overall effect of the higher sulphur levels may be summarised as follows:

(1) The addition of sulphur improves the tensile ductility for all heat treatment cycles, with the exception of the one-stage 1250°C treatment. Quenching from 1250°C causes the highest hardness recorded.

(2) Sulphur additions also enhance the impact toughness provided the correct sulphur control is exercised. The ITT is shifted approximately 30°C per 100 ppm sulphur addition.

(3) The optimum impact toughness is derived from ageing at 850°C prior to SHT at 1050°C, while the optimum tensile ductility is achieved by ageing at 850°C subsequent to 1050°C.

(4) Prior and post ageing is effective in alleviating the severe tensile embrittlement following SHT at 1250°C. It is interesting to note that reasonable toughness is maintained in the alloy solutionised at 1250°C despite the severe loss of tensile ductility, but this in turn is lost by ageing to restore the ductility.

OVERHEATING

The isothermal behaviour of the monoclinic CrS species is consistent with that reported for the sulphides of the (Mn,M)S type. The CrS displays a high degree of deformability, which causes it to be extruded in the form of stringers aligned in the rolling direction. Subsequent homogenisation over the temperature range 850-1050°C enables restoration of the surface energy, whereby the stringers are resolved into globular spheroids. Overheating occurs when the SHT temperature is raised to 1250°C, and the sulphides are taken into solution. There is then no restraint on grain growth by the particles. Re-precipitation occurs both intragranularly and at the grain boundaries during cooling. This confirms observations by Schultz and McMahon (1973) of overheating, causing CrS dissolution

in the vicinity of 1250°C.

The severe tensile embrittlement in the alloy solutionised at 1250°C is patently the result of subsequent reprecipitation of the sulphur. While the intragranular dispersoid hardens the matrix and increases the flow stress, precipitation at the grain boundary promotes an intergranular fracture mode, as evidenced by the number of intercrystalline facets in Figure 4.37(b). Many of the grains also exhibit evidence of intergranular microvoid coalescence, which signifies overheating.

While the overheating embrittlement detracts from the impact resistance, this is by no means as pronounced as might be expected. This is borne out by the results of Baker and Johnson (1973) who found that the overheated sulphides have no detrimental effect on the fracture toughness of high strength steels.

The tensile ductility of the overheated alloy is restored by ageing. In the case of the prior ageing treatment, spheroidisation is accomplished before SHT. The low surface to volume ratio of the spheroids ensures greater stability over that of the stringers and hence only partial dissolution of the sulphide particles takes place at 1250°C. Less sulphur is therefore available for re-precipitation during cooling. As in the case of the carbide and nitride precipitates, post-ageing relieves the intragranular sulphide precipition by coarsening, which improves dislocation mobility but reduces the impact toughness. This once again leads to the conclusion that the impact toughness is less sensitive to intragranular precipitation than it is to grain boundary precipitation.

FISSURE FORMATION

The appearance of fissures in the impact fracture surfaces of the alloy treated at 850/1250°C parallel to the plate surfaces denotes planes of weakness which fracture ahead of the crack to relieve the triaxial stress state. Fissure formation is generally thought to be the product of elongated ferrite grains and a preferred orientation as a result of deformation. Nucleation usually occurs

at non-metallic second phase particles, and may give rise to cracks which propagate in a brittle manner. Mintz (1980) has gone as far as arguing that the critical event for brittle propagation is the ability for intergranular decohesion to take place.

Examination of the grain morphology and sub-structure in the 850/1250°C alloy shows that the spheroids are capable of pinning the boundaries despite partial dissolution. Grain growth at 1250°C occurs by competitive coalescence of the sub-grains, but this is retarded in the through-thickness direction by the linear trails of spheroidised stringers. This results in elongated grains with straight boundaries. Conditions are therefore ripe for lamellate fissure, especially in light of the tendency towards intergranular failure.

SLIP INITIATION

The action of the sulphide inclusions in initiating plastic flow is demonstrated by the sub-surface particles contained within the slip-lines in Figure 4.41. Taken in conjunction with the improved ductility in the alloys containing a dispersion of carbonitrides, it is apparent that a distribution of second phase particles is effective as slip sources in promoting plastic deformation in the Fe-40Cr alloy. Observations of dislocations in Fe-40Cr alloys suggest that even at the low sulphur levels the particles are important sources of dislocations in this otherwise source-poor material. The significance of this to the brittle fracture resistance lies in the fact that particles may induce slip in response to a stress field or applied stress.

PRISMATIC DISLOCATION GENERATION

Estimates of the stress distribution at the CrS particle/matrix interface caused by differential thermal expansion effects show that its magnitude is of the order of the matrix yield stress and therefore sufficient for prismatic dislocation generation according to the Tresca criterion. This is borne out by transmission microscopy which directly shows the formation of primary arrays at

the sulphide particles. An increase in the impact toughness has been coupled with a high density of dislocations associated with a uniform distribution of these sources.

Assuming that a stress-free state exists around the spheroid at its formation temperature, cooling results in stresses of a tensile nature being set up at the matrix/particle interface. The magnitude of these stresses hinges on the change in temperature, and higher temperatures are expected to result in an increase in the prismatic dislocation production. It is therefore not immediately apparent why the alloy cooled from 1050°C should evidence a lower density of dislocations compared with the alloy aged at 850°C prior to 1050°C, since both are cooled from the same final temperature. Nevertheless, this causes an increase in the impact toughness. A possible reason for this difference lies in the formation temperature of the spheroids, being 850°C in the case of the prior-aged alloy, but 1050°C in the simple annealed alloy. Aside from possible slight changes in the particle size that this may cause, it is also meaningful to consider the nature of the interfacial stresses derived from heating the prior-aged alloy from its stress-free state at 850°C. Heating to 1050°C causes the particle to expand relative to the matrix, which is a premise for tessellated stressing of a dilatational nature. For example, Equation 4.2 applied over the range 850°C-1050°C gives an estimate of the operative reduced shear stress as 257MPa. Since the yield stress of non-dispersion hardened chromium steels at 800°C ranges from 100-170MPa [Smithells (1976)], it is evident that tessellated stresses may give rise to plastic accommodation on rapid heating. However, diffusional processes are expected to anneal out any interfacial stresses or dislocations at the higher soaking temperature, once again leaving the particles in a stress-free state. In any event, the net effect of heating from the intermediate temperature is to create a higher misfit (assuming particle stability), which in turn implies a larger tesellated potential for dislocation generation on cooling and a higher dislocation density. This may provide an additional explanation for the superior toughness of the prior-aged alloys.

The fact that smaller sulphides are not active as dislocation sources is accounted for by the Brooksbank-Andrews model which predicts a critical radius for a given set of thermal conditions. Nevertheless, it is true that even the smaller particles can support a residual stress field which may be additive to an external stress field such as that ahead of a crack tip. This is given further consideration in the final discussion.

One additional point deserves comment, and that concerns the "void-forming potential" of the sulphides as coined by Brooksbank and Andrews. The present study has found no evidence of separation of the particle from the matrix, notwithstanding the predicted high interfacial stresses. Indeed, the interfacial strength is sufficient to support the tessellated stresses. There is some evidence to suggest that the sulphide spheroids have a faceted morphology (see for example Figure 4.16(a)), which would favour strong interfacial bonds, and possibly even limited coherency, as well as facilitating the nucleation of interfacial dislocations.

4.6 Fe-40Cr WITH ALLOYING ADDITIONS

4.6.1 Results

The mechanical properties of Fe-40Cr were examined from the perspective of secondary alloying additions which may impart the requisite impact toughness and corrosion resistance. Nickel is expected to increase the fracture resistance by the alloy softening mechanism identified in Section 2.3.1. The gettering of residual carbon and nitrogen by niobium is necessary from the point of view of preventing embrittling grain boundary precipitation, also linked to grain boundary sensitisation. Ruthenium is added to take advantage of the cathodic modification process for enhanced passivation in reducing acid media. Each alloying addition contributes unique features to the deformation process, and these are considered in turn.

4.6.1.1 Mechanical Properties

The tensile behaviour of alloys modified with 2% Ni, 0.2% Nb and 0.2% Ru respectively is shown in Figures 4.42-4.44. A summary of the results is contained in Table 4.7, with the properties of the base alloy included for purposes of comparison.

The effect of the alloying additions on grain size is shown in Table 4.8.

TABLE 4.8 Effect of Alloying Additions on Grain Size

Heat Treatment	Grain Size (Microns)			
	LI	NI	NB	RU
1h1050°C	181	80	68	291
1h1250°C	306	410	323	304

TABLE 4.7 Test Results: Properties of Alloyed Fe-40Cr

Cycle	Heat Treatment	UTS (MPa)				0.2% PS (MPa)				%EI				HV_{50}				Cv (RT) (J/cm^2)			
		LI	NI	NB	RU	LI	NI	NB	RU	LI	NI	NB	RU	LI	NI	NB	RU	LI	NI	NB	RU
1	1h 1050°C	564	630	521	553	448	576	448	448	23	20	17	18	206	230	199	214	8	43	9	8
2	1h 1050°C	569	673	523	607	494	581	451	540	19	18	20	20	224	242	212	229	35	87	19	21
3	1h850/1h1050°C	554	619	520	552	448	560	407	458	22	21	31	24	212	229	201	222	13	59	12	12
4	1h850/1h1250°C	560	659	561	611	474	550	486	535	15	17	19	20	228	259	220	238	79	93	11	17
5	1h1050/1h850°C	491	570	486	502	321	504	392	384	26	26	22	34	187	214	189	200	17	51	9	9
6	1h1250/1h850°C	460	532	494	476	367	469	418	387	21	19	27	20	190	208	195	197	35	76	13	17

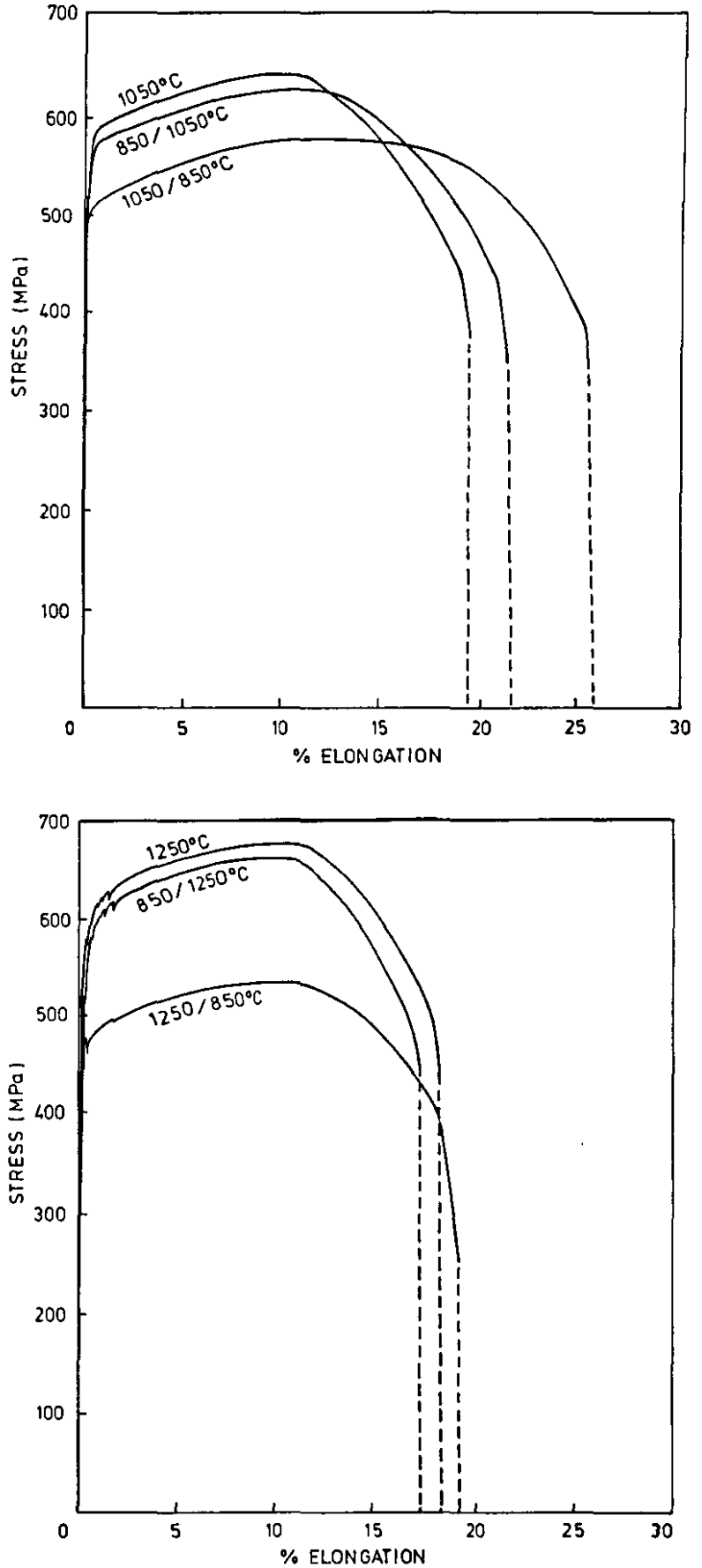

FIGURE 4.42 Tensile characteristics of Fe-40Cr-2Ni

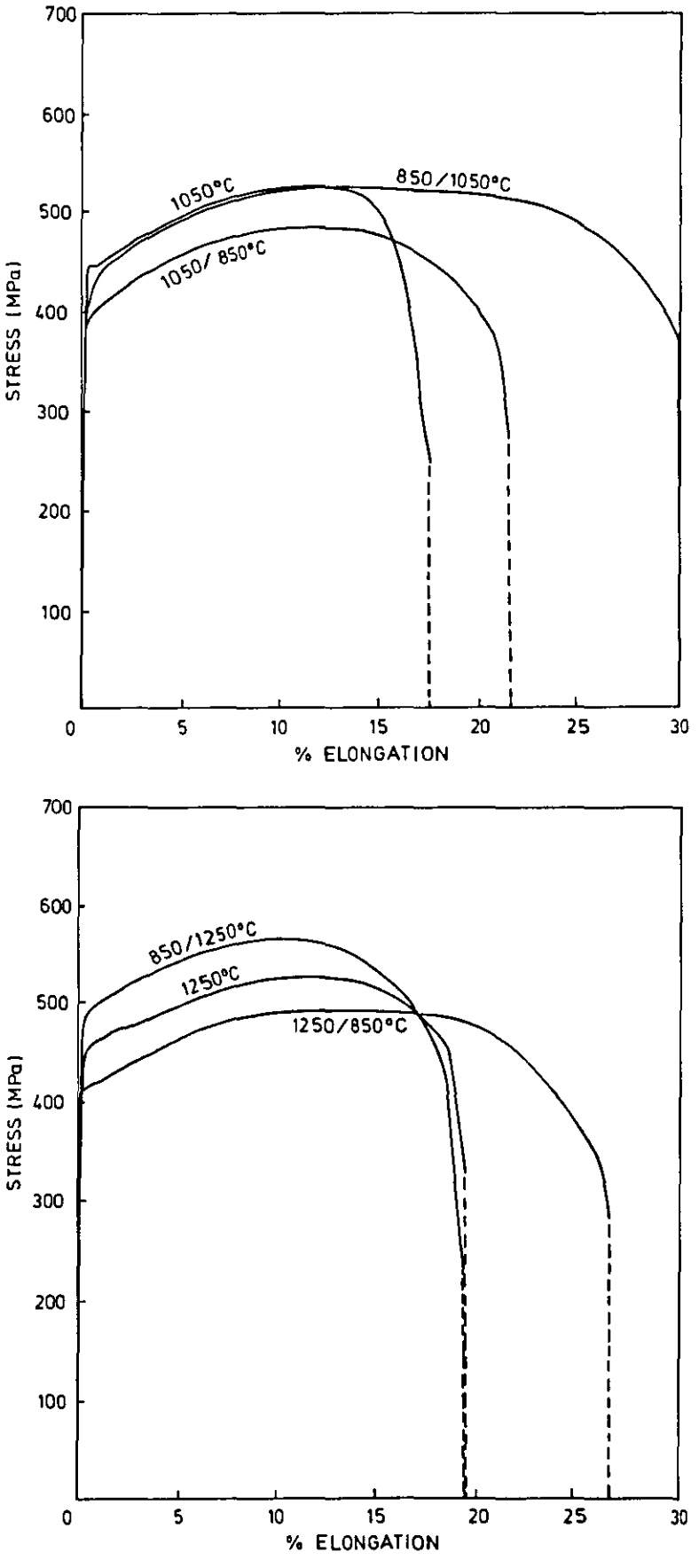

FIGURE 4.43 Tensile characteristics of Fe-40Cr-0.2Nb

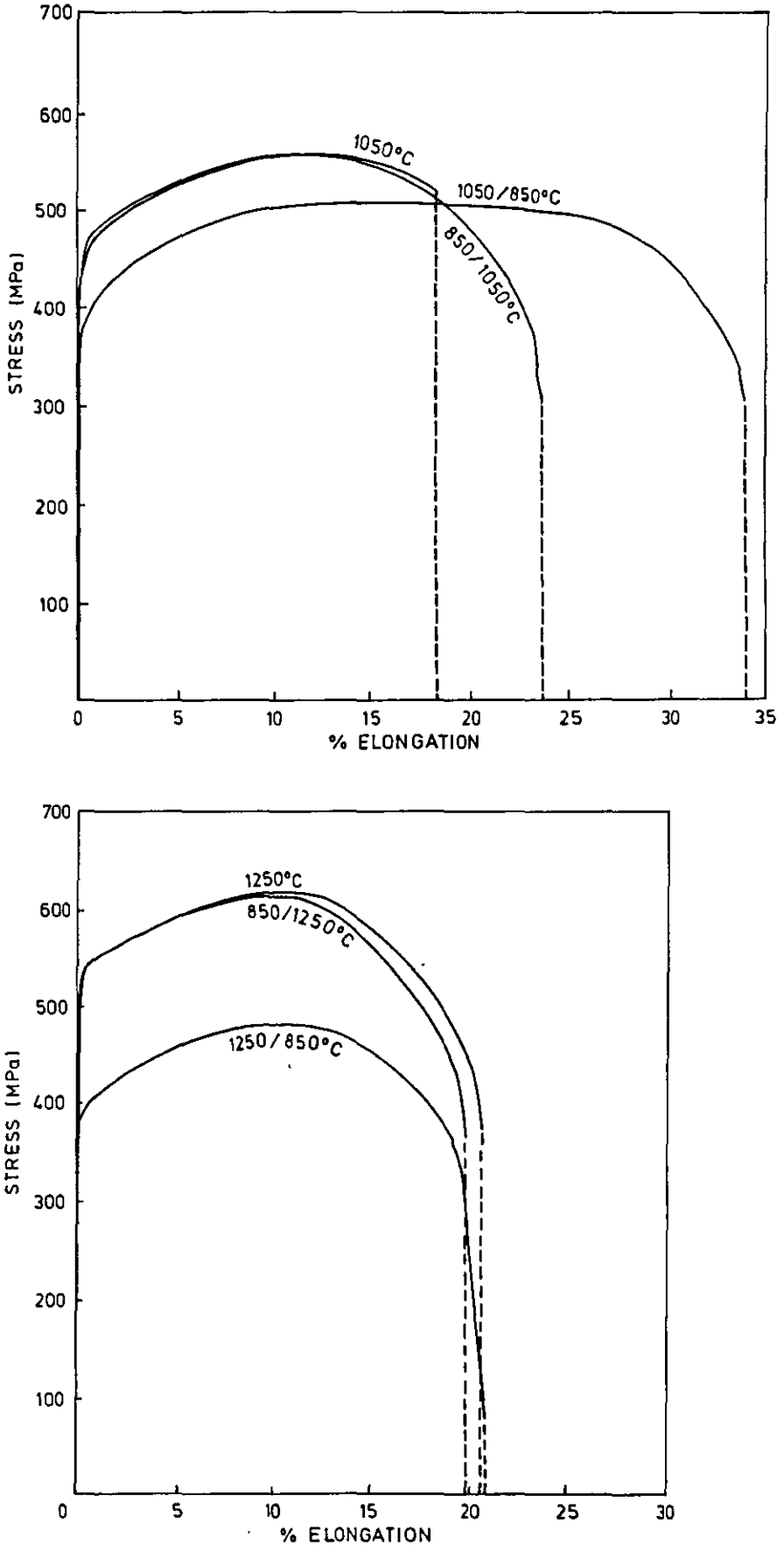

FIGURE 4.44 Tensile characteristics of Fe-40Cr-0.2Ru

4.6.1.2 Fe-40Cr-2Ni

The addition of nickel resulted in a marked increase in strength at RT, but the strain to fracture was unaffected as compared with the base alloy. At the same time the RT impact resistance was substantially improved for all heat treatment conditions. As in the case of the base alloy, the 1250°C SHT was more effective than 1050°C in promoting toughness, and greater toughness was achieved by prior-ageing. However, unlike the base alloy, ageing subsequent to SHT resulted in only a small loss of toughness.

The tensile characteristics followed similar trends over the different annealing cycles to those exhibited by the unalloyed species. SHT at 1250°C increased the strength over that achieved at 1050°C, and the maximum strain to fracture followed post-ageing treatments. However, the tensile curves of the nickel alloy were unique in exhibiting serrated yielding at RT. This was characterised by load drops and audible clicks during deformation, and was linked to twinning by arresting the deformation and examining a transverse section through the deformed gauge length. The incidence of twinning increased in specimens deformed at lower temperatures, although this did not impair the strain to fracture. (Figure 4.45). Nevertheless, the lower temperatures resulted in an increase in strength and a tendency to brittle fracture.

Examination of the polished surfaces of the impact specimens also showed a high density of twins in addition to the plastic slip bands. (Figure 4.46).

Figure 4.47 shows TEM micrographs of a specimen taken from a deformed region. Twinning in the form of deformation shear bands can be seen, associated with a high degree of plastic deformation.

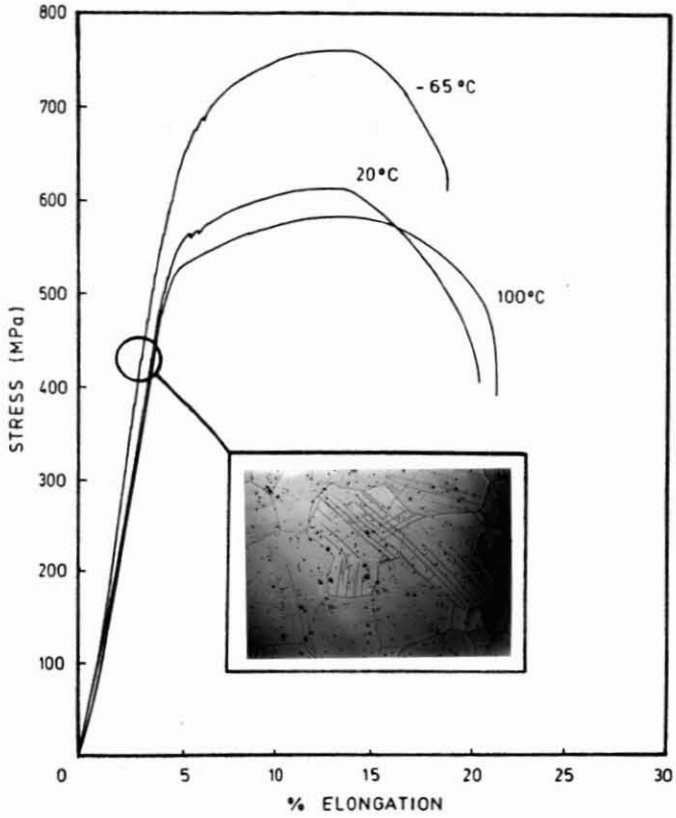

FIGURE 4.45 Isothermal tensile characteristics of Fe-40Cr-2Ni showing serrated yielding and an increased rate of work-hardening as a result of mechanical twinning (1250°C)

FIGURE 4.46 Polished deformation surface of an impact specimen of Fe-40Cr-2Ni, showing mixed twinning and plastic slip

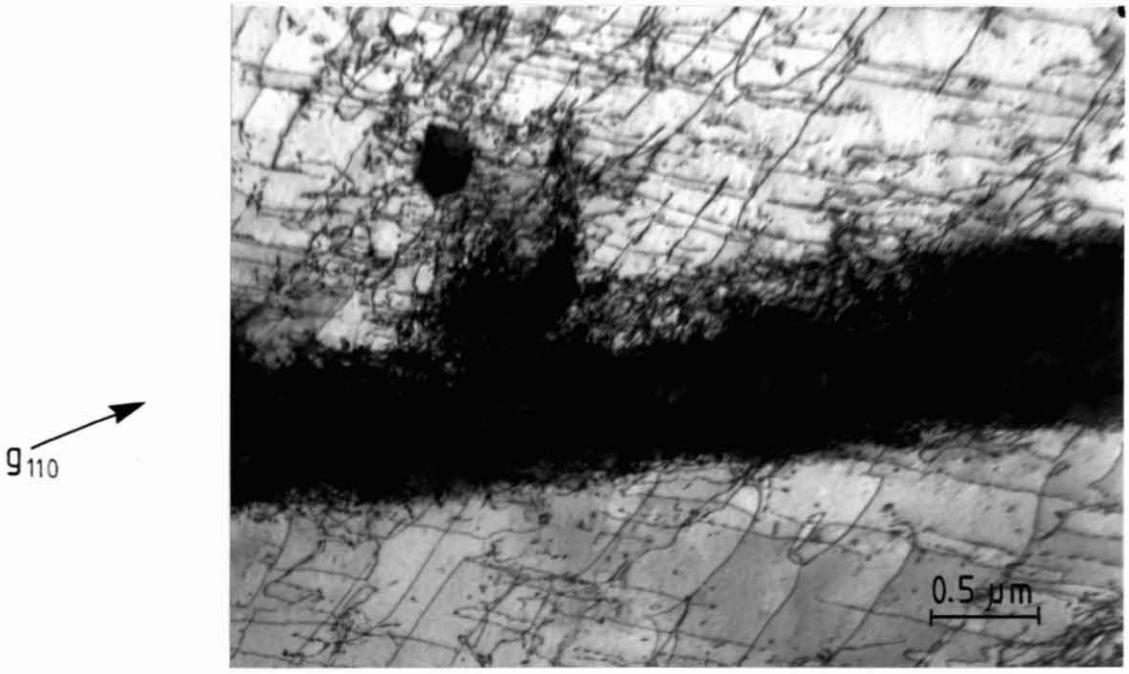

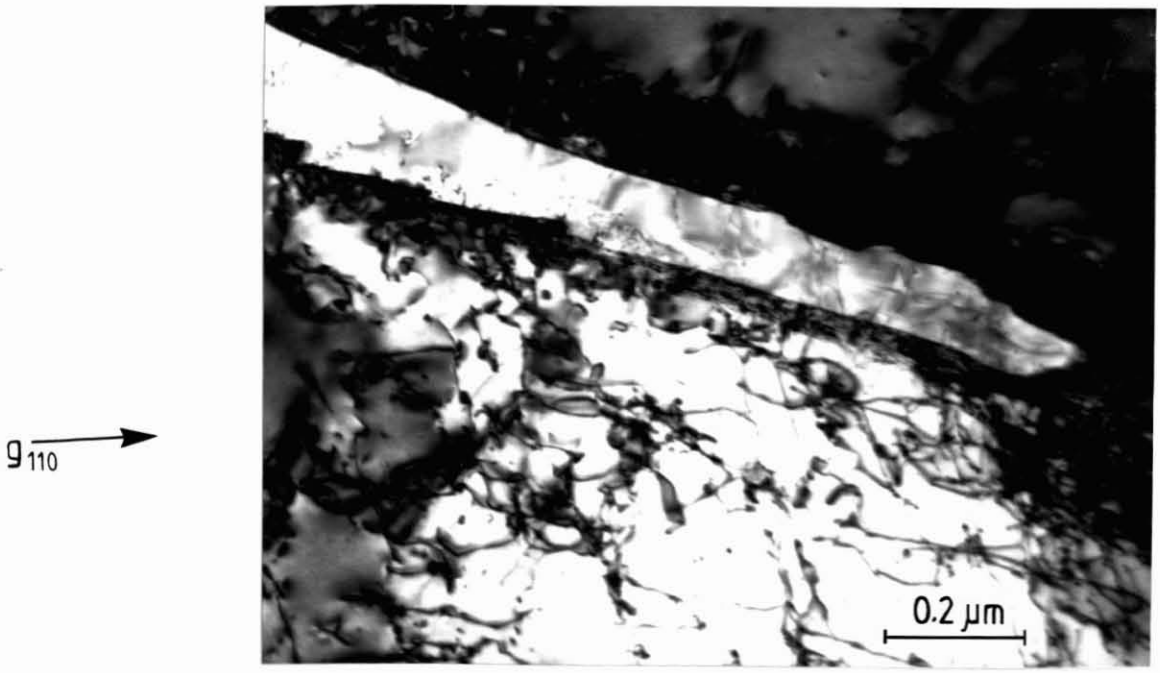

FIGURE 4.47 Examples of twinning in Fe-40Cr-2Ni. Sections taken from a deformed region show twin lamellae in the form of shear bands with high plastic strain gradients

4.6.1.3 Fe-40Cr-0.2Nb

The niobium addition was roughly 2,2x the stoichiometric equivalent of the (C+N). The behaviour of the niobium alloy deviated in part from that of the other alloys as a result of additional phase relationships, in particular the expected formation of the submicroscopic Nb(C+N) below 900°C.

The tensile characteristics of the niobium alloy generally exhibited superior ductility to the base alloy. Unlike the other systems the optimum ductility was achieved by prior- rather than post-ageing at 1050°C. Furthermore, the 1250°C treatment was found to increase the strength as well as the strain to fracture in most cases. Alloying with niobium reduced the hardness, although this caused hardening relative to the base alloy in the case of post-ageing. The superstoichiometric addition of niobium also caused a reduction in the RT toughness.

The niobium addition is a powerful retardent of the recrystallisation kinetics. For example, partial recovery following the 850/1050°C cycle is shown in the TEM micrograph in Figure 4.48. The net effect was an order of magnitude refinement in the grain size of the alloys heat treated at 1050°C, but normal grain growth at 1250°C to give a polygonal ferrite morphology.

The effect of pre-straining on the RT impact toughness is illustrated in Figure 4.49. The alloy showed a brittle response following cold rolling when annealed at 1050°C, but became progressively tougher up to an optimum degree of prior-deformation when annealed at 1250°C. The cause of this difference became clear from transmission microscopy, shown in Figure 4.50. Material annealed at 1050°C, and known to have a dislocation substructure, showed a heavily work-hardened structure following pre-straining. Dense tangles and banding were evident after a reduction of only 5%. In the case of the material annealed at 1250°C, a uniform dislocation network was observed, despite greater degrees of deformation.

FIGURE 4.48 Recovered substructure in Fe-40Cr-0,2Nb (850/1050°C)

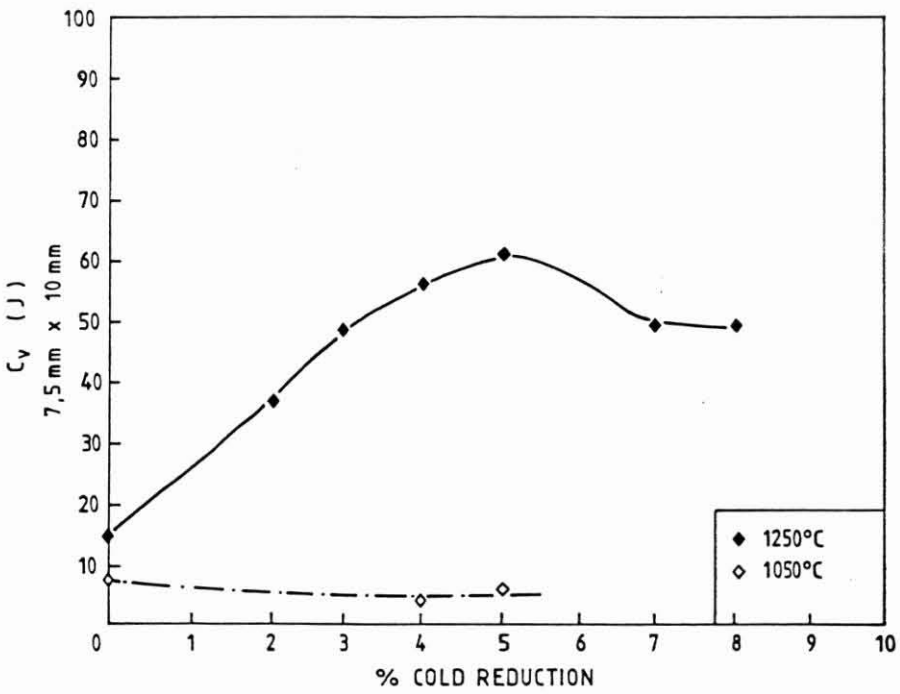

FIGURE 4.49 Effect of pre-straining on the RT impact toughness of Fe-40Cr-0.2Nb

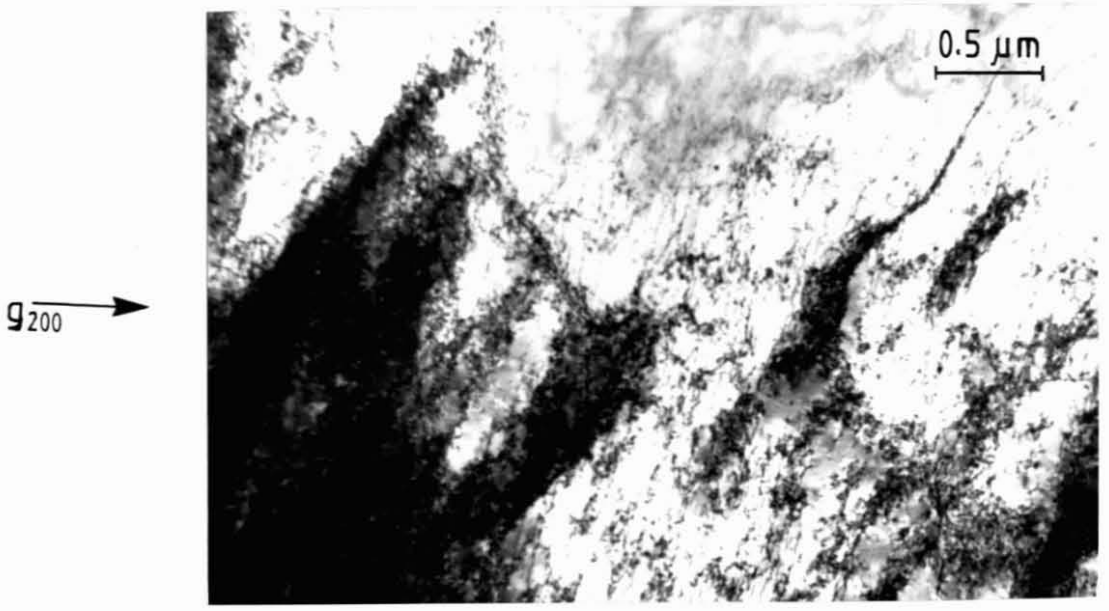

(a)

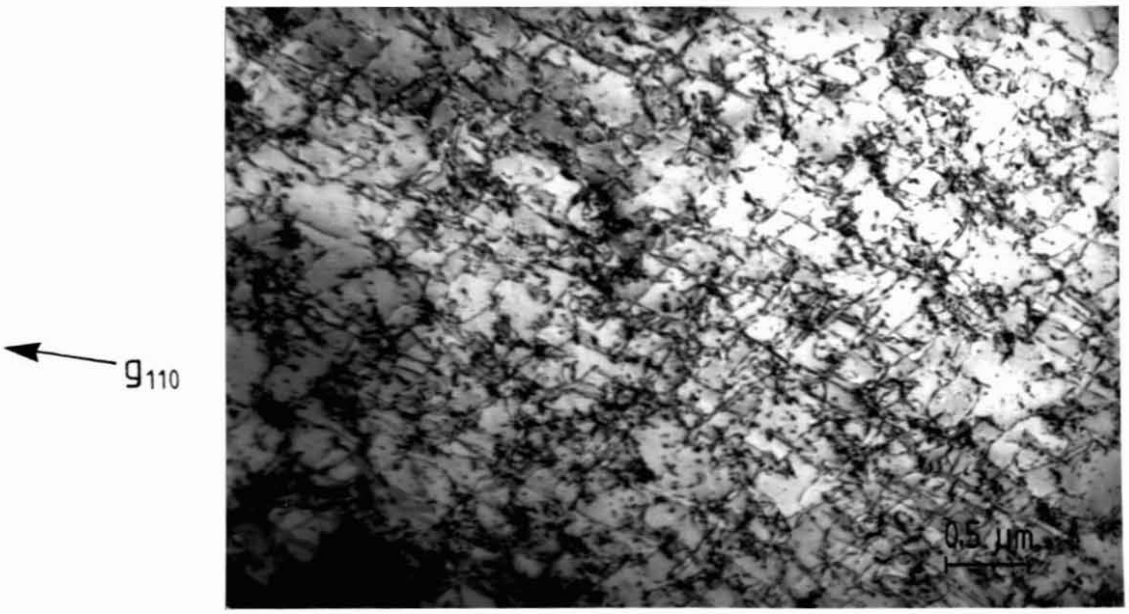

(b)

FIGURE 4.50 Effect of pre-straining on microstructure of Fe-40Cr-0,2Nb

(a) 1050°C, 5% CR - Work-hardening
(b) 1250°C, 7% CR - Uniform dislocation density

4.6.1.4 Fe-40Cr-0.2Ru

The mechanical characteristics of the ruthenium alloy elicited the following significant points:

(1) The ruthenium addition caused a substantial strengthening effect. The hardness increased for all heat treatments, and the tensile fracture mode exhibited a significant brittle component;

(2) SHT at 1250°C resulted in an increase in strength relative to SHT at 1050°C;

(3) The ruthenium addition impaired the RT impact toughness.

Of particular interest in the ruthenium alloy was the response of grain growth to the annealing ranges. Soaking at 1050°C was characterised by rampant grain growth, although 1250°C left the ferrite grain size unchanged relative to the base alloy, as shown in Table 4.8. Optical micrographs are shown in Figure 4.51. The salient feature to be noted is the wavy grain boundary morphology following simple annealing at 1050°C as compared with the equiaxed ferrite grain structure in the base alloy (see for example Figure 4.11). This is indicative of recovery coalescence of low-angle boundaries, clearly demonstrated in Figure 4.51(b). This led to the conclusion that grain growth occurred by the coalescence of sub-grains at temperatures up to 1050°C, while the 1250°C treatment yielded a fully recrystallised morphology attained by the migration and impingement of high angle boundaries.

The RT impact toughness of the ruthenium alloy showed no response to pre-straining, evidently as a result of the work-hardening by the sub-structure.

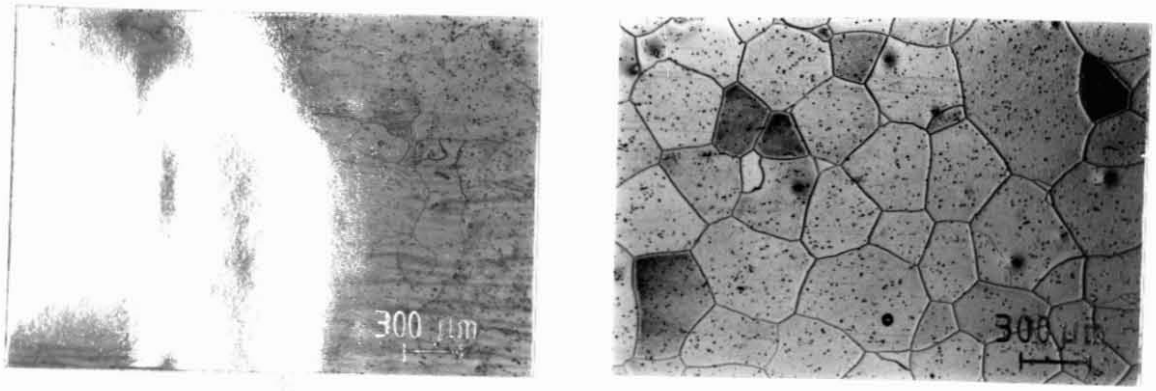

(a) 1050°C 1250°C

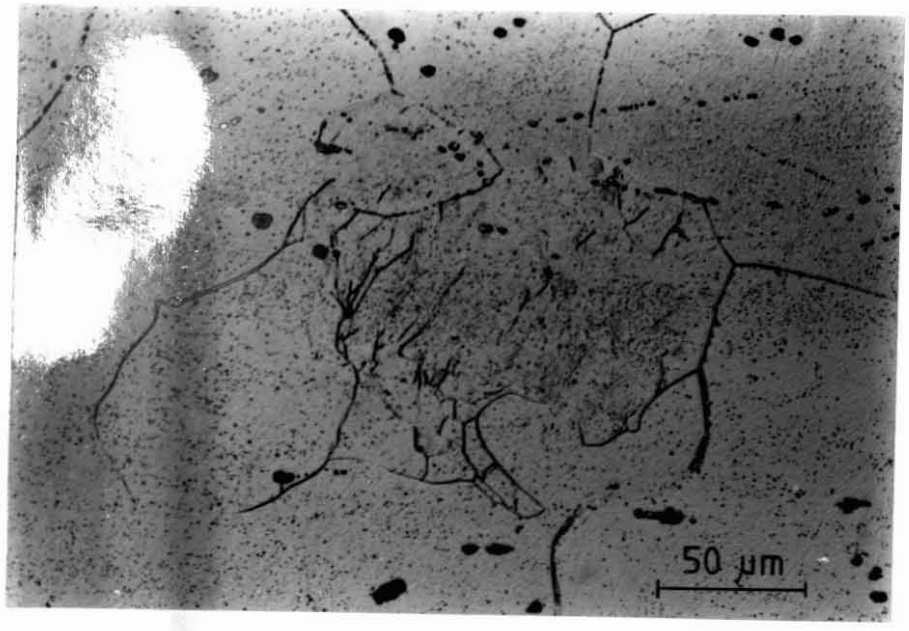

(b)

FIGURE 4.51 Grain morphology of Fe-40Cr-0,2Ru (1050°C) - Solution A.

(a) Secondary grain growth, showing wavy boundaries. The recrystallised structure is shown for comparison
(b) Grain growth by recovery coalescence

4.6.2 Comment

Of all the alloys studied, the most potent solid solution strengthening is achieved by the addition of 2% nickel. An increase in the tensile strength and hardness is manifest for all heat treatment conditions, while the tensile ductility is little changed. A favourable shift in the DBTT to well below 0°C was previously noted by DeMarsh (1986) for the Fe-40Cr-2Ni alloy. The above results show an improvement in toughness under an extended range of conditions. The mechanism of solid solution softening by nickel has therefore been hallmarked.

The observation of an increased tendency to deformation twinning with the addition of nickel substantiates the results reported by other authors (Section 2.3.1). The pronounced occurrence of twinning in the alloys annealed at 1250°C may be accounted for by (1) the higher flow stress, and (2) the larger grain size, both of which favour twinning.

The preponderance of twinning at cryogenic temperatures in the alloys of Nakano et al (1978) was not matched by the Fe-40CrNi alloy, but this is not surprising in view of the higher chromium content and smaller nickel additions. The alloys reflect a clear progression to twinning control at lower temperatures, but the relatively low twin density supported by the small nickel content limits the contribution of the twinning to the total deformation.

It is apparent from the tensile curves in Figures 4.42 and 4.45 that fracture is not coincident with the onset of twinning in the nickel alloy, which indicates an increased ability for stress accommodation at terminating twins. The occurrence of good impact toughness, even in the alloy subjected to post-ageing provides additional evidence for enhanced stress relief and dissipative plastic work at the crack tip of the nickel alloy. Despite the coarsening of the grain boundary phase, shown to be critical in the base alloy, the local stress field of the crack is sufficiently lowered to ensure stable

crack growth. Thus the addition of nickel has an analogous effect to crack-tip shielding by dislocations introduced heterogeneously. The mechanism whereby this is assisted is suggested by the TEM micrographs in Figure 4.47. Twin formation within the deformed region appears to precede plastic flow which subsequently distorts the crystallographic definition of the twin band. This is in agreement with the general principle that twinning is suppressed by pre-straining [Reid (1981)] and that the dislocations, once formed, would pre-empt twinning. Following the formation of the shear band, the plastic slip becomes localised in the twin region. The question then revolves around the chronological relationship between the plastic deformation in relation to the passage of the crack. Two scenario's present themselves for consideration:

(1) The twin, nucleated by the local stress field of the crack, is propagated ahead of the crack where it triggers plastic slip to blunt the crack;

(2) Twinning and slip occur independently in response to the crack field (although the time scale for twinning is much smaller) and plastic slip accumulates at the shear band boundaries to give the appearance of associated dislocation activity.

In both cases the twins contribute to the work hardening, but whereas in the first instance the twins provide an active mechanism for blunting, in the second they simply supplement the total strain energy of the crack. The role of twinning is developed further in the final discussion.

The additions of small quantities of niobium and ruthenium have a pronounced effect on the restoration processes during annealing of the warm-worked alloy. In the case of the niobium alloy, both the recovery and the recrystallisation kinetics are retarded by the ostensible precipitation of the niobium from solid solution. Complete solutionising and recrystallisation is only achieved with the higher 1250°C treatment. The mechanical properties are therefore greatly influenced by the occurrence of a subgrain structure. Suffice it to note at this stage that neither the tensile ductility nor the RT impact toughness benefit from the highly stable dislocation substructure. This is highlighted by the effect of pre-straining on the toughness. The sub-boundaries cause

severe work-hardening, whereas the fully recrystallised matrix allows the introduction of a uniform distribution of mobile dislocations which are effective in blunting the crack despite the solid solution strengthening by the niobium. It is once again apparent that an optimum dislocation density exists whereafter strain-hardening causes the toughness to diminish.

The failure of the ruthenium alloy to recrystallise at 1050°C points to a reduced drive for recrystallisation. Since recrystallisation is usually advanced by a reduction in the cellularity of the substructure, the increase in the recrystallisation temperature must be attributed to an increase in the Stacking Fault Energy (SFE) in the absence of any secondary phases. Although care must be taken when raising the concept of a SFE in bcc metals, the term is used here in the loose sense to describe the relative ease of cross-slip by dislocations. In the simplest analysis recovery depends on the ability of dislocations to leave the slip plane, and since lowering of the SFE causes the dislocations to be extended on the slip plane, a greater thermal activation is needed to cause them to constrict in order to crossglide or climb. An increase in the SFE therefore ensures a greater freedom for cross-slip during recovery, and thus a high degree of mobility of the low-angle sub-boundaries. The ruthenium alloy therefore favours restoration by recovery, and the favourable energetics sustain recovery and sub-grain coalescence up to higher temperatures. A higher SFE also implies a higher rate of work-hardening, which means that in terms of the Petch model, the cleavage fracture stress is more readily attained by strain effects. This and the contribution of the substructure to dislocation entanglement, explains the failure of the ruthenium to respond to pre-straining.

4.7 SUMMARY OF RESULTS

The ductile response of a range of alloys based on the Fe-40Cr composition was evaluated as a function of the annealing practice and alloy chemistry.

Following deformation in the warm-working region ($T=0.4\ T_m$) static recovery of low interstitial Fe-40Cr alloys takes place during annealing below 850°C to give rise to a partially recrystallised sub-grain structure. The recrystallisation kinetics are retarded by increasing the volume fraction of second phase particles, and examples of impeded recovery by precipitates of niobium, chromium carbides, oxides and sulphides have been found. The formation of a recovered grain structure is also promoted by the addition of ruthenium, which elevates the recrystallisation temperature, ostensibly by increasing the boundary mobility.

Full recrystallisation to give an equiaxed ferrite grain structure is achieved at an annealing temperature of 1050°C, but temperatures of the order of 1250°C are required to ensure complete dissolution of any secondary phases. Subsequent quenching from the SHT temperature forces precipitation of the interstitials intragranually and at grain boundaries, despite levels as low as 100 ppm (C+N).

Ageing the Fe-40Cr alloy at an intermediate temperature prior to or subsequent to solutionising has pronounced but opposing effects on toughness and ductility. Prior-ageing at 850°C enhances the impact toughness, whereas post-ageing promotes the tensile ductility at the expense of toughness. In each case the mechanical response has been interpreted in terms of the microstructural parameters:

Prior-ageing is associated with a recovered dislocation substructure which contributes to the overall work-hardening. Although the substructure is effectively pinned at ambient temperatures, and inert to the brittle fracture process, results suggest that the dislocation arrays may be activated to contribute to crack blunting at higher temperatures. It has also been shown that the prior-recovered substructure increases the rate of heterogeneous precipitation during cooling from SHT by creating additional sites for preferential nucleation, and therefore changes the precipitate distribution. In respect of the sulphide inclusions, the role of ageing

prior to SHT was further interpreted in terms of spheroidisation of the wrought sulphide stringers and enhanced prismatic dislocation generation. Thus the effect of the prior-ageing may be described in terms of a change in the precipitation and recrystallisation characteristics.

Ageing following SHT is basically a coarsening treatment, allowing the re-deposition of the finer matrix precipitates at the grain boundaries. This reduces the flow stress of dislocations moving through the matrix and has as a consequence an improvement in the tensile ductility. At higher strain rates the coarse particles provide fast-crack initiation sites which is reflected in a loss of impact toughness. The effect of the ageing treatment may be nullified by reheating to the SHT temperature to dissolve the grain-boundary phase and restore the impact toughness.

A study of high interstitial Fe-40Cr alloys has allowed the characterisation of the excess phases. Separate additions of carbon and nitrogen have delineated the relative contributions of each interstitial element to the deformation process, and resolved the apparent conflict in results reported in the literature. Quenching from the elevated temperatures causes a change in the precipitate morphology and distribution. In the case of the high carbon alloy, precipitation from solid solution at high quench rates takes the form of Widmanstatten plates on crystallographic habit planes, and is accompanied by a homogeneous intragranular dispersoid. The carbide precipitates cause a drop in the hardness of the alloy. In the case of the high nitrogen alloy, the precipitation occurs as a high density of fine, coherent strain centres, which causes precipitation hardening relative to the low interstitial alloy. Both the carbon and the nitrogen alloy may be 'overaged' by coarsening at 850°C following SHT.

The impact toughness as measured by the ITT is improved by the introduction of mobile dislocations into the matrix. There exists an optimum free dislocation density whereby the crack is blunted and propagates in a high energy, ductile manner. Beyond the optimum density, dislocation interactions give rise to work-hardening and a fall-off in the toughness. Under the same conditions, nowever, the presence of coarse grain boundary particles causes brittle failure despite the increased matrix plasticity. Thus given the scenario whereby there exists a critical particle size for the initiation of a non-equilibrium crack, the application of a coarsening

treatment (or an increase in the total interstitial content) results in the attainment of a critical particle size at the given testing temperature, which causes fast fracture irrespective of the dislocation density.

The uniform distribution of incoherent particles in the matrix changes the macro-yield behaviour of the Fe-40Cr alloys. To wit, an increase in ductility has been related to coarse carbide, nitride and sulphide particles which favour strain localisation and thereby serve to increase the number of dislocation sources which may be activated in response to a local or far-field stress.

Elastic analysis of the stress distribution at the sulphide particle/matrix interface has shown that stresses of the order of the matrix yield stress may be generated as a result of differential thermal expansion effects, leading to the formation of primary prismatic dislocation arrays which increase the mobile dislocation density.

The response of the Fe-40Cr alloy to three minor alloying additions differs qualitatively in each case. The addition of 2wt% nickel improves the fracture resistance at low temperatures and high strain rates. The nickel is associated with an increased incidence of mechanical twinning. Since the stresses at terminating twins are effectively accommodated by the nickel alloy, this provides an additional deformation mechanism for stress relief. In addition, evidence to link the twinning to a more direct crack-blunting mechanism has been presented. However, the true efficacy of the nickel appears to lie in the well-documented alloy softening at high strain rates. The ability to accommodate the twinning and other stresses in the crack tip vicinity provides for enhanced crack blunting even in the event of embrittling secondary phases which nucleate fast cracks.

Super-stoichiometric niobium additions in the ratio Nb/(C+N)=2 improve the ductility of the alloy. Given the appropriate thermal treatment, niobium leaves the solid solution to react with residual carbon and nitrogen to inhibit embrittlement and sensitisation. Over-stabilisation causes a loss of impact resistance, but it has been shown that the toughness may be enhanced by simply increasing the dislocation density of the fully recrystallised alloy.

Finally, the addition of 0.2% ruthenium has a profound effect on the restoration processes of recovery and recrystallisation, as has already been mentioned. An increase in the SFE raises the recrystallisation temperature, with the consequence that annealing at 1050°C advances recovery coalescence. The recovered structure in all cases adversely affects the corrosion resistance and reduces the passive region.

CHAPTER 5

DISCUSSION

5.1 TOUGHNESS AS A FUNCTION OF THE FREE DISLOCATION DENSITY

The micromechanisms of fracture and the ability of the alloy to deform plastically in response to a local stress are inextricably related. Results have shown that the processes governing brittle fracture and those relating to dislocation emission and motion are both determined by the dislocation mobility.

From the outset, a distinction must be made between ductile behaviour at nominal strain rates and that at high strain rates. In the case of the former, dislocation mobility is determined by long range obstacles to dislocation migration, examples being dispersoids or boundaries. At high strain rates, commensurate with high dislocation velocities, dislocation mobility is governed by the intrinsic lattice friction and viscous drag effects, and the number of free dislocations becomes more important.

The propagation of a non-equilibrium crack may be understood from dynamic principles. The crack tip system is specified in terms of the plastic deformation in the crack tip field of influence, the lattice resistance or viscous drag on dislocation motion, and the fast crack velocity. In this case the operative stresses are short range order. Crack instability leading to brittle fracture is coincident with crack initiation when (1) the break-out of a crack across a brittle second phase particle providesa crack at the ferrite/particle interface of velocity of order greater than that at which the dislocations are able to move, or (2) there is an insufficient dislocation density to modify the emission conditions at the crack tip. In order to satisfy the conditions that the strain rate equal the product of the dislocation density and the dislocation velocity, an increased crack velocity requires that the dislocation density be increased accordingly, but also to take account of the shrinking crack influence field and the viscous drag effects on plastic slip which become more pronounced at higher velocities.

The provision of mobile dislocations by external means, in this case pre-straining by cold-rolling, has proved effective in raising the impact resistance, or, more accurately, decreasing the ITT. The ITT clearly increases with particle size, as may occur when the particles are coarsened, or when the total (C+N) level is raised. The velocity of the fast crack at the particle/ferrite interface in turn depends on the particle size, and the conditions for cleavage are therefore met at that size which, for a given testing temperature and strain rate, just provides a crack of velocity greater than that at which dislocations may be induced to move and multiply to cause blunting.

Studies such as those by Mintz et al (1982) have shown that above a critical carbide thickness, no further deterioration in the impact behaviour is observed. This critical point represents a transfer to a different fracture criterion, namely the ability to propagate a carbide crack in the ferrite matrix and across the next boundary, where the carbide effectively acts as a barrier to crack propagation. This constitutes a regime of little practical significance to the system under investigation, where the C+N is limited to 200 ppm.

The model proposed by Smith (1966) first suggested that the initiation of a fast crack within a second phase particle is derived from local stresses set up by plastic slip in the form of a pile-up blocked at the particle. This advanced the premise of a dislocation mechanism for cleavage initiation. The results of the pre-straining studies show that small degrees of plastic deformation (of the order of 1-2%) do indeed facilitate brittle fracture, with an accompanying loss of impact toughness. Similarly, in the coarse carbide material, pre-straining causes a loss of fracture resistance. There therefore appears to exist a regime below the DBTT whereby the introduction of plastic strain initially assists the initiation of micro-cracks. In terms of the Petch model outlined previously (Section 2.4) this may be explained on the basis of work-hardening to attain the cleavage fracture stress.

There remains the question of whether a fast crack, once having propagated across the ferrite/particle interface, may be arrested before it reaches the next barrier - that is to say, whether the magnitude of the crack velocity relative to the dislocation activity in the crack influence field may be made to become sub-critical. In effect this means changing the fracture conditions from that of initiation control to that of growth

control. The experimental evidence presented by Hahn (1984) shows that no dislocations are associated with the propagating crack, and that blunting and crack arrest only occur at a barrier, in this case the next grain boundary. No evidence to the contrary has been found in the present study. Below the ITT no degree of external ductility suffices to blunt a propagating crack. In all cases the evidence for crack blunting points to accommodation of the particle-sized crack prior to transfer into the next ferrite grain rather than arrest during propagation through the ferrite. The rate-controlling step is therefore the propagation of a microcrack through the interface. The crack, once transferred, runs with a super-critical velocity in a brittle manner.

5.2 PARTICLE-INDUCED DUCTILITY

A combination of factors contribute to the inherently low dislocation density of the Fe-40Cr system. These include:

(1) the high degree of chemical refinement to eliminate residual impurities,
(2) the absence of any phase transformation stresses, and
(3) the large grain size.

The ITT of the Fe-40Cr base alloys is shifted to well below ambient temperatures in response to a small amount of plastic deformation which has as a result a uniform but relatively low density of mobile dislocations in the matrix. A comparable dislocation density is readily induced by the punching of primary prismatic loops at a sparse distribution of active second phase particles.

Prismatic punching to accommodate tessellated stresses represents one method of harnessing particle sources. The activation of a small number of sulphide inclusions is sufficient to raise the matrix plasticity to the extent that the ITT is again lowered to below ambient temperatures. There is clearly an optimum size and volume fraction for the particles in maximising the ductile response.

A further construction may be placed on the role of the inclusions in dispersion toughening. The model proposed by Lin and Thomson (Section 2.5) requires that an indeterminate dislocation source be available for triggering by the local crack k-field to alter the emission conditions at the crack-tip. As has been demonstrated, this "source" may

take the form of dislocations introduced heterogeneously by pre-straining or thermal stresses. Alternatively, it is apparent that the particles may induce localised slip in response to an external stress, such as that of the crack field. The initiation of slip at sulphide particles has, in fact, been demonstrated in the high resolution scanning microscopy of the deformed region. Apart from the stress concentration factor associated with the particles, elastic analysis has illustrated the presence of large residual thermal stresses at the particle interface which, as has already been pointed out, may be additive to the imposed stress fields, assisting dislocation nucleation even though the residual stress itself may be insufficient to spontaneously produce dislocations. The triggering of slip at the sulphide particles therefore provides a means of crack blunting as envisaged by Lin and Thomson.

Li and Sanday (1986) have approached dispersion toughening from a different angle. Considering the residual stresses at the particles, they have demonstrated mathematically that if the particles are under hydrostatic tension, a crack may be attracted into the particle and blunted. Under these conditions a periodic array of inclusions may increase the toughness in proportion to the volume fraction of inclusions, the misfit strain, and the square root of the inclusion spacing. Inclusions under hydrostatic pressure on the other hand, will resist crack entrance so that the crack will propagate between inclusions. In either case there is an internal stress field which may resist crack growth.

Dispersion toughening has been conceptualised on several other levels. For instance, Evans (1972) has accounted for the increase in fracture strength brought about by a dispersoid by postulating a line tension effect as the crack bows between obstacles in its slip plane, effectively pinning the crack. Wilcox et al (1972) attributed a reduction in the DBTT of thoriated chromium to slip dispersal by particles such that critical stress or strain concentrations for crack nucleation are more difficult to achieve. Alternative theories of crack blunting by intersection with the particle, or crack deviation such as that proposed by Li and Sanday (1986) have already been mentioned. The essential concept is that the impact resistance may be improved by a dispersion of second phase particles.

The ready availability of slip sources in the form of second phase

particles is also predisposed to improving the ductile flow characteristics at nominal strain rates. Strain gradients have been identified at coarse carbide, nitride and sulphide particles in the present study (see Figures 4.26(c) and 4.28(a), associated with improved tensile ductility. At low strain rates, sufficient time is allowed for local stress accommodation at the particles, resulting in substantial plastic deformation prior to the accumulation of sufficient stress to create a crack at the particle/ferrite interface. Thus the crack-tip is presented with conditions of prior deformation to effect the necessary blunting. Unfortunately at high strain rates most particles have interface properties which promote cleavage. The formation of plate-like carbides and nitrides on habit planes, sulphide stringers with a high aspect ratio, and oxides with a low decohesion strength have all been shown to be undesirable in this regard.

The effective utilization of residual impurities as secondary-phase dislocation sources offers an elegant step towards cost-effective production of ductile alloys. The current study has harnessed the unique thermal and mechanical properties of sulphides to the advantage of toughness and ductility. Reference to Figure 2.14 shows that few other inclusions have a similar potential for thermal dislocation generation. The shape and distribution of the sulphides may be controlled by simple thermo-mechanical processing. In addition the corrosion resistance has been shown to be relatively inert to the CrS species. The chromium carbonitride species, on the other hand have proved to be unsuitable from the point of view of impact toughness and corrosion resistance. However, improvements in toughness and ductility, and corrosion resistance stand to be gained by use of stabilising elements to form more stable carbonitride species. Unfortunately the precipitates all suffer from high temperature instability, and use of more stable dispersoids such as ThO_2 may be beneficial, as suggested by the work of Wilcox et al (1972). A further possibility lies in the use of rare earth metal (REM) additions in conjunction with sulphur for inclusion shape modification. The effect of small REM additions of up to 0.3% was previously studied by Hermanus (Section 2.2.5). The production of higher melting point sulphides with lower aspect ratios would greatly extend the thermal range over which a sulphide dispersoid could be obtained.

Finally, there exists the possibility of enhanced dislocation formation by the intrinsic intermetallic phases such as sigma. The viability of a sigmatised alloy cannot be countenanced at this stage in light of what is known of the influence of the brittle phase on the impact and corrosion resistance. Nevertheless, the enhanced formation of sigma phase to increase the inter-phase dislocation density, followed by rapid dissolution of the sigma phase at higher temperatures to leave a residual dislocation substructure has been proposed by De Marsh (1986), and presents an interesting study.

5.3 THE ROLE OF BOUNDARIES IN THE FRACTURE PROCESS

The results of the study have shown that both the macro-ferrite grain boundaries, as well as the low angle sub-grain boundaries introduced by recovery annealing are intimately associated with the initiation and growth control of a crack. In effect, brittle cleavage initiation has been linked to the occurrence of second phase particles, primarily at the grain boundaries, which transfer non-equilibrium or fast-cracks across the particle/ferrite interface. The low-angle boundaries, on the other hand occur under conditions which can lead to crack blunting. Consideration is given to each of these in turn.

GRAIN BOUNDARIES

The effect of grain size on the impact toughness is obscured by the competing influence of the particle size in the present study, a result which is also reflected in the conflict in the published literature. The grain boundaries constitute the principal nucleation sites for dynamic cracks as a result of the propensity for intergranular precipitation under all heat treatment conditions. Given sufficiently coarse precipitation, a reduction in the grain size therefore implies an increased frequency in the crack initiation events. However, the apparent anomaly whereby an increase in the grain size leads to improved impact resistance in the Fe-40Cr alloys may more reasonably be explained by the greater degree of dissolution and re-precipitation of carbo-nitrides intragranularly following cooling from the higher temperatures with which the coarser grain size is associated. Thus, experiment has shown that a solutionising temperature of 1250°C is more effective in dissolving the carbides than

1050°C. Grain growth at the higher temperature, associated with greater diffusion paths to the grain boundary areas, accompanied by rapid cooling therefore forces a fine, intragranular dispersion of sub-critical sized particles, with an improvement in the resistance to cleavage initiation. Similarly, a reduction in the grain-size of at least an order of magnitude is expected to improve the resistance to fast crack initiation by diluting the grain boundary precipitation over a larger area. This, in fact, is reflected in the results of Grubb (1982) who observed an ITT reduction of 160°C for a grain size reduction from 600 to 27 microns in high interstitial, unstabilised Fe-26Cr alloys.

A systematic study of the toughness as a function of grain size and carbide thickness lies beyond the scope of the present study. Nevertheless, the elegant treatment of Petch (1986) has provided a model to relate the two parameters which begs to be tested empirically. The results of this study largely support the Petch model, in so far as

(1) for a given carbide thickness, grain refinement has little effect on toughness over a given range of grain sizes, and
(2) the measured effect of grain size is outweighed by the carbide dimensions, which often leads to the anomalous increase in toughness with grain size because of concurrent refinement in the carbide dimensions.

The grain size also plays several important secondary roles. In the first instance a large grain size is associated with a greater tendency to twinning. The grain boundaries act both as sources as well as barriers for terminating twins. The alliance of the twin lamellae with the plastic deformation process has been demonstrated in the nickel alloys, and grain size may consequently play an important role in this respect. Secondly, and more importantly, the grain boundaries have been identified as important sources of dislocations for ductility, and several instances of dislocation emission at grain boundaries have been presented. In the pre-straining studies, for example, a smaller degree of deformation was required for impact toughness in the smaller grained alloys. This is borne out by Lewis and Pickering (1982) who report an increase in the work hardening rate of fully recrystallised structures by a refinement in the ferrite grain size. Kestenbach (1977) has noted that the formation of cell walls usually occurs near the grain boudaries, an observation which is backed by the current study.

LOW ANGLE BOUNDARIES

The formation of low-angle sub-boundaries within the macro-ferrite grains by polygonization in the final stages of recovery causes localised strain, which can conceptually be represented as an array of dislocations which take up the mismatch across a small misorientation between sub-grains. A low-angle array is shown in Figure 5.1.

No clear description of the role of sub-boundaries on the plastic deformation process exists in the literature, although several indirect

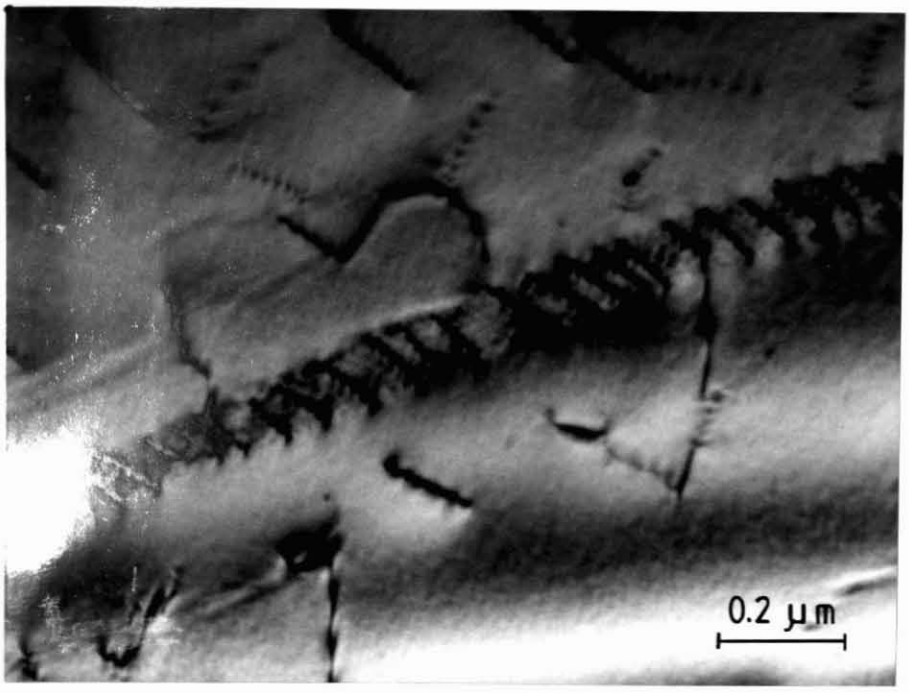

FIGURE 5.1 Sub-array in Fe-40Cr recovered at 850°C

inferences have been made. The increase in strength caused by a sub-grain structure has already been noted. Analyses based on a modified Petch relationship suggest that the ability of sub-boundaries to resist the passage of dislocations or the transference of slip is equal to that of grain boundaries. The sub-boundaries may interact strongly with, trap or allow dislocations to pass through, suffering the formation of jogs [McQueen (1977)]. The results of pre-straining of Fe-40Cr in the recovered condition show that the substructure is unequivocally related to work-hardening. In terms of the Alden model (Equation 2.9) the sub-boundaries reduce the mobile dislocation density by an increased rate of trapping.

There is an alternative view that the sub-boundaries dissociate under stress to act as sources of dislocations. [Garrod and Wain (1965)]. In the present system, the boundary arrays are ineffective barriers to cleavage at ambient temperatures, particularly since prior-ageing is associated with enhanced intragranular precipitation at the sub-boundaries. Figure 5.2 shows the transfer of a brittle crack through the sub-grains without deflection. The boundary dislocations are therefore effectively pinned, especially in the presence of precipitates, and the release of a dislocation means sequential unpinning of the nodes as reported by Lindroos and Miekkoja (1968). This process is necessarily thermally activated, and at higher temperatures there exists the possibility that the dislocations have sufficient freedom to interact with the stress field of a crack. This accounts for an enhanced impact resistance noticed in Fe-40Cr alloys which are prior-recovered. Similarly, under slow strain rates some results suggest that the sub-structure is beneficial to the tensile ductility (See for example Table 4.1, where the recovered alloys display the maximum ductility). There is However, further evidence to show that changes in the mechanical properties may be related to modified precipitation effects brought about by the sub-structure.

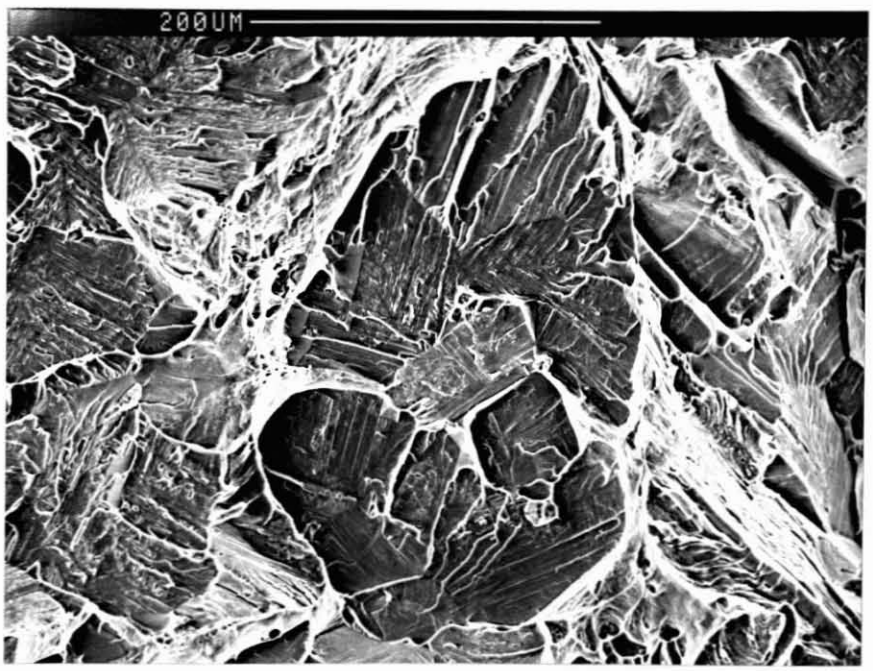

FIGURE 5.2 Cleavage crack path through sub-boundaries at ambient temperature

The influence of a dislocation sub-structure on the precipitation kinetics has been examined in detail by researchers such as Stumpf (1968) and Smith (1975). It is now well established that at high dislocation densities, rapid solute transport along the paths provided by the dislocation network becomes significant, and the enhanced diffusion processes facilitate precipitation. The role of the sub-boundaries in solute transport is further extended by the fact that they may be pinned by the precipitates, leading to the development of an interconnecting network between the precipitates. As a result coarsening, or Ostwald ripening, by means of which the more stable precipitates grow at the expense of the smaller particles, is facilitated.

The provision of a stable sub-structure also increases the kinetics of heterogeneous precipitate nucleation during cooling compared to the recrystallised condition by providing additional nucleation sites. This is also generally considered to decrease the tendency toward sensitization by minimising the amount of carbide precipitated inter-granularly. [Sedriks (1978)]. It is clear that a reduction in the grain boundary precipitation advances the cleavage fracture resistance.

The role of a prior-ageing treatment at 850°C can therefore be described in terms of a change in the recrystallisation and precipitation characteristics. While prior-ageing holds benefits for the impact toughness of Fe-40Cr alloys, the corrosion properties are impaired by a recovered substructure. The sub-structure also prevents the application of pre-straining to further reduce the ITT. The usefulness of the treatment therefore appears limited.

5.4 HIGH TEMPERATURE EMBRITTLEMENT

The construction placed on observations of high temperature embrittlement in the literature is clearly subject to the testing conditions and alloy chemistry. There is no doubt that high temperature embrittlement is essentially related to precipitation of secondary phases during cooling from super-saturated solid solution. Since this occurs both intra- and intergranularly, the effect on the mechanical properties varies with the strain rate. The occurrence of a fine intragranular dispersoid has been shown to be detrimental to the tensile ductility, but does not necessarily

impair the impact toughness. On the other hand, grain boundary precipitation is more favourable to the tensile ductility, but causes impact embrittlement at a critical precipitate thickness, as discussed. The resistance to intragranular crack initiation has previously been attributed to restriction by the fine dispersion on the dislocation motion necessary to form a stress concentration [Martin (1980)]. It is only when the intragranular precipitates attain a size sufficiently coarse to initiate a fast crack that the toughness is adversely affected.

The relative contribution of the precipitate species to embrittlement has been isolated. Nitrides cause embrittlement primarily by a precipitation hardening reaction associated with coherent strain centres in the matrix, which increase the flow stress. By contrast tne precipitation of incoherent carbides which act as localised plastic strain centres promotes the tensile ductility and strain to fracture. However, both carbides and nitrides in the over-aged condition provide low energy crack initiation centres in the form of plate and grain boundary precipitates at high strain rates.

5.5 THE EFFECT OF NICKEL ADDITIONS

In the simplest analysis the addition of nickel is associated with solid solution strengthening and an increase in the flow stress at ambient temperatures. At high strain rates and low temperatures the nickel addition enhances toughness and ductility, which is consistent with the behaviour of systems in which the alloy chemistry exhibits solution softening. This provides a basis for interpretation of the results in terms of enhanced dislocation dynamics.

Solute-induced changes in the fracture behaviour do not occur as the result of any real changes in the true fracture strength of an alloy, but rather are due to changes in the resistance to plastic deformation and the ease of stress relaxation processes at sites of stress concentrations. Stress accommodation may take the form of slip or mechanical twinning, and evidence has shown that the addition of nickel facilitates both of these deformation mechanisms in Fe-40Cr. In general, twinning is favoured by an increased resistance to plastic slip, and therefore lower temperatures and high strain rates are expected to suppress slip in favour of twinning.

Since these conditions also favour the propagation of brittle fracture, the role of the nickel solute must be resolved in terms of whether

(1) the facilitation of twinning provides an active mechanism for plastic deformation and stress relief supplemental to slip,
(2) whether the twin lamellae promote slip, or
(3) whether twinning is simply a by-product of the deformation process.

The development of twinning in the nickel alloy has been associated with good ductility and impact toughness, and this has been linked on a microstructural level to enhanced plastic deformation processes. However, it should be pointed out that twinning is not the exclusive domain of the nickel alloy, but has been observed in varying degrees in all the other alloys studied, being typical of the rhenium ductilising effect characterised by Stephens and Klopp (Section 2.3.1). In these cases there was nothing to suggest that twinning promoted the fracture resistance, and the occurrence of twinning was always associated with the brittle fracture condition. What distinguishes the nickel alloy therefore, is an ability to reconcile the stresses accompanying twinning with plastic deformation. The theory of alloy softening, which invokes a mechanism of enhanced dislocation dynamics based on a modified lattice friction, can in principle explain a greater capacity for plastic deformation and hence stress accommodation at sites such as terminating twins, twin boundaries and crack tips. Given the increased ability to deform mechanically, it is reasonable to advance the likelihood of a synchronised response of plastic deformation to twinning stresses.

The strain-rate dependence of the Fe-40Cr system implies that stresses for brittle crack initiation are reached before stress accommodation can occur. Since the observed times of formation of twins can be of the order of several micro-seconds [Honeycombe (1984)], mechanical twinning is particularly suited to high strain-rate stress accommodation at the crack tip. Observations of the dislocation activity at these shear bands indicates that the primary twins can subsequently act as centres for plastic slip and thus crack blunting. The sequence of events may therefore be given by:

local crack stress field
↓
high strain rate formation of primary twins ahead of the crack
↓
initiation of plastic slip at twin boundaries
↓
crack blunting

The mutual interaction between mechanical twinning and slip can therefore be simply stated: The addition of nickel to the Fe-40Cr alloy promotes both twinning and slip. The twinning stresses are sustained by enhanced stress accommodation, and in turn facilitate slip.

The flip side of the coin, namely that twinning is a by-product of the deformation process, can also be argued on the basis of an enhanced slip mechanism. Twinning usually requires a higher stress to initiate it than does slip, and the simultaneous movement of all the atoms in the twin band is therefore improbable. Several dislocation models for progressive twinning have consequently been postulated, and it seems clear that dislocations are also directly responsible for mechanical twinning. [Honeycombe (1984)]. The origin of the increased twinning in the nickel alloy is therefore in all probability traceable to the solution softening mechanism which is associated with enhanced dislocation activity. The fact remains that the twin lamellae contribute to overall work-hardening in the crack region.

An alternative view, namely that the addition of nickel may modify the twin growth rate, thereby extending the time for accommodation processes to occur, requires further experimental study.

The desired ductilization at high strain rates has been produced in no less than three ways. Each of these mechanisms have been related to an effective increase in the dislocation mobility at the crack tip. Pre-straining serves to increase the dislocation density within the crack influence field. Similarly prismatic punching at second phase particles provides an additional source of dislocations. Finally, the addition of nickel improves the cleavage resistance by enhanced stress accommodation of local stresses. Each mechanism represents a practical solution for the fabrication of tough Fe-40Cr alloys. From the engineering point of view, alloying with nickel holds several advantages. The addition of as little as 2wt%Ni increases the strength of the alloy without impairing the tensile ductility. The nickel is easily added to the melt and does not require a complex annealing practice to control the formation of secondary phases. From the corrosion point of view, the use of nickel in stainless alloys is well established. There is the additional advantage of applications in cast products, which precludes the use of mechanical means to alter the microstructure. Further development of Fe-40Cr alloys with minor nickel additions is therefore justified.

5.6 THE RELATIONSHIP BETWEEN CORROSION RESISTANCE AND DUCTILITY

This study has emphasised the importance of a dualistic approach to the alloy development of corrosion resistant alloys. Elucidation of the microstructural effects is central to both the mechanical as well as the corrosion properties since both are determined by the chemical composition and fabrication route.

A number of microstructural parameters have been studied and linked to the fracture process in Fe-40Cr alloys. These include the occurrence of second phase particles, the dislocation substructure, and controlled alloying additions to impart specific properties. The effect of some of these variables on the general and localised corrosion resistance has been demonstrated by electrochemical testing in reducing acid and also chloride environments. In most cases it is found that factors debilitating to the impact toughness and ductility also impair the corrosion resistance. The major conclusions of the corrosion studies detailed in Appendix A may be summarised as follows:

(1) A recovered sub-structure destabilises the passivity. The optimum corrosion resistance is obtained by ensuring full recrystallisation.
(2) Cathodic modification by 0,2% ruthenium additions improves the passivation kinetics, but promotes recovery annealing associated with a sub-structure.
(3) In the absence of stabilising additives to getter the interstitials, the Fe-40Cr alloys are prone to grain boundary attack under all conditions.
(4) The alloys exhibit good pitting resistance in aqueous chloride environments.
(5) The addition of 500 ppm sulphur has only a slight negative effect on the pitting potential. Pitting occurs primarily at the chromium-enriched oxide phases.
(6) Small amounts of cold work may be tolerated without destabilising the passivity.

It is usually accepted that high temperature embrittlement and loss of corrosion resistance are related phenomena. As with other stainless steel systems, intergranular attack is coupled to the precipitation of grain boundary phases with resulting depletion of chromium in the adjacent matrix. Grain boundary sensitisation and loss of impact resistance are

therefore intimately linked. The post-ageing treatment in the vicinity of 850°C in unstabilised alloys is therefore undesirable from both points of view.

The use of stabilising elements such as niobium to prevent intergranular precipitation holds merit for both the mechanical and the corrosion properties. In this case correct manipulation of heat treatment cycles is necessary to ensure (1) full recrystallisation, and (2) complete reaction of the residual impurities with the niobium. This brings several considerations to the fore. In the first place, a greater degree of alloying brings with it the problems associated with the increased kinetics of intermetallic phase formation. Furthermore, prolonged soaking at an intermediate temperature to ensure complete reaction with the residual interstitials coincides with the formation of sigma phase. The desirability of avoiding the intermediate ageing treatment therefore becomes apparent. This leaves the alternative approach of over-stabilising to promote gettering. Studies by Tullmin (1988) have indicated that stabilising ratio's of as high as 35 are necessary to ensure adequate gettering during cooling from the solutionising temperature. While over-stabilisation brings about a loss of impact toughness, the present study has shown how this may be overcome by, for example, pre-straining.

Before rejecting the utility of a post-ageing treatment outright, it should be pointed out that the concurrent improvement in the tensile ductility lends itself to forming processes such as cold pressing. This allows fabrication subsequent to which solutionising can be carried out to restore the primary impact and corrosion resistance.

Recovery annealing of the wrought microstructure to establish a stable sub-boundary network as opposed to full recrystallisation has been associated with an improvement in the impact toughness. Unfortunately, the sub-structure causes a loss of corrosion resistance due to a greater site density for preferential attack at the corrosion surface. The presence of (1) second phase particles or (2) solutes which retard the recrystallisation kinetics consequently hold an inherent potential for promoting localised attack. The use of niobium is a case in point. In addition, it seems clear that a small addition of ruthenium results in a recovered grain structure at temperatures of 1050°C and below. This is attributed to an increase in the SFE. The conditions for cathodic

activation are considerably restricted as a consequence, and necessitate higher annealing temperatures (or a greater degree of cold work) to create a driving force for recrystallisation.

The nature of sensitisation of the sub-boundaries appears to be the result of preferential attack at intragranular precipitation. The mechanism whereby the dislocation network increases the number of nucleation sites has already been discussed. As in the case of boundaries of higher misorientation, selective pitting at the low-angle boundaries therefore arises from compositional fluctuations. It is pertinent to note that only certain grains are attacked, which is consistent with an orientation dependence of pitting at either fresh or decorated dislocations in high chromium alloys.

The corrosion tests confirm the effectiveness of ruthenium as a cathodic modificant. Provided the correct annealing cycles are carried out, the addition of 0,2% Ru causes only a slight change in the mechanical properties, this being associated mainly with an increase in the flow stress.

The removal of the chromium-rich oxide phases also benefits the mechanical/corrosion properties. The oxides provide sites for microcrack initiation, as well as being prime sites for pitting attack. Considerable advantages therefore stand to be gained by deoxidation of the alloy melts via the addition of gettering agents such as aluminium.

In as much as the sulphides stabilise the substructure and form grain-boundary precipitates, additions of sulphur impair the corrosion resistance. In themselves the chromium sulphide spheroids are relatively noble as compared with other inclusions, and resistant to pitting.

Finally, the corrosion tests have established that small cold reductions of the order of 10% cause little change in the corrosion resistance. Thus a uniform dislocation network is relatively immune to attack as compared with the recovered dislocation sub-arrays. This is an important consideration in that forming processes typically involve deformations in the region of 5% [Redmond et al (1981)] and can usefully be harnessed to improve the toughness.

5.7 THE DEVELOPMENT OF TOUGH Fe-40Cr ALLOYS

In summary, an understanding has been gained of some of the microstructural variables governing the deformation processes in ferritic alloys. The principles outlined in this study obviously extend to other systems, such as the lower chromium steels. The parameters critical for good toughness in Fe-40Cr alloys may be summed up as follows:

(1) The state of the residual elements must be controlled to preclude the formation of secondary phases associated with brittle crack initiation events.
(2) It has been shown that the impact toughness is not necessarily correlated with the tensile ductility. Good toughness relies on the number of mobile dislocations available to interact with the crack front.

In addition, the corrosion characteristics place several further constraints on the fabrication practice, viz.

(1) The elimination of a recovered dislocation substructure must be ensured to prevent destabilisation of the passivity.
(2) Stabilisation of the residual impurities is essential to prevent grain boundary sensitisation.

Careful control of the fabrication procedure has enabled the production of tough, corrosion-resistant Fe-40Cr alloys. The efficacy of standard procedures such as isothermal heat treatment cycles and pre-straining by cold rolling for increasing toughness has been demonstrated.

Although use has been made of high purity raw materials to make the alloys on a laboratory scale, the routine attainment of similar levels of refinement in modern commercial practice has made the production of high purity alloys viable.

The advantages of minor alloying additions are self-evident. Of particular importance is the improvement in the mechanical properties gained by relatively small amounts of nickel. No attempt has been made to optimise these additions with respect to the thermo-mechanical schedules or alloy

composition, and considerable scope remains to evaluate the response of the system to larger nickel additions.

Dispersion toughening, in this case by the exploitation of the controlled residual element, sulphur, has also proved effective. Recommendations for the use of more stable dispersoids have already been mentioned. Once again it remains to optimise the dispersoid distribution relative to the alloy composition.

Cathodically modified alloys based on a composition of Fe-40wt%Cr must ultimately rely on a range of alloying additions to impart the requisite properties. Thus the alloy may eventually be any combination of

Fe-40Cr
- + PGM - cathodic modification
- + Ni - strength and toughness
- + Nb,Ti - stabilisation of interstitials
- + REM - inclusion shape control
- + S - dispersion toughening
- + Mo - enhanced pitting resistance

Notwithstanding the resulting complexity in the alloy chemistry, which inevitably detracts from the philosophy of a simple binary alloy, the development of Fe-40Cr base alloys is deemed practicable from the alloy engineering point of view.

A final point regarding the material economics is worth noting. The disproportionate cost of the PGM additions may ultimately necessitate re-evaluation of their use in bulk alloys. Studies into their use as surface coatings on the base alloy rather than as additions to the melt have recently been proposed. This concept may bring the alloy system one step closer to commercial feasibility.

CHAPTER 6

CONCLUSIONS

6.1 MAJOR CONCLUSIONS

A series of experimental alloys based on an Fe-40Cr composition have been studied in the wrought condition. The mechanical properties were examined in relation to a series of isothermal annealing treatments comprising ageing and solutionising cycles which terminated in a quench from the final soaking temperature. The plastic deformation and fracture mechanisms have been rationalised in terms of the microstructural parameters:

1. The toughness of the alloys at high strain rates is due to their resistance to dynamic fast crack initiation rather than crack propagation. Once initiated, a fast crack propagates to failure in a brittle manner. Dynamic crack initiation sites for cleavage are provided primarily by grain boundary precipitates of a critical thickness, but also by coarse intragranular second phase particles. Since the degree of the precipitation is a function of the extent of supersaturation of solid solution, the toughness of the base alloy is directly related to the total interstitial content.

2. The impact toughness is enhanced by increasing the mobile dislocation density up to an optimum level, and this has been achieved in two ways:

   (1) Pre-straining by cold reductions of up to 10% of fully recrystallised plate.
   (2) Prismatic punching of primary dislocation loops at second phase particles in response to tessellated or local stresses.

   In both cases the effect is to achieve external blunting and/or shielding at the crack tip.

3. The overall ductility is improved by increasing the number of dislocation sources in the form of second phase particles which act as local strain centres.

4. The formation of a recovered sub-structure is associated with a greater impact toughness, evidently related to a modification of the precipitation processes, and a contribution to the work-hardening component at the crack-front.

6.2 OTHER CONCLUSIONS

1. The high temperature embrittlement phenomenon following quenching from the solution heat treatment temperature is the result of precipitation at the grain boundary sites. The impact toughness is not governed by fine incoherent intragranular precipitation, although this impairs the tensile ductility. The strain to fracture is a function of the dislocation mobility, rather than the dislocation density, and depends on the ability of the dislocations to migrate unhindered through the matrix. The tensile ductility may be recovered by a coarsening treatment which favours precipitation at the grain boundaries, but this in turn compromises the impact toughness.

2. The carbide and nitride precipitates have an independent effect on the mechanical properties. The precipitation of carbides promotes ductility by acting as local plastic strain centres at nominal strain rates, whereas the nitrides cause overall strengthening.

3. The addition of nickel raises the flow stress at ambient temperatures and nominal strain rates, but advances solid solution softening at low temperatures and high strain rates by enhanced local stress accommodation. This is accompanied by a high incidence of mechanical twinning, which provides an additional mechanism for stress relief, and contributes to plastic blunting of the crack.

4. The secondary phases have been successfully isolated by analytical transmission microscopy. The carbide phase has been identified as the chromium-enriched complex fcc $M_{23}C_6$, although carbides of the metastable M_7C_3 type may be introduced under the non-equilibrium cooling conditions. The nitride phase is probably the hexagonal Cr_2N. An oxide

phase, the hcp Cr_2O_3, or 'escolaite', was identified, being rich in chromium, but also containing smaller amounts of iron and aluminium. The sulphide species was classified as the monoclinic CrS type. No evidence of the tcp sigma phase was found in the alloys subjected to the standard heat treatment schedules.

A range of Fe-40Cr alloys were selected for localised corrosion studies using potentiodynamic techniques. The corrosion resistance was found to be related to the alloy chemistry and processing route:

5. The passivity of the alloys in acid media is destabilised following recovery annealing which results in the formation of a dislocation substructure.

6. The addition of 0.2% ruthenium as a cathodic modificant renders the alloy prone to restoration by recovery up to 1050°C, which subsequently impairs the corrosion resistance. It is therefore necessary to effect full recrystallisation at higher temperatures to ensure the optimum corrosion resistance.

7. The alloys show a high resistance to pitting in chloride media, although this is compromised by the presence of the chromium-enriched oxide phases.

REFERENCES

AARONSON, H.I., "Observations on Interphase Boundary Structure," J. Microscopy, Vol. 102, Pt3, Dec., 1974, pp275 - 300.

ABO, H. et al, The Role of Carbon and Nitrogen on the Toughness and Intergranular Corrosion of Ferritic Stainless Steels," Stainless Steel '77, Conf. Proc., London, England, Sep. 26-27, 1977, Barr, R.Q. (Ed), Climax Molybdenum Co., 1977, pp35 - 48.

ALDEN, T.H., "Theory of Mobile Dislocation Density: Application to the Deformation of 304 Stainless Steel," Metall. Trans. A., Vol.18A, Jan., 1987, pp51 - 62.

ALDEN, T.H., "Theory of Plastic and Viscous Deformation," Metall. Trans. A., Vol. 18A, May, 1987, pp811 - 826.

ANDERSSON, J-O., "A Thermodynamic Evaluation of the Fe-Cr-C System," Metall. Trans. A., Vol. 19A, March, 1988, pp627 - 636.

ANGERS, L., FINE, M.E. and WEERTMAN, J.R., "Effect of Plastic Deformation on the Coarsening of Dispersoids in a Rapidly Solidified Al-Fe-Ce Alloy," Metall. Trans. A., Vol.18A, April, 1987, pp555 - 562.

ANGLADA, M., NASARRE, M. and PLANELL, J.A., "High Temperature Mechanical Twinning of Two Fe-Cr-Mo-Ni Ferritic Stainless Steels," Scripta Metall., Vol. 21, 1987, pp931 - 936.

ARGON, A.S. and IM, J., "Separation of Second Phase Particles in Spheroidized 1045 Steel, Cu-0.6 Pct Cr Alloy, and Maraging Steel in Plastic Straining", Metall. Trans. A., Vol.6A, 1975, pp839 - 851.

ASHBROOK, R.W. and MARDER, A.R., "The Effect of Initial Carbide Morphology on Abnormal Grain Growth in Decarburized Steels," Metall. Trans. A., Vol. 16A, May, 1985, pp897 - 906.

ASHBY, M.F., GELLES, S.H. and TANNER, L.E., "The Stress at which Dislocations are Generated at a Particle-Matrix Interface," Phil. Mag., Vol. 19, No. 160, April, 1969, p757.

ASHBY, M.F. and EMBURY, J.D., "The Influence of Dislocation Density on the Ductile-Brittle Transition in BCC Metals," Scripta Metall., Vol. 19, 1985, pp557 - 562.

BAKER, T.J. and JOHNSON, R., "Overheating and Fracture Toughness," J. Iron and Steel Inst., Nov., 1973, pp783 - 791.

BALL, A., BULLEN, F.P. and WAIN, H.L., "The Ductile/Brittle Transition for Chromium Pressurized at 10-25 kbars,"
Mater. Sci. Eng., Vol. 3, 1968/69, pp283 - 288.

BALL, A. and BULLEN, F.P., "Pressurization Effects in Chromium,"
Phil. Mag., Vol.22, No.176, Aug, 1970, pp301 - 315.

BARBANGELO, A., "Influence of Nonmetallic Inclusions on Fatigue Crack Growth in a Structural Steel,"
J. Mater. Sci., Vol. 20, 1985, pp2087 - 2092.

BARCIK, J., "The Kinetics of Sigma-Phase Precipitation in AISI 310 and AISI 316 Steels,"
Metall. Trans. A., Vol. 14A, April, 1983, pp635 - 641.

BARCIK, J., "The Process of Sigma-Phase Solution in 25 Pct Cr-20 Pct Ni Austenitic Steels,"
Metall. Trans. A., Vol. 18A, July, 1987, pp1171 - 1177.

BEECH, J. and WARRINGTON, D.M., "M_7C_3 to $M_{23}C_6$ Transformation in Chromium Containing alloys,"
J. Iron and Steel Inst., May, 1966, pp460 - 468.

BELL, T. and KUMAR, D., "Thermochemical Production of Nitrogen Stainless Steels,"
Metals Technol., Sept., 1978, pp293 - 301.

BEREMIN, F.M., "Cavity Formation from Inclusions in Ductile Fracture of A508 Steel,"
Metall. Trans. A., Vol. 12A, May, 1981, pp723 - 731.

BINDER, W.R. and SPENDELOW, H.O., "The Influence of Chromium on the Mechanical Properties of Plain Chromium Steels,"
Trans. ASM, 1951, 43, 759.

BOTTA, W.J., CHRISTIAN, J.W. and TAYLER, G.,"Solution Hardening and Softening in Nb-Zr Single Crystals,"
Phil. Mag. A., Vol. 57, No. 5, 1988, pp703 - 716.

BRENNER, S.S., MILLER, M.K. and SOFFA, W.A., "Spinodal Decomposition of Iron-32 at % Chromium at 470°C,"
Scripta Metallurgica, Vol. 16, 1982, pp831 - 836.

BREWER, L. and CHANG, S-G., "Constitution of Ternary Alloys,"
ASM Metals Handbook, 8th Ed., Vol.8, 1973, p422.

BRIANT, C.L. and BANERJI, S.K., "Tempered Martensite Embrittlement and Intergranular Fracture in an Ultra-High Strength Sulfur Doped Steel,"
Metall. Trans. A., Vol. 12A, Feb., 1981, pp309 - 319.

BRIANT, C.L. and BANERJI, S.K. (Eds), "Treatise on Materials Science and Technology,"
Vol. 25, Embrittlement of Engineering Alloys, Academic Press, 1983.

BRIANT, C.L., "Grain Boundary Segregation of Phosphorous and Sulfur in Types 304L and 316L Stainless Steel,"
Metall. Trans. A., Vol. 18A, April, 1987, pp691 - 699.

BROOKSBANK, D. and ANDREWS, K.W., "Stress Fields Around Inclusions and their Relation to Mechanical Properties,"
J. Iron. Steel. Inst., April, 1972, pp246 - 255.

BROWN, E.L., BURNETT, M.E., PURTSCHER, P.T. and KRAUSS, G., "Intermetallic Phase Formation in 25Cr-3Mo-4Ni Ferritic Stainless Steel,"
Metall., Trans. A., Vol. 14A, May, 1983, pp791 - 800.

BROWN, L.M., WOOLHOUSE, G.R. and VALDRE, U., "Radiation - Induced Coherency Loss in a Cu-Co Alloy,"
Phil. Mag., 17, 1968, p781.

BROWN, L.M. and WOOLHOUSE, G.R., "The Loss of Coherency of Precipitates and the Generation of Dislocations,"
Phil. Mag., Vol. 17, p781.

BYWATER, K.A. and DYSON, D.J., "The Precipitation of Cr_2N in 17%Cr Steels,"
Metal Science, Vol. 9, 1975, pp155 - 162.

CHANDRA, T. and KUCHLMAYR, R., "Effect of Strain Rate on Sigma Formation in Ferrite-Austenite Stainless Steel at High Temperatures,"
J. Materials Science, Vol. 23, 1988, pp723 - 728.

CHOMEL, P and COTTU, J.P., "Influence of Substitutional Elements on Flow Stress in Iron at Low Temperature,"
Acta Metall., Vol. 30, 1982, pp1481 - 1491.

COTTRELL, A.H., "Theory of Brittle Fracture in Steel and Similar Metals,"
Trans. Met. Soc. AIME, April, 1958, pp192 - 202.

CURRY, D. and KNOTT, J.F., "Effects of Microstructure on Cleavage Fracture Stress in Steel,"
Metal Science, Vol. 12, 1978, pp511 - 514.

CURRY, D.A. and KNOTT, J.F., "Effect of Microstructure on Cleavage Fracture Toughness of Quenched and Tempered Steels,"
Metal Science, Vol. 13, 1979, p341 - 345.

DAWSON, W.M. and SALE, F.R., "Enthalpies of Formation of Chromium Carbides,"
Metall. Trans. A, Vol. 8A, Jan., 1977, p15.

DEAN, M.S. and PLUMBRIDGE, W.J., "Prediction of Sigma Phase Formation in Stainless Steels,"
Nucl. Energy, Vol. 21, No.2, April, 1982, pp119 - 135.

DEMARSH, E.A., "A Study of the Embrittlement and Toughening of Fe-40% Cr Alloys,"
M.Sc Thesis, Univ. Witwatersrand, Johannesburg, 1986.

DEMO, J.J., "Mechanism of High Temperature Embrittlement and Loss of Corrosion Resistance in AISI Type 446 Stainless Steel,"
Corrosion, Vol. 27, 1971, pp531 - 544.

DEMO, J.J., "Structure, Constitution and General Characteristics of Wrought Ferritic Stainless Steels,"
ASTM STP 619, ASTM, 1977.

DEVERELL, H.E., "Toughness Properties of Vacuum Induction Melted High-Chromium Ferritic Stainless Steels,"
Toughness of Ferritic Stainless Steels, ASTM STP 706, R.A. Lula, (Ed), ASTM, 1980, pp184 - 201.

DRACHINSKIY, A.S., MOISEYEV, V.F. and TREFILOV, V.I., "Conditions of the Slip-To-Twinning Transition,"
Fiz. Metal. Metalloved., 19, No.4, 1965, pp602 - 611.

DRYDEN, J.R., DEAKIN, A.S. and PURDY, G.S., "Elastic Analysis of Deformation Near a Spherical Carbon Particle Embedded in Iron,"
Acta Metall., Vol. 35, No. 3, 1987, pp681 - 689.

EMBURY, J.D., "Plastic Flow in Dispersion Hardened Materials,"
Metall. Trans. A., Vol. 16A, Dec., 1985, pp2191 - 2200.

EVANS, A.G.,
Phil. Mag., Vol. 26, p1327.

FORGENG, W.D. and FORGENG, W.D., (Jr), "Constitution of Ternary Alloys,"
ASM Metals Handbook, 8th Ed., Vol. 8, 1973, p402.

GARROD, R.I. and WAIN, H.L., "Dislocation Arrangements and Brittleness in Chromium,"
J. Less - Common Metals, Vol. 9, 1965, pp81 - 94.

GLADMAN, T., "Developments in Stainless Steels,"
Metals and Materials, J. Inst. Metals, Vol. 4, No. 6, June, 1988, pp351 - 355.

GOL'DSHTEYN, Ya. E. et al, "High Temperature Brittleness of a Ferritic Chromium Steel,"
Russian Metallurgy, 1983, pp91-94.

GROBNER, P.J. AND STEIGERWALD, R.F., "Effect of Cold Work on the 885F (475) Embrittlement of 18Cr-2Mo Ferritic Stainless Steels",
J. Metals, Vol. 29, No. 7, 1977, P17.

GROOM, J.D.G., AND KNOTT, J.F., "Cleavage Fracture in Prestrained Mild Steel,"
Metal Science, Vol. 9, 1975, pp390 - 400.

GRUBB, J.F. AND WRIGHT, R.N., "The Role of C and N in the Brittle Fracture of Fe-26Cr,"
Metall. Trans. A., Vol. 10A, Sept., 1979, pp1247 - 1255.

GRUBB, J.F., WRIGHT, R.N. and FARRAR, P., "Micromechanisms of Brittle Fracture in Titanium-Stabilised and Alpha-Prime Embrittled Ferritic Stainless Steels,"
Toughness of Ferritic Stainless Steels, ASTM STP 706, R.A. Lula (Ed.), ASTM, 1980, pp56 - 76.

GRUBB, J.F., "Brittle Fracture of Ferritic Stainless Steel,"
Ph.D Thesis, Rensselaer Polytechnic Institute, Troy, New York, April, 1982.

HAHN, G.T., "The Influence of Microstructure on Brittle Fracture Toughness,"
Metall. Trans. A., Vol. 15A, June, 1984, pp947 - 959.

HALIM, A., DORMAGEN, D., DUNNEWALD - ARFMANN, H., TWICKLER, M., TWICKLER, R.and DAHL, W., "Application of Micromechanical Models for Predicting Fracture Toughness of Sulphide Controlled Fe510 Steels,"
Nucl. Eng. Design, 105, 1987, pp59 - 64.

HAOQUAN, W., SPEAR, W.S. and POLONIS, D.H., "Influence of Annealing and Ageing Treatments on the Embrittlement of Type 446 Ferritic Stainless Steel,"
J. Matls. Eng, Vol. 9, No. 1, 1987, pp51 - 61.

HARDING, A., Personal Communication, MINTEK, RSA.

HASSAN, D.F. and ARSENAULT, R.J., "Substitutional - Interstitial Interactions in B.C.C. Alloys,"
Treatise on Materials Science and Technology, Vol. 1,
H. Herman (Ed.), Academic Press, 1972.

HERMANUS, M.A., "The Development of a Tough High Chromium Ferritic Stainless Steel,"
M.Sc. Thesis, Univ. Witwatersrand, Johannesburg, March, 1986.

HESLOP, J. and PETCH, N.J., "The Ductile-Brittle Transition in the Fracture of Alpha-Iron,"
Phil. Mag., Vol. 3, 1958, pp1128 - 1136.

HIGGINSON, A., "The Passivation of Fe-Cr-Ru Alloys in Acidic Solutions,"
Ph.D Thesis, Univ. Manchester, June, 1987.

HONEYCOMBE, R.W.K., "The Plastic Deformation of Metals,"
2nd Ed., Edward Arnold, 1984.

HULL, D., "Introduction to Dislocations,"
Int. Series on Mater. Science. Technology, Vol. 16,
2nd Edition, Pergamon Press, 1979.

JAFFE, R.I. and HAHN, G.T.,
DMIC Rep. No. 182, Battelle Memorial Institute,
Columbus, Ohio, 1963.

JOHNSON, L. and ASHBY, M.F., "On the Generation of Dislocations at Misfitting Particles in a Ductile Matrix,"
Phil. Mag., Vol. 20, 1969, p1009.

JOKL, M.L., VITEK, V., McMAHON, C.J. and BURGERS, P., "On the Micromechanics of Brittle Fracture: Existing vs Injected Cracks,"
Acta Metall., Vol. 37, No.1, 1989, pp87 - 97.

JOLLEY, W., "Effect of Mn and Ni on Impact Properties of Fe and Fe-C Alloys,"
J. Iron. Steel. Inst., Feb., 1968, pp170 - 173.

JONES, D.A. and MITCHELL, J.W., "Observations of Helical Dislocations in Silver Chloride,"
Phil. Mag., 3, 1958, p1.

JONES, R.H., "Predicting the Stress-Strain Behaviour of Polycrystalline Alpha-Iron Containing Hard Spherical Particles,"
Metall. Trans., Vol. 4, Dec., 1973, pp2799 - 2808.

KAMEDA, J., "A Kinetic Model for Ductile-Brittle Fracture Mode Transition Behaviour,"
Acta Metall., Vol. 34, No.12, 1986, pp2391 - 2398.

KIESSLING, R., "Non-Metallic Inclusions in Steel,"
Second Ed, The Metals Society, London, 1978.

KINOSHITA, N., "Brittle Cracking in Extra Low Interstitial Ferritic Stainless Steels,"
Stainless Steels '84, Proc. Conf. Chalmers Univ. of Technology, Göteborg, 3-4 Sept., 1984, Inst. of Metals, London, 1985.

KLOPP, W.D., "A Review of Chromium, Molybdenum and Tungsten Alloys,"
J. Less Common Metals, 42, 1975, pp261 - 278.

KUBIN, L.P. and LOUCHET, F., "Description of Low-Temperature Interstitial Hardening of the B.C.C. Lattice from in situ Experiments,"
Phil. Mag. A, Vol. 38, No.2, 1978, pp205 - 221.

KUO, K.H. and JIA, C.L., "Crystallography of $M_{23}C_6$ and M_6C Precipitated in a Low Alloy Steel,"
Acta Metall., Vol. 33, No. 6, 1985, pp991 - 996.

KWON, D., "Interfacial Decohesion Around Spheroidal Carbide Particles,"
Scripta Met., Vol. 22, 1988, pp1161 - 1164.

LAGNEBORG, R., "Stress for Twin-Induced Fracture,"
Trans. Metall. Soc. A.I.M.E., Vol. 239, Oct., 1967, pp1661 - 1662.

LEE, J.K. and JOHNSON, W.C., "Re-examination of the Elastic Strain Energy of an Incoherent Ellipsoidal Precipitate,"
Acta Metall., Vol. 26, 1978, pp541 - 545.

LEITCH, J.E., "The Role of Interstitial Nitrogen in the Precipitation Hardening Reactions in High-Chromium Ferritic Steels,"
M.Sc. Thesis, Univ. Cape Town, September, 1987.

LEITCH, J.E. and BALL, A., "The Microstructure of an Aged Ferritic Stainless Steel Containing Nitrogen,"
Proc. E.M.S.S.A., Vol. 9, Port Elizabeth, 1979, pp47 - 48.

LESLIE, W.C., "Iron and Its Dilute Substitutional Solid Solutions,"
Metall. Trans., Vol. 3, Jan., 1972, pp5 - 26.

LEWIS, M.H.,
Acta Metall., Vol. 14, 1966, pp1421 - 1428.

LEWIS, D.B. AND PICKERING, F.B., "Development of Recrystallization Textures in Ferritic Stainless Steels and Their Relationship to Formability,"
Advances in the Physical Metallurgy and Applications of Steels, Proc. Int. Conf. Metals. Soc., Univ. Liverpool, 21-24 Sept., 1981,
The Metals Society, London, 1982.

LI, J.C.M., "Dislocation Sources,"
Dislocation Modelling of Physical Systems, Proc. Int. Conf., Gainesville, Florida, USA, June 22-27, 1980, Pergamon Press, 1980.

LI, J.C.M., and SANDAY, S.C., "Dispersion Toughening,"
Acta Metall., Vol. 34, No. 3, 1986, pp537 - 543.

LIN, I.H. and THOMSON, R., "Cleavage, Dislocation Emission, and Shielding for Cracks under General Loading,"
Acta Metall., Overview No.47, Vol. 34, No.2, 1986, pp187-206.

LIN, I.H. and THOMSON, R., "The Influence of Dislocation Density on the Ductile-Brittle Transition in BCC Metals,"
Scripta Metall., Vol. 20, 1986, pp1367 - 1371.

LINDROOS, V.K. and MIEKKOJA, H.M., "Knitting of Dislocation Networks by Means of Stress-Induced Climb in an Aluminium-Magnesium Alloy,"
Phil. Mag., Vol. 17, 1968, pp119 - 133.

LUDWIGSON, D.C. and LINK, H.S., "Further Studies on the Formation of Sigma in 12 to 16 Per Cent Chromium Steels,"
Advances in the Technology of Stainless Steels and Related Alloys, ASTM STP No. 369, ASTM, April, 1965.

MAGNIN, T. and MORET, F., "Mechanical Twinning in Ferritic Stainless Steels,"
Scripta Metall., Vol. 16, 1982, pp1225 - 1228.

MARTIKAINEN, H.O. and LINDROOS, V.K., "Grain Boundary Structural Changes During Annealing and High Temperature Deformation of Ferritic Stainless Steel,"
Acta Metall., Vol. 11, No.7, 1985, pp1223 - 1234.

MARTIN, J.W., "Micromechanisms in Particle-Hardened Alloys,"
Cambridge University Press, 1980.

McFARLAND, W.H. and CRONN, J.T., "Spheroidization of Type II Manganese Sulphides by Heat Treatment,"
Metall. Trans. A., Vol. 12A, May, 1981, pp915 - 917.

McMAHON, C.J. and COHEN, M.,
Acta Metall., Vol. 13, 1965, pp591 - 604.

MINTEK, "A Corporate Report,"
Supplement to S.A. Financial Mail, 11 July, 1986, P39.

MINTZ, B., "Influence of Grain Boundaries on Fissure Formation During Impact Testing of Ferritic Stainless Steels,"
Metals Technol. Vol. 7, March, 1980, pp127 - 129.

MINTZ, B. and ARROWSMITH, J.M., "Impact Properties of Fe-13Cr Thick Plate,"
Toughness of Ferritic Stainless Steels, ASTM STP 706, R.A. Lula (Ed.), ASTM, 1980, pp313 - 335.

MINTZ, B., MORRISON, W.B. and COCHRANE, R.C., "Influence of Grain Boundary Carbide Thickness and Grain Size on the Impact Properties of Steels,"
Advances in the Physical Metallurgy and Applications of Steels, Proc. Int. Conf. Metals Soc., Univ. Liverpool, 21-24 Sept., 1981, The Metals Society, London, 1982.

MOHLA, P.P. and BEECH, J., "Effect of Cooling Rate on the Morphology of Sulphur Inclusions,"
J. Iron and Steel Inst., Feb., 1969, p177.

MONTEMAYOR-ALDRETE, J.A., SOULLARD, J., GOMEZ - RAMIREZ, R. and CALLES, A.,
"The Creation Rate of Mobile Dislocation Density in a Creep Experiment,"
Scripta Metall., Vol. 20, 1986, pp1075 - 1078.

MURTY, Y.V., et al, "Initial Coarsening of Manganese Sulphide Inclusions in Rolled Steel During Homogenization,"
Metall. Trans. A., Vol. 6A, 1975, pp2031 - 2035.

NAGAKAWA, J. and MESHII M., "Rationalization of Softening and Hardening Effects by Interstitial Atoms in B.C.C. Metals,"
Strength of Metals and Alloys, Proc. 5th. Int. Conf., Aachen, Germany, 1979.

NAKANO, K., KANAO, M. and HOSHINO, A., "Effect of Nickel Content and the Austenite Phase on Low Temperature Toughness and Embrittlement Behaviour of Fe-26%Cr Alloys,"
Trans. National Research Inst. for Metals, Vol. 20, No. 1, 1978, pp1 - 12.

NICHOL, T.J., "Mechanical Properties of a 29Pct Cr-4Pct Mo-2Pct Ni Ferritic Stainless Steel,"
Metall. Trans. A., Vol. 8A, Feb., 1977, pp229 - 237.

NICHOL, T.J., DATTA, A and AGGEN, G., "Embrittlement of Ferritic Stainless Steels,"
Metall. Trans. A., Vol. 11A, April, 1980, pp573 - 585.

OHASHI, N., ONO, Y., KINOSHITA, N. and YOSHIOKA, K., "Effects of Metallurgical and Mechanical Factors on Charpy Impact Toughness of Extra-Low Interstitial Ferritic Stainless Steels,"
Toughness of Ferritic Stainless Steels, ASTM STP 706, R.A. LULA (Ed.), ASTM, 1980, pp202 - 220.

OHR, S.M., "Introduction to Viewpoint Set on Dislocation Emission from Cracks,"
Scripta Metall., Vol. 20, 1986, pp1465 - 1466.

PARK, K., LA SALLE, J.C. and SCHWARTZ, L.H., "Mechanical Properties of Spinodally Decomposed Fe-30wt%Cr Alloys: Yield Strength and Ageing Embrittlement,"
Acta Metall., Vol. 34, No. 9, 1986, pp1853 - 1865.

PATSKEVICH, I.R. et al, "Effect of Nitrogen on the Properties of Low-Carbon Ferritic Steel with 25% Cr,"
Metal Science and Heat Treatment, Vol. 17, 1975, pp780 - 782.

PETCH, N.J., "The Influence of Grain Boundary Carbide and Grain Size on the Cleavage Strength and Impact Transition Temperature of Steel,"
Acta Metall., Vol. 34, No. 7., 1986, pp1387 - 1393.

PETCH, N.J., "The Influence of Some Substitutional Alloys on the Cleavage of Ferritic Steels,"
Acta Metall. Vol. 35, No. 8, 1987, pp2027 - 2034.

PICKERING, F.B., "The Effect of Composition and Microstructure on Ductility and Toughness,"
Toward Improved Ductility and Toughness, Kyoto Int. Conf., 1971, pp9 - 31.

PICKERING, F.B., "Some Aspects of the Heat Treatment of Welded Corrosion and Heat-Resisting Steels,"
The Metallurgical Evolution of Stainless Steels, F.B. Pickering (Ed.), ASM, 1979.

PLUMTREE, A. and GULLBERG, R., "The Influence of Interstitial Content on the Ductile-Brittle Transition Temperature of Fe-25Cr Ferritic Stainless Steels,"
J. Testing and Evaluation, JTEVA, Vol. 2, No. 5, Sept., 1974, pp331-336.

PLUMTREE, A. and GULLBERG, R., "Influence of Interstitial and Some Substitutional Alloying Elements,"
Toughness of Ferritic Stainless Steels, ASTM STP 706,
R.A. Lula (Ed.), ASTM, 1980, pp34 - 55.

POLLARD, B., "The Effect of Titanium on the Ductility of 26% Chromium Low Interstitial Ferritic Stainless Steel,"
Metals Technology, Jan., 1974, pp31 - 36.

POWELL, D.J., PILKINGTON, R. and MILLER, D.A., "The Precipitation Characteristics of 20%Cr/25% Ni - Nb Stabilised Stainless Steel,"
Acta Metall., Vol. 36, No. 3, 1988, pp713 - 724.

PRIESTNER, R. and LESLIE, W.C., "Nucleation of Deformation Twins at Slip Plane Intersections in B.C.C. Metals,"
Philosophical Mag., Vol. 11, No. 113, May, 1965, p895.

REDMOND, J.D., "Toughness of 18Cr-2Mo Stainless Steel,"
Toughness of Ferritic Stainless Steels, ASTM STP 706, R.A. Lula (Ed.), ASTM, 1980, pp123 - 144.

REID, C.N. and GILBERT, A., "Dislocation Structure in Chromium, Chromium-Rhenium, and Chromium - Iron Alloys,"
J. Less-Common Metals, 10, 1965, pp 77-90.

REID, C.N., "A Review of Mechanical Twinning in Body-Centred Cubic Metals and its Relation to Brittle Fracture,"
J. Less-Common Metals, 9, 1965, pp105 - 122.

REID, C.N., "The Association of Twinning and Fracture in BCC Metals,"
Metall. Trans. A., Vol. 12A, March, 1981, pp371 - 377.

RICE, J.R. AND THOMSON, R,
Phil. Mag., Vol. 29, 1975, p73.

RITCHIE, R.O., KNOTT, J.F. and RICE, J.R., "On the Relationship Between Critical Tensile Stress and Fracture Toughness in Mild Steel,"
J. Mech. Phys. Solids, Vol. 21, 1973, p395.

RITCHIE, R.O. and KNOTT, J.F., "On the Influence of High Austenitizing Temperatures and 'Overheating' on Fracture in a Low Alloy Steel,"
Metall. Trans., Vol. 5, March, 1974, pp782 - 785.

ROBSON, G.G. and SMITH, F.J., "Platinum 1988,"
Johnson Matthey, May, 1988.

SAITO, S. et al, "On the Embrittlement and Toughness of High Purity Fe-30Cr-2Mo Alloy,"
Toughness of Ferritic Stainless Steels, ASTM STP 706, R.A. Lula (Ed.), ASTM, 1980, pp77 - 98.

SAITO, N., ABIKO, K. and KIMURA, H., "Reduction of Intergranular Fracture in Fe-P Alloys by the Addition of Nickel,"
Mater. Sci. Engin. A., 102, 1988, pp169 - 174.

SCHULZ, B.J. and McMAHON, C.J., "Fracture of Alloy Steels by Intergranular Microvoid Coalescence as Influenced by Composition and Heat Treatment,"
Metall. Trans., Vol. 4, Oct., 1973, pp2485 - 2489.

SEDRIKS, A.J., "Metallurgical Control of Localised Corrosion of Stainless Steels,"
Stainless Steel '87, Proc. Int. Conf., Univ. York, 14-16 Sept. 1987, Institute of Metals, 1988.

SEMCHYSHEN, M., BOND, A.P. and DUNDAS, H.J., "Effects of Composition on Ductility and Toughness of Ferritic Stainless Steels,"
Towards Improved Ductility and Toughness, Conf. Proc., Kyoto International Conference Hall, Oct., 1971, pp239 - 253.

SHAW, M.P., ROBINSON, J.M., WOLFF, I.M. and BALL, A., "Microstructural Influences on the Plastic Deformation of High Chromium Ferritic Alloys,"
Proc. ICSMA 8, Tampere, Finland, Pergamon, 1988, pp439 - 444.

SHEPPARD, T. and RICHARDS, P., "Structural and Substructural Observations During Thermomechanical Processing of Two Ferritic Stainless Steels,"
J. Matls. Science, 22, 1987, pp1642 - 1650.

SIMS, T.C. and HAZEL, W.C., "The Super Alloys,"
Wiley Interscience, 1972.

SMITH, A.F., "Low-Temperature Diffusion of Chromium in a Fine-Grained Austenitic Stainless Steel with Varying Dislocation Densities,"
Metal Science, Vol. 9, No. 9, Sept., 1975, pp425 - 429.

SMITH, E.,
Proc. Conf. Physical Basis of Yield and Fracture, Inst. Physics and Physical Soc., Oxford, 1966, p36.

SMITHELLS, C.J., "Metals Reference Book,"
5th Edition, Butterworths, 1976.

STEIGERWALD, R.F., "The Effects of Metallic Second Phases in Stainless Steels," Corrosion, Vol. 33, No. 9, Sept., 1977, pp338 - 343.

STEPHENS, J.R. and KLOPP, W.D., "Enhanced Ductility in Binary Chromium Alloys," Trans. Metall. Soc. AIME, Vol. 242, Sept., 1968, pp1837 - 1843.

STOLOFF, N.S., "Effects of Alloying on Fracture Characteristics," Fracture, Vol. 6, H. Liebowitz (Ed.), Academic Press, 1969.

STREICHER, M.A., "Stainless Steels: Past, Present and Future," Stainless Steel '77, Conf. Proc., London, England, Sept. 26-27, 1977, Barr, R.Q. (Ed), Climax Molybdenum Co., 1977, pp1 - 34.

STREICHER, M.A., "Alloying Stainless Steels with the Platinum Metals," Platinum Metals Review, Vol. 21, No. 51, 1977, pp51 - 55.

STUART, M. and RIDLEY, N., "Thermal Expansion of Some Carbides and Tessellated Stresses in Steels," J. Iron. Steel. Inst., Dec., 1970, pp1087 - 1092.

STUMPF, W.E., "Effect of Matrix Structure and Concurrent Fatigue on Carbide Coarsening," Ph. D. Thesis, Univ. Sheffield, July, 1968.

SUZUKI, S., TANII, S., ABIKO, K. and KIMURA, M., "Site Competition Between S and C at Grain Boundaries and Their Effects on the Grain Boundary Cohesion in Iron," Metall. Trans. A., Vol. 18A, June 1987, pp1109 - 1115.

TAILLARD, R., "Twinning in 19wt% Chromium Steels Hardened by the Precipitation of the Intermetallic Compound NiAl," Scripta Metall., Vol. 16, 1982, pp49-54.

TETELMAN, A.S. and McEVILY, A.J. (Jr), "Fracture of Structural Materials," John Wiley and Sons Inc., New York, 1967.

THIELSCH, H., "Physical and Welding Metallurgy of Chromium Stainless Steels," The Welding Journal, 30, May, 1951, pp209-250.

THOMSON, R., "Physics of Fracture," Solid State Physics, Vol. 39, Ehrenreich, M. and Turnbull, D. (Eds), Academic Press, 1986.

TOMASHOV, N.D., CHERNOVA, G.P. and USTINSKI, E.N., "The Corrosion and Electrochemical Behaviour of Ductile Chromium Alloys," Plat. Met. Rev., Vol. 23, No. 143, 1979, pp143 - 149.

TOMITA, Y., "Effect of Hot-Rolling Reductions on Shape of Sulfide Inclusions and Fracture Toughness of A.I.S.I. 4340 Ultrahigh Strength Steel,"
Metall. Trans. A., Vol. 19A, June, 1988, pp1555 - 1561.

TSANN, L., EVANS, A.G. and RITCHIE, R.O., "Stochastic Modelling of the Independent Roles of Particle Size and Grain Size in Transgranular Cleavage Failure,"
Metall. Trans. A., Vol. 18A, April, 1987, pp641 - 651.

TULLMIN, M.A.A., ROBINSON, F.P.A. and CORTIE, M.B., "Corrosion Resistance of 40% Cr Ferritic Stainless Steels and the Effects of Stabilising Elements",
Proc. E.M.S.S.A., Vol. 18, 1988, pp183 - 184.

UEMATSU, Y. and YAMAZAKI, K., "Formation of Deformation Band and Recrystallisation Behaviour of Fully Ferritic Stainless Steels Under Hot Rolling Process,"
Stainless Steels '87, Proc. Int. Conf., Univ. York, 14-16 Sept., 1987, Institute of Metals, 1988.

VAN ZWIETEN, A.C.T.M., "The Effect of Interstitials on the Dynamic Toughness Properties of Fe-40Cr,"
M.Sc. Thesis, Univ. Witwatersrand, Johannesburg, August, 1987.

WEATHERLEY, G.C. and NICHOLSON, R.B., "An Electron Microscope Investigation of the Interfacial Structure of Semi-Coherent Precipitates,"
Phil. Mag., 17, 1968, pp801 - 831.

WEISS, B. and STICKLER, R., "Phase Instabilities During High Temperature Exposure of 316 Austenitic Stainless Steel,"
Metall. Trans. A., Vol. 3, April, 1972, pp851 - 866.

WILCOX, B.A., VEIGEL, N.D. and CLAUER, A.H., "Ductile-Brittle Transition of Thoriated Chromium,"
Metall. Trans., Vol. 3, Jan., 1972, pp273 - 283.

WILSON, A.D., "Homogenization of Sulfide Inclusions in Low Alloy Steel,"
Metall. Trans. A., Vol. 8A, Jan., 1977, pp201 - 202.

WOLFF,I.M., "Melting Problems in High Chromium Ferritic Irons,"
Final Year Dissertation, Univ. Witwatersrand, Sept., 1985.

WOLFF, I.M., SHAW, M.P. and BALL, A., "Observations on Preciptiation in High Chromium Ferritic Alloys,"
Proc. E.M.S.S.A., Vol. 17, 1987, pp161 - 162.

IOOD, G.S. and BALL,A., "An Investigation of the Early Stages of the Precipitation of Nitrogen in Chromium",
Phil. Mag., Vol. 27, No. 4, April, 1975, pp785-799.

IOOD, J.R., "Effect of Residual Elements and Mo Additions on Annealed and Welded Mechanical Properties of 18Cr Ferritic Stainless Steels,"
Toughness of Ferritic Stainless Steels, ASTM STP 706,
R.A. Lula (Ed.), ASTM, 1980, pp145 - 160.

IOODYATT, R.L. and KRAUSS, G., "Iron-Chromium-Carbon System at 870°C,"
Metall. Trans. A., Vol. 7A, July, 1976, pp983 - 989.

IRIGHT, R.N., "Toughness of Ferritic Stainless Steels,"
Toughness of Ferritic Stainless Steels, ASTM STP 706,
R.A. Lula (Ed.), American Society for Testing and Materials,
1980, pp2 - 33.

'ASUNAKA, T. and KANAO, M., "Fracture Characteristics of 475°C Embrittled 30% Cr Ferritic Stainless Steels,"
Trans. I.S.I.J, 1979, p69.

'UBETS, Y.Y. et al., "Mechanism of Plastic Deformation and Low Temperature Embrittlement of the Alloy Cr-45AT% Fe,"
Fiz. Metal. metalloved., 35, No. 3, 1973, pp609 - 617.

APPENDIX A

LOCALISED CORROSION OF Fe-40Cr ALLOYS

SYNOPSIS

General and pitting corrosion tests were carried out on a selection of alloys based on a composition of Fe-40wt%Cr to complement studies into the operative ductilising mechanisms. The effects of three metallurgical variables on the localised corrosion processes were investigated; these being:

(a) controlled sulphur additions;
(b) pre-straining by cold work to increase the strain energy;
(c) Recovery annealing to give a sub-grain structure.

In addition, attention was given to the cathodic modification of these alloys by small additions of the PGM ruthenium.

1. INTRODUCTION

The polarization characteristics of a typical stainless steel are shown schematically in Figure A.1. The stability of the large passive region is a covering effect of the protective oxide film at the corrosion surface. Cathodic cavitation, on the other hand, is an electrochemical effect. The addition of a PGM to the Fe-Cr system causes a spontaneous shift of the cathodic potential into the passive region by promoting the hydrogen evolution reaction in reducing acid media, as shown.

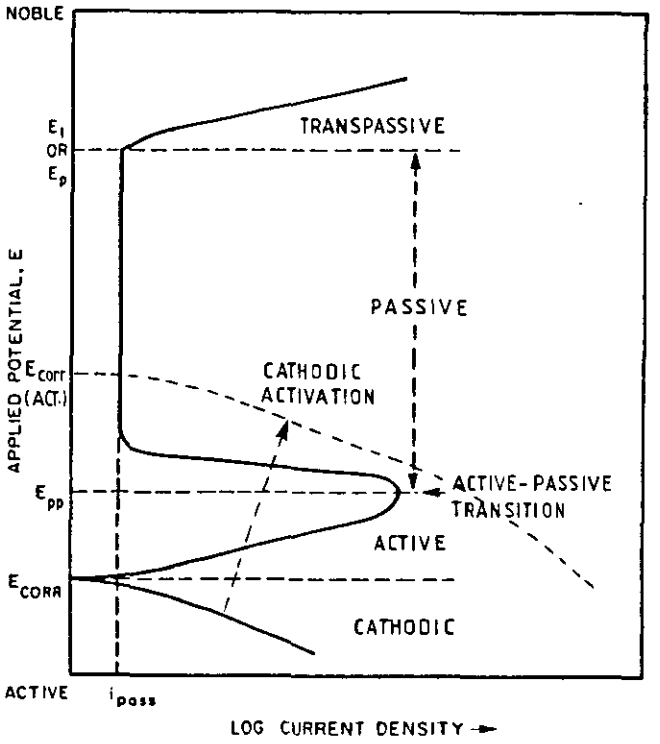

FIGURE A.1 Polarization Curve of Fe-Cr, showing the effect of cathodic modification

The distribution of the cathodic element in the base alloy has been the subject of investigations by Delport and Roux (1986) and Miller et al (1987). Delport and Roux identified a surface segregation effect by palladium in Fe-40Cr. The oxidation of palladium results in a surface layer of high chromium diffusivity which apparently enhances the kinetics of passivity. A surface segregation effect was also noted by Miller and

colleagues, who found that palladium favoured the ferrite/ferrite boundaries in a Type 4130 Steel, where it formed a mono-atomically thick adsorbate layer. Thomashov et al (1979) on the other hand, have identified separate islets of the noble metal phase on the surface of the alloy rather than a homogeneous layer, covering only some 1% of the alloy surface. Although the exact location of the cathodic element is uncertain, the action of the cathodic addition as a catalyst for hydrogen evolution appears to be well established. There is, however, also evidence to suggest that dissolution of the base alloy, to concentrate the cathodic element at the surface, inhibits the anodic dissolution rate of the base alloy by causing a smaller current and charge density at passivation [Higgenson (1987)].

While the benefits of cathodic element additions for the general corrosion resistance have been amply demonstrated, far less attention has been given to the susceptibility of Fe-40Cr alloys to localised attack, and in particular, the effect of the cathodic modificants on the localised corrosion processes. Factors which may lead to the localised breakdown of the passive film are illustrated in Figure A.2.

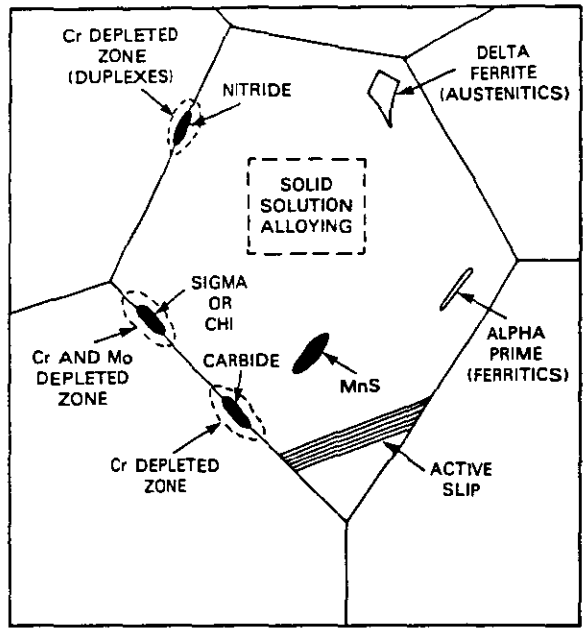

FIGURE A.2 Metallurgical Variables affecting the Localised Corrosion Behaviour of Stainless Steels [Sedricks (1987)]

The purpose of the study is to examine three aspects of the resistance of Fe-40Cr Alloys to localised corrosion, which may be motivated as follows:

(1) The controlled addition of sulphur to Fe-40Cr alloys has been shown to improve the impact resistance by increasing the number of prismatic dislocation sources. The notion that sulphides are the major source of pitting in stainless steels makes it necessary to examine the feasibility of dispersion toughening by sulphides in practice.

(2) The impact toughness of Fe-40Cr alloys is improved by increasing the mobile dislocation density. Since plastic deformation may be expected to increase the odds for stress corrosion, the effect of pre-strain on the corrosion behaviour must needs be assessed.

(3) The optimum impact resistance has been associated with heat treatments designed to introduce a low-angle sub-grain structure. In addition to increasing the dislocation density, the sub-structure has also been shown to modify the precipitate distribution. The sub-structure is characteristic not only of recovery-annealed alloys, but also of alloy systems in which the recrystallisation kinetics have been altered. Retarded recrystallisation has been noted in stabilised alloys, alloys where second phase particles pin the sub-structure, and also as a result of substitutional alloying additions which modify the so-called stacking fault energy (SFE). The cathodic element ruthenium is an example of the latter.

2. EXPERIMENTAL PROCEDURE

The general and pitting corrosion of a selection of Fe-40Cr alloys was studied as a function of the alloy composition and heat-treated condition using accelerated potentiodynamic polarization tests. A description of the experimental alloys is given in Table A.1. The experimental parameters are summarised in Table A.2.

TABLE A.1 Experimental Alloys

Designation	Description	Composition (wt%)	Heat Treatment		Condition
1	Fe-40Cr	Base	1h1050°C	+ quenched	Recrystallised
2	Fe-40Cr	Base	1h850/1h1050°C	+ quenched	Recovered sub-structure
3	Fe-40Cr	Base	1h1050°C	+ quenched	Recrystallised/ 5% pre-strain
4	Fe-40Cr-S	0,04 S	1h850/1h1050°C	+ quenched	Spheroidised/ Recovered
5	Fe-40Cr-0.2Ru	0,2 Ru	1h1050°C	+ quenched	Recovered sub-structure

TABLE A.2 Experimental Parameters

Variable	General Corrosion Scans	Pitting Scans
Specimen Format:	15,7mm diam. x 3mm	15,7mm diam. x 3mm
Solution:	10 Vol% H_2SO_4	500ppm Cl + 300ppm SO_4
Temperature:	45°C	30°C
Scan Rate:	0,7mV/sec	0,7mV/sec
Initiated: (w.r.t. SCE)	E_{corr}-250mV	E_{corr}
Terminated: (w.r.t. SCE)	1200mV	Reversed above $10^3 uA/cm^2$
Equilibration:	1 hr	1 hr

The specimens were mechanically lapped to a 3 micron finish and mounted in insulating retaining gaskets. The temperature was maintained in an isothermal water bath. De-aeration was effected by bubbling through with chemical purity argon gas. Each test was repeated using separate specimens to ensure reproducibility. The corroded surfaces were studied by means of scanning electron microscopy.

3. EXPERIMENTAL RESULTS

The potentiodynamic scans carried out in the 10% H_2SO_4 solution are illustrated in Figures A.3 - A.7

Traces of the pitting scans in the 500ppm Cl + 300ppm SO_4 aqueous solution are shown in Figures A.8 - A.12.

The results of the electrochemical tests are summarised in Tables A.3 and A.4.

TABLE A.3 Test Results: General Corrosion Scans in 10% H_2SO_4

Result	Alloy 1	Alloy 2	Alloy 3	Alloy 4	Alloy 5
Free Corrosion Potential: E_{corr} (mV)	-438	-150	-425	-125	-213
Pitting Potential: E_p (mV)	+888	-113	+825	- 50	+175
Passive Range: E_p-E_{pp}mV)	1 314	37	1 250	75	388
Passivation Current: i_{pass}(uA/cm^2)	0,62	1,15	0,63	1,15	0,42
Corrosion Current: i_{corr} (uA/cm^2)	24,18	5,46	15,99	7,39	8,86
Corrosion Rate: (Cathodic)	2,42mmpy	0,55mmpy	1,60mmpy	0,25mmpy	0,89mmpy

With reference to Table A.3, the relative corrosion behaviour of the alloys may be summarised as follows:

(1) The fully recrystallised Alloy 1 exhibits passive behaviour over the widest range of conditions. Full passivation is achieved at a low passivation current, up to the maximum potential recorded, viz. E_p=888mV;

(2) The application of an intermediate ageing treatment to introduce a recovered sub-grain structure results in minimal passivity, with an accompanying unfavourable shift in the passivation current. The behaviour of the high sulphur Alloy 4, subjected to the same heat treatment is almost identical to that of the base alloy;
(3) Pre-straining of the fully recrystallised alloy to introduce a cold-worked dislocation sub-structure marginally constricts the range of passivity but leaves the passivation current unaffected;
(4) The addition of ruthenium is effective in lowering the passivation current, but the passive range is severely reduced.

Paradoxically, the free corrosion potential E_{corr} is shifted in the more noble (positive) direction for those alloys exhibiting poor passive behaviour. This is also reflected in the corrosion rates calculated by the Polarization Resistance technique.

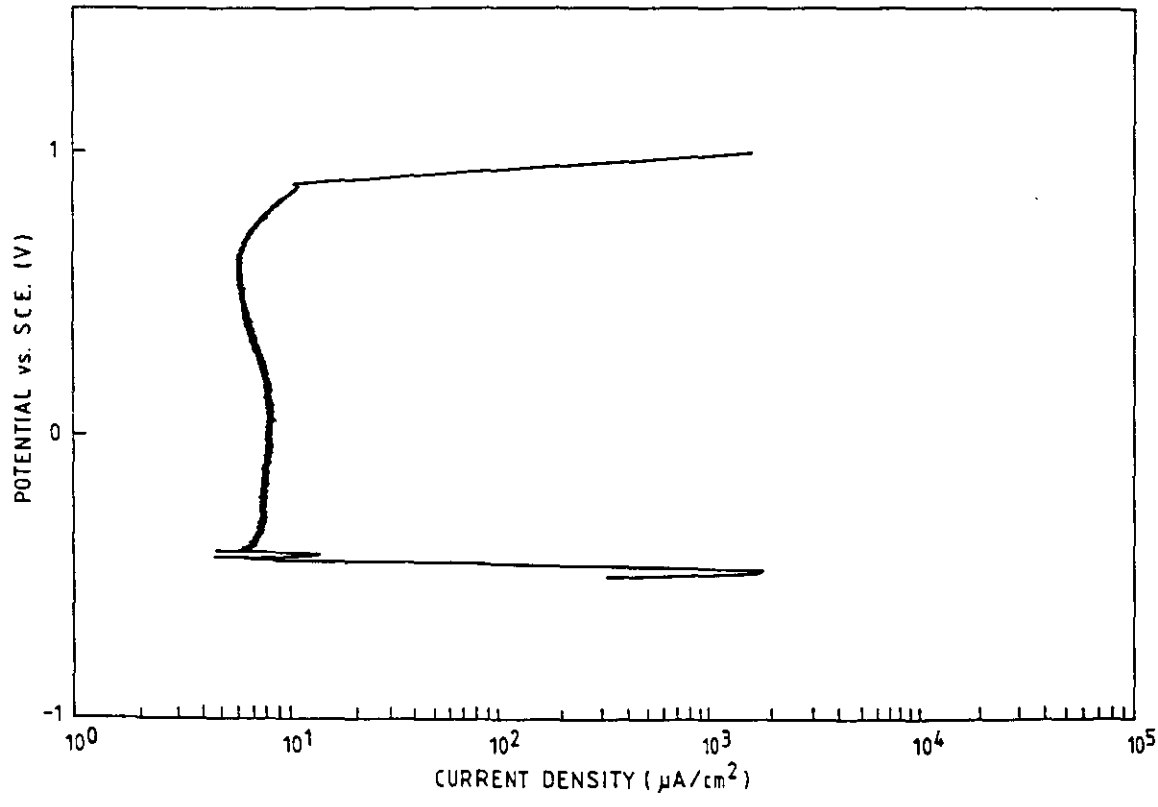

Figure A.3 Potentiodynamic Scan - Alloy 1: Fe-40Cr Fully Recrystallised (10% H_2SO_4)

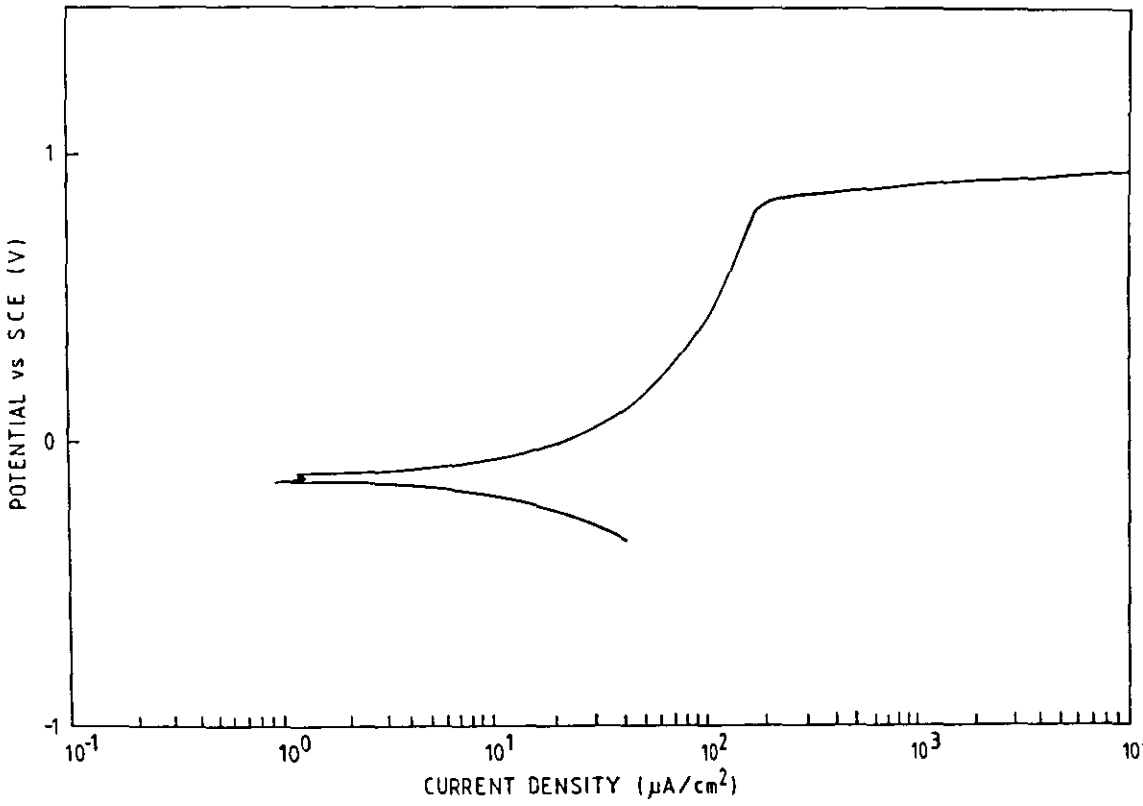

Figure A.4 Potentiodynamic Scan - Alloy 2: Fe-40Cr Partially Recovered ($10\%\ H_2SO_4$)

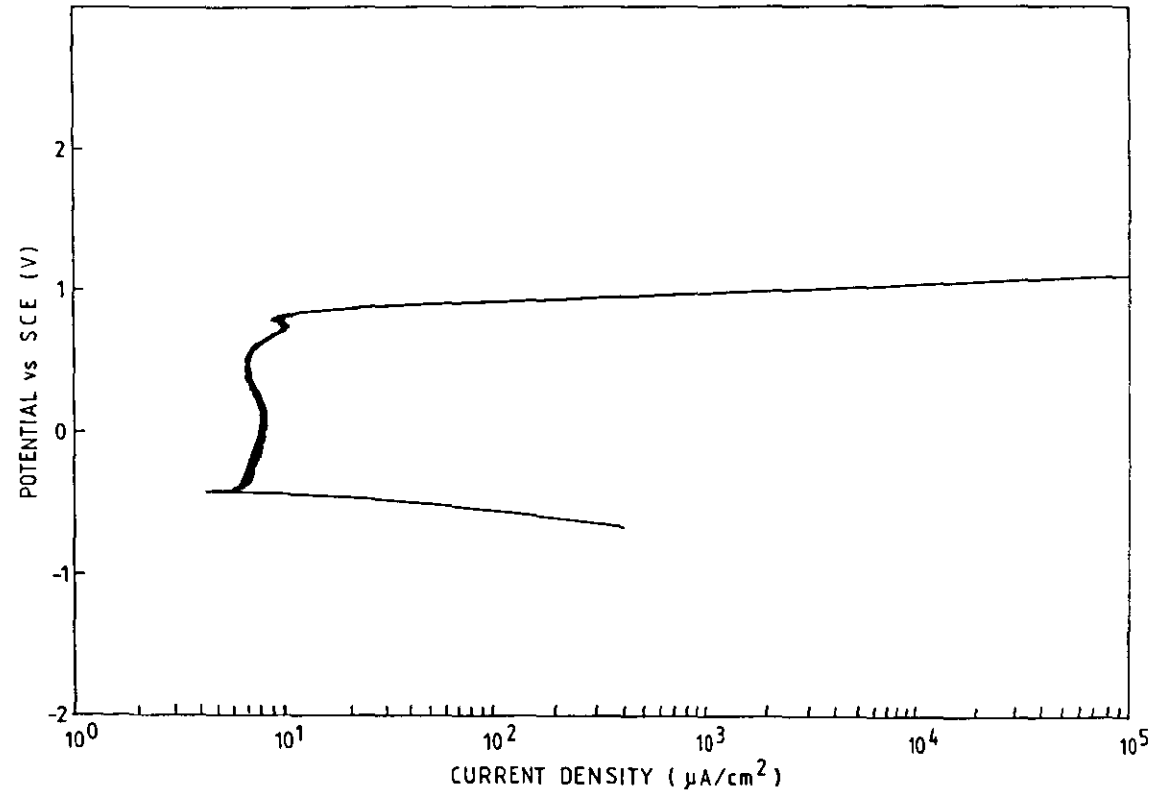

Figure A.5 Potentiodynamic Scan - Alloy 3: Fe-40Cr 5% Pre-strain ($10\%\ H_2SO_4$)

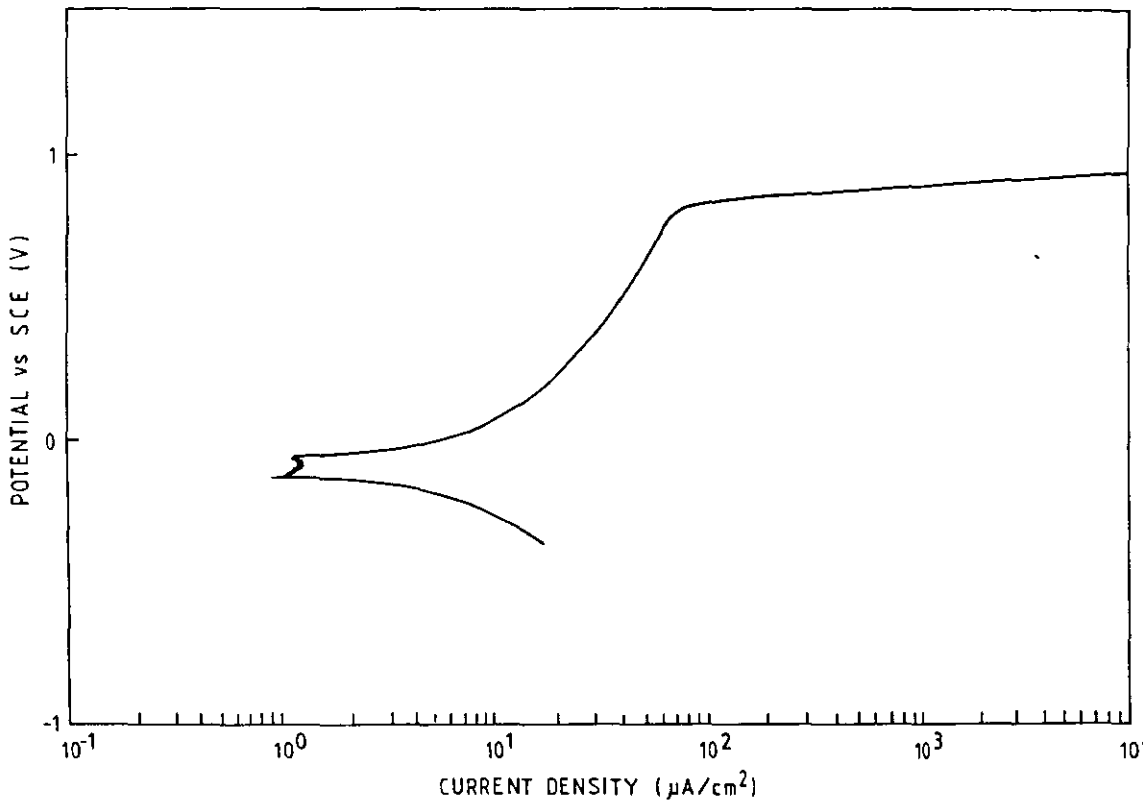

Figure A.6 Potentiodynamic Scan - Alloy 4: Fe-40Cr-S (10% H_2SO_4)

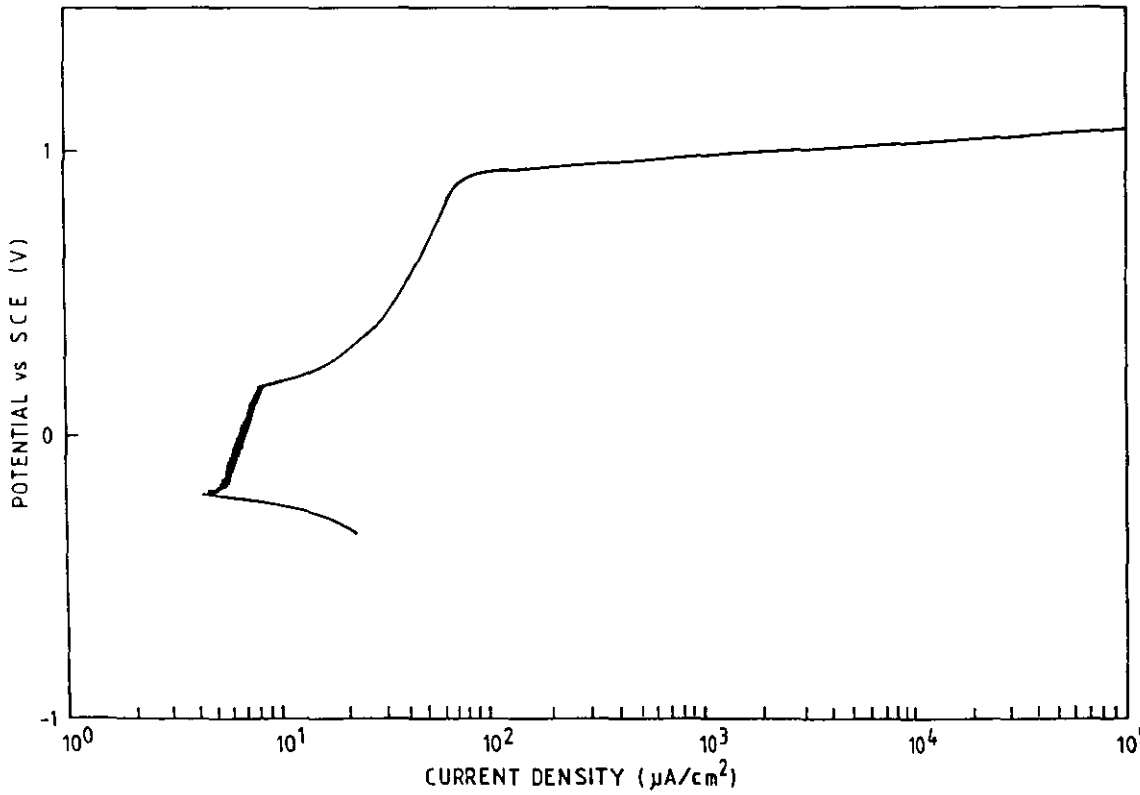

Figure A.7 Potentiodynamic Scan - Alloy 5: Fe-40Cr-0.2Ru (10% H_2SO_4)

TABLE A.4 Test Results: Pitting Scans in 500ppm Cl + 300ppm SO_4 Aqueous Solution

Result	Alloy 1	Alloy 2	Alloy 3	Alloy 4	Alloy 5
Free Corrosion Potential: E_{corr} (mV)	-225	-50	-200	-75	-425
Pitting Potential: E_p (mV)	+675	+625	+650	+725	+700
Passive Range: E_p-E_{corr} (mV)	900	675	1 125	800	1 125
Passivation Current: i_{pass}(uA/cm^2)	2,98	3,11	2,80	3,68	2,72
Protection Potential: E_{prot} (mV)	+825	+850	+925	+775	+900

The following observations hold for the pitting behaviour of the Fe-40Cr alloys.

(1) In all cases the alloys spontaneously passivate, and are resistant to pitting over a wide passive region;

(2) Reversal of the scan causes the trace to intersect the forward scan with a small hysteresis loop, indicating ready re-passivation and a high protection potential;

(3) The ruthenium alloy exhibits the lowest passivation current and the widest range of stability;

(4) The prior-aged base and high sulphur alloys exhibit a reduced resistance to pitting, although this is not as severe as the loss of general corrosion resistance;

(5) Pre-straining the recrystallised alloy causes a slight reduction in the pitting potential, but leaves the range of passivity unaffected.

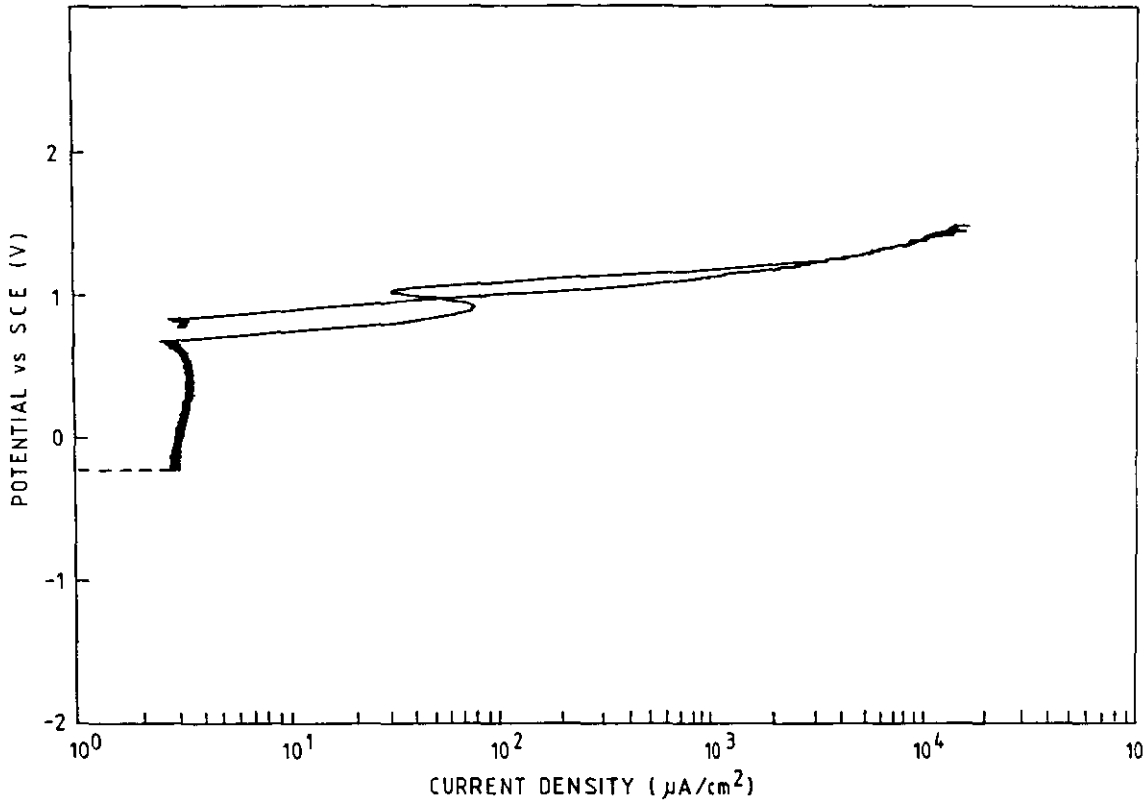

Figure A.8 Pitting Scan for Alloy 1: Fe-40Cr Fully Recrystallised (500 ppm Cl + 300 ppm SO_4)

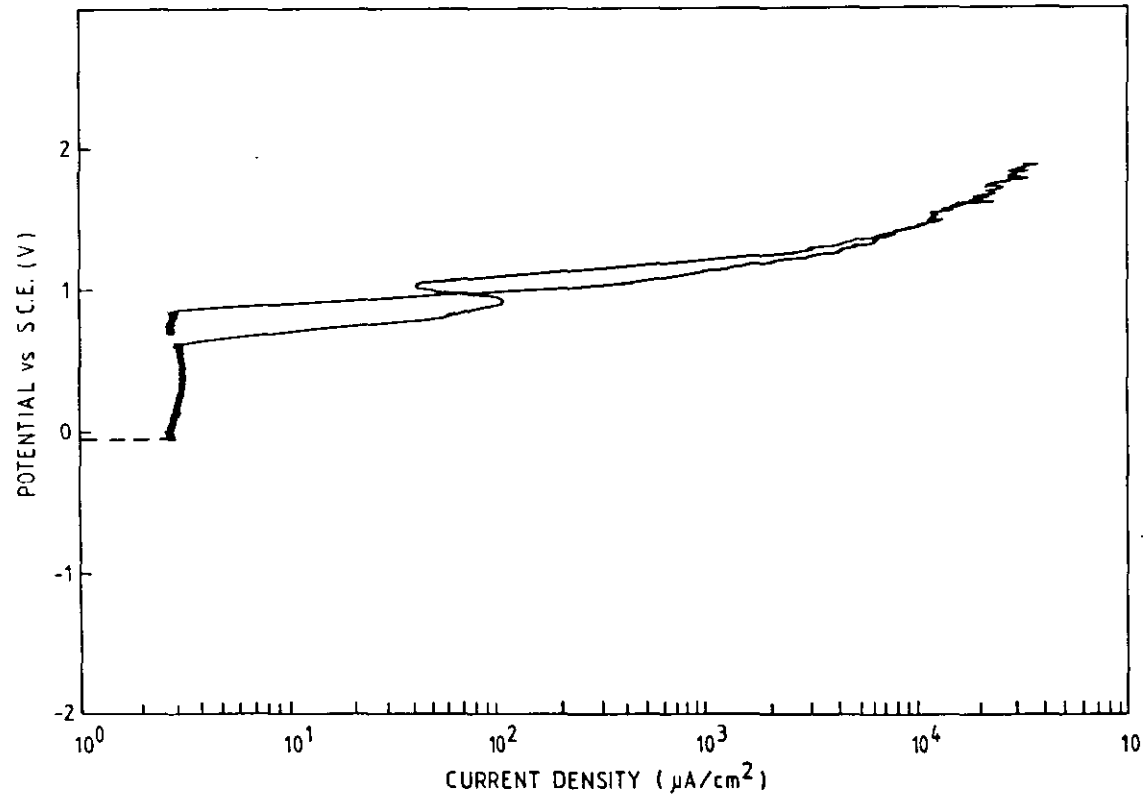

Figure A.9 Pitting Scan for Alloy 2: Fe-40Cr Partially Recovered (500 ppm Cl + 300 ppm SO_4)

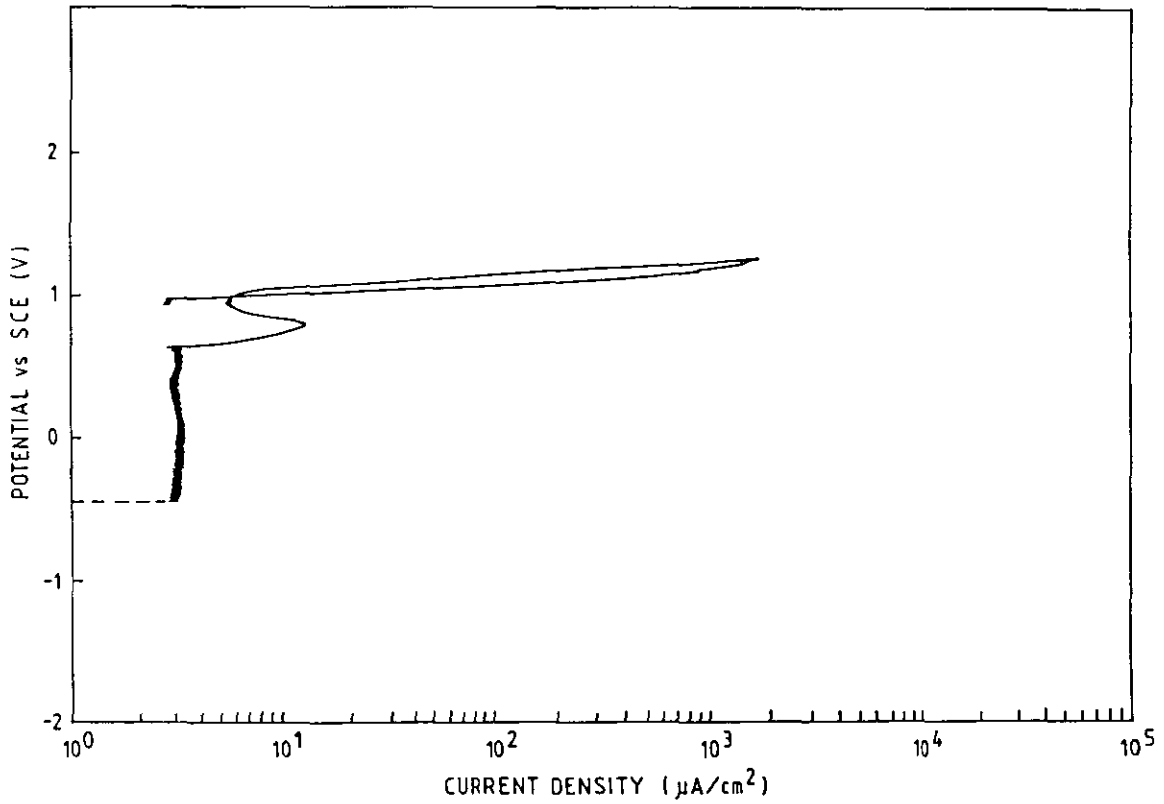

Figure A.10 Pitting Scan - Alloy 3: Fe-40Cr 5% Pre-strain (500 ppm Cl + 300 ppm SO_4)

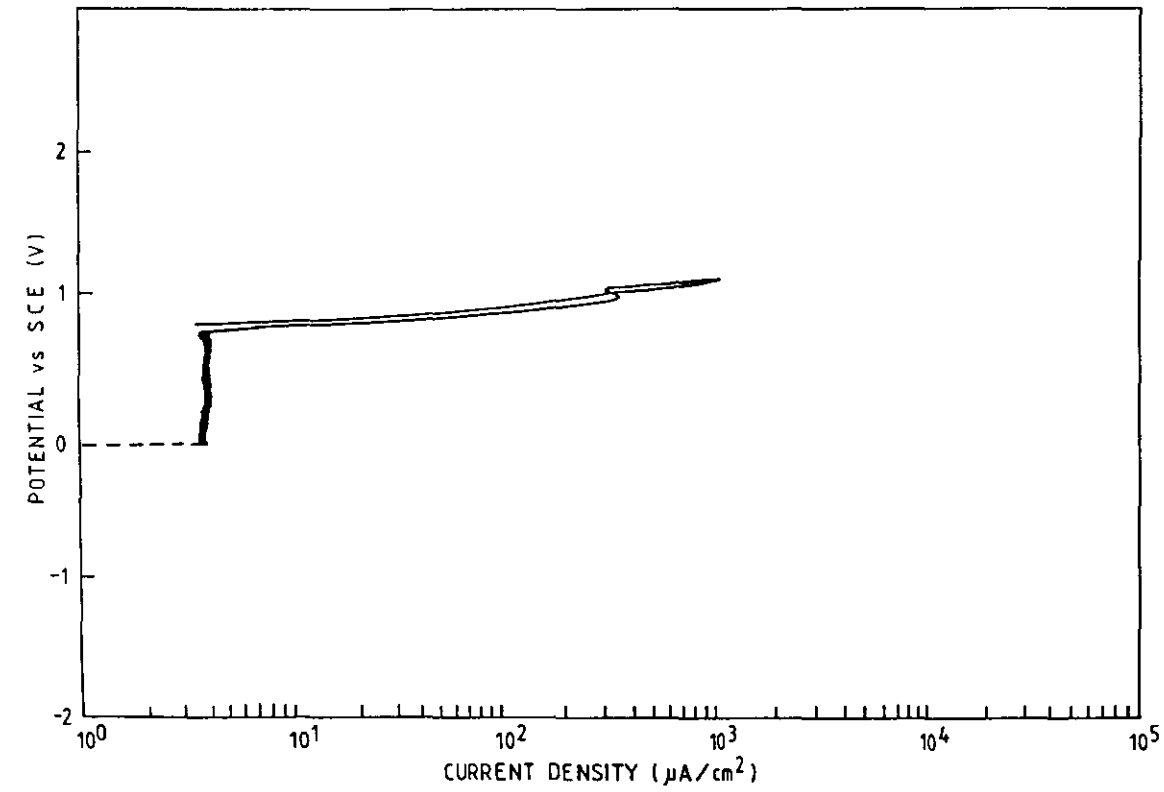

Figure A.11 Pitting Scan - Alloy 4: Fe-40Cr-S (500 ppm Cl + 300 ppm SO_4)

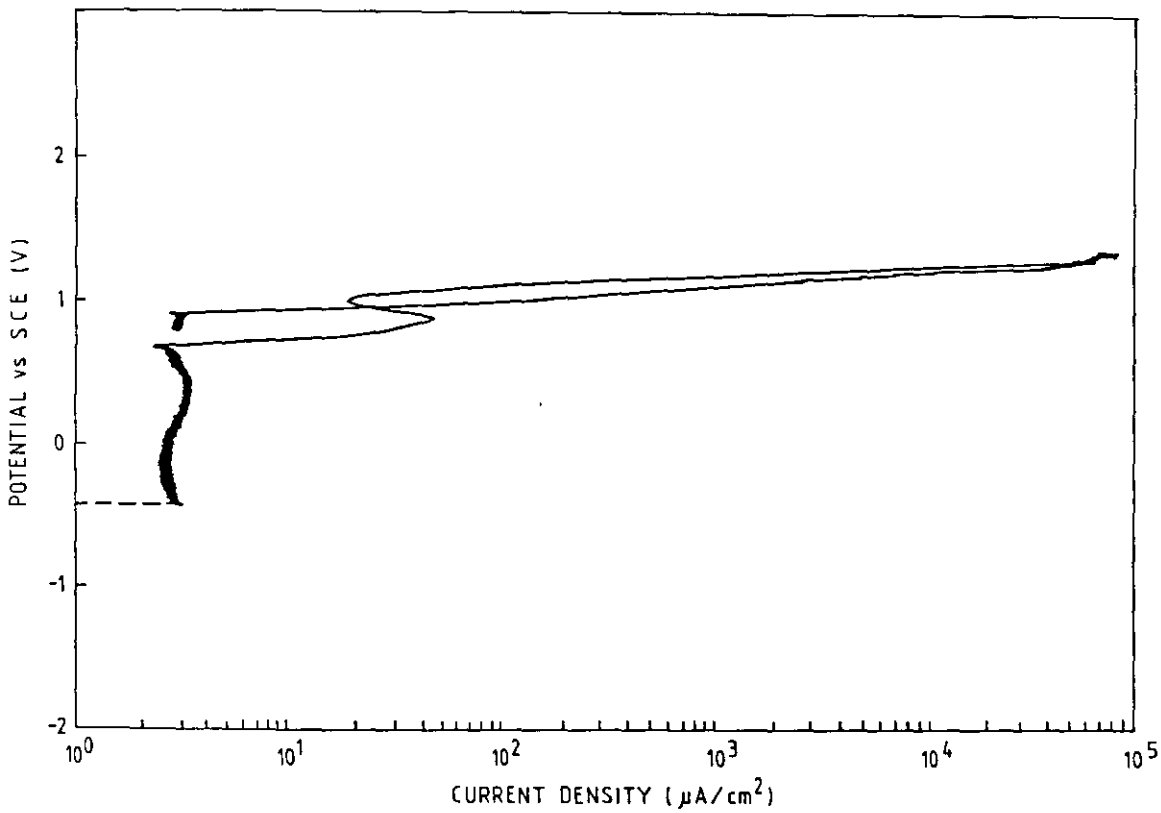

Figure A.12 Pitting Scan - Alloy 5: Fe-40Cr-0.2Ru (500 ppm Cl + 300 ppm SO_4)

Examination of Corroded Surfaces

The corrosion faces were studied by scanning electron microscopy and the results are shown in Figures A.13 - A.16.

The transpassive region was characterised by localised and general pitting. Preferential attack occurred at the chromium enriched oxide inclusions and at the grain boundaries. In the case of the recovered alloys, attack occurred at the sub-boundaries, as well as at prior-ferrite boundaries as shown.

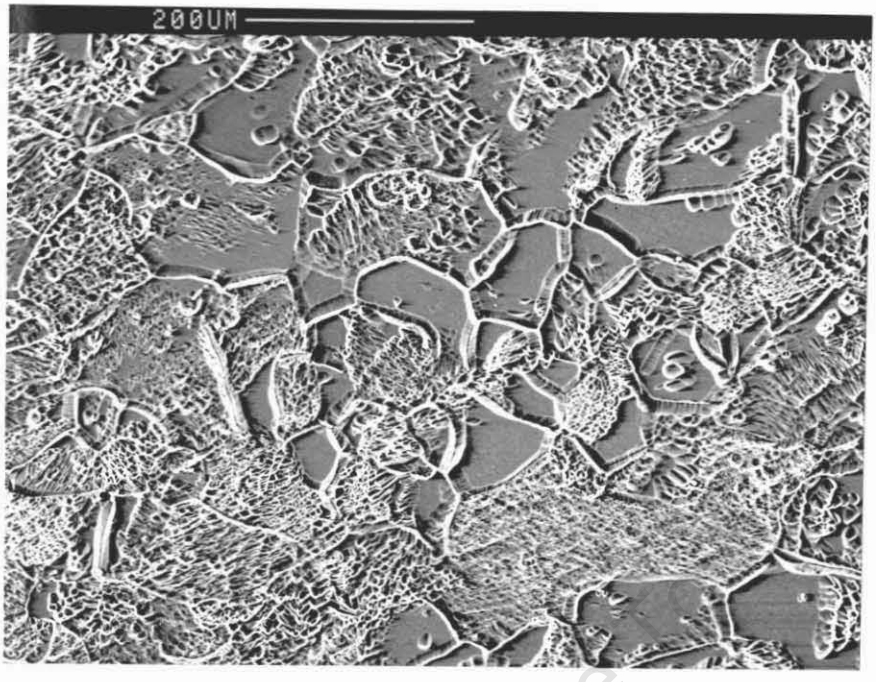

Figure A.13 Corroded Surface showing general transpassive attack - Alloy 4 (10% H_2SO_4)

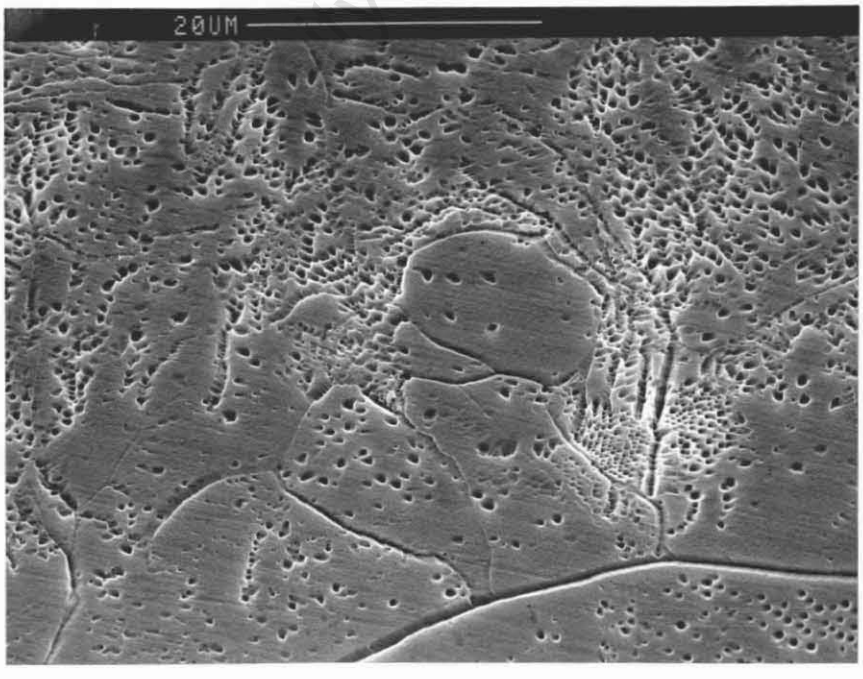

Figure A.14 Pitting Attack at sub-boundaries - Alloy 2 (10% H_2SO_4)

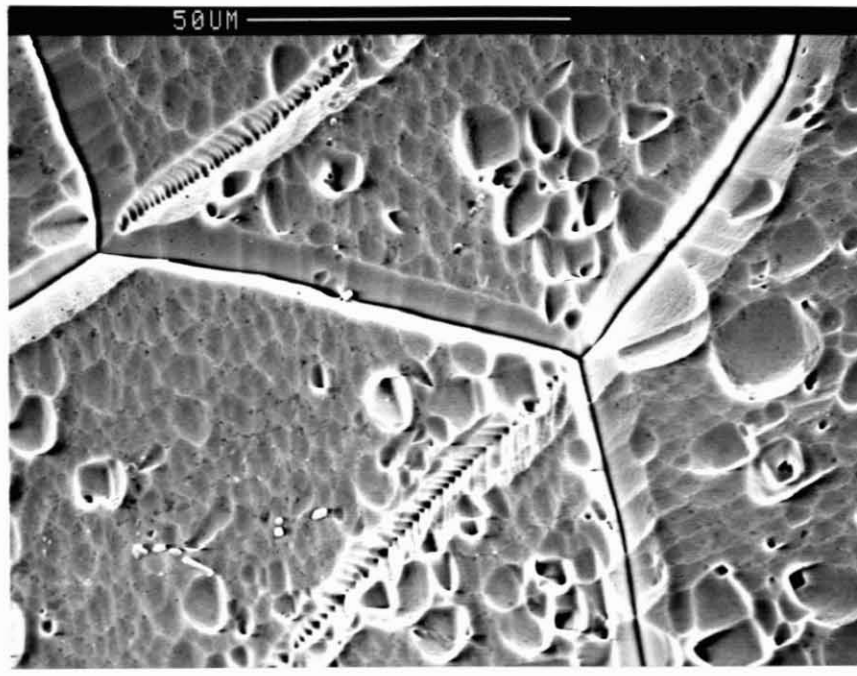

Figure A.15 Attack at grain boundaries and prior-ferrite boundaries - Alloy 2 (10% H_2SO_4)

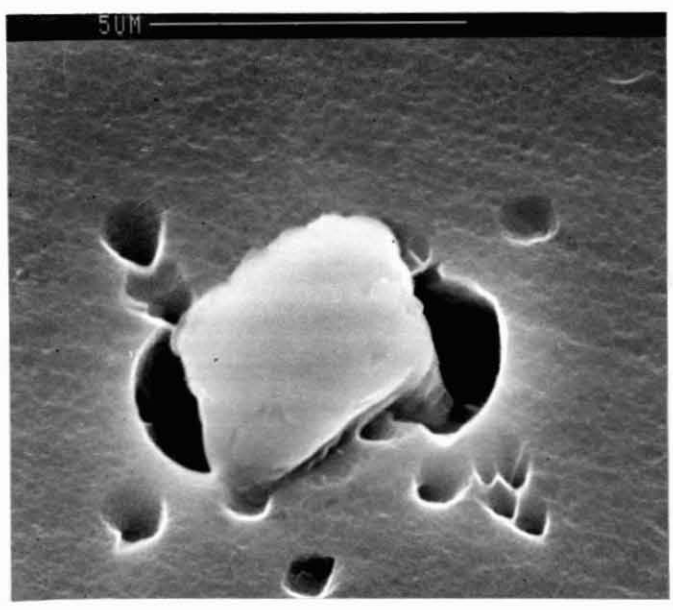

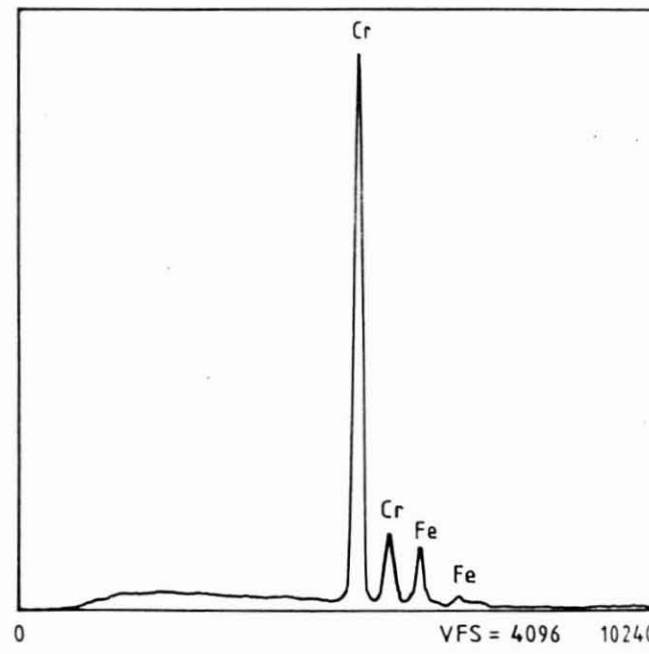

Figure A.16 Pitting attack at chromium-enriched oxide inclusions - Alloy 1 (10% H_2SO_4)

4. DISCUSSION

The results of the potentiodynamic corrosion and pitting studies show that localised corrosion may be initiated at any one of several microstructural inhomogeneities. To wit, preferential attack occurs at (1) grain boundaries, (2) prior-ferrite boundaries, (3) sub-boundaries and (4) second phase inclusions.

In the first analysis, these sites represent high energy surfaces which may in principle modify the corrosion thermodynamics, but the preferential attack is more probably linked to compositional variations with which these microstructural features are associated.

4.1 Intergranular Corrosion

Transmission electron microscopy has shown that in all cases quenching from the solutionising temperature results in precipitation at the grain boundaries. Since these precipitates are invariably chromium-enriched, grain boundary corrosion, as with other stainless steels, can be explained by invoking a theory of chromium depletion in the adjacent regions. This is commonly referred to as sensitisation, and is overcome in practice by re-annealing at an intermediate temperature to re-diffuse chromium into the denuded regions. Unfortunately, the present study has shown that post-anneal heat treatments are conducive to coarsening of the grain boundary phase, with implications for the impact resistance. It is therefore important to eliminate grain boundary precipitation by stabilisation of the interstitial solutes.

Since the stabilising practice usually demands prolonged soaking at intermediate temperatures (conducive to both carbonitride and sigma phase formation) the approach adopted with the Fe-40Cr alloys has been to over-stabilise the alloy to promote gettering of the interstitials. For example, Tullmin et al (1988) have shown that super-stoichiometric additions of as much as 35(C+N) are necessary to effect intergranular corrosion resistance in low interstitial Fe-40Cr alloys. Although this causes solid solution strengthening, the present study had shown that

the over-stabilised alloys may be rendered ductile by simple cold reduction to increase the dislocation density.

4.2 Corrosion of the Cold-worked Structure

Plastic strain is known to compromise the corrosion resistance, particularly as the result of localised internal stresses which promote stress corrosion. The introduction of a limited degree of pre-strain into the matrix may therefore be expected to prejudice the corrosion resistance. In this case, cold work of the order of 5%, necessary for adequate toughness, has been shown to exert only a slight influence on the passivity and general pitting resistance.

4.3 Corrosion of the Recovered Structure

Selected attack has been unequivocally correlated with the initiation of pitting at sub-grain boundaries, comprising low-angle dislocation arrays. The occurrence of a dislocation sub-structure was previously linked to enhanced solute transport and a change in the precipitation kinetics due to the provision of additional nucleation sites. The increased intragranular solubility of the solute elements as a result of the sub-boundaries has been shown to reduce the susceptibility of stainless steels to grain-boundary sensitization [Sedriks (1979)]. It appears however, that this decoration of the sub-boundaries leads to preferential attack. Uhlig (1948), for example, has noted that pitting occurs in stainless steels annealed at intermediate temperatures which induce carbide precipitation.

The important influence of a sub-structure on the corrosion resistance has implications for the alloying practice. Both the addition of stabilising elements as well as the addition of elements for cathodic modification alter the recrystallisation kinetics of Fe-40Cr. In the case of niobium, recovery is retarded by pinning of the sub-arrays. The addition of ruthenium elevates the recrystallisation temperature by changing the boundary energy. Care must therefore be taken to ensure complete recrystallisation, although once again this means a play-off against the mechanical properties.

4.4 Pitting Attack at Sulphides

The addition of 500ppm sulphur to Fe-40Cr impairs the corrosion resistance in so far as the sulphide particles stabilise the sub-structure. Provided that the state of the sulphides is adequately controlled, there is no apparent loss of intergranular corrosion resistance or pitting resistance. In stainless steels the sulphide inclusions are usually solid solutions of the (Mn,M)S type, and their conductivity varies with the amount of M in solution. It has been suggested that pitting may be inhibited by lowering the Mn/M ratio of sulphides in favour of more noble phases like Cr and Ti sulphides, which have a wider thermodynamic stability range. [Sedriks (1987)]. Experimental evidence has shown that the breakdown potential of steel with Mn-free sulphides is nearly as high as for sulphur-free steels of the same composition [Kiessling (1978)]. This is borne out by the above results, which give little indication of preferential pitting at the CrS spheroids. This suggests that greater amounts of sulphur than the 0,03% max. limit recognised for super-ferritic steels might be tolerated.

4.5 Cathodic Modification

The effects of a 0,2% ruthenium addition on the passivation characteristics are largely overridden by the influence of the recovered substructure. Nevertheless, it is significant to note that the ruthenium alloy shifts the free corrosion potential E_{corr} in the noble direction relative to the base alloy with a similar thermal history in the case of the general corrosion tests, as well as reducing the passivation current. Similarly, the pitting resistance in the chloride aqueous solution is substantially better, and the ruthenium alloy once again records the minimum current for passivation. The addition of cathodic elements therefore holds advantages for the localised corrosion resistance, provided that the appropriate annealing practices are observed.

5. CONCLUSIONS

General and pitting corrosion was studied electrochemically in reducing 10% H_2SO_4 and chloride environments respectively for a range of Fe-40Cr alloys. The following may be concluded:

(1) A recovered sub-structure promotes localised attack which destabilises the passivity. The optimum corrosion resistance is obtained by ensuring full recrystallisation.
(2) The addition of the cathodic element ruthenium increases the resistance to localised attack. However, ruthenium promotes recovery annealing at the normal recrystallisation temperature, with a loss of corrosion resistance as a result of the sub-structure.
(3) Grain boundary attack occurs in all cases in the absence of a stabilisation practice.
(4) The addition of 500ppm sulphur has only a slight negative effect on the pitting potential of the alloy in the spheroidised condition.
(5) Pre-straining by cold deformation of the order of 5% may be tolerated without impairing the passivity or pitting resistance.
(6) The Fe-40Cr alloys all exhibit excellent pitting resistance in chloride environments, although severe pitting occurs at the chromium-enriched oxide inclusions.

6. REFERENCES

DELPORT, W.E. and ROUX, J.P., "The Surface Segregation and Oxidation of Chromium and Palladium in High Chromium Stainless Steel,"
Corr. Science, Vol. 26, No. 6, 1986, pp407 - 417.

HIGGENSON, A., "The Passivation of Fe-Cr-Ru Alloys in Acidic Solutions,"
Ph.D Thesis, Univ. Manchester, June, 1987.

MILLER, M.K., BRENNER, S.S. and BURKE, M.G., "The Distribution of Palladium in a Pd- Modified 4130 Steel,"
Metall. Trans. A., Vol. 18A, April, 1987, pp519 - 523.

SEDRIKS, A.J., "Corrosion of Stainless Steels,"
Wiley - Interscience, 1979.

SEDRIKS, A.J., "Metallurgical Control of Localized Corrosion of Stainless Steels",
Proc. Int. Conf., Stainless Steels '87, 14 - 16 Sept., 1987, York, Inst. of Metals, 1988.

STREICHER, M.A., "Alloying Stainless Steels with the Platinum Metals,"
Plat. Met. Rev., Vol. 21, No. 51, 1977, pp51 - 55.

TOMASHOV, N.D., CHERNOVA, G.P. and USTINSKI, E.N., "The Corrosion and Electrochemical Behaviour of Ductile Chromium Alloys,"
Plat. Met. Rev., Vol. 23, No. 143, 1979, pp143 - 149.

TULLMIN, M.A.A., ROBINSON, F.P.A. and CORTIE, M.B., "Corrosion Resistance of 40% Cr Ferritic Stainless Steels and the Effects of Stabilising Elements",
Proc. E.M.S.S.A., Vol. 18, 1988, pp183 - 184.

UHLIG, H.H., "The Corrosion Handbook",
Wiley, 1948.

APPENDIX B

PUBLICATIONS

STRENGTH OF METALS AND ALLOYS

(ICSMA 8)

Proceedings of the 8th International Conference
on the Strength of Metals and Alloys
Tampere, Finland, 22–26 August 1988
(Eds) Kettunen, P.O., Lepistö, T.K., Lehtonen, M.E.
Volume 1 - Pergamon Press

Microstructural Influences on the Plastic Deformation of High Chromium Ferritic Alloys

M. P. Shaw, J. M. Robinson, I. M. Wolff and A. Ball

Department of Materials Engineering, University of Cape Town, Rondebosch 7700, South Africa

ABSTRACT

The transition from brittle to ductile behaviour of a wrought 40 wt. % Cr-Fe ferritic alloy appears to be intimately associated with the presence of mobile dislocations, the occurrence of which is controlled by the thermo-mechanical processing route. The influence of a sparse population of sulphide precipitates on the production of mobile dislocations, and the subsequent effect of cooling rate during quenching, is considered in terms of the distribution of dislocations and their influence on the ductile/brittle transition during room temperature deformation.

KEYWORDS

Mobile dislocations, ductile/brittle transition, transmission electron microscopy, ferrite, interstitials.

INTRODUCTION

The 'super-ferritic' alloys, containing up to 40% Cr, hold considerable promise for applications where a combination of good corrosion resistance and toughness are of prime importance (Abo and colleagues, 1977). However, one of the factors limiting their utilisation is the susceptibility to brittle failure at room temperature (see e.g. Steigerwald and colleagues, 1977). Control of the ductile/brittle transition has proved to be elusive, despite deliberate efforts to minimise interstitial contents in order to promote ductility. The potentially encouraging strength and toughness levels occur in a frustratingly unpredictable manner. Part of the reason for this is associated with difficulties in process control together with the flaw sensitivity of the alloys (De Marsh, 1986). It is clear that a detailed mechanistic knowledge of the influence of a wide range of microstructural parameters on the ductile/brittle transition is required.

The material investigated is a 40 wt. % Cr-Fe alloy with a deliberately minimised interstitial content (~120ppm) in order to minimise the formation of Cottrell 'atmospheres' and undesirable amounts of grain boundary precipitation. The material was examined in the wrought condition, having undergone an extended thermo-mechanical processing cycle terminating in a quench from the final rolling temperature. The grain size is variable but

but tends to be large at an average value of 100 μm.

Here we report on some microstructural observations pertaining to precipitate/matrix interactions that appear to encourage ductile behaviour. The influence of quenching rates on subsequent dislocation distributions, and deformation features that become evident during tensile deformation and fracture, are discussed.

OBSERVATIONS

Thin foil specimens for transmission electron microscopy were prepared by conventional twin-jet electropolishing techniques using a solution of 5% perchloric acid in ethanol at -20°C. Specimens were examined from four different specimens, that had been quenched from 1050°C at different rates in order to investigate the effect on mechanical properties (see Fig. 3).

Intragranular matrix precipitation, comprising a relatively non-uniform distribution of spheroidal precipitates, was observed to be associated with a ductility increase after water quenching (Wolff, Shaw and Ball, 1987). Transmission electron microscopy subsequently revealed that the precipiates were associated with a high density of $^{a}/_{2}\langle 111\rangle$ dislocation loops, which had apparently been 'punched out' from the precipitate/matrix interface (see Fig. 1). These prismatic dislocation loops would seem to be associated with differential thermal contraction coefficients between precipitate and matrix causing local plastic deformation during quenching, or differences in specific volume during precipitate growth (see e.g. Honeycombe, 1984). Subsequent examination by electron diffraction and energy dispersive X-ray microanalysis in the transmission electron microscope revealed that the precipitates were chromium sulphides (CrS) having a monoclinic crystal structure. Other dislocations were also present in the form of a background population of small loops.

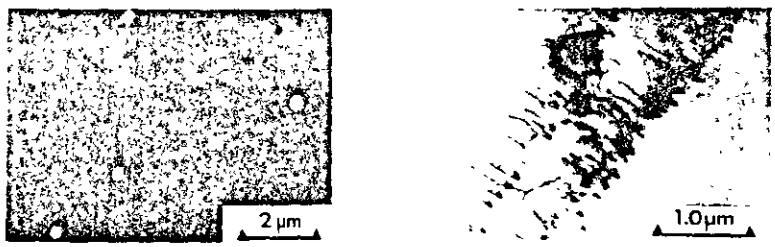

(a) (b)

Fig 1. (a) SEM image (combined secondary and back scattered electrons) from an etched cross-section of a quenched specimen showing CrS spheroids. (b) TEM (bright field image) of CrS precipitate showing sections of 'punched out' dislocation loops. Specimen water quenched from 1050°C.

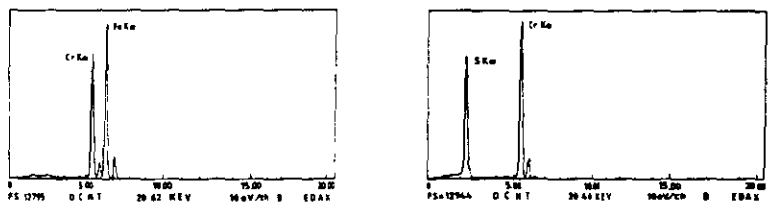

(a) (b)

Fig. 2. EDS spectra from (a) matrix, (b) spheroidal precipitate.

The enhanced ductility, apparently induced by the 'in-situ' production of free dislocations during quenching, was found to be markedly influenced by the cooling rate and is illustrated in Fig. 3.

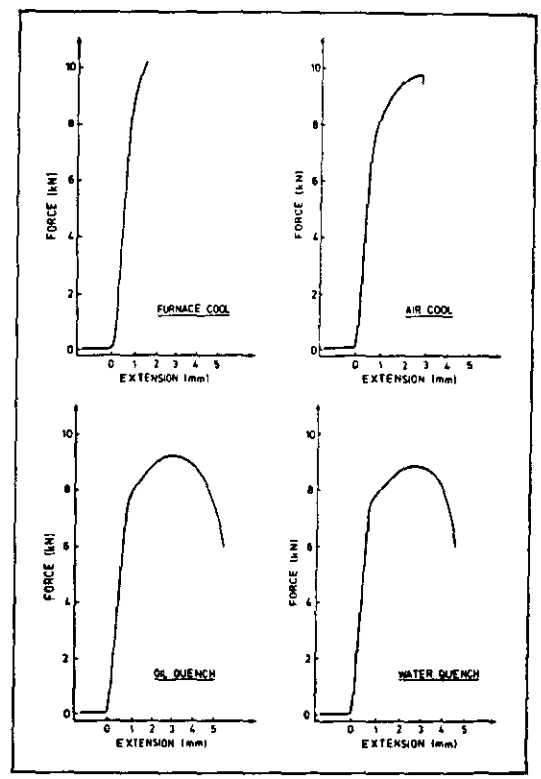

Fig. 3. Load/extension curves from room temperature tensile tests illustrating the influence of cooling rate, during quenching from 1050°C, on ductility.

Transmission electron microscopy of foils taken from material cooled at the rates corresponding to Fig. 3 revealed significant differences in dislocation density and distribution. Both dislocation line segments and the smaller background loops showed a marked decrease in density as the cooling rate was decreased. Figure 4 shows examples from the ductile water quenched and oil quenched specimens and it is evident that the slower quench has allowed growth of the small dislocation loops to occur. Electron micrographs from the two specimens which behaved in a brittle manner showed a complete absence of dislocation loops and only isolated matrix dislocation lines. Care was taken to ensure that foil thicknesses sufficient to ensure the retention of dislocations were examined; areas where dislocation loss from thinner regions had occurred were avoided.

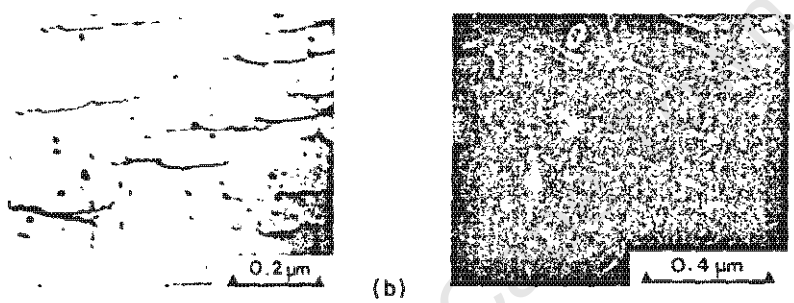

Fig. 4. Transmission electron micrographs from (a) water quenched and (b) oil quenched specimens, showing the change in dislocation density and loop growth at slower cooling rates. Some evidence of dislocation line pinning is apparent in (a), (b) is a weak beam image.

The relative contribution of the dislocation lines and the smaller loops to subsequent plastic deformation is not clear at present. However, interestingly, there is some evidence to suggest that local pinning and dipole formation of dislocation lines in the water quenched specimen is occurring (Fig. 4).

During subsequent tensile testing the electropolished specimen surfaces were observed in order to identify any surface deformation features which may act as fracture nucleation sites. Examination in the SEM of both brittle and ductile specimens, at 2kN load intervals during straining, and of the final fracture surfaces, indicated that micro-void coalescence was operative prior to failure and that there were no obvious surface features responsible for fracture initiation. Figure 5 shows some of the typical surface features that developed during tensile straining in a ductile sample. Optical examination of cross-sections through the fracture surfaces indicated that mechanical twinning, in the form of Neumann bands, was a commmon feature of plastic deformation in both brittle and ductile specimens. In addition, there was evidence (see Fig. 6) that abrupt changes in crack propagation direction are associated with a local increase in deformation twinning. Whether the twinning is induced by the strain field of the propagating crack or the twins cause changes in crack direction is unclear at present.

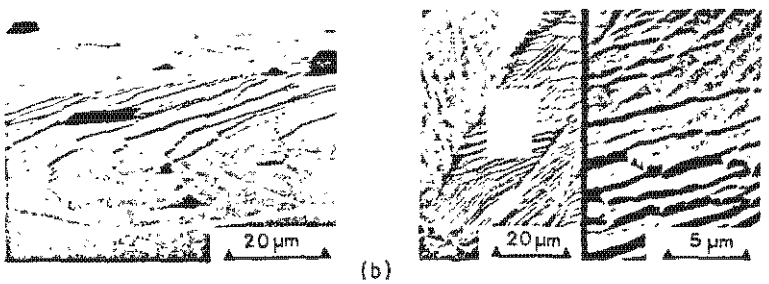

(a) (b)

Fig. 5. Secondary electron SEM images of surface deformation markings from a pre-polished tensile specimen after plastic straining. Intersecting 'wavy' surface slip steps are evident (a) oblique view of surface slip steps, (b) intersecting 'wavy' slip steps.

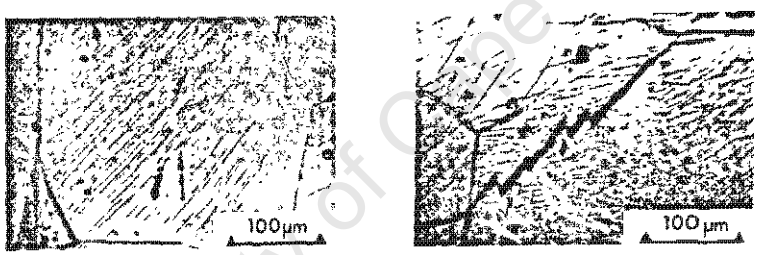

(a) (b)

Fig. 6. Optical micrographs of fracture surface cross-sections showing (a) parallel twins (Neumann bands) in a single grain adjacent to the fracture surface, (b) transgranular cracking in association with Neumann bands in the vicinity of changes in crack direction.

SUMMARY AND DISCUSSION

The observations, in a smiliar manner to pure chromium, indicate that ductility of 40% Cr-Fe alloys is dependent upon the availability of freshly introduced unpinned dislocations (Ball and Bullen, 1970, Bullen and colleagues, 1964). The solubility of both carbon and nitrogen in Fe-Cr alloys is known to decrease rapidly with decreasing temperature (see e.g. Pollard, 1974), and this would encourage the clustering of interstitials at dislocation strain fields. The observation that apparently freshly introduced dislocations are present after relatively rapid quenching suggests that these dislocations play an important role during subsequent plastic deformation. Importantly, these defects are present only in the specimens exhibiting ductile behaviour. The more extended cooling periods apparently allow a sufficient degree of dislocation rearrangement - by either climb or stress relieving slip - to remove those required for a significant degree of subsequent ductility. The observation of apparently impeded matrix dislocations in the water quenched specimen suggests that the smaller loops may be important features in plastic flow.

Surface features observed after plastic straining of the pre-polished gauge length of tensile specimens are consistent with those expected from multiple slip in b.c.c. metals, the intersecting 'wavy' slip steps being expected from 'pencil' glide. However, the scale of these features would suggest that they may act as effective stress raisers, if sufficiently developed, and may be expected to provide crack nucleation sites under suitable circumstances. Clearly, deformation twinning eventually plays a significant role, as evidenced by the micrographs taken near fracture surfaces and cracks. However, the contribution of conventional slip appears to be dominant during the earlier stages of plastic flow.

In summary, quenching rates rapid enough to ensure the retention of freshly introduced mobile dislocations - either by precipitate/matrix interactions, quenching stresses or point defect agglomeration - seem necessary to ensure ductility during room temperature deformation.

The authors gratefully acknowledge the support of The Council for Mineral Technology (MINTEK), Randburg, South Africa.

REFERENCES

Abo, H., Nakazawa, T., Takemura, S., Onoyama, M., Ogawa, H. and Okeda, H. (1977). Stainless Steel '77. Climax Molybdeunum Co (U.S.A.), p. 35.
Ball, A. and Bullen, F.P. (1970). Phil. Mag., 22, 176, 301.
Bullen, F.P., Henderson, F., Hutchison, M.M. and Wain, H.L. (1964). Phil. Mag., 9, 98, 285.
De Marsh, E.A. (1986). M.Sc. Thesis. University of the Witwatersrand, Johannesburg.
Honeycombe, R.W.K., (1984). The Plastic Deformation of Metals (2nd ed.). Edward Arnold (London), p. 197.
Pollard, B. (1974). Metals Technology, 1, 31.
Steigerwald, R.F., Dundas, H.J., Redmond, J.R. and Davison, R.M. (1977). Stainless Steel '77. Climax Molybdenum Co. (U.S.A.), p. 57.
Wolff, I.M., Shaw, M.P. and Ball, A. (1987). Proc. Electron Microscopy Society of Southern Africa. 17, p. 161.

Elektronmikroskopievereniging van Suidelike Afrika JOHANNESBURG (1987)

OBSERVATIONS ON PRECIPITATION IN HIGH CHROMIUM FERRITIC ALLOYS

I.M. Wolff, M.P. Shaw and A. Ball

Department of Materials Engineering, University of Cape Town

This paper concerns some transmission electron microscope observations on precipitation phenomena in high chromium 'super-ferritic' alloys. The material discussed here is a 40 wt.% Cr-Fe base alloy that has an intentionally minimised interstitial content in order to promote ductility in a system that is notoriously susceptible to brittle fracture[1]. The observations presented here represent some preliminary results from the initial stages in a more extensive study of microstructural influences on properties[2].

Thin foil specimens for transmission electron microscopy were prepared by conventional twin-jet electropolishing techniques using a solution of 5% perchloric acid in ethanol at -20°C.

Matrix precipitation, of an as yet unidentified compound, was observed to be associated with a ductility increase in wrought alloys after a complex thermo-mechanical processing cycle terminating in an isothermal treatment. Fig. 1 shows a bright-field image of a spheroidal matrix precipitate associated with this ductility increase. Significantly, precipitation is associated with the apparent 'punching out' of a relatively high density of a/2 ⟨111⟩ dislocation loops (sections of which are visible in Fig. 1). These are likely to be associated with differential thermal expansion coefficients or differences in specific volume between precipitate and matrix causing local plastic deformation during precipitate growth, as suggested by Honeycombe[3]. Closer examination of the matrix revealed a relatively high, but inhomogeneous, population of small dislocation loops associated with a region of higher general dislocation density, but not noticeably with adjacent precipitation (as shown in Fig. 2). The relative contribution of the larger prismatic loops and the smaller 'matrix' loops to subsequent plastic flow is presently under investigation[2]. The commonly observed brittle behaviour of alloys in this system can be logically associated with the absence of mobile dislocations under normal circumstances and, despite the low interstitial content of the alloys investigated, the production of mobile precipitate-induced dislocations allied with an increase in ductility is worthy of further investigation.

Fig. 3 illustrates the occurrence of grain boundary precipitates that are morphologically consistent with $M_{23}(C,N)_6$[4]. These precipitates are confined to only a proportion of the high angle grain boundaries present and there is some evidence to suggest that they are particularly associated with boundaries of higher misorientation. Low-angle sub-boundaries (see Fig. 4) show no evidence of precipitation and are typically represented by extensive 'clean' dislocation arrays.

Interestingly, selected area diffraction studies indicate that the spheroidal precipitates responsible for dislocation production are inconsistent with both cubic and hexagonal structures. Furthermore, examination of patterns from various zone axes cannot be reconciled with the tetragonal σ phase structure, which may be expected to occur in these alloy systems. Current work utilising convergent beam electron diffraction and energy dispersive X-ray spectrometry should enable the various precipitate structures and compositions to be clarified.

The authors gratefully acknowledge the support of Mintek.

References

1. Steigerwald, R.F., Dundas, H.J., Redmond, J.D. and Davison, R.M., (1977), Stainless Steel '77, Pub. Climax Molybdenum Co. (U.S.A.), p.p. 57-79.
2. Wolff, I.M., (1987), current research for Ph.D. thesis.
3. Honeycombe, R.W.K., (1984), The Plastic Deformation of Metals (2nd ed.), Pub. Edward Arnold (London), p. 197.
4. Edington, J.W., (1976), Practical Electron Microscopy in Materials Science, Vol. 4, Pub. MacMillan (London), p. 38.

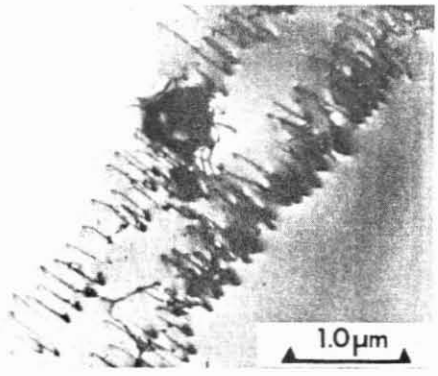

Fig. 1: A spheroidal matrix precipitate acting as a dislocation source.

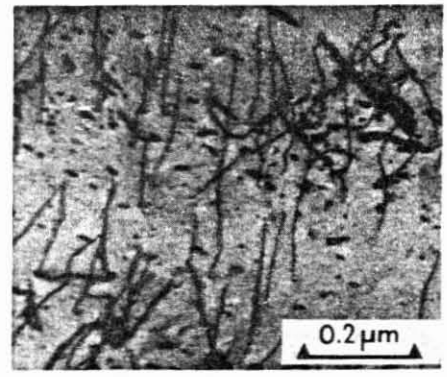

Fig. 2: Small dislocation loops in a region of higher dislocation density.

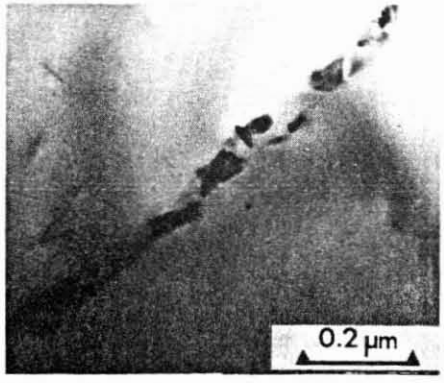

Fig. 3: Grain boundary precipitation.

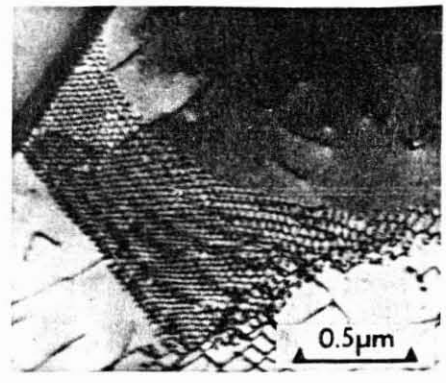

Fig. 4: A low-angle sub-boundary revealed by a dislocation array.